Winter 2008

Experimental Investigation of Active Control of Bluff Body Vortex Shedding

Ilteris Koc
Old Dominion University

EXPERIMENTAL INVESTIGATION OF ACTIVE CONTROL OF BLUFF BODY VORTEX SHEDDING

by

ILTERIS KOC
B.S. June 2001, Gazi University, Turkey
M.S. August 2003, Old Dominion University

A Dissertation Submitted to the Faculty of
Old Dominion University in Partial Fulfillment of the
Requirement for the Degree of

DOCTOR OF PHILOSOPHY

AEROSPACE ENGINEERING

OLD DOMINION UNIVERSITY
December 2008

Approved by:

Colin P. Britcher (Director)

Oktay Baysal (Member)

Drew Landman (Member)

Stephen P. Wilkinson (Member)

ABSTRACT

EXPERIMENTAL INVESTIGATION OF ACTIVE CONTROL OF BLUFF BODY VORTEX SHEDDING

Ilteris Koc

Old Dominion University, 2008

Director: Dr. Colin P. Britcher

Mean and fluctuating forces acting on a body are strongly related to vortex shedding generated behind it. Therefore, it is possible to obtain substantial reductions of at least the unsteady forces if vortex shedding is controlled or its regularity is reduced. While conventional active flow control methods are mainly concerned with direct interaction with, and alteration of, the mean flow about a body, modern techniques involve altering existing flow instabilities using relatively small inputs to obtain large-scale changes of mean flows. Aerodynamic flow control may be intended to delay or suppress boundary layer separation through creation of a boundary layer downstream from the control input that is able to withstand adverse pressure gradients imposed by the outer (global) flow.

In the present work, aerodynamic characteristics of a circular cylinder at Re=156,000 and an axisymmetric body (ogive cylinder) at Re=170,000 are first analyzed using a proposed phase averaging technique for the Particle Image Velocimetry (PIV) data. Later, the effect of plasma actuators on the aerodynamic characteristics of these bodies is investigated.

When plasma actuators were placed 10° upstream of the separation point on the circular cylinder, momentum addition, and maybe the effect of local heating, modified the streamwise pressure gradient, leading to the establishment of a thinner boundary layer downstream. Phase synchronization of vortex shedding was also obtained for Re=156,000 for a narrow frequency band of the carrier signal of the actuators when they operated with a 90° phase shift. To the knowledge of the author no other method has been shown to achieve vortex shedding control up to this high a Reynolds number.

Effects of the different configurations of plasma actuators on the circumference, on the base, and in a streamwise direction were investigated for the ogive cylinder. It was observed that direct alteration of the mean flow about a body was not as effective as the boundary layer flow control where the flow instabilities are exploited. Also, the three dimensionalities in this flow made it significantly more complex to analyze.

Anneme, babama ve tüm aileme…

ACKNOWLEDGMENTS

It is a hard task to name and thank all the people who contributed to this achievement. The decision to come to ODU more than six years ago turned out to be one that permanently changed my life, on a professional as well as personal level. ODU, with its diverse, stimulating and constantly changing crowds of like-minded souls, has been an inextinguishable source of academic and personal challenges for me.

I would like to thank first and foremost my advisor Dr. Colin P. Britcher, who, with his wisdom, not only mentored me but also presented a constant example of how to be a director and a researcher.

A sincere and special thank you is owed to my committee members Dr. Oktay Baysal, Dr. Drew Landman, and Mr. Stephen Wilkinson for their valuable guidance and support. Dr. Baysal has guided me since my first day in the U.S. and supported meduring all those years. Dr. Landman was always someone I could depend on for his knowledge and help. This work involved cooperation from the NASA Langley Research Center and Mr. Wilkinson has provided very valuable support and guidance to this work; without him this work would not be possible.

Among all the many friends I made in Norfolk, I would like to particularly thank Dr. Mehti Koklu, with whom I not only shared my office but also many ups and downs of my life. Thank you for providing help in all times of need.

I am also greatly indebted to my dear friend Dr. Kursat Kara for generously spending his time editing this dissertation.

I would also like to thank my friends Bedri Yagiz, Omer San and my longtime house-mates Rifat Tuzcuoglu and Olcay Sahin for enduring my seemingly endless worries and complaints of what was actually a very quick period.

I am also very grateful to my friend Ashish Tamhane, without whom the long hours of experiments in the lab would be very hard and boring. I would also like to acknowledge Tom Galloway and Kevin Colvin from Batten Model Shop for helping me build experimental models.

Also, I would like to thank my family, whose love and attention made the time and distance between us appear much less than it really was. I could never come to this point without their support and love. Special thanks go to my future family, my beloved one, my fiancée Semanur Kirici for her continuous presence, support and encouragement. Thank you for understanding me when I had to spend time away from you.

Last but not least, I want to remember Erdinc Karakas, Murat Cinar, Yilmaz Kaplan, and all the countless friends that I met over the years and who all helped make my stay in Norfolk one that I will treasure and remember forever.

NOMENCLATURE

Variables

C_x	Drag Coefficient
C_y	Lift Coefficient
Cp_b	Base pressure coefficient
d	Diameter of the cylinder or width of the bluff body
D	Drag
E_b	Breakdown voltage of electric field
f_s	Vortex shedding frequency, Hertz
h	Lateral spacing
l	Longitudinal spacing
L	Lift
P	Power input
Re, R_d	Reynolds Number
St	Strouhal number
T	Thrust
u_{max}	Maximum induced velocity
U	Flow velocity
V_j	Bleed velocity

Greek Symbols

$\Delta\beta$	Azimuthal angle
ν	Kinematic viscosity

φ	Phase angle
μ	Phase averaged value
τ_w	Skin friction vector
τ	Time displacement
ΔV	Voltage drop

Acronyms

ATT	Angular triggering technique
CCD	Charge coupled device
DBD	Dielectric-barrier discharges
DES	Detached Eddy Simulation
DNS	Direct numerical simulation
EHD	Electrohydrodynamic
LDA	Laser Doppler Anemometer
LES	Large Eddy Simulation
MEM	Micro-electromechanical-system
MHD	Magnethohyrodynamic
OAUGDP	One Atmosphere Uniform Glow Discharge Plasma
PATT	Predictive Angular Triggering Technique
PIC-DSMC	Particle-in-cell direct-simulation-Monte-Carlo
PIV	Particle Image Velocimetry
RANS	Reynolds Averaged Navier Stokes equations
r.m.s.	Root mean square value x'

r.p.m.	Revolution per minute
RF	Radio frequency
TTT	Tracking triggering technique
URANS	Unsteady Reynolds Averaged Navier Stokes equations

Mathematical Operators

{}	ensemble average
⟨⟩	phase average

TABLE OF CONTENTS

Chapter Page

LIST OF FIGURES

LIST OF TABLES

1. INTRODUCTION

1.1 Background

Flows over bodies opposing unbounded fluids are referred to as external flows[1]. External flows have been studied extensively due to their many practical applications[2]. Some of the features of external flow fields can be seen in Figure 1.1 where flow over an airfoil is presented. The freestream flow divides into two after facing the stagnation point on the body. The flow velocity at the surface goes to zero as a result of the no-slip condition. On both surfaces the boundary layer forms. In some cases boundary layer thickness increases considerably, and the flow in the boundary layer becomes reversed in the downstream direction[3]. This results in decelerated flow particles being moved outwards, causing the boundary layer to separate from the surface, which causes formation of vortices and large energy losses in the wake of the body. Viscous wakes are highly decelerated flow regions whose pressure distributions deviate remarkably from the wakes in frictionless fluids. This pressure region, which is actually the result of the boundary layer separation, can be used to explain the large drag of bluff bodies. At present, relatively little is known about developed separations, separation in transonic flow, three-dimensional boundary-layer separation, unsteady separation, etc. Future research in these areas is needed.

The format of this dissertation is based on *AIAA Journal.*

1.2 Objectives

The current study addresses a classical 2-D flow and a particular aspect of one of the simplest 3-D flows. A circular cylinder in crossflow was chosen for the 2-D case due to the extensive documentation of this flow structure. An axisymmetric base flow, an ogive cylinder, was chosen for the 3-D case owing to its geometric simplicity and range of possible applications. This research aims to carefully characterize the wake structure then investigate the possibility of some level of active control of this structure. Influencing the aerodynamic characteristics of both bodies using an active flow control device is a first step to active control in more challenging cases such as road vehicles. Plasma actuators were selected as good candidates for control actuators with these types of highly unsteady wakes.

1.3 Bluff Body Flows

Classification of bodies is made with respect to the features of the flow field they produce when they are immersed in a cross-stream (or are moving through still fluid), namely "streamlined" and "bluff bodies". Streamlined bodies have thin boundary layers that are completely attached over their surface. The wake that they leave behind is thin, generally steady and contains vorticity. Simplified potential flow and boundary layer theory can be used to deduce the aerodynamic forces acting on these bodies. On the other hand, bluff bodies have early and/or extensive boundary layer separation from their surface and wakes with significant lateral dimensions and unsteady velocity fields. Bluff body flows generally cannot be explained with simplified mathematical definitions, and the forces

acting on them may be evaluated either from the solution of the complete Navier-Stokes equations or from the results of experiments[4].

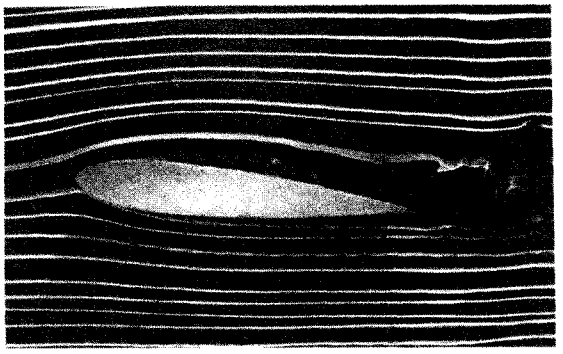

Figure 1.1 Separated flow over an airfoil[5]

Orientation of the body in a flow is also important in classification of the flow type. Streamlined bodies may become bluff bodies for some flow conditions (Figure 1.2). This brings another type of grouping of aerodynamic bodies according to their "degrees of bluffness". Some of the criteria in defining bluffness can be defined as the ratio between the cross-flow dimensions of the separated wake and of the body or to the extent of the body surface immersed in the separated wake. As a result of the flow type the amount and level of the vorticity and consequently the forces acting on the bodies, which has the greatest importance both from the aerodynamic and from the design points of view, are determined.

Generally, aerodynamic loads have mean and time-varying components (which may be characterized, for example, by their r.m.s. values and by their frequency spectra). Due to factors such as turbulence effects, the upstream flow can be time dependent, and the fluctuating loads can be significant. Fluctuating loads may also be significant for the

flows when the wake produced by the body itself has more-or-less regular fluctuations. In general one may say that, for steady upstream flow, streamlined bodies are characterized by steady wakes and loads, whereas for bluff bodies the opposite is true.

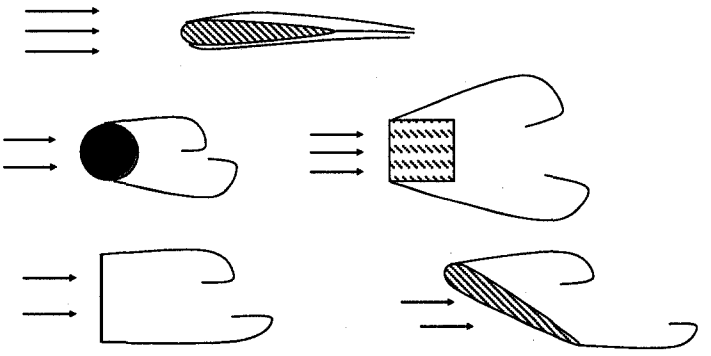

Figure 1.2 Streamlined and bluff bodies

1.3.1 Flow Over Two-dimensional Bodies

One of the most important aerodynamic force components is drag. Due to significant increase in pressure drag deriving from the boundary layer separation, bluff bodies typically have at least one order of magnitude higher drag coefficients than streamlined bodies.

The drag force acting on a body may also be explained in energetic terms. Indeed, the work done in a certain time interval by the drag force is equivalent to the increase in the total energy (i.e. the sum of the internal and kinetic energies) of the whole fluid field in the same time interval. In subsonic/incompressible flow this variation could strictly be connected to the amount of perturbation energy present in the wake of the body. In this manner, differences in the energy content of the wakes of different bodies may be related

to different values in drag. This explanation helps us to better understand different values of drag coefficients and also leads to a rationale for drag reduction approaches.

Figure 1.3 shows an airfoil (a streamlined body) and a cylinder (a bluff body) having the same total drag under same freestream conditions. The reason for these two bodies to have the same drag value despite the huge difference in their sizes is due to the 15 to 20 times higher drag coefficient of the cylinder. The flow field behind these bodies explains why the cylinder has a higher drag coefficient. As can be seen from Figure 1.4, the airfoil leaves an extremely thin wake, which gives rise to very small perturbation energy[5]. On the other hand, the circular cylinder shows a highly energetic wake (with a large pressure drag component), characterized by the presence of a double row of alternate concentrated vortices (known as a Karman vortex street). This vortex shedding phenomenon is typical of all two-dimensional bluff bodies, and has a great practical importance. If the frequency of the vortex shedding coincides with one of the natural frequencies of a structure they may induce remarkable oscillations.

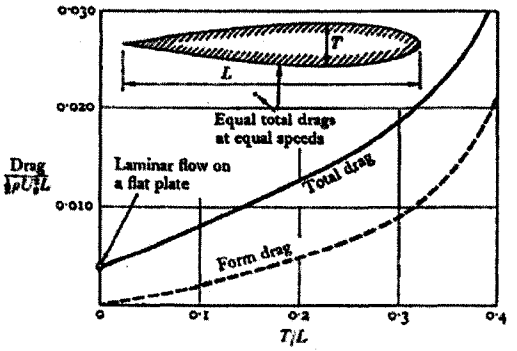

Figure 1.3 Comparison of an airfoil and a circular cylinder with same total drag (Batchelor 1967)[4]

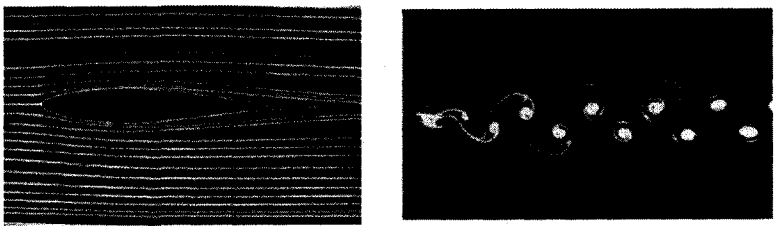

Figure 1.4 Flow Field around bodies a) Airfoil, b) Circular Cylinder (Van Dyke 1982)[5]

1.3.2 Periodic Wake Structures

A special feature of interest with bluff body flows is the periodic wake structure. In 1911, using results from the wind tunnel, Theodore von Karman made an analysis of the alternating double row of vortices behind a flat body in a fluid flow which is now known as the Karman Vortex Street (Figure 1.5)[6]. The name came from the way that the vortices alternated in position on the two sides of the double row in an arrangement similar to that of streetlights on the two sides of a street[7]. The vortex street is just a special type of unsteady separation over bluff bodies such as the flat plate shown in Figure 1.5. The vortex street is highly periodic having a frequency which is proportional to U/D, where D is the length of the bluff body measured transverse to the flow and U is the incoming flow speed. This periodicity is responsible for the "singing" of telephone wires. In fact, vortex streets are almost always involved when the wind generates a fairly pure tone as it blows over obstacles.

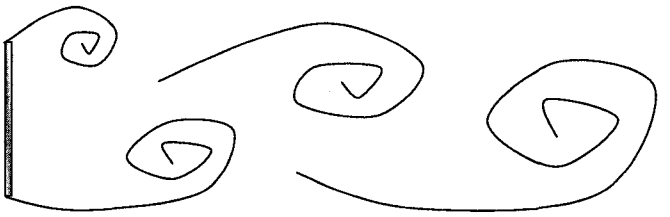

Figure 1.5 Von Karman Vortex Street behind a Flat Plate

If the density and viscosity of the fluid are known and the diameter of the body is given, the frequency measured at the wake can be used in the definition of Strouhal number to calculate the flow velocity. Vortex shedding generating from steady subsonic flow over circular smooth cylinders is dependent on Reynolds number. Significant Reynolds number regimes are shown in Figure 1.6[8].

At Reynolds numbers below Re=5, flow is unseparated and follows the cylinder contours. For Reynolds numbers between $5 \leq Re \leq 45$, the flow separates and a symmetric pair of vortices forms. The streamwise length of the vortices is a function of Reynolds number, increasing monotonically with increasing Reynolds number. This length reaches three cylinder diameters at Re=45. After this point, increasing Reynolds number results in an unstable wake and breaking away of one of the vortices. A laminar periodic wake with vortices of opposite sign (vortex street) is formed[9]. For the range of $150 \leq Re \leq 300$, the vortex wake becomes turbulent, although the boundary layer on the cylinder stays laminar[10].

In the subcritical range, $300 \leq Re \leq 1.5 \times 10^5$, laminar boundary layers separate at about 80° aft of the nose of the cylinder and there is strong periodic vortex shedding. In the range $1.5 \times 10^5 \leq Re \leq 3.5 \times 10^6$, which is called the transitional range, the cylinder boundary layer becomes turbulent, the separation points move aft to 140°, and the drag coefficient of the

cylinder drops to 0.3[9]. In this range, laminar separation bubbles and three-dimensional effects disrupt the regular vortex shedding process and broaden the spectrum of shedding frequencies for smooth surface cylinders[11]. Regular vortex shedding is reformed with a turbulent cylinder boundary layer in the supercritical range ($Re > 3.5x10^6$)[12].

In 1912, Von Karman showed that the ratio of the longitudinal to lateral spacing of an ideal, staggered vortex street was h/l=0.281 (Figure 1.7). It was also shown by recent studies that the lateral spacing drops to a minimum a few diameters downstream of the cylinder and then increases[13]. Sarpkaya showed that the longitudinal spacing (l) to cylinder diameter (D) is almost constant for most of the vortex streets[14]. Griffin et al. found $4.8<l/D<5.2$ and typically the distance between vortices is five cylinder diameters[15]. These values were observed for the near wake; also it is observed that the downstream vorticity decreases[14]. As a result the staggered vortex pattern expands laterally in accordance with asymptotic laws of turbulent wakes[9].

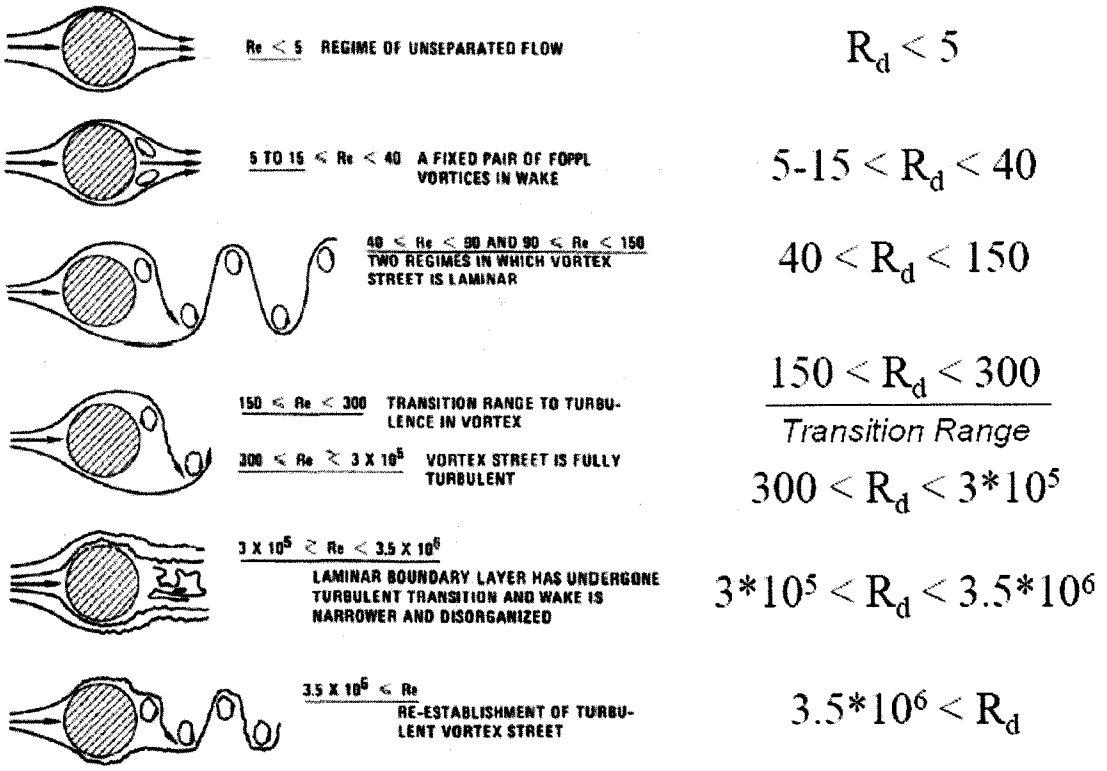

Figure 1.6 Fluid flow regimes across smooth circular cylinders[8]

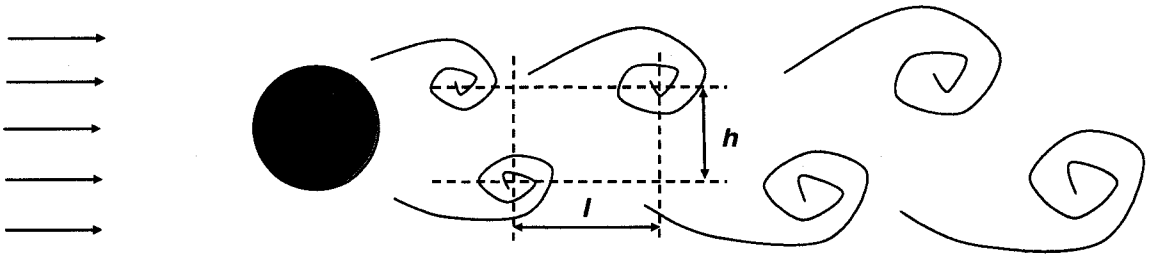

Figure 1.7 Von Karman Vortex Street

Dimensional analysis shows that the frequency of vortex shedding, f_s, is governed by the Strouhal number. The Strouhal number is the dimensionless proportionality constant between the predominant frequency of vortex shedding and the free stream velocity divided by the cylinder width,

$$f_s = \frac{StU}{D}$$

where f_s is the vortex shedding frequency in Hertz, D is the diameter of the cylinder or width of the bluff body and U is the flow velocity. The Strouhal number is a dependent variable of the Reynolds number. However, experimental investigations show that the Strouhal number is about constant across a wide range of the Reynolds number (10^2 ~ 10^7). The Strouhal number is about 0.18 for a cylinder within a Reynolds number range of 300 ~ 10^7. The relation between Reynolds number and the Strouhal number for circular cylinders can be seen in Figure 1.8.

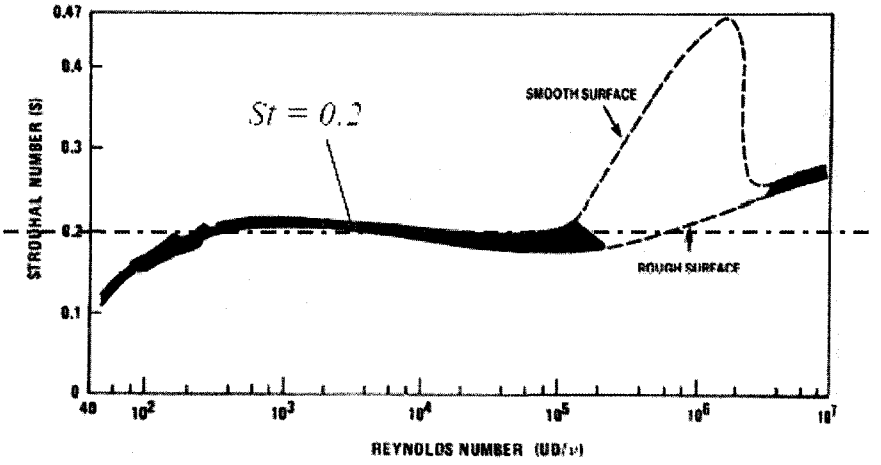

Figure 1.8 Strouhal number- Reynolds number relationship for circular cylinders[9]

Noncircular cross-sections also shed vortices. Figure 1.9 shows Strouhal numbers for noncircular sections and some three-dimensional bodies. Vortex street wakes of different geometries show similar trends.

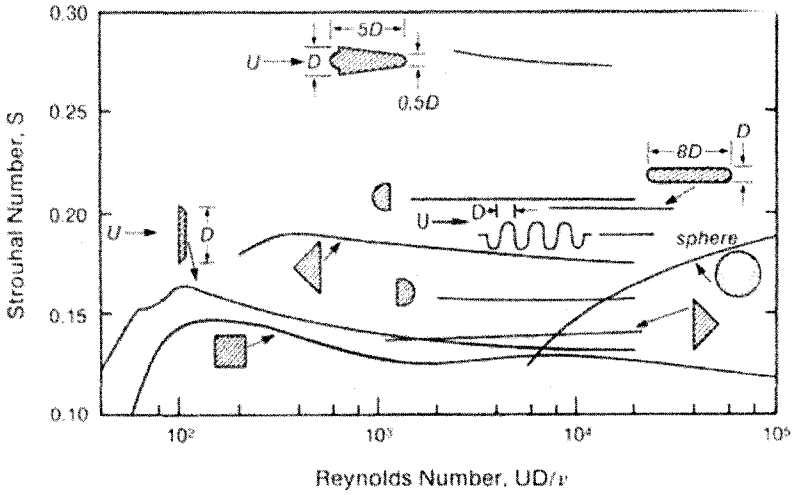

Figure 1.9 Strouhal numbers for noncircular sections and some three-dimensional bodies[9]

A vortex street wake is formed by the interaction of two free shear layers trailing behind a body. Researchers have suggested defining a "universal" Strouhal number for any bluff section based on the separation distance between shear layers. Defining D in Strouhal number formula as the width of the separation points gives a Strouhal number of 0.2 for a wide range of Reynolds numbers regardless of the section geometry. This property of vortex shedding makes it possible to use the vortex shedding frequency as the design basis for fluid flow meters[16].

$$St = \frac{f_s D}{U}$$

Another important point about the vortex shedding process is that in high Reynolds number flows vortex shedding from a stationary cylinder wanders over a narrow band of frequencies with a range of amplitudes and is not constant along the span[17].

Forces generated by the vortex shedding

Alternating vortex shedding causes oscillations in lift and drag forces. The oscillations in lift force for a cylinder occur at the vortex shedding frequency, while they occur at twice the vortex shedding frequency for drag force (Figure 1.10).

Force coefficients can be defined as follows:

$$C_x = \frac{D(t)}{\frac{1}{2}\rho U^2 d}$$

$$C_y = \frac{L(t)}{\frac{1}{2}\rho U^2 d}$$

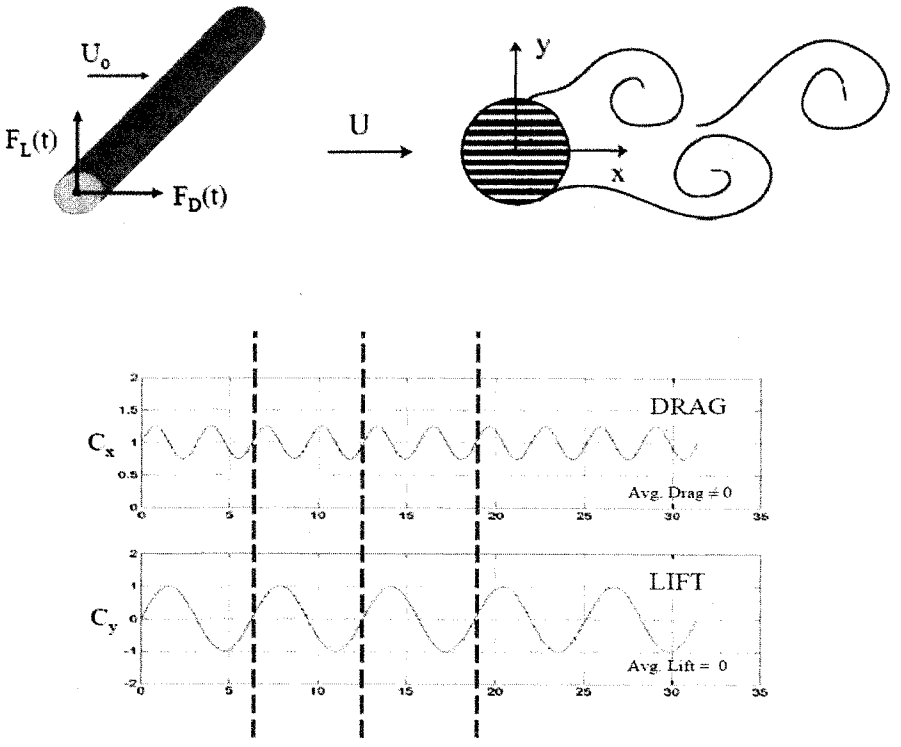

Figure 1.10 Lift and drag forces generated on a cylinder[18]

If the frequency of the shedding is close to a structural frequency, resonance can occur, usually with unpleasant results. As an example, oscillating forces caused the Tacoma Narrows Bridge to collapse in 1940.

1.3.3 Flow Over Three-dimensional Bodies

Flows around three-dimensional bodies still cannot be explained easily due to complexity of the flow configurations and the numerous influencing parameters. Thus, load predictions on three-dimensional bodies are often made based on experimental studies of common shapes.

Bluff body wakes are complex since they involve the interactions of three shear layers: boundary layers, a separating free shear layer, and a wake at the same time[19]. The nominally 2-D vortex shedding process has been described in many review papers in the past decade. However, very little attention has been given to 3-D vortex shedding phenomena. Despite having extensive new results available there are no review papers known to this author addressing this aspect in great detail.

Three-dimensional conditions are present, due to the shape of the considered bodies (extrinsic), to the possible non-uniformity of the incoming freestream (intrinsic), or to the occurrence of both these conditions[4]. The mean and time-varying forces are fundamentally dependent on the behavior of the vorticity introduced in the wake as happens in the two-dimensional case. Current studies of 3-D phenomena show that long-standing controversies assumed to have two-dimensional origins were indeed related to 3-D phenomena[4].

In general, an isolated, low-aspect-ratio three-dimensional body of revolution has lower aerodynamic loads than those on a two-dimensional body of analogous cross-section (Figure 1.11)[20]. This can be explained by the disturbance caused by a three-dimensional body being lower due to the possibility of flow in an additional direction; however, the characteristics of the forces mainly depend on the modifications of the flow structures and of the vorticity field in the separated wake.

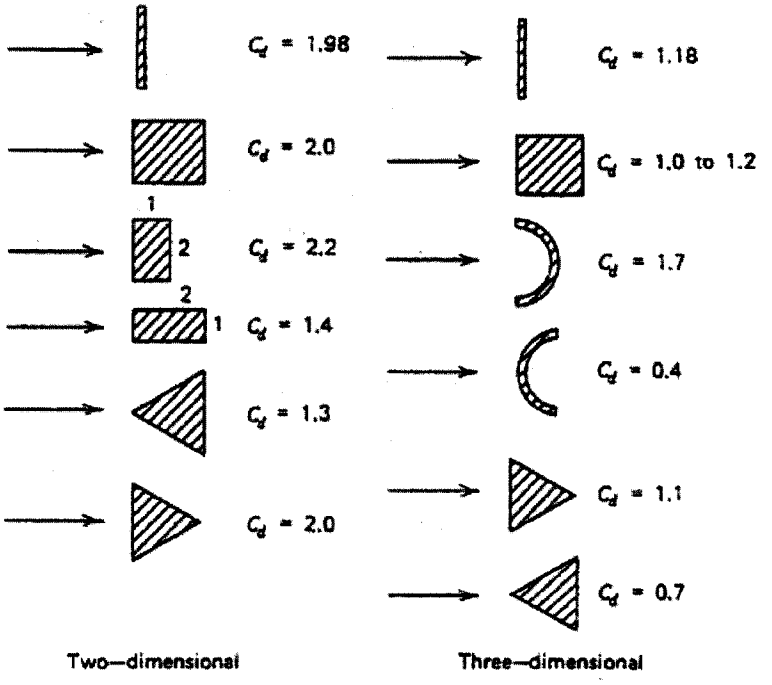

Figure 1.11 Drag coefficients of two-dimensional and three-dimensional bodies[20]

Considering the finite-length cylinder in Figure 1.12, one can see that the low pressure existing in the wake region causes a flow around the free-ends of the body. This incoming flow penetrates inside the wake, widens it, and displaces the rolling up of the vortices detaching from the sides. As a result, unlike the two-dimensional case, widening of the wake and the consequent reduction of the vortex shedding frequency occur.

Increase of the base pressure due to the flow entering the wake, a lower value of the perturbation energy induced by the lower-intensity shed vortices and drag reduction are observed.

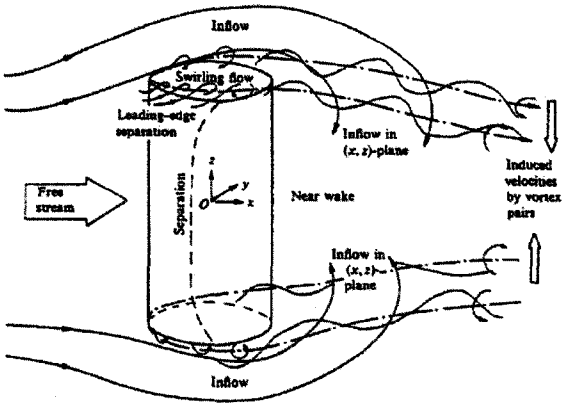

Figure 1.12 Flow around a finite length cylinder[20]

Williamson[19] categorized vortex patterns into three groups, namely "Laminar Shedding Regime", "Transition Regime", and "Higher Reynolds Regime". However rather than attempting to describe the vortex dynamics in both unseparated and separated wakes for different types of 3-D and nominally 2-D body shapes, he presented an overview on circular cylinder wakes over a wide range of Reynolds numbers due to its engineering significance and simplicity for both experimental and computational studies.

Many experiments have been carried out for the bluff body wake, including measuring Strouhal numbers, coefficients of lift and drag, base pressure, separation points, surface shear stress, wake velocity measurements such as mean and fluctuation velocity profiles and Reynolds stresses, and estimates of the length and width of the "vortex formation" region. Particularly important are the plots of the Strouhal number St or base pressure

coefficient Cp_b (used as base suction coefficient ($-Cp_b$), rather than the base pressure itself) as a function of the Reynolds number. In contrast to some of the other parameters of the flow, the base pressure responds sensitively to the changes in flow instabilities and phenomena throughout the Reynolds number range (Figure 1.13).

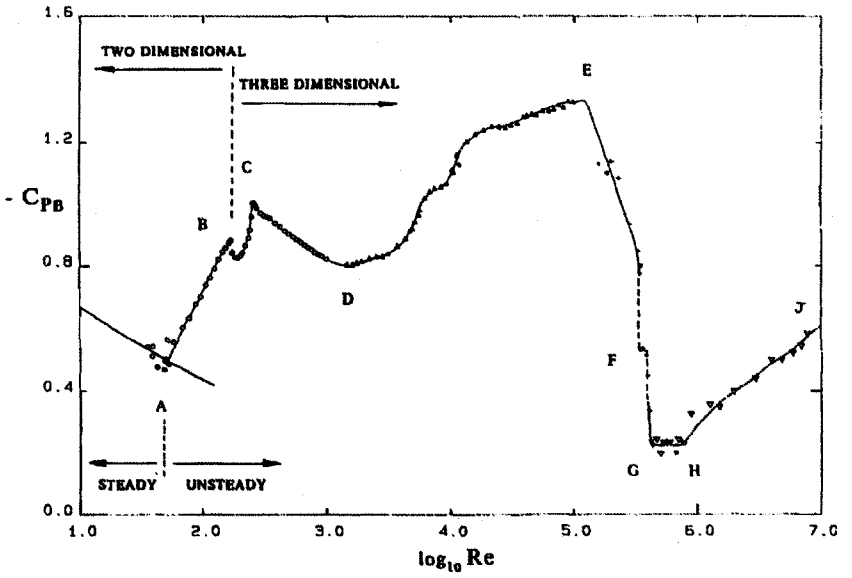

Figure 1.13 Base suction coefficient – Reynolds Number for a circular cylinder[19]

Figure 1.14 shows the instabilities involved in the development of turbulence in the wake. As the Reynolds number increased (down the page) wake turbulence experiences the following major instabilities:

The formation of primary Karman vortices

The inception of small-scale streamwise vortex structures

The formation of very large-scale 3-D structures (vortex dislocations)

The development of shear-layer instability vortices, which are themselves prone to 3-D instability of small scale.

Williamson also explained several 3-D vortex dynamics phenomena such as cellular shedding, vortex dislocations, oblique shedding, phase shocks and expansions, and vortex loops in his extensive review. Studies of flow around a bluff body with streamlined forebody and blunt base showed that vortex shedding in a shear flow occurs with spanwise cells, with a constant frequency in each cell. It was shown that vortices can shed at some oblique angles (typically 15-20°) to the axis of the cylinder what is known as oblique shedding. This shedding can occur with different patterns according to the end conditions. By manipulating end conditions at low Reynolds numbers both parallel and oblique shedding can be induced. Parallel or oblique shedding has a close relationship with the oscillating fluid forces acting on the body. When oblique shedding occurs, these forces are not in phase along the span, so their instantaneous spanwise-integrated value is lower. It was also shown that oblique shedding could occur from a ring in the form of helical vortices. This suggests that this phenomenon is intrinsic to the flow, even if it can be controlled by end conditions. Another important three-dimensional feature is the possible coexistence, along the span, of cells with shedding at different frequencies. Furthermore, in the regions at the boundary between these cells, large-scale three-dimensional structures are found, known as vortex dislocations or vortex splitting where vortices adapt their frequency to that of the neighboring ones.

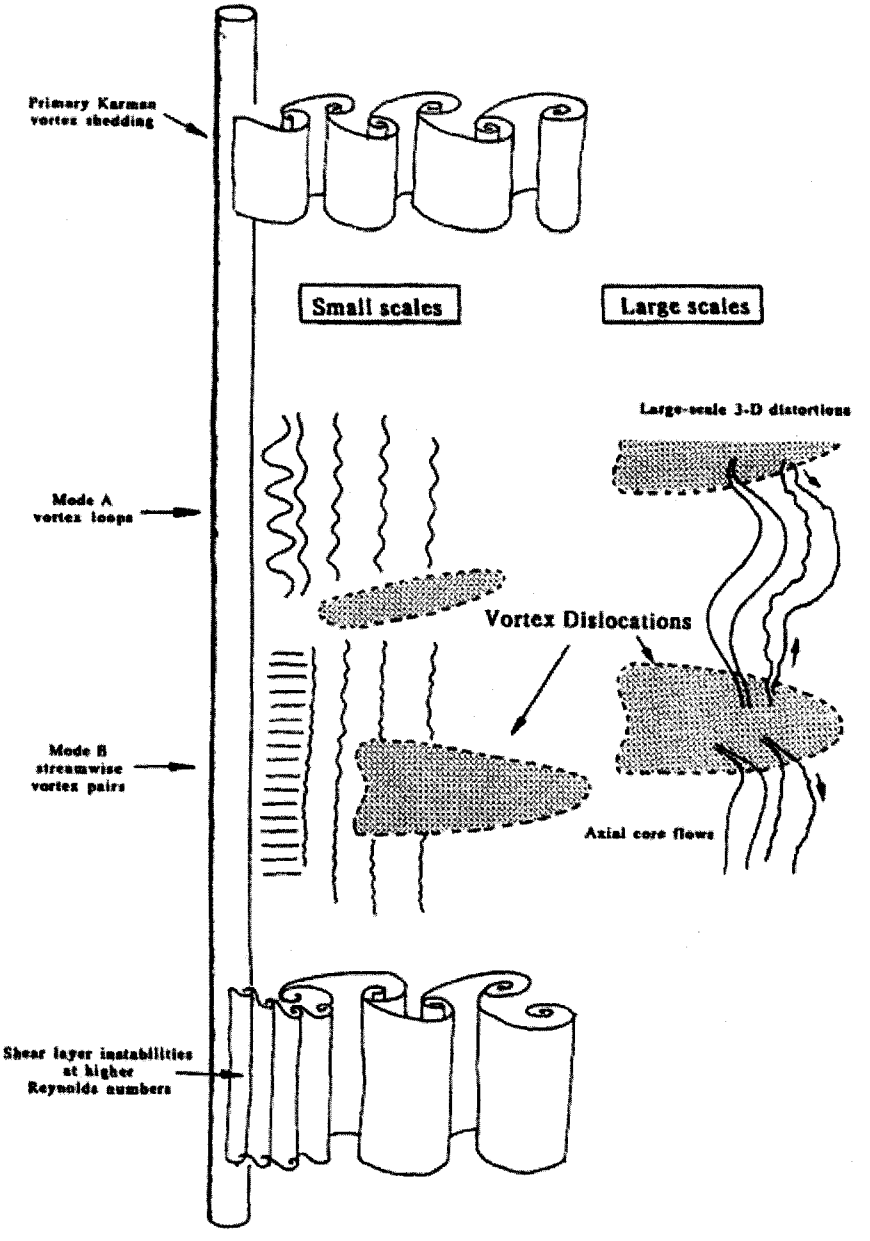

Figure 1.14 Instabilities involved in the development of turbulence in the wake[19]

1.3.3.1 Analytical and Experimental Description of Three-Dimensional Separation

The description and the physical understanding of three-dimensional separated flows are difficult primarily because of the improper use of terms linked to two-dimensional flows. Transformation from known two-dimensional structures to the more mysterious three dimensional flows requires a substantial reconsideration of concepts, such as separation and reattachment points, separated bubble, recirculation zone, and limiting streamlines, which are inappropriate for use in three-dimensional flows. Introduction of notions such as skin friction lines, critical points, separation (or attachment) lines, separation (or attachment) surfaces, and topological rules are needed to describe 3-D flow fields[21].

Since separation is linked to the existence of viscosity, whose effects are reflected in boundary layers, the surface of a body should be investigated to explain separation. More precisely the shear stress at the wall, which is a vector field in three-dimensional flows, should be monitored. The trajectories of this field are the skin friction lines, sometimes called limiting streamlines since they are the limit of a streamline when the distance to the wall becomes zero. Skin friction lines covering a body which forms a skin friction line pattern are helpful but not sufficient in defining separation. Therefore the outer field flow structure needs to be examined as well.

Considering a two-dimensional space, where the components of the skin friction vector τ_w are denoted by $\tau_x(x, z)$ and $\tau_z(x, z)$ along x- and z-axis, respectively; skin friction lines can be defined by the following time independent equation for a steady flow:

$$\frac{dx}{\tau_x(x,z)} = \frac{dz}{\tau_z(x,z)}$$

These equations define an infinite number of solution curves called characteristic lines or trajectories that are associated with the skin friction lines introduced above. In general, only one trajectory passes through a point on the surface. The only points that do not satisfy this rule are the singular points of the system where the skin friction vanishes and the equation reduces to:

$$\tau_x(x, z) = \tau_z(x, z) = 0$$

Trajectories in the vicinity of a singular point $P_0(x, z)$ can be found by solving a first order Taylor series expansion. The conditions for a nontrivial solution lead to an eigenvalue problem introducing the Jacobian matrix below,

$$F = \begin{vmatrix} \frac{\partial \tau_x}{\partial x} & \frac{\partial \tau_z}{\partial x} \\ \frac{\partial \tau_x}{\partial z} & \frac{\partial \tau_z}{\partial z} \end{vmatrix}$$

Where p = -(trace of F) and q= (determinant of F), then the eigenvalues are:

$$S_{1,2} = \frac{-p \pm \sqrt{p^2 - 4q}}{2}$$

The real or imaginary character as well as the sign of the eigenvalues S_1 and S_2 determines the behavior of the skin friction lines around the singular point (or critical point P_0). Figure 1.15 shows the possible different behaviors experienced according to the

eigenvalues on [p, q] plane and Figure 1.16 presents the skin friction lines in the vicinity of the critical point.

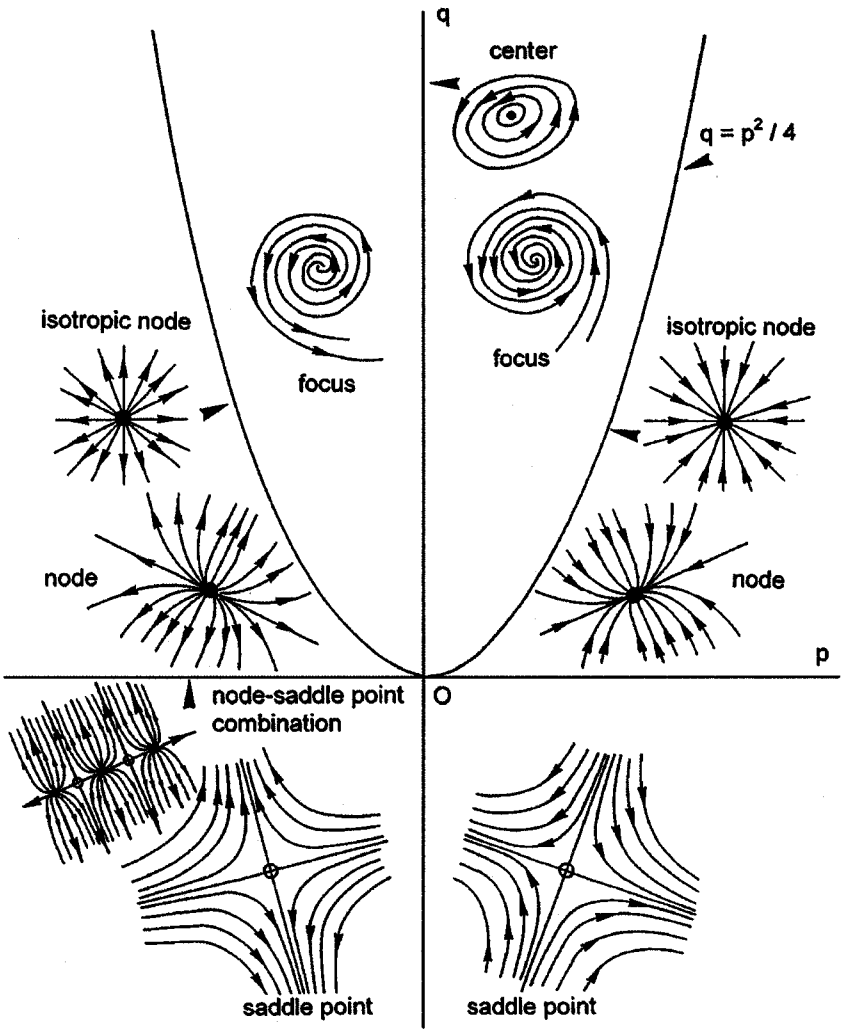

Figure 1.15 Classification of the critical points in the [p, q] plane[21]

If the two eigenvalues S_1 and S_2 are real and have the same sign, the singular point is called a node. If they are not equal, all the trajectories except one have a common tangent at P_0 (Figure 1.16a). If the two eigenvalues are equal (points located on the parabola of

equation q=p2/4), all the trajectories have different slopes at P_0, and the node is called an isotropic node (Figure 1.16b). If both eigenvalues are real but have opposite signs, the singular point is a saddle point. For this case only two trajectories go through the singular point P_0, where the other trajectories form hyperbolic shape, as shown in Figure 1.16c. If the eigenvalues are complex conjugates, all of the trajectories end in the singular point and spiral around it to form a focus (Figure 1.16d). If p is zero and q is positive, no line passes through the singular point and the trajectories are closed curves in the form of an ellipse (Figure 1.16e). This singular point is called a center. For two-dimensional separation cases the critical point becomes an infinite set of node-saddle point combinations distributed along a common line (Figure 1.16f).

The following general characterization of separation in three-dimensional flow can now be made: A flow past a body is separated if the skin friction line pattern contains at least one saddle point[21]. For a three-dimensional velocity field the following two singularities are considered:

1. Three-dimensional saddle point, which is associated with a two-dimensional node on the body surface and two-dimensional saddle points in the outer field.

2. Three-dimensional focus associated with a two-dimensional focus on the obstacle and an isolated line passing through the center of the focus (Figure 1.17a). The other streamlines spiral around this line forming a helical shape which corresponds to a tornado-like vortex.

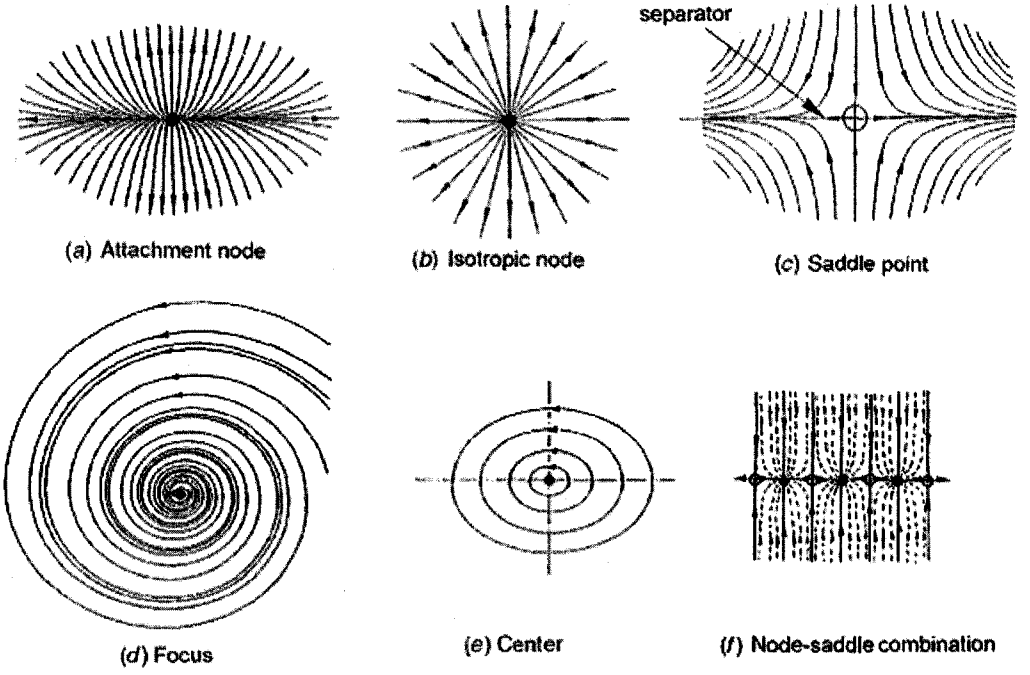

Figure 5 The different critical points.

Figure 1.16 Different critical points[21]

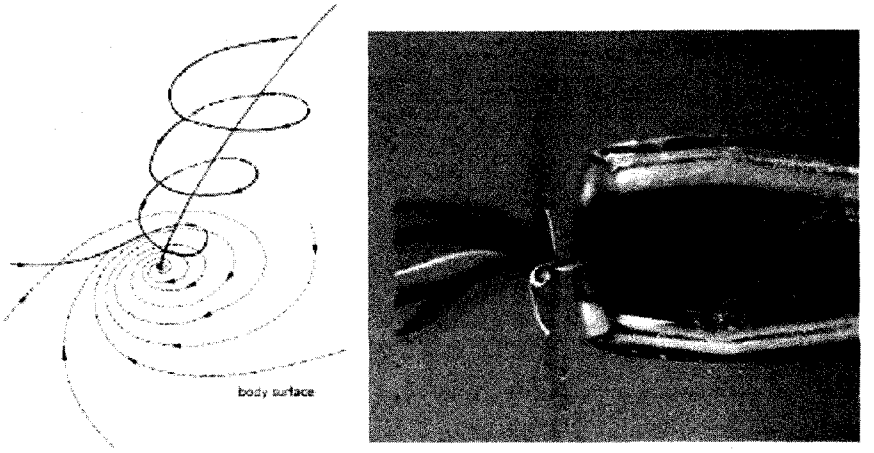

Figure 1.17 Three-dimensional focus[21]

Using the information provided so far some practical flows will be investigated in the following section[21].

Flow over Cylindrical Obstacles

A separated region exists behind a cylinder with separation surfaces starting from each side of the cylinder. Figure 1.18 shows the topology of the skin friction pattern behind a cylinder. To obtain the presented topology, two foci F_1 and F_2 must be introduced behind the cylinder, and at least three saddle points, S_3, S_4, and S_5, must exist along with the separation lines (S_5), (S_6), and (S_7). Two other separation lines (S_3) and (S_4) start from two sides and rolls over downstream of the cylinder generating two vortices.

In Figure 1.19 two tornado-like vortices are shown behind an obstacle (cylinder on flat plate), in addition to the horseshoe vortices forming ahead of the obstacle. They result from the rolling up of the separation surfaces emanating from the separation lines located on the obstacle. Their trace on the plate is presented by the foci F_1 and F_2. If the obstacle has a finite height, the two vortices are deflected by the general stream and entrained downstream.

Base Flows

Base flows have always attracted much attention since they can be related to the global performance of a vehicle (drag, stability). However, even for axisymmetric afterbodies, turbulent base flow prediction remains a challenging problem and no completely satisfactory result is yet provided by the existing turbulence models. For base flows the simplest case is the axisymmetric afterbody (circular cross section) without a jet. For this case, as

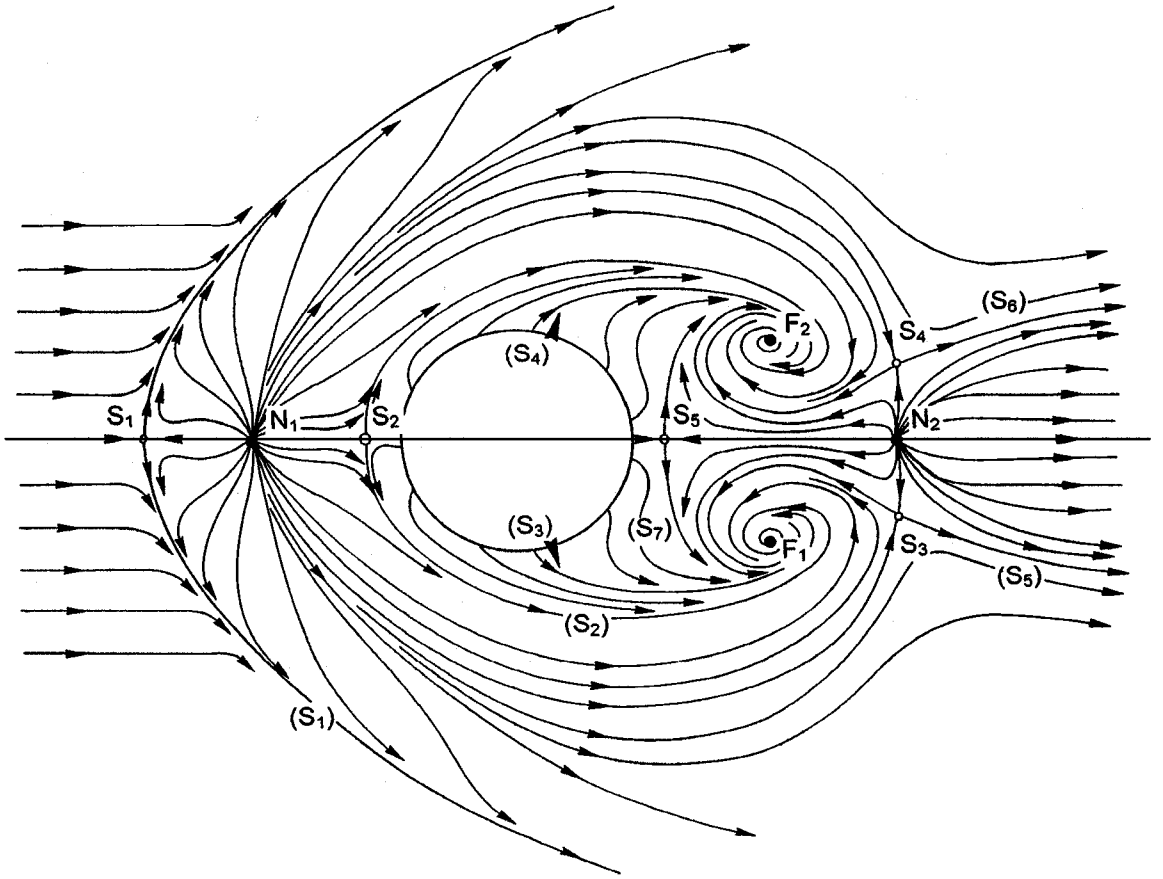

Figure 1.18 Separation behind a cylindrical obstacle[21]

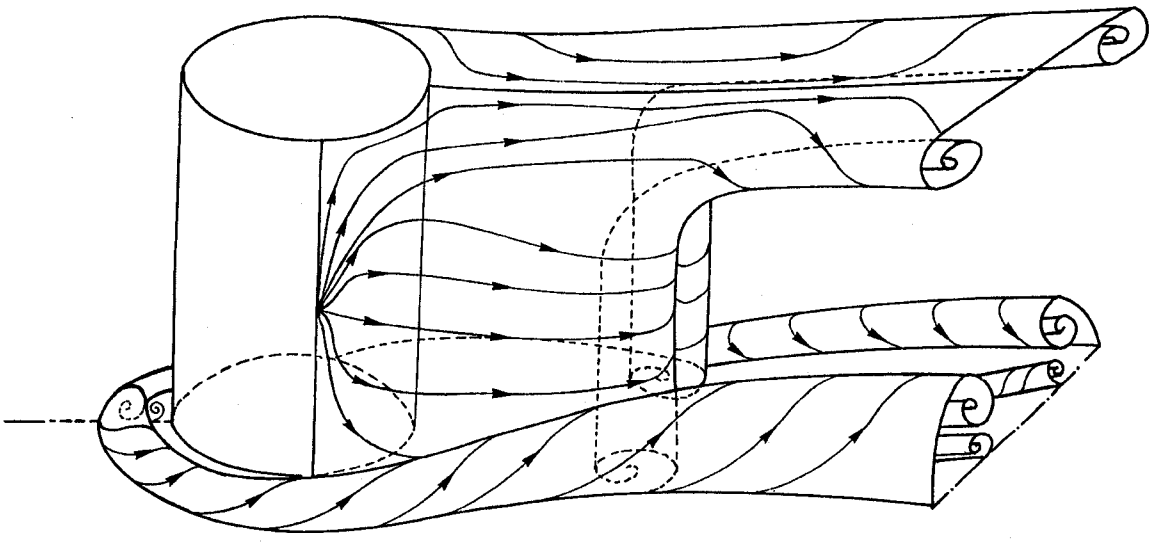

Figure 1.19 Vortex system induced by an obstacle[21]

shown in Figure 1.20a, two large recirculation bubbles, which are the trace in the visualization plane of a toroidal vortex, exist. If the flow is perfectly axisymmetric, the traces of this vortex form two centers that are special foci as seen in the topological interpretation of Figure 1.20b. In this case, the streamlines are closed curves rotating around C_1 and C_2; the recirculating flow is separated from the outer stream by the separators (S_1) and (S_2) that pass through the saddle point S_4. Since it is hard to realize a perfectly axisymmetric structure in real life, more realistic flow topology can be seen in Figure 1.20c, where the centers C_1 and C_2 are replaced by two foci F_1 and F_2. The presence of a central jet changes the flow organization as shown by the photograph in Figure 1.21a and the sketch in Figure 1.21b. In this case, the toroidal vortex is bounded by a separator (S_1) ending on the base at the half saddle point S_2 (and the symmetric point). The outer flow streamlines first flow around the bubble, then bend rapidly in the downstream direction due to the entrainment effect of the jet.

Due to the complexity and great variety of the possible three dimensional flow configurations, and the high number of influencing parameters, the present level of knowledge does not allow reliable predictions to be made for general cases. Therefore, it is necessary to rely upon experimental data bases. Careful experiments have shown the presence and importance of three-dimensional features in nominally two-dimensional configurations. It is essential to understand how these features influence the different facets of the problem, like the amount of vorticity being shed from the separation points, its spatial concentration, the vortex formation position, the shedding frequency, etc. Today, although our knowledge of three-dimensional flows is extensive, there are many

questions remain to be understood. However, with the increasing power of computers and the developing experimental techniques the body of knowledge expands rapidly.

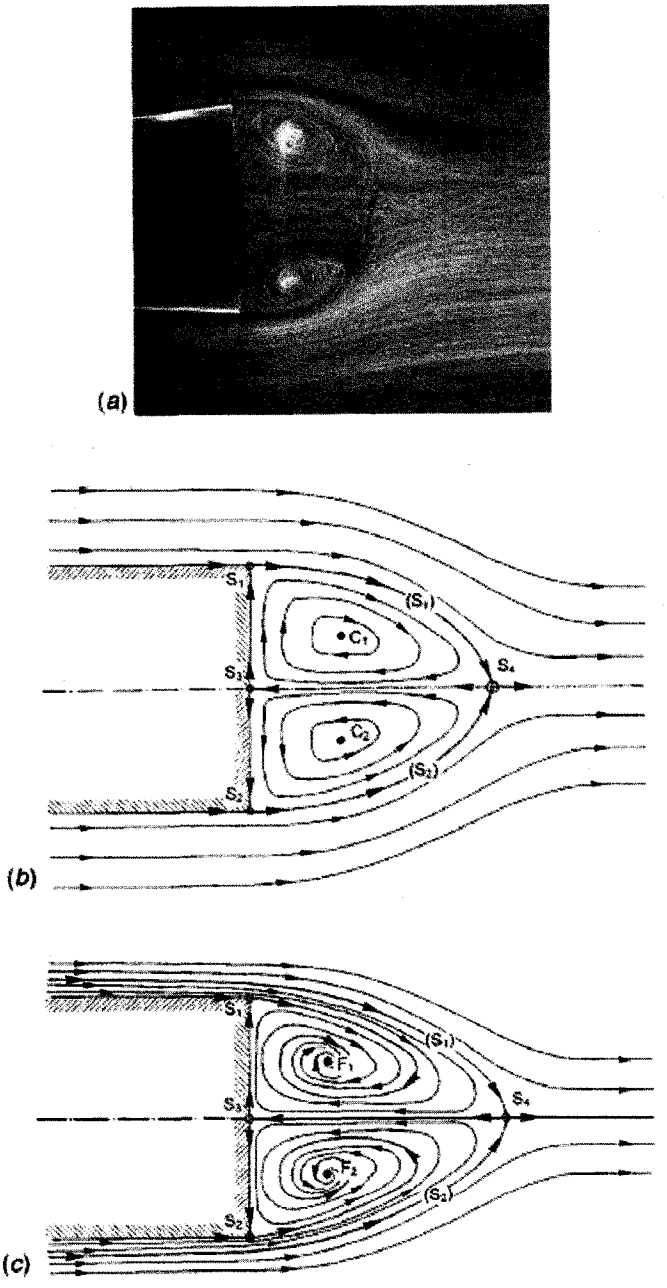

Figure 1.20 Flow behind an axisymmetric body: a) air-bubble visualization, b) topological sketch of an axisymmetric body, c) topological sketch of a body with slight axisymmetric defect[21]

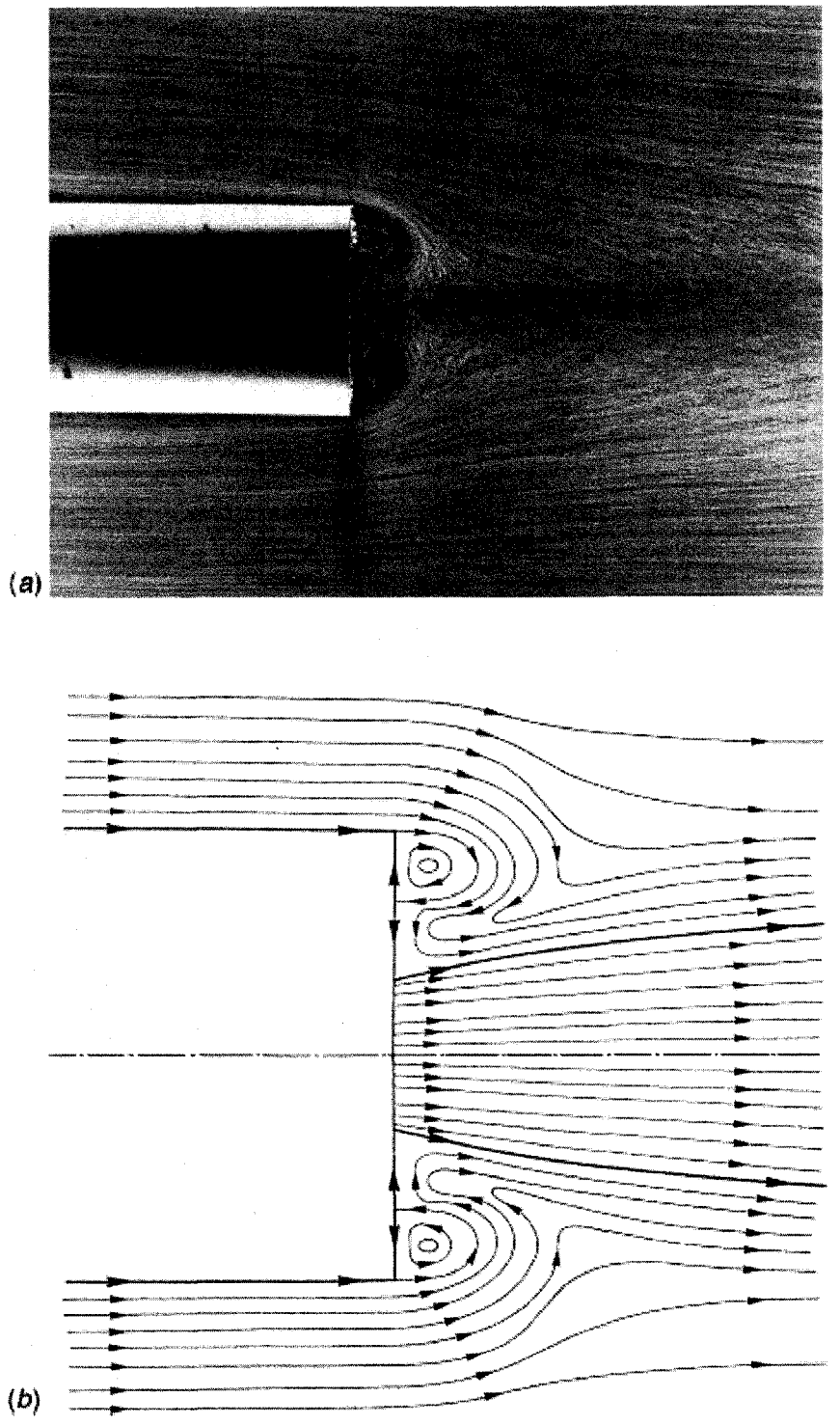

Figure 1.21 Flow behind an axisymmetric body with central jet[21]

1.4 Flow Control

From the above discussions of flow over bluff bodies, the relationship between increasing drag and increasing width of their wakes (due to the larger distance between oppositely-signed vorticity) and the connection with the presence of regularly-shed concentrated vortices can be observed. It can also be concluded that the perturbation energy (and thus the drag) of a bluff body can be reduced (without significantly changing the width of its wake) by preventing the vorticity from concentrating in restricted cores. This may be achieved by interfering with the vortex-shedding process. Avoiding the occurrence of the separation of the boundary layer along a straight line can be an example of modifying the vortex shedding (which may be seen to be a necessary condition for regular vortex shedding to take place). For this purpose various types of protuberances may be placed along the span of the body (Figure 1.24). More drastic variations of the body contour may be used if possible (Figure 1.25). Using these methods drag reductions as high as 50% may be obtained[22]. Restraining vortex shedding is also effective in avoiding the fluctuating cross-flow forces and the related oscillatory phenomena.

By modifying the structure or the flow, the vortex-induced vibration and the related increase of mean drag can be significantly reduced[9].

Streamlining cross section: Minimizing separation will minimize vortex shedding and this will reduce the drag.

Adding a vortex suppression device: Using the add-on devices in Figure 1.26 for suppression of vortex-induced vibration of cylindrical structures in wind and marine applications is found to be effective.

The topic of flow control will be discussed in more detail and from an aerodynamics perspective in chapter 4.

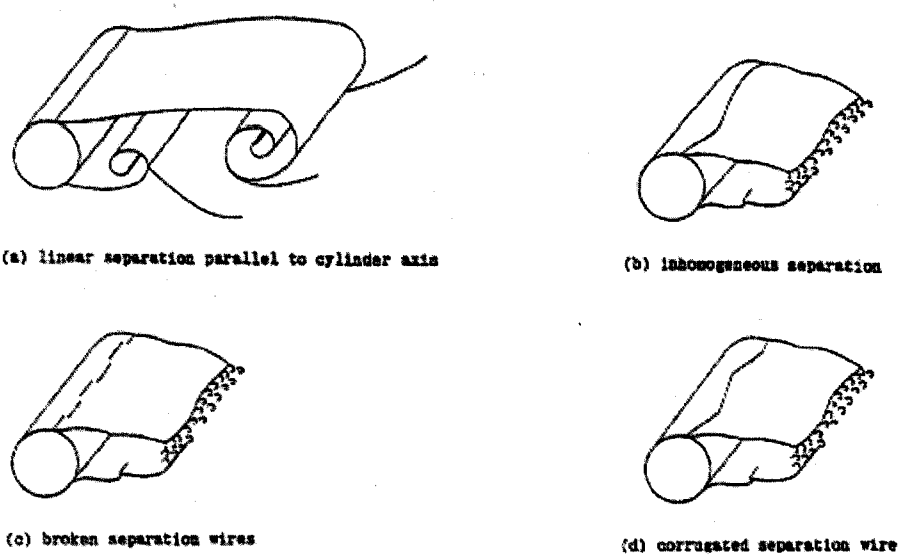

Figure 1.24 Influence of separation line on wake structure for a circular cylinder[22]

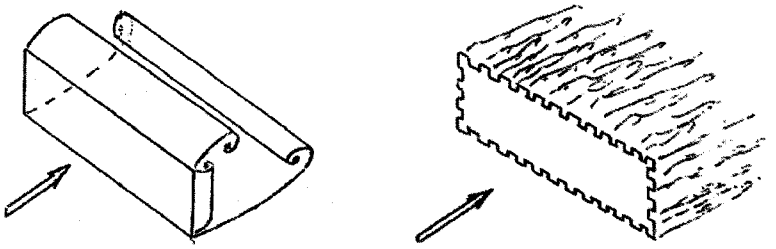

Figure 1.25 Effect of serrated contour on wake[22]

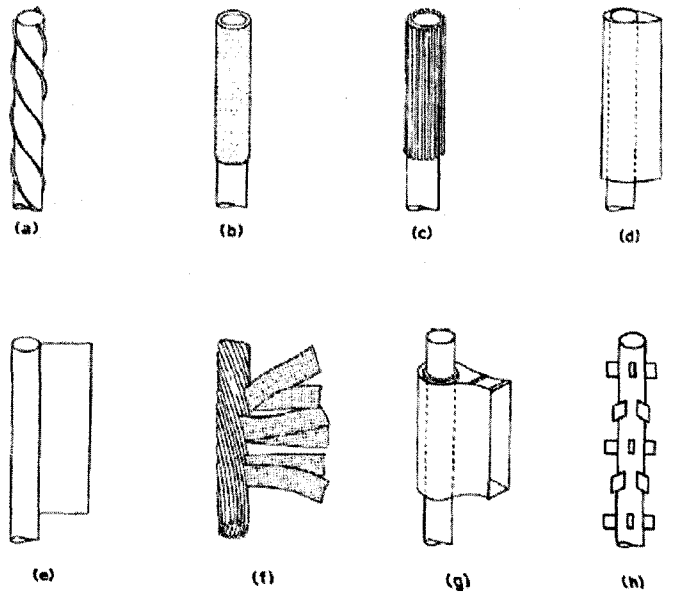

Figure 1.26: Add-on devices for suppression of vortex induced vibrations of cylinders a) helical strake, b) shroud, c) axial slats, d) streamlined fairing, e) splitter, f) ribboned cable, g) pivoted guiding vane, h) spoiler plates[9]

1.5 Statement of the Problem and Motivation

Mean and fluctuating forces acting on a body are strongly related to vortex shedding and the unsteady wake generated behind it. Therefore it is possible to obtain significant force reductions if vortex shedding is controlled or its regularity is reduced.

For this reason, to modify the wake of a bluff body in a favorable way, the following objectives are established for this research:

Investigate the wake behind a circular cylinder in crossflow and an axisymmetric base (ogive cylinder). The latter has seen less attention relative to the research on 2D vortex shedding behind cylinders.

Quantitatively document the unsteady velocity field behind the circular cylinder and the ogive cylinder in the light of previous research.

Design an actuator that can influence the wake structure and if possible, help reduce drag.

Investigate the effect of flow excitation by the actuators on the wake structure from the body.

Aerodynamic flow control intends to delay or suppress boundary layer separation by techniques such as creation of a boundary layer downstream from the control input that is able to withstand adverse pressure gradients imposed by the outer (global) flow. Numerous passive and active flow control techniques have been developed to suppress or reduce boundary layer separation causing a substantial increase in performance of practical flows such as airfoils, turbines, compressors, and diffusers, etc.

Vortex generators, control discs, splitter plates, and creating geometrical modifications to generate 3-dimensionalities are used as passive control techniques; while base bleeding, acoustic forcing, micro-electromechanical-systems (MEMS), oscillating wires, oscillation of the models (usually cylinders), electro magnetic fields, ionic wind and synthetic jets, and electrohydrodynamic fields are used as active flow control methods.

Lately extensive research have been carried out on electrohydrodynamic forces and it has been found that surface direct-current (DC) corona and alternating (AC) dielectric-barrier discharges (DBDs) also seem to stabilize boundary layers where separation may otherwise occur. In either of the DC or AC discharge configurations, the discharge generates a plasma in the immediate vicinity of the surface. Electrodes (which are often simply metallic strips between a dielectric sheet) can be configured such that the net force due to the ion drift is along the streamwise direction to suppress the flow separation.

However plasma actuators are also used to influence the flowfield by changing gas properties near the surface by local heating in the discharge region.

Plasma actuators possess advantages when compared to other flow control devices in several ways such as:

Electronic Structure: Completely electronic, with no need for mechanical parts, thus they can withstand high forces.

Size: These actuators are scalable in size and electrodes can be constructed as small as 0.5 mm and as large as 20 cm. They also have a low-profile and can be laminated onto surfaces without requiring slots or cavities.

Mass: They are light-weight.

High bandwidth: High bandwidth enables fast response for feedback control.

High energy density: Phased plasma actuators are capable of producing significant effects with a minimum power input.

2. LITERATURE SURVEY

2.1 Background

Vortex shedding behind bluff bodies has been an area of interest to researchers for decades. A vast amount of literature is available since the early 1900's[4]. Besides these scientific materials, flow visualization drawings by painters like Leonardo da Vinci are also available (Figure 2.1).

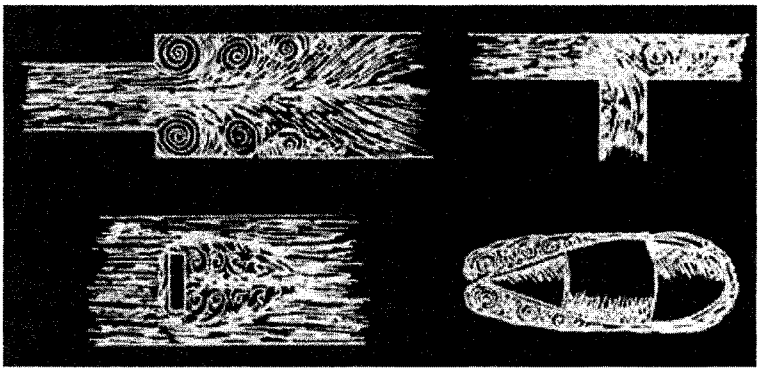

Figure 2.1 Vortex shedding visualizations by Leonardo da Vinci (1452-1519)

Theodore Von Karman was the first researcher who explained the area extensively. He published his findings in 1911[23] and 1912[24] and therefore the double row of vortices of opposite sign shed from a cylinder became known as a Karman Vortex Street in his honor.

2.2 Control of Vortex Shedding

There has long been interest by researchers in controlling bluff body wakes. Most efforts have been concentrated on reducing drag and improving lift properties. Many scientists have studied controlling or suppressing vortex shedding from bluff bodies in order to

reduce drag, vibrations, and noise[25, 26]. Meanwhile, increasing vortex shedding, which might help processes like mixing of two fluids, has not been studied as extensively[26]. Several reviews of vortex shedding are available, mostly dealing with vortex shedding from a circular cylinder due to its practical importance and experimental simplicity.

Axisymmetric wakes have been studied for different bodies like spheres[27], discs, circular cylinders[28], and more general bodies of revolution. In these studies existence of a single vortex spiral or a pair of counter-rotating spirals is sometimes observed in the wake, corresponding to a flapping of the wake in a quasi-fixed plane[26].

Ogive cylinders have been of special interest to scientists due to their geometric simplicity and application to projectiles. Alcorn and Britcher previously conducted several experiments on an ogive geometry focusing on the wake structure and behavior[29]. They made tests to investigate base pressures, wake stagnation point location, effect of incoming boundary layer velocity profile and wake periodicity (predominant frequency and coherence measurements). They found out that despite large variations in base pressure coefficient with varying Reynolds number or boundary layer trip location, all base pressure measurements collapse onto single curves when plotted against incoming boundary layer momentum thickness. They also examined the wake structure and the drag coefficient with varying base slant angle. They noticed the large changes in drag coefficient occurring for small changes of base slant angle around 45 degrees. The two wake types investigated were quasi-symmetric turbulent closure (low slant angles) and longitudinal vortex flow (high slant angles).

Fuchs, Merker, and Michel[30, 31] performed cross-spectral measurements in the axisymmetric wake of a disk. The symmetry imposed by the disk allowed for an illustrative description of the large-scale wake structures by examining elementary modes of instability or azimuthal constituents. They showed that only a small number of modes were necessary to describe the unsteady behavior of an axisymmetric bluff body wake or jet. Based on their work Alcorn and Britcher also defined three modes of vortex flow as follows. The mode m=0 can be called axisymmetric since its magnitude and phase are independent of $\Delta\beta$ (azimuthal angle). This mode is similar to vortex rings found in a laminar shear layer shed from a circular jet[29]. The m=1 mode changes sign of velocity perturbation twice from $0°<\Delta\beta<360°$. It may be positive on one half of the circle and negative on the other half. Therefore m=1 is a helical structure characteristic of vortex shedding. The m=2 mode change sign four times from $0°<\Delta\beta<360°$ and is known as the quadrupole structure. These organized structures in the wake of a cylinder aligned with the flow can be seen in Figure 2.2. In their cross spectral analysis Alcorn and Britcher also demonstrated existence of helical disturbances that have no preferred orientation using the respective power spectra of two spatially separated points. Monkewitz et al. also confirmed the spiral nature of the large-scale vortex structure in the wake by phased-locked measurements of the instantaneous streamwise velocity field $\langle V_x \rangle(x,r)$ (Figure 2.3).

2.3 Numerical Work on Vortex Shedding

Numerical solutions of vortex flows behind bluff bodies, including force calculations, have not been easy for researchers due to insufficient computational power for high

Reynolds number flows, which is the case for most of the applications of interest. This has directed scientists to use simpler models that describe the flow physics. Viscous effects can be neglected for sufficiently high Reynolds numbers and potential-flow methods used when the correct amount of vorticity is generated and its dynamics are reproduced with enough accuracy[4].

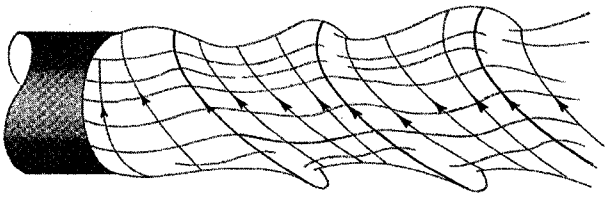

Figure 2.2 Wake of a cylinder aligned with the flow[29]

Neglecting viscosity, researchers developed discrete vortex methods in 1970s where ideal point vortices are used to simulate the vortex shedding in certain time intervals. These methods are briefly reviewed by Sarpkaya[32]. An attempt to improve these models is made by Chorin to take viscosity into account[33]. However his considerable efforts did not show any substantial superiority to the previous simpler models. Kamemoto and Ojima solved the same ogive cylinder used in experimental cases numerically (private communication). In their vortex blob method they used N=2400 points, for a Reynolds number of $Re=1.7x10^5$ and for a time interval of $\Delta t=1x10^{-4}$ and attack angles of $\theta= 0,20°$ (Figure 2.4).

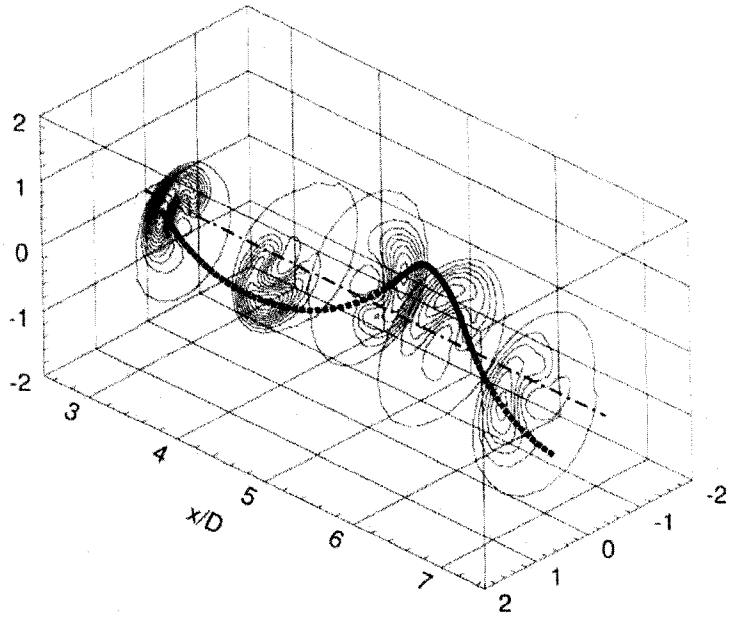

Figure 2.3 Helical vortex shedding[34]

It is noted by Buresti that accurately predicting vortex shedding using potential-flow models is not easy. Besides the need to use several adjustable parameters restricts models to be used only for certain flow conditions. Thus developers should clearly note the physical aspects that cannot be predicted by their models.

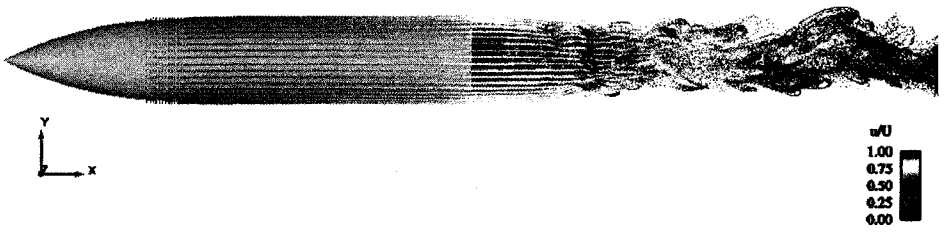

Figure 2.4 Instantaneous Velocity Vectors with Vortex Elements

On the other hand, Direct Numerical Simulation (DNS) of complete Navier-Stokes equations might allow better understanding of the physics of the vortex shedding.

Although DNS has been restricted to low Reynolds numbers ($Re<10^4$) information that cannot be obtained by experimental work such as evolution of the complete vorticity field can be derived. To overcome the Reynolds number restriction, methods like Reynolds Averaged Navier Stokes equations (RANS) and Large Eddy Simulation (LES) are used. It was noted by Buresti and Fureby that encouraging results were obtained by using three-dimensional LES, while RANS and two-dimensional LES applications were not satisfactory.

2.4 Inhibition of Vortex Shedding

Mean and fluctuating forces acting on a body are strongly related to vortex shedding generated behind it. Therefore, it is possible to obtain substantial reductions of at least the unsteady forces if vortex shedding is controlled or its regularity is reduced[4]. Selection of the flow control method to use can be made according to whether the goal is to alter the instantaneous mean velocity distribution or to alter the flow instabilities thereby changing the flow structure. While conventional active flow control methods are mainly concerned with direct interaction with, and alteration of, the mean flow about a body modern techniques involve altering existing flow instabilities using relatively small inputs to obtain large-scale changes of mean flows. Aerodynamic flow control may be intended to delay or suppress boundary layer separation through creation of a boundary layer downstream from the control input that is able to withstand adverse pressure gradients imposed by the outer (global) flow. Numerous passive and active flow control techniques have been developed to suppress or reduce the boundary layer separation which

otherwise causes a substantial loss of performance in practical flows such as airfoils, turbines, compressors, diffusers etc[35].

2.4.1 Passive Flow Control

A common passive flow control device is a vortex generator[36] which is used on the wings of commercial aircraft. Vortex generators produce streamwise vorticity and provide a mechanism for the transfer of momentum from the outer flow into the boundary layer.

Strykowski and Sreenivasan[37] placed a second cylinder of about 1/8 - 1/20 of the main cylinder diameter in the wake of the main cylinder. They suppressed the shedding for a limited Reynolds number range of 40-100 by placing the cylinder in an appropriate location.

Weickgenannt and Monkewitz analyzed the effect of a control disc mounted on an axisymmetric body with blunt based body of revolution in more detail, a configuration first studied by Mair[38]. They defined four vortex shedding regimes by increasing the control disc distance from the base, namely no effect, a sharp increase of vortex shedding activity and total drag, reduced activity, and an independent activity region where the flow around the main body and the disc become independent and drag forces for these two are additive. Hot-wire and LDA measurements were made to understand the instability mechanism leading to high vortex shedding activity.

Among other methods, one of the most effective passive control methods is the use of splitter plates, which was first introduced by Roshko[10, 39]. A splitter plate is a plate positioned downstream of the body aligned parallel to the free stream direction (Figure 2.5). This plate avoids or delays the interaction of the shear layers separating from two

sides of the body. If the plate is long enough, separated shear layers attach on the plate with two almost steady recirculation regions. The shear layers join again downstream of the plate forming a low-momentum wake, which experiences instabilities. This new wake oscillates with different degrees of amplitude and regularity and thus fluctuating forces are reduced significantly. For example, there may be reductions in drag as much as 50%. Roshko found out that the existence of the plate caused vortex formation to occur downstream of the plate. He also investigated the effect of the distance between the plate and the body. He observed that further downstream movement of the plate results in the original flow configuration with the original vortex shedding.

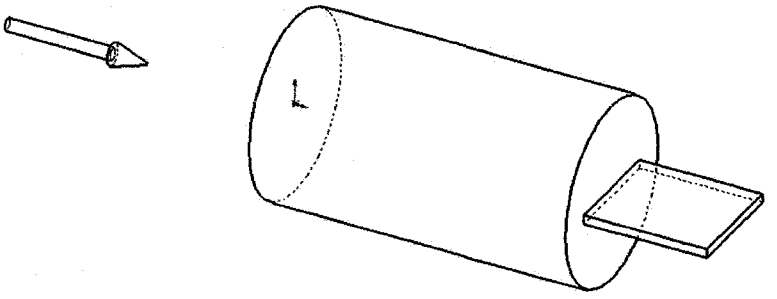

Figure 2.5 Splitter plate on a bluff body

Effects of splitter plates have also been studied numerically. Kwon & Choi used a DNS to model the flow behind a circular cylinder with a splitter plate[40]. They showed that the friction on the plate reduces the total drag of the configuration when the plate is shorter than the recirculation bubble. Maull noted that using a short splitter plate helps delay vortex formation while longer splitter plates might stop the vortex shedding altogether[41]. Monkewitz explains this by the fact that the splitter plate imposes zero transverse

velocity along the wake centerline and hence suppresses the absolute unstable sinuous mode of the vortex shedding[42].

Another successful passive control application can be found in the papers by Howard et al.[43, 44]. They investigated performance of passive techniques such as circumferential grooves, small transverse and swept grooves, passive porous surfaces, large longitudinal grooves, and vortex generators for controlling moderate, two dimensional, turbulent flow separation experimentally. They conducted surface static pressure measurements and oil flow visualizations to compare these techniques. While transverse grooves, longitudinal grooves, and vortex generators were shown to reduce reattachment distances and increase pressure recovery; swept groove and passive porous surface configurations were shown to increase separation.

Bushnell et al. showed that "almost all of the 2-D separated flows contained embedded cells of 3-D (mean) flow" including the 2-D (unswept) cylinder case[45]. It was also noted that the majority of the turbulent separated flows were unsteady with dominant frequencies generated by cavity recirculation and large-scale shear layer eddies. He showed examples of flow control techniques such as serrated trailing edges, splitter plates, adjacent bodies, passive bleed, spanwise geometrical variability, cavities/trapped vortices, vortex generators, and excitation of the fluctuating velocity field.

Forces acting on a two dimensional bluff body due to vortex shedding can also be modified by producing geometrical three dimensionalities capable of reducing the regularity of the shedding[4]. Using a cavity in the base, using serrated profiles on a blunt trailing edge to produce differences in shedding frequency[46] or using small irregular

protuberances on a circular cylinder to avoid uniform separation of the boundary layer are some examples of interfering with vortex formation. Another common method is using helical strakes to reduce the spanwise correlation of the shed vortices. Information about different geometrical modifications was mentioned in chapter 1.4 and also can be found in the paper by Zdravkovich[47].

2.4.2 Active Flow Control Methods

Flow control denotes any mechanism or any practice applied to control or modify the behavior of the fluid flow in order to accomplish a desired goal. A main objective of flow control is to overcome the effects of viscous boundary layers, generally skin friction and separation[48].

Some of the flow control objectives can be named as transition delay, separation prevention, drag reduction, lift augmentation, turbulence suppression, noise abatement, and heat and mass transfer enhancement. Prandtl pioneered the modern science of flow control at the beginning of the twentieth century[49].

Successful active flow control examples can be found in recent literature. Some of the methods used can be named as base bleed, acoustic forcing, micro-electromechanical-system (MEMS), oscillating wires, oscillation of the model (usually cylinders), electro magnetic fields, ionic winds and synthetic jets. Each of these techniques will now be discussed briefly.

Base Bleed

Base bleed is used in a similar way to the small splitter plates. In this method an air flow is driven in streamwise direction through a slot of width d on the base of the blunt body having height h. This configuration is characterized by the base bleed coefficient: $C_q = V_j d / Vh$. Where V is the freestream velocity and V_j is the bleed velocity. A description of this method was given by Bearman[50] and more information can be found in the paper by Tanner[46]. This technique is been used by researchers both in experimental and in numerical studies. An example of numerical study was the work of Clements reported in the paper of Maull[51] where he showed that base bleed delayed vortex formation.

Sevilla and Bazan[34] studied the large–scale helical vortex shedding regime in the wake of an axisymmetric body with a blunt trailing edge at high Reynolds numbers. Their experimental and stability analysis showed that there is a region of absolute instability in the near wake. They believed that this instability promoted the large-scale helical vortex shedding downstream of the recirculating zone. Blowing from the base of the slender body was tried to suppress the vortex shedding. It was shown that applying a sufficient amount of base bleed achieves suppression of the vortex shedding.

Acoustic Forcing

External and internal acoustic excitation methods are also used successfully as active flow control methods to prevent separation. Ahuja and Burrin[52] presented data for both external acoustic forcing (sound impinging on an airfoil from an external source) and internal acoustic forcing (sound emanating from within the airfoil through a slot in the surface) for a NACA 65(1)-213 airfoil. They showed that using external acoustic sources

helped increase the maximum lift coefficient and delay the stall angle to higher values. They also showed that internal forcing can delay separation on a high-lift airfoil. Huang, Maestrello, and Bryant[53] applied internal acoustic forcing at twice the shedding frequency increasing the maximum lift coefficient and delaying the stall angle. Hsiao, Liu, and Shyu[54] used internal acoustic forcing on an airfoil and a circular cylinder. They showed that for low post-stall angles of attack at constant sound pressure level the most effective forcing frequency is that which "locks in" the separated shear-layer instability, and is applied near the separation point.

MEMS

Liu and Brodie[55] presented a feedback control of the separation point at Re=25,000 by active transition control of the boundary layer. They used a micro-electromechanical-system (MEM), shear-stress sensor arrays, and a thin spanwise slit for the acoustic perturbation of the boundary layer over a cylinder. Using the sensors measuring the separation point and vortex shedding to set the acoustic perturbations to the boundary layer frequencies, instability-driven acceleration of the transition process is produced. This resulted in separation delay of the boundary layer.

Oscillating Wire

Another flow control method that utilizes the principle of introducing periodic disturbance to the flow is to use an oscillating wire. Bar-Sever[56] delayed separation over a wide range of frequencies (with decreased effectiveness below St ~1) by introducing velocity fluctuations in the shear layer of an airfoil.

Cylinder Oscillation

Schumm et al.[57] used oscillation of an oblong cylinder to suppress the vortex shedding at Re = 56; they applied a forcing frequency of about 1.8 times the natural vortex shedding frequency and relatively small cylinder oscillations. They also used wake heating and rotational oscillation to suppress the shedding. Fujisawa et al.[58] managed to suppress the shedding and reduce the aerodynamic forces using feedback control at Re = 6700. They used a hot-wire sensor for the feedback source.

Electromagnetic Fields

Electromagnetic force is also used for the purpose of flow control. It is well-known that the body force known as Lorentz force is generated in a conducting fluid flow subjected to an electric field and a magnetic field non-parallel to one another[59]. Researchers have been using this method in flow control area because of the advantage of having no moving parts and therefore the potential of miniaturization.

Henoch and Stace[60] investigated a turbulent boundary layer flow subjected to a magnethohyrodynamic (MHD) body force in the streamwise direction. They showed that the MHD force decreased turbulence intensity up to 30%.

Suction/Blowing

Blowing and suction is one of the most popular flow control techniques. Roussopooulos[61] conducted feedback control using a speaker by analyzing the velocity and phase information obtained at a point in the wake. Park et al.[62] accomplished complete suppression of vortex shedding at Re = 60 using a pair of blowing/suction sluts on a cylinder and a single feedback sensor located in the wake.

Synthetic Jets

Smith et al.[63] performed experiments using an isolated 2-D synthetic jet and two adjacent synthetic jets issuing in quiescent air. They also provided benchmark data for numerical studies. NASA Langley Research Center (LaRC) held a workshop on CFD validation of synthetic jets and turbulent separation control in March 2004 (CFDVAL2004). They provided three sets of experimental data to validate CFD codes: (1) a slot synthetic jet issuing into quiescent air, (2) a circular synthetic jet interacting with a flat plate turbulent boundary layer, and (3) separation control of flow over a hump by steady suction / blowing or a synthetic jet.

Researchers have studied, 2-D and 3-D simulations of flow fields controlled by synthetic jets using URANS, LES, DES and DNS methodologies. The majority of the numerical studies in the literature are performed for 2-D configurations. A limited number of 3D simulations are also available. Rizzetta et al.[64] investigated the flow field of a slot synthetic jet by direct numerical simulation (DNS). They examined several aspects of the actuator configuration such as cavity geometry and jet Reynolds number. The fully vectorized time-accurate 3D code FDL3DI was used in their study. They compared their result to the experiments of Smith and Glezer[65] for the time-mean vertical velocity in the flow field. Because of the limitations of computational resources, the semi-span length of the jet nozzle in the simulation was only 10 % of the experimental value[65]. On the whole, 3D computations agreed only qualitatively with the data.

2.5 Previous Work on Plasma Actuators

It has been found that surface direct-current (DC) corona and alternating (AC) dielectric-barrier discharges (DBDs) also seem to stabilize boundary layers where separation may otherwise occur[66-72]. In either of the DC or AC discharge configurations, the discharge generates a plasma in the immediate vicinity of the surface. Electrodes (which are often simply metallic strips between a dielectric sheet) can be configured such that the net force due to the ion drift is along the streamwise direction to suppress the flow separation or electrodes can also be configured to induce separation, generating an unusually large wake. While this is undesirable from an aerodynamic perspective; it can be suitable for applications such as flow mixing[73].

Malik et al.[74] first used DC corona discharge (or "ion wind") to manipulate flat plate boundary layers. Reporting drag reduction on the order of 20% for freestream velocities up to 30 m/s and 15 kV applied voltage, they concluded that drag reduction was largely voltage-dependent, and that multiple discharges might be used to obtain better efficiencies[75]. The use of corona discharges to produce and accelerate ions via the generation of an ion wind and hence to alter the thickness of boundary layers has been well studied[67, 68, 76]. El-Khabiry and Colver[77], in their numerical study, presented corona discharge induced drag reduction as much as 50% in flows with Reynolds number of 10^5 for flat plates. They observed that drag reduction decreased with increasing freestream velocity and decreasing potential difference between the wire electrodes. However, their discharge configuration was difficult to scale and integrate into practical devices. Artana[67] produced velocities up to 17.5m/s while Moreau[78] produced induced velocities

of about 3m/s in freestream flow velocities as high as 25m/s using corona discharge over flat plates. Roth et al.[66, 69, 79] presented the possibility of flow control using uniform radio frequency (RF) glow discharge surface plasma in a low speed wind tunnel. Wilkinson[80] investigated oscillating, weakly ionized surface plasma to reduce the viscous drag of turbulent boundary layers. Since it was reported that spanwise oscillations of a wall can reduce drag up to 40%, it was also thought that plasma induced body forces in high electric field gradients due to a surface plasma along strip electrodes could also be configured to oscillate the flow. His results showed that while a small oscillation could be obtained, the effect was lost at low frequencies (<100Hz). Furthermore, a mean flow that complicates the effect was generated. He presented hot-wire and pitot probe data as well as phase-averaged images revealing the plasma structure.

Plasma actuators have drawn a lot of attention and have been used in many applications in recent years[81]. Some applications of plasma actuators include low Re separation control[82, 83], lift enhancement on airfoils[84, 85], virtual flaps and slats for airfoil flow control[86], low pressure turbine blade separation control[86-90], near-wake flow control[68] (with plasma sheet actuators), wake (Karman Vortex Street) phase synchronization from multiple cylinders[91], circular cylinder wake vortex control[92], landing gear noise reduction[93], and to control the coherent structures in a planar, weakly compressible, free shear layer[94]. Although most of the applications mentioned above are restricted to incompressible flows, some high speed applications such as axisymmetric jet forcing using arc plasma based configurations have been also reported[95].

Numerical Work

Although most of the plasma based flow control research is based on experimental studies, there are also several published numerical works. Current models generally use an electrohydrodynamic (EHD) body force term to simulate the effect of plasma actuators on the external flow[75].

Shyy et al.[96] calculated the time-averaged electrostatic body force acting on the fluid and then added this to the 2-D steady, incompressible, Navier-Stokes equations to solve for the entire flowfield considering a linear approximation for the electric field distribution. Suzen et al.[97, 98] introduced the body force as the product of net charge density and electric field in the Navier-Stokes equations. Hall et al.[99] used a potential flow approach to model the behavior of a plasma actuator, where a doublet element was used to imitate the actuator-induced velocity field. Orlov and Corke[100, 101] used the body force expression developed by Enloe et al.[70], and a lumped electric circuit model was used to compute the electric potential and volume of plasma. Besides the simplified models mentioned above more sophisticated particle physics and plasma chemistry based approaches were also used. Font et al.[102-104] used a particle-in-cell direct-simulation-Monte-Carlo (PIC-DSMC) method to model the interaction between various ionic species. Shang[105] solved the time-dependent Maxwell's equations along with particle concentration equations to compute the electromagnetic field distribution of a dielectric barrier discharge.

Optimization of the Parameters Affecting Plasma Performance

Dielectric barrier discharges can produce diffuse uniform coverage, depending on the gas used, ambient pressure, electrode separation, operating voltage, and frequency as has

been presented by Pons et al.[106] in their parametric studies. However, in practice, the plasmas generated in air are often filamentary and made up of individual electron avalanche discharges.

Based on large scale integral measurements of thrust output, voltage and plasma emission measurements, and simulations, Enloe et al.[70] presented that the power input, P, to the plasma is nonlinear with the voltage drop, ΔV, across the dielectric, and that both the maximum induced velocity, u_{max}, and thrust, T, are proportional to input power, such that

$$T \propto u_{max} \propto P \propto \Delta V^{7/2}$$

They also noted that thrust is greater for a "positive" waveform as opposed to a "negative" waveform, even though the bulk plasma structure is the same. The "positive" waveform appears to produce a more uniform discharge.

Effects of the factors such as input power, input voltage, input frequency, electrode geometry, actuator orientation, dielectric material, dielectric thickness, freestream Re, pressure gradient, plasma chemistry and humidity of air have been investigated by many researchers to optimize the performance of plasma actuators. Baughn et al.[107] measured velocity profiles at several locations upstream and downstream of a plasma actuator, and calculated the body force using a control volume momentum balance approach. For freestream velocities in the order of few m/s they showed that the force was not affected by the imposed crossflow. They also presented that for a constant voltage, body force production increased as input ac frequency increased (between 5 and 20 kHz) for nearly constant input power. Porter et al.[108] examined the effects of individually varying input ac

voltage and frequency by measuring the body force produced by steady operation of a plasma actuator. They concluded that while the time-averaged body force is linearly proportional to input ac frequency between 5 and 20 kHz (for constant input voltage), it was nonlinear with the input voltage (for constant frequency). Further, they observed that the actuator "blows" (with higher magnitude) and "sucks" (with lower magnitude) the fluid during each cycle.

Roth and Dai[79] investigated the effects of dielectric material, electrode geometry, input frequency and input voltage on the flow velocity induced by a plasma actuator. They observed that the type of dielectric material affects the plasma volume, the distribution of electric field lines (dictated by the dielectric constant value), and the dielectric heating power loss (which, in turn, is proportional to input AC frequency and electrode area). They found that while alumina has a higher dielectric constant, Kapton has higher dielectric strength and quartz and Teflon have lower heating loss factors. Teflon was found to generate higher induced flow velocities for lesser power input compared to quartz. They used Teflon as the dielectric material for their remaining parametric studies. The width of the bottom electrode was found to have negligible effect on both the maximum induced velocity and input power per unit length of the actuator. However they found that the gap distance between the electrodes had a significant effect (optimum for d = 1 to 2 mm) on the induced flow velocity.

2.6 Three Dimensionality and Interference Effects

There have been a vast number of papers published on circular cylinders and Karman vortex streets while there has been less work done on three-dimensional bluff bodies. It is

obvious that the three-dimensional flow around a bluff body base is complicated. Even the pseudo-two dimensional flow around a circular cylinder with vortex shedding is still not easy to resolve when realizing that the flow shows some three-dimensionality and the spanwise correlation of the vortices is not high[51]. There are some similarities in two-dimensional flows and three-dimensional flows and some conclusions related to the first can be carried over to the latter, however other results are not applicable.

Maull noted that any introduction of three-dimensionality into the base flow has an effect on the vortex shedding and consequently upon the base pressure. Many methods such as segmented trailing edge, part-span splitter plates, and part-span cavities and some other methods are reviewed by Tanner[46]. It was noted by Maull that the differences between two- and three dimensional base flows are great, and it is not necessarily true that drag reduction devices which work for two dimensional flows will work for three dimensional flows.

Numerically, it is possible to compare the results of the two-dimensional and three-dimensional computations, in order to single out the differences in the flow field and aerodynamic forces generated by these three-dimensional features. Mittal has shown that there are significant differences between the two types of the computations for both the mean and the fluctuating forces[109]. While three-dimensional computations are in agreement with the experimental results, two-dimensional computations gave much higher mean drag and fluctuating lift forces.

3. DATA SAMPLING AND ANALYSIS

3.1 Classification of Data

Any data representing a physical phenomenon can be described as deterministic or nondeterministic (random). Deterministic data can be described by an explicit mathematical relationship, where nondeterministic data cannot be expressed by such a relationship, i.e. there is no way to predict an exact value at a future instant of time. Classification of deterministic and random data can be seen in Figure 3.1.

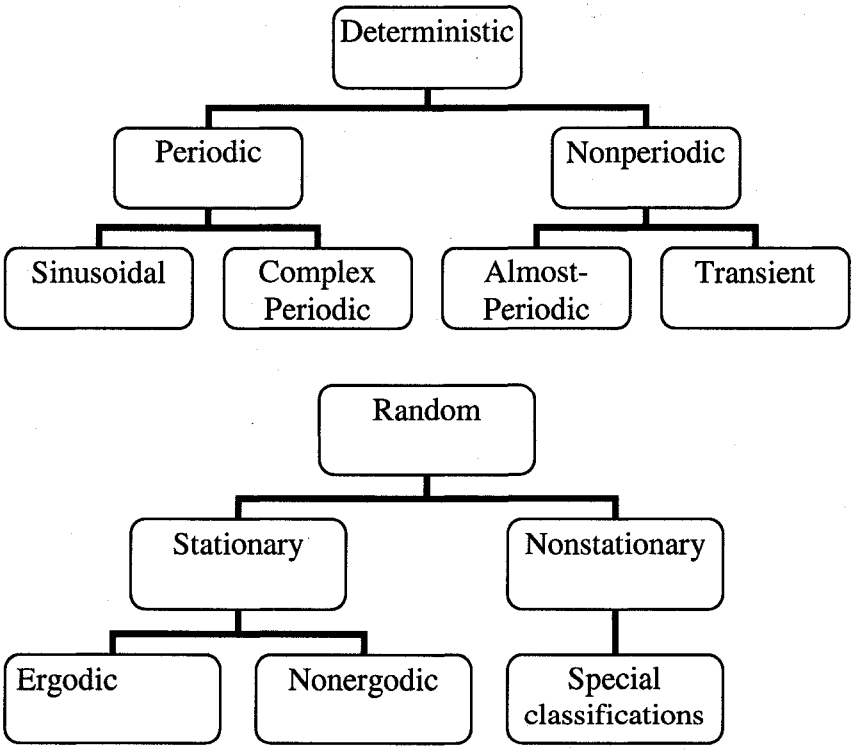

Figure 3.1 Classification of Data Types[110]

As mentioned above each observation of a random data will be unique and infinitely large time histories can be recorded. A single time history representing a random phenomenon is called a sample function (also called a sample record when observed over a finite time interval). The group of all possible sample functions that the random phenomenon might have formed is called a random process or a stochastic process (Figure 3.2). Hence a sample record of data for a random physical phenomenon may be considered as one physical realization of a random process. When a physical phenomenon is considered in terms of a random process, the properties of the phenomenon can hypothetically be described at any instant of time by computing average values over the collection of sample functions that describe the random process. Figure 3.2 shows a collection of sample functions that forms a random process.

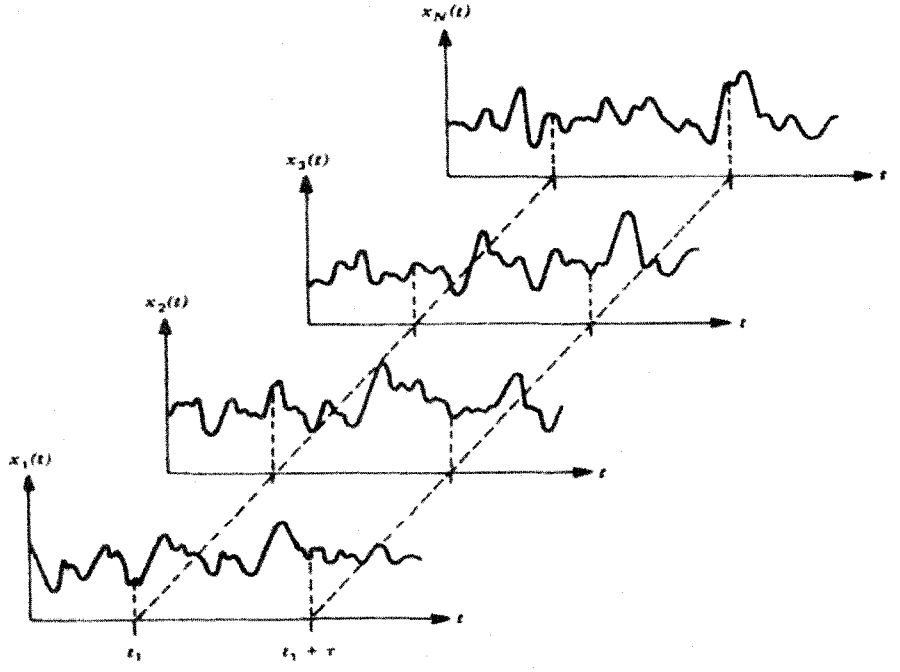

Figure 3.2 Ensemble of time-history records defining a random process[110]

The mean value (first moment) of the random process at some time t_1 can be computed by summing the instantaneous value of each sample function of the ensemble at time t_1, and dividing by the number of sample functions. Similarly a correlation (joint moment) between the values of the random process at two different times (autocorrelation function) can be computed by taking the ensemble average (the ensemble average of a random process, x(t), is shown as {x(t)}) of the product of instantaneous values at two times, t_1 and $t_1+\tau$.

$$\mu_X(t_1) = \lim_{N\to\infty} \frac{1}{N} \sum_{k=1}^{N} x_k(t_1)$$

$$R_x(t_1, t_1+\tau) = \lim_{N\to\infty} \frac{1}{N} \sum_{k=1}^{N} x_t(t_1) x_k(t_1+\tau)$$

For the cases where $\mu_x(t_1)$ and $R_x(t_1, t_1+\tau)$ vary as time t_1 varies the random process {x(t)} is said to be nonstationary. For the cases where $\mu_x(t_1)$ and $R_x(t_1, t_1+\tau)$ do not vary as time t_1 varies {x(t)} is said to be weakly stationary. In these cases the mean value is constant and the autocorrelation function depends only on the time displacement τ. For the cases where all possible moments and joint moments are time invariant, {x(t)} is said to be stationary. If the ensemble averages of a stationary random process are equal to the averages obtained from the time integral over different sample functions, the random process is called ergodic[110].

Data acquired in this study was a special set of nonstationary random processes with periodic properties at finite intervals of τ_0. For practical purposes ergodic properties are assumed during data analysis from a single realization of the experiment (a single sample function of the random process). Adopting the above definitions, random processes described by phase averaging are called periodic ergodic[111].

Averages of stationary ergodic random processes are calculated from time integrals, on the other hand averages of periodic ergodic data are calculated from the sum of discrete instants of time, which differ by an integer multiple of the period τ_0. As an example, for a fluctuating quantity x(t), the phase average $\mu_x(\tau)$ for a given $\tau \in [0; \tau_0]$ is:

$$\mu_X(\tau) = \lim_{N\to\infty} \frac{1}{N} \sum_{k=1}^{N} x_k(k\tau_0 + \tau)$$

Where $t = k\tau_0 + \tau$ is substituted for the time t. τ denotes the population of samples that the phase average is calculated from, where different 'τ's show different populations. The total number of different populations is defined by the period τ_0 and the temporal resolution of the implemented measurement method[111].

3.2 Bin Averaging

The temporal resolution of some of the measurement techniques is limited to the length of the measurement interval (record interval). Hence, each period τ_0 is subdivided into elementary intervals that are called bins. Each bin is defined by an interval of phase angle ϕ, that has a value between 0 and 2π. Later phase averages are calculated using the

samples which were collected in the same bin. Estimates of the mean X(ϕ) and the root mean square value x'(ϕ) are calculated as follows;

$$X(\phi)=\frac{1}{N(\phi)}\sum_{k=1}^{N(\phi)}x_k(\phi)$$

$$x'(\phi)=\sqrt{\frac{1}{N(\phi)-1}\sum_{k=1}^{N(\phi)}(x_k(\phi)-X(\phi))^2}$$

When large numbers of samples are used this method (bin averaging) gives accurate estimates. On the other hand the accuracy decreases with a decreasing number of samples; hence other averaging methods needs to be used when there are not enough samples or when sampling time is critical. Other methods suggested by researchers include weighted averaging, and Fourier averaging[111]. In this study a satisfactory number of samples were collected in a reasonable time, so the bin averaging method was applied successfully.

Sampling of the Data

The periodic near wake behind a bluff body presents unsteady velocities with high gradients, strong turbulent fluctuations and a three-dimensional pattern. These features require a velocity measurement technique which has high spatial and temporal resolution. Particle Image Velocimetry (PIV) is a promising method due to its high spatial resolution and being non-intrusive, however it only has fair frequency response. In order to overcome the low sampling rate problem, sampling methods and supplementary

equipment can be used. In this study velocity signals acquired through a hot-wire anemometry system are used together with PIV system.

In the test section fixed frame of reference, the velocity around an ogive cylinder with an axisymmetric inflow varies periodically at a frequency; hence the statistical analysis of the turbulent flow cannot be obtained through time averaging of velocity histories acquired in a measurement point. Instead phase sampling methods are used to calculate true ensemble averages, referring the velocity field to the flow angular position. Statistics are based on a large number of time histories, each one representing an experimental instant[112].

3.3 Phase Sampling Approaches

Two main methods are used to analyze the phase averaged velocity fields around periodic flow generating bodies; the time acquisition method and the angular triggering technique. In the first method, several time histories of a velocity field at a space fixed point are recorded. In the second method velocity is saved once per period based on selection of an angular position (i.e. specific phase angle). The time acquisition method is widely used due to substantial time savings compared to the angular triggering method since the latter method uses only one trigger signal per period. On the other hand with the time acquisition method the number of required samples for a particular phase angle is not guaranteed and the recorded samples might not be enough for accurate investigation of the velocity field at this phase angle. Consequently, the time acquisition method is suggested to be used for fast analysis of a periodic wake, while the angular triggering

technique is recommended for accurate investigations of highly turbulent flow regions where data storage capacity might be restrictive.

In this research two phase sampling methods are used. First an implementation of the angular triggering technique (ATT), namely the Predictive Angular Triggering Technique (PATT) is introduced. In this method the flow structure is monitored using a single channel hot-wire anemometer. Flow phase and frequency is obtained by using statistical tools such as bandpass filtering and FFT. Knowing the phase and frequency of the flow, a desired future time is chosen for the acquisition of the data (a trigger signal is sent to start data acquisition), and every time that point (including an n x period delay if necessary) is reached a trigger signal is sent to the PIV laser system, i.e. the trigger is "phase locked" to the flow structure (Figure 3.3).

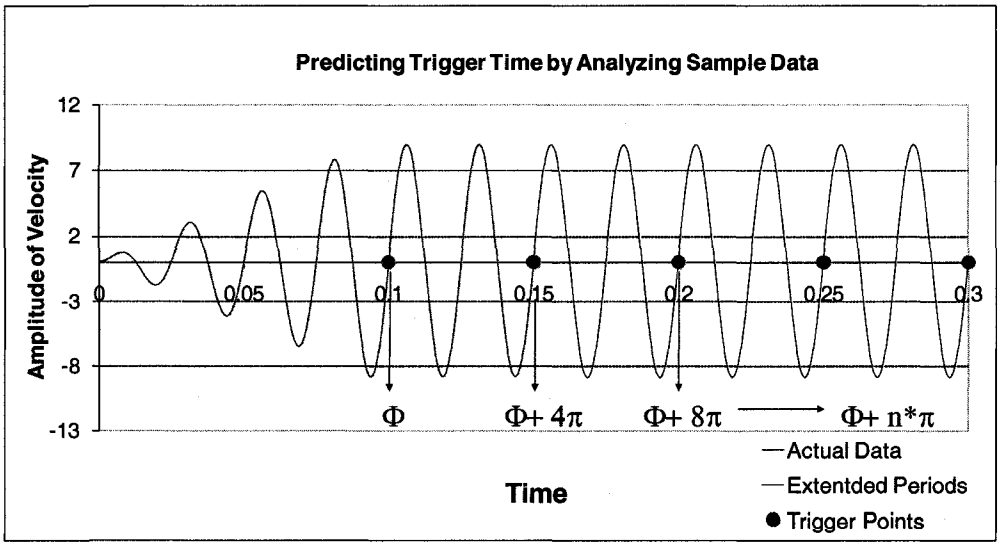

Figure 3.3 Predictive Angular Triggering Technique

While this method was suitable for periodic structures whose frequency is in the order of 1-10 Hz, it was not appropriate for use in flows with higher frequencies because of the

limitations of available hardware. To negate those limitations, the tracking triggering technique (TTT) is chosen to analyze the flow field. In this process laser triggers sent through the synchronizer (observed by monitoring the voltage pulses sent from the synchronizer) are saved, while the velocity and the phase information of the flow are also recorded by the help of the hot-wire signal. The velocity data is used to match a sine wave (Figure 3.4). This sine wave is then used to match the recorded images to the corresponding flow position. After grouping the images saved over a defined interval, ensemble averages of the samples are calculated for each desired instance (Figure 3.5).

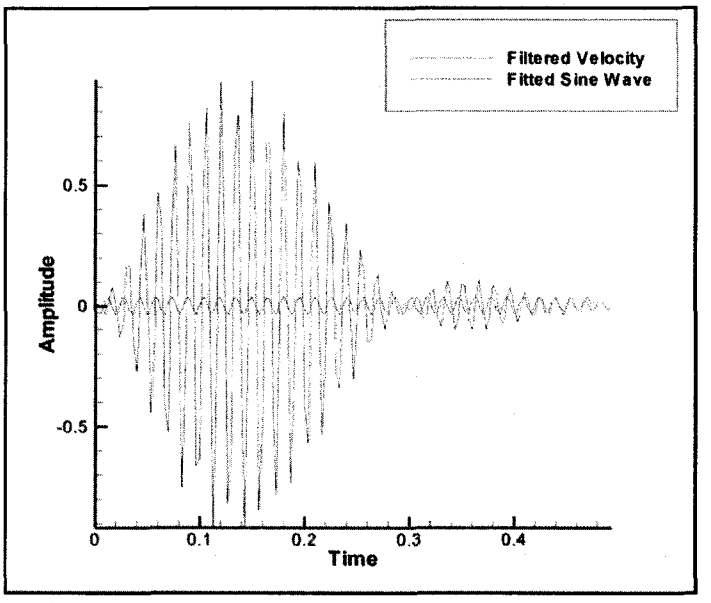

Figure 3.4 Matching raw data to a sine wave for associating image to flow structure

Samples are arranged inside angular slots (or bins) of width ε. The sample Vi(t*) is acquired when flow structure position was φ(t*), is put in slot

$$\varphi K - \varepsilon/2 < \varphi(t^*) < \varphi K + \varepsilon/2$$

Where the slot center is φK and ε is chosen to obtain the maximum spatial resolution.

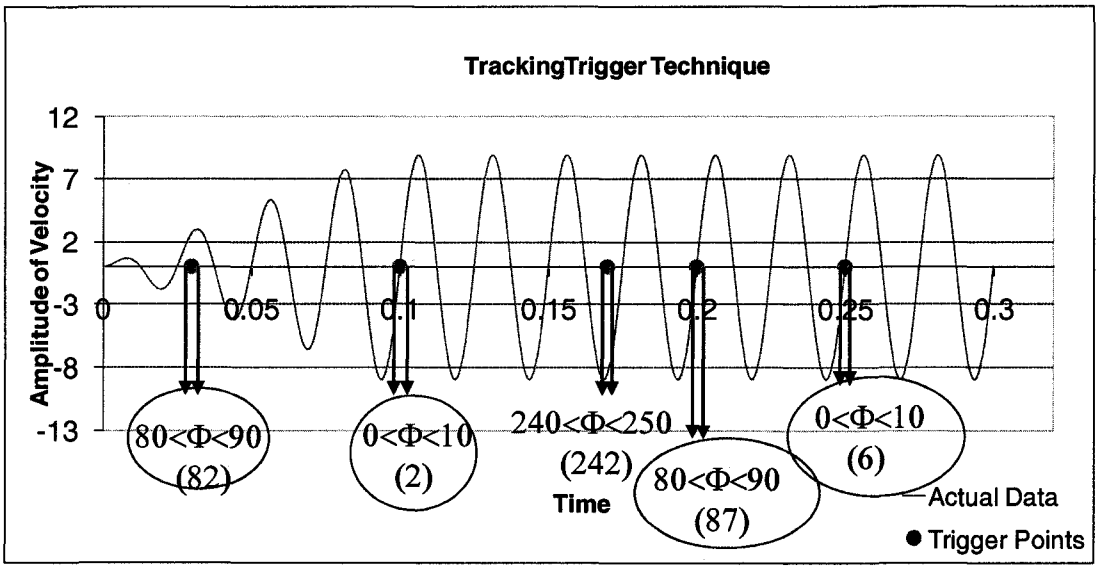

Figure 3.6 Tracking Triggering Technique

4. FLOW CONTROL

4.1 Background

In recent years, there has been much emphasis on the development of flow control devices that can improve aerodynamic performance by such means as flow laminarization or separation control. Flow control denotes any mechanism or any practice applied to control or modify the behavior of the fluid flow in order to accomplish a desired goal. Arguably, the main challenge of flow control is to overcome the effects of viscous boundary layers, generally skin friction and separation[113]. Improving aerodynamic performance has potential benefits across a wide range of applications, such as savings in fuel costs, and achievement of more economically competitive and environmentally sound industrial processes involving fluid flows[49].

Some of the objectives of flow control areas can be listed as transition delay, separation prevention, drag reduction, lift augmentation, turbulence suppression, noise abatement, and heat or mass transfer enhancement. Prandtl pioneered the modern science of flow control at the beginning of the twentieth century[49].

Flow control methods can be classified according to whether external energy and a control loop are used or not. Passive control devices do not need any auxiliary power or a control loop. Active flow control techniques require a control loop and energy expenditure in some form. Control loop structures are classified into predetermined or reactive categories. Predetermined control is based on an open loop structure and does not need any sensing of flow conditions. For this case, steady or unsteady energy is input

regardless of the flow behavior. In reactive control, the output parameter is continuously adjusted by control input based on appropriate measurements, either by an open feedforward loop or a closed feedback loop (Figure 4.1). Reactive control divides into adaptive, physical-model-based, dynamical systems-based, and optimal control categories[49] (Figure 4.2).

(a) Predetermined,

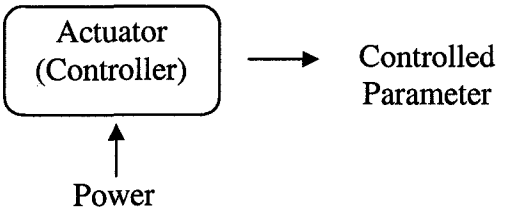

(b) Reactive, feedforward, open-loop control

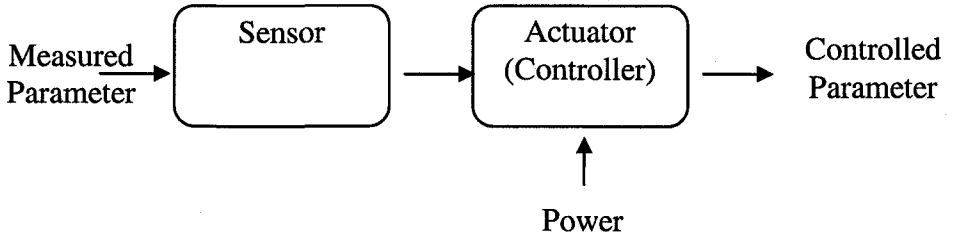

(c) Reactive, feedback, closed-loop control

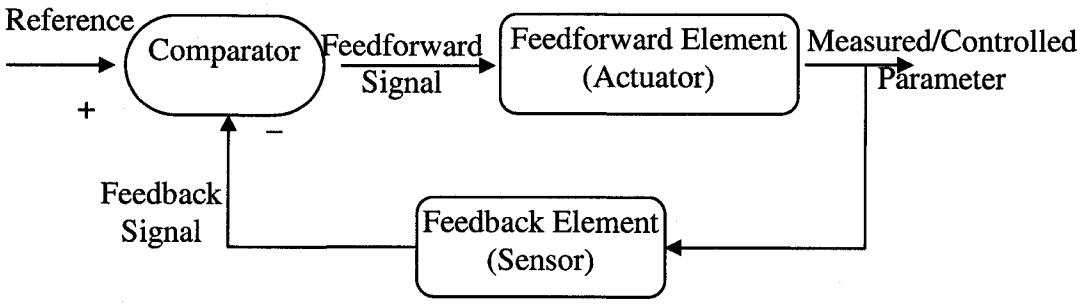

Figure 4.1 Control Loop Types for Active Flow Control

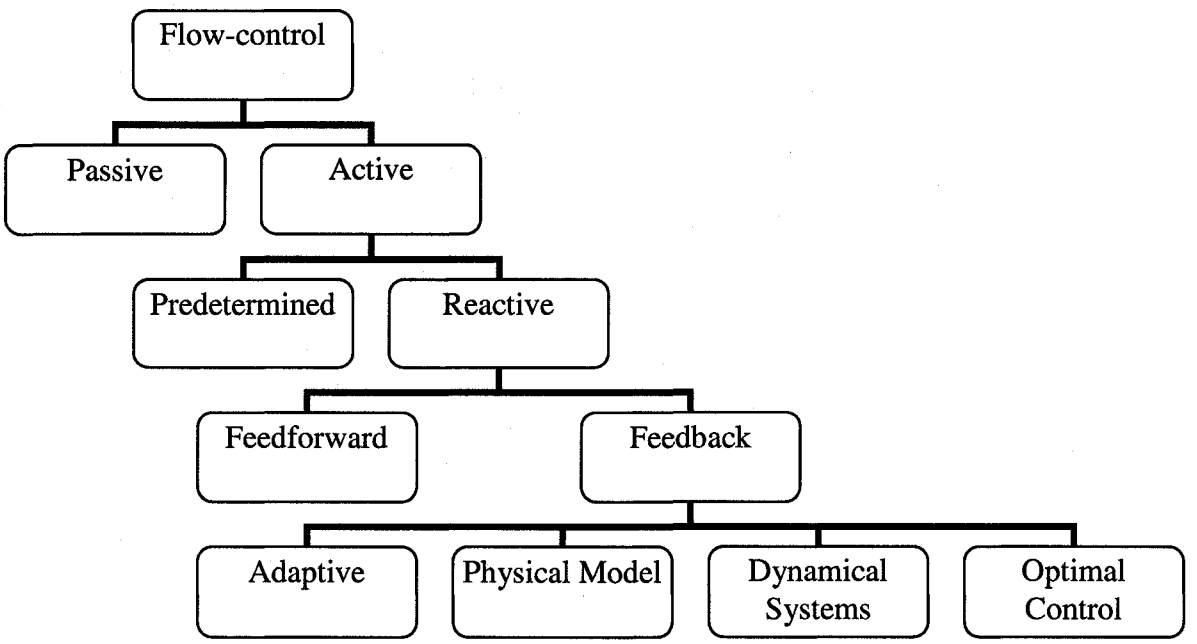

Figure 4.2 Flow Control Classifications

4.2 Flow Control Classifications

Another classification of the flow control methods can be made according to whether the control technique alters the instantaneous mean velocity distribution or whether it alters the flow instabilities thereby changing the flow structure. Conventional active flow control methods are mainly concerned with direct interaction with, and alteration of, the mean flow about a body. Modern techniques involve altering existing flow instabilities using relatively small inputs to obtain large-scale changes of mean flows. In many flow control cases, particularly closed loop applications, unsteady actuation is required for optimal performance when it can be controlled. If the unsteady actuation can be synchronized with the characteristic time scales of the flowfield, actuator power requirements and performance can be optimized[114].

Boundary layer control includes any mechanism or process through which the boundary layer of a fluid flow is caused to behave differently than it normally would were the flow developing naturally along a smooth straight surface[49]. Boundary layer flow control can be classified according to whether the technique is applied at the wall or away from the wall. Heating and cooling a surface and mass transfer from a surface are examples of flow control methods applied at the wall. Using large-eddy breakup devices, acoustic wave bombarding, using additives, using electromagnetic and electrohydrodynamic body forces are examples for flow control away from the wall.

Flow control actuators used frequently by researchers include synthetic jets, piezoelectric benders, powered resonance tubes, plasma actuators, pulsed jets, fluidic oscillators, and steady blowing or suction[114]. Selection of a flow control actuator often is driven by the requirements of the application. In recent years, a variety of impressive flow control results have been achieved by many researchers by vectoring of periodic excitation of turbulent jets[115], modifications of aerodynamic characteristics of bluff bodies[4, 47], using sound waves to improve lift and drag of airfoils[53], control of external and internal flow separation and cavity oscillations[46].

4.3 Control of Vortex-Shedding

Numerous researchers have addressed the control of vortex shedding behind bluff bodies, especially circular cylinders. In these works researchers have focused on suppressing the vortex shedding, separation control, and lock-in or synchronization of the shedding[42]. Controlling vortex shedding can be used to reduce drag, increase lift, suppress noise, decrease vibration, and increase mixing or heat transfer. The technique to achieve the

vortex shedding control is chosen according to the objective and the Reynolds number of the flow. Both active and passive control and feedback control systems have been variously used[4, 47].

4.3.1 Suppression of the Absolute Instability and Vortex Shedding

Knowing that the absolute instability is the reason for the vortex shedding, many researchers have directed their efforts at suppressing the absolute instability by active or passive means[42]. Examples of passive control of vortex shedding from cylinders include using end plates[116], splitter plates[117], placing a control disk behind the base of a body[26] (Figure 4.3), and placing a secondary cylinder in the flow[118]. Forces acting on a two dimensional bluff body due to vortex shedding can also be modified by producing geometrical three dimensionalities capable of reducing the regularity of the shedding[4]. Using a cavity in the base, using serrated profiles on a blunt trailing edge to produce differences in shedding frequency[46] or using small irregular protuberances on a circular cylinder[18] (Figure 4.4) to alter the separation of the boundary layer are some examples of interfering with vortex formation. Another common method is using helical strakes to reduce the spanwise correlation of the shed vortices. Further information can be found in the paper by Zdravkovich[47].

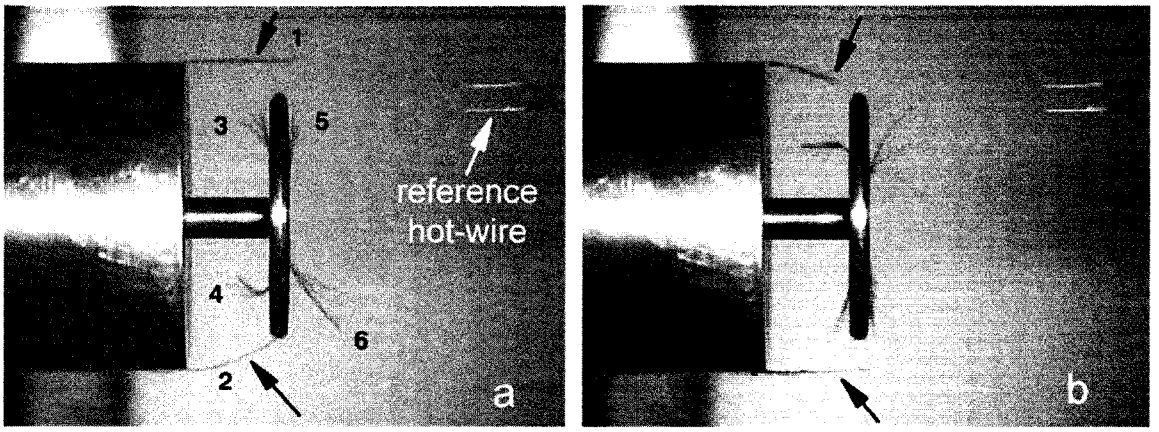

Figure 4.3 Affect of a control disk, phase difference between (a) and (b) is $\Delta\Phi = \pi$[26]

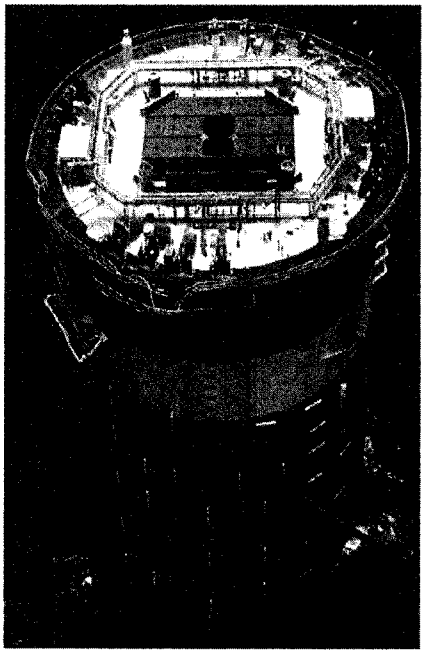

Figure 4.4 Protuberances on a circular spar platform[18]

Successful active flow control examples can be found in more recent work. Some of the methods used can be listed as base bleeding[34] (Figure 4.5), acoustic forcing, micro-electromechanical-system (MEM), oscillating wires, oscillation of the model (usually cylinders), electromagnetic fields, ionic wind, plasma actuators[119], and synthetic jets[120].

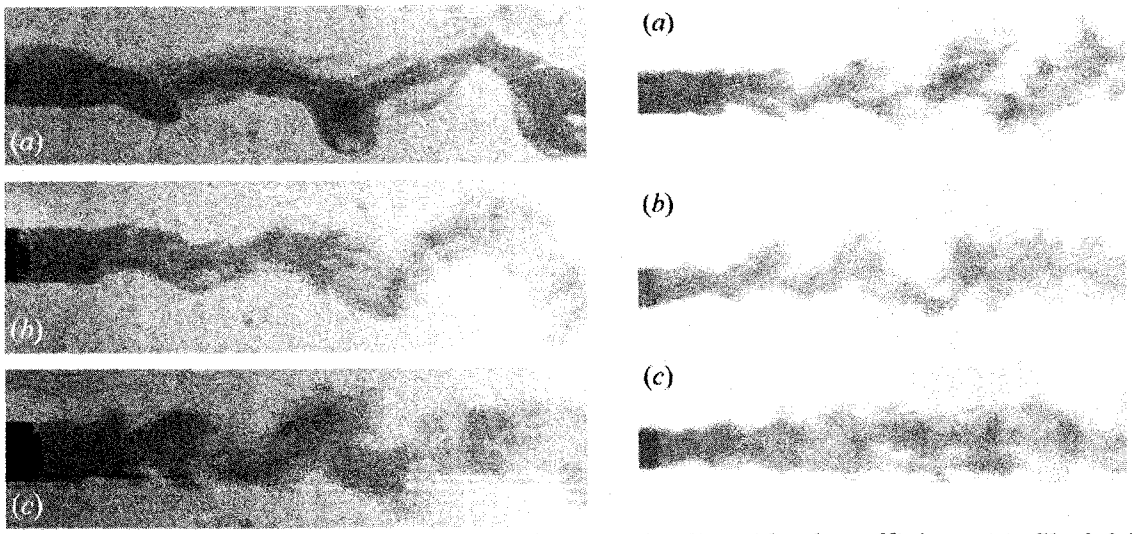

No bleed, (a) Re=1075, (b) Re=1900, and (c) Re=2650

Bleeding, bleed coefficient: (a) *Cb*=0.04, (b) *Cb*=0.09, and (c) *Cb*=0.13

Figure 4.5 Base bleeding[34]

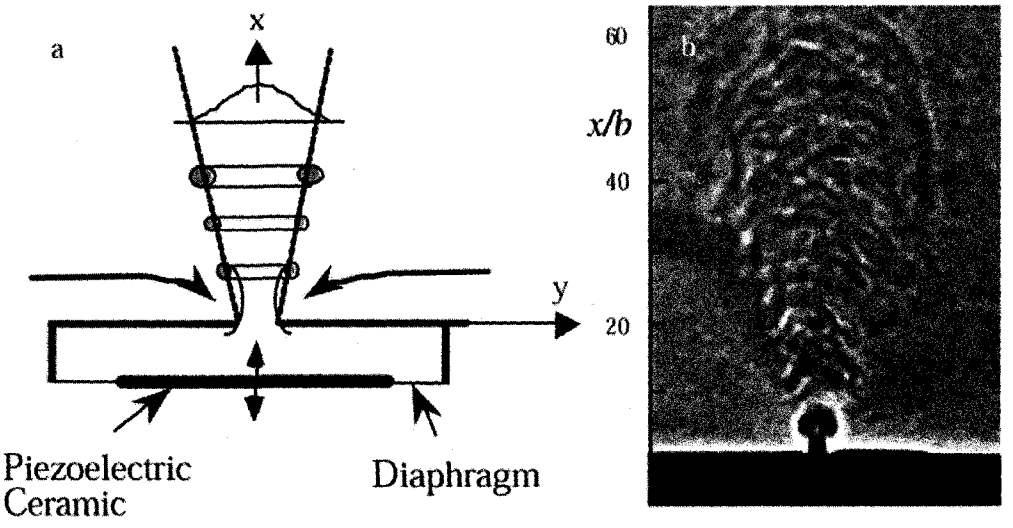

Figure 4.6 Schematic diagram of a synthetic jet actuator and Schlieren image of a rectangular synthetic jet[120]

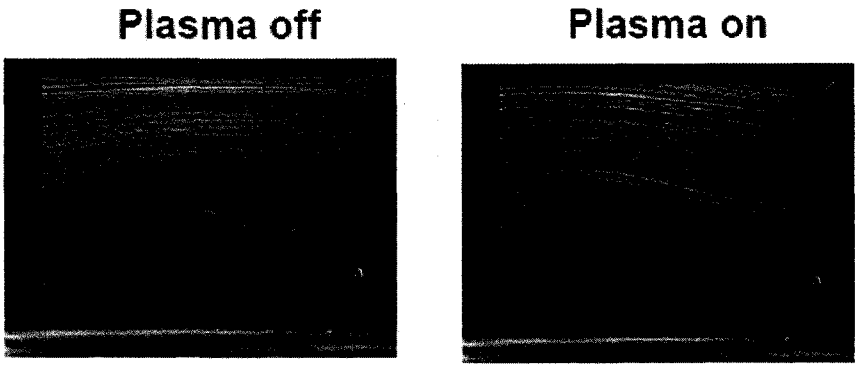

Figure 4.7 Separation control using plasma actuators[119]

4.3.2 Synchronization of Vortex Shedding

The phenomenon variously known as synchronization, wake capture, resonance, or phase-locking, is used by many investigators to lock-on vortex shedding with forcing. When a cylinder oscillates at a frequency close to the frequency of the vortex shedding from the cylinder, vortex shedding tends to lock on to the oscillation frequency. The range of lock-on frequencies increases with increasing oscillation amplitude. The usual Strouhal relations are not observed during lock-on.

Various flow control methods used for vortex shedding synchronization with excitation are reviewed by Griffin and Hall[121]. An important result of synchronization is the increase in the spanwise correlation of the vortex shedding.

Synchronization of vortex shedding can be achieved by the transverse[14], in-line[122] or rotational[123] oscillation of the cylinder. Another method to obtain lock-on was used by Blevins[124] by applying acoustic excitation behind a cylinder. He experienced that the amplitude of the vortex shedding, the spectral peak at the shedding frequency, and the spanwise coherence of the vortex shedding increased with increasing sound pressure whereas the frequency band around the Strouhal frequency decreased.

4.3.3 Present Flow Control Methodology

The capability to estimate, efficiently alter and maintain a flow state relies on the control authority of available actuators. Although the selection of the actuator depends on the application it is going to be used, three general criteria can be presented to evaluate their performance. The first criteria is based on actuators force or linear momentum generation capability as it operates in still fluid, while considering its weight, volume and power consumption. The second criteria is simply the actuator peak velocity relative to the free-stream velocity, where generally a velocity ratio greater than 0.1 and/or momentum coefficient greater than 0.01% is preferred. The third, application dependent, criterion is based on the improvement of the controlled performance (e.g., lift to drag ratio) of a certain application, when the power consumption (and also the weight) of the actuation system are taken into account[125].

In the present work an actuator without mechanical parts, with high bandwidth, and which is easy to construct was needed to alter the wake of a bluff body. Hence, the current study focuses on active flow control by means of plasma actuators due to their advantages such as robustness, simplicity, and ability for real-time control at high frequencies. These actuators are also scalable in size, hence were easily placed on the test models.

5. PLASMA ACTUATORS

5.1 Background

When heat is added to a solid, it first undergoes a phase transition from the solid to the liquid state and then from the liquid to the gaseous state. If further heat is added to the gas, the forces binding the electrons to the atoms in the gas are overcome by thermal agitation, and the gas forms an electrically conducting plasma. This state is known as the fourth state of matter and it can be produced using very high temperatures, strong constant DC electric fields, or radio frequency (RF), or microwave electromagnetic fields. Plasma can be found everywhere in nature and ninety-five percent of our universe is made up of plasma. Among many other applications where one might encounter plasma in everyday life are fluorescent lights, fabrication of microelectronic devices, flat panel television screens, and welding[126].

5.2 Electrical Discharges

When an electric field with adequate amplitude is applied on a gas volume to create "electron-ion pairs by electron impact ionization of the neutral gas", a gas discharge is created[127]. Traditional gas discharges at low pressures generally employed separated facing electrodes. These two electrodes produce either a direct current (DC) or alternating current (AC) electric field. When the amplitude of the electric field is greater than the breakdown electric field, E_b, plasma is generated.

Most of the aerodynamic flow control applications require actuators operating near atmospheric pressure[127]. There are different sources of plasma that can be operated at one

atmosphere. For example, in regions of high electric field near sharp points where electrically stressed gas is present, a corona discharge may exist if the electric field exceeds that for breakdown of the gas. Applications of corona discharges include electrostatic precipitators, xerography, modifying the surface properties of materials, optical pumping of CO_2 lasers, large-area mercury-free fluorescent lamps, flat plasma display panels, ozone generation[128] and air freshening. However, drawbacks of corona sources include formation of ozone, X-rays, NO_2, nitric acid (in the presence of water vapor), and production of audible and RF noise. In the field of aerodynamics, corona discharges have been used successfully for altering the characteristics of boundary layer flows[74]. Boundary layers thickness was reduced by many researchers using corona discharges to produce and accelerate ions via the generation of an ion wind[67, 68, 76, 77]. It was reported[74] that the ion wind generated by these corona discharges reduced drag by as much as 50% for flows at Reynolds number of $\sim 10^5$. However, application of the discharge configuration on practical devices was difficult due to scaling and integration problems.

DC and AC electric discharges are also used in flow control applications. AC discharges are preferred over DC ones since they form self-limiting discharges by virtue of the charge build-up on the dielectric surface. Without this feature, the discharge would breakdown into a thermal arc with attendant control and materials problems. However, it is possible to obtain similar flow forcing effects using DC discharges. By using a current limiting resistor formation of the thermal arc can be prevented for DC discharges. Hence, some of the new, emerging ideas use combinations of AC/DC excitation.

The current-voltage diagram in Figure 5.1 shows the regimes of classical DC electrical discharge[129]. Corona discharges occur from D to E on the diagram; whereas dielectric barrier discharges operate in the normal glow region from F to G.

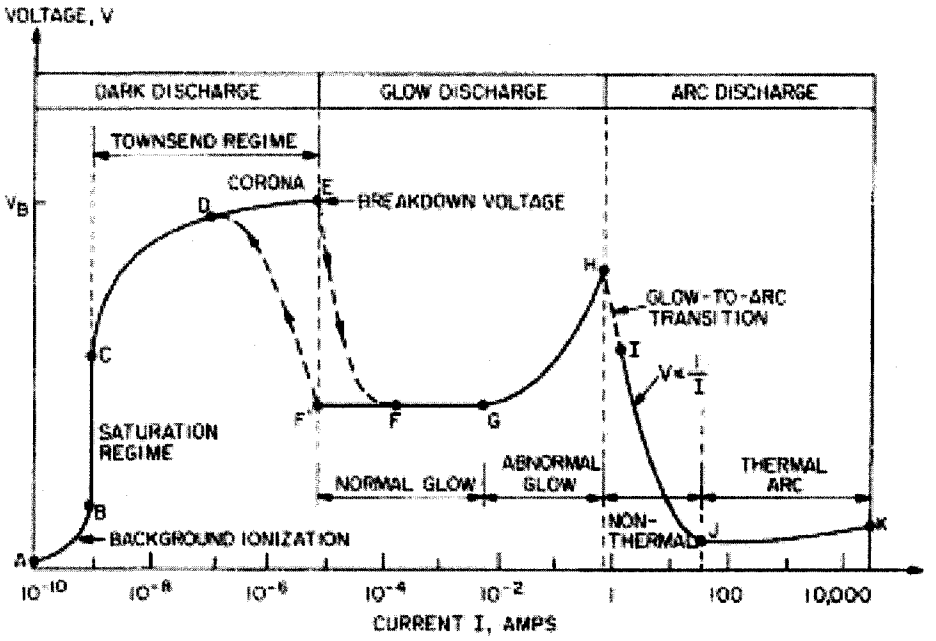

Figure 5.1 Regimes of classical DC electrical discharge[129]

5.3 Dielectric Barrier Discharge (DBD)

Dielectric Barrier Discharge (DBD) devices can be operated at one atmosphere. DBD is generated in the space between two electrodes, at least one of which is covered with an insulating dielectric material. The applied AC voltage causes air to ionize over the covered electrode. The ionized air, in the presence of the electric field produced by the asymmetric placement of the electrodes, generates a body force acting on the charged particles and, via collisions, on the bulk neutrally charged air molecules[127]. This body force is the main factor in aerodynamic flow control.

During plasma actuator operation, for one-half of the AC cycle electrons move from the electrode to the dielectric and accumulate locally, whereas during the reverse half of the cycle, surface discharges on the dielectric produce electrons that move to the electrode. This cycle is on the order of a few tens of nanoseconds for atmospheric pressure[127]. To produce the power needed for the actuators a signal generator, amplifier and step up transformer are needed (Figure 5.3).

In principle, DBD can generate diffuse uniform coverage, depending on the gas used, ambient pressure, electrode separation, operating voltage, and operating AC frequency, as has been shown through the parametric studies of Pons et al.[106]. The more commonly observed phenomena in atmospheric studies using the system in Figure 5.3 is a striated discharge[136].

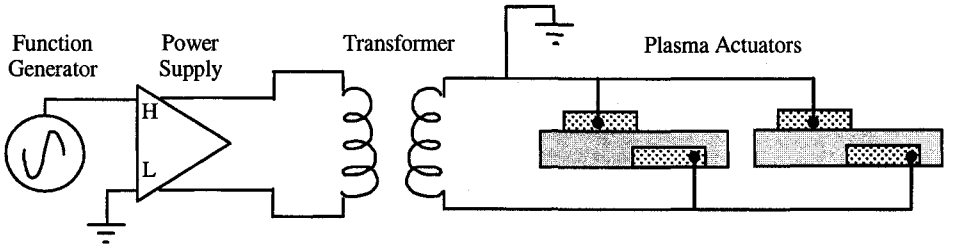

Figure 5.3 Actuator electronic setup for plasma actuators

5.4 Performance of Plasma Actuators

5.4.1 Efficiency and Optimization of the Plasma Actuators

Investigations of Roth et al.[79] showed that use of a single actuator was sufficient for flow re-attachment on a NACA 0015 airfoil with increase of the stall angle by 5 degrees in a

freestream airflow of 2.85 m/s (Figure 5.6). Although only a velocity of 2 to 5 m/s could be induced from a single actuator they can accomplish re-attachment of free stream flows with much higher velocity. Wind tunnel experiments of Opaits et al.[130] confirmed that the stall angle of a NACA-0015 airfoil was increased from 15 to 21 degree using a single plasma actuator on the leading edge with a free-steam flow velocity as high as 75m/s. This result showed a promising future for plasma actuator applications and researchers[119, 126, 129, 131-133] made several studies to improve the performance of these actuators. To maximize the horizontal component of the induced boundary layer flow velocity and to obtain better efficiency from these actuators, several parameters such as actuator geometry, type of the dielectric material (Table 5.1), as well as the operating frequency and voltage can be selected.

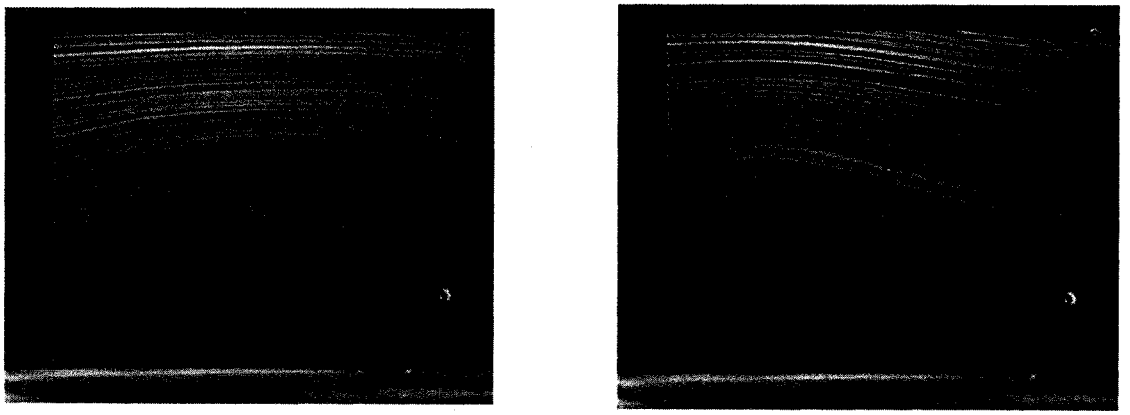

Figure 5.6 Flow attachment using plasma actuators[79]

5.4.1.1 Factors Affecting the Plasma Production

Data from an extensive set of measurements of the input power and flow horizontal velocity as functions of the dielectric material, the electrode geometry (Figure 5.7), the voltage, and the frequency summarized below[70, 127, 134].

a. Dielectric Material:

As shown in Table 5.1 materials have different electrical characteristics which effect plasma production. Among those materials listed, quartz and Teflon were found to be the best dielectric materials in terms of providing the highest induced flow velocities for the least power input. However, Kapton is also preferred by many researchers due to its high dielectric strength.

Table 5.1 Characteristics of some Dielectric Materials[79]

Material	Mass Density ρ (kg/m^3)	Dielectric Constant (ε_r) (room temperature)	Dielectric Strength (E) (room temperature)	Dielectric loss tanδ (1 MHz)	Loss Factor ε_r.tanδ
Teflon	2160	2.1	11.2 kV/mm	0.0001	0.00021
Quartz	2200	5	25 kV/mm	0.00001	0.00005
Glass	2600	3.8	10 kV/mm	0.004	0.0152
Lexan	1190	2.9 (1 MHz)	16 kV/mm	0.0085	0.02465
PC Board	1690	5	16.8 kV/mm	0.005	0.025
Kapton	1420	3.5	154 kV/mm	0.009 (100kHz)	0.0315

b. Electrode Geometry

Post[135] and Enloe[70] et al studied the effects of the geometry (Figure 5.7) on actuator performance and showed that major factor was the asymmetric setup of the electrodes. They also showed that the width of the lower electrode should be sufficiently large for plasma formation. It was also presented that a small gap or overlap of the electrodes does not change the performance of the actuators. However slight overlap was found to produce more uniform plasma.

c. Applied Voltage and Frequency

Orlov[134] showed that plasma velocity was increasing with increasing voltage analyzing the light emission from the plasma actuators (Figure 5.8). However Haack[136] showed that

beyond 9 kV_{p-p}, pressure drag reduction decreases for circular cylinders due to presence of laminar separation bubbles. Post[135] showed that best results were obtained when the applied voltage was in the form of "positive saw tooth". Orlov also showed that plasma velocity increases linearly with the AC frequency (Figure 5.8).

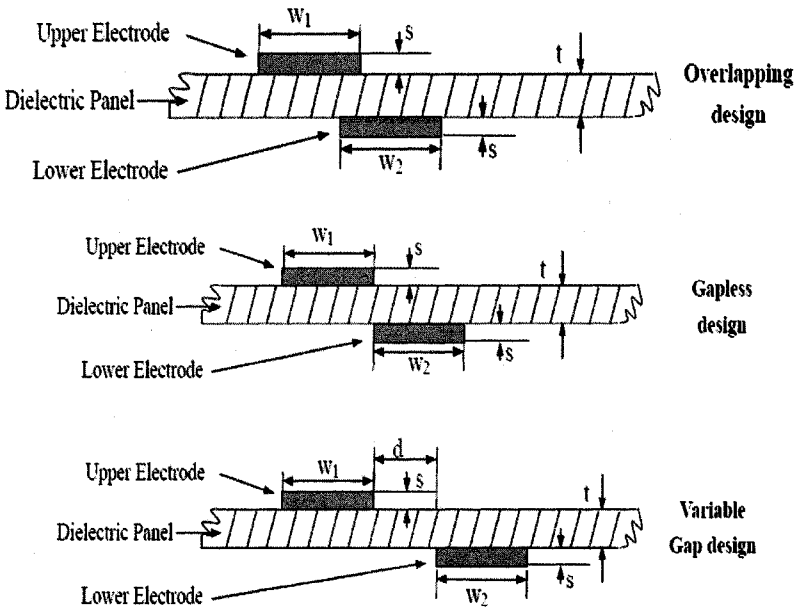

Figure 5.7 Dimensional parameters of plasma actuators[79]

5.4.2 Robustness of Plasma Panels

Previous tests for robustness of plasma panels showed that long-term, repeated use for flow re-attachment or flow control is feasible. Results from air jet tests, water spray tests, and wear tests were reported to have no significant problems. These actuators were also found to be electrically safe and easy to maintain[126].

5.4.3 Advantages of Using Plasma Actuators

Plasma actuators have the ability to create a glow discharge at atmospheric pressure. The electrodes used for these actuators have characteristics which lend themselves to practical

engineering applications, such as simplicity and robustness. In the present work an actuator without moving parts and with high bandwidth was preferred due to ease of construction and the high frequency flow fluctuations in the wake of a bluff body. These actuators are also scalable in size, hence were easily placed on the test models.

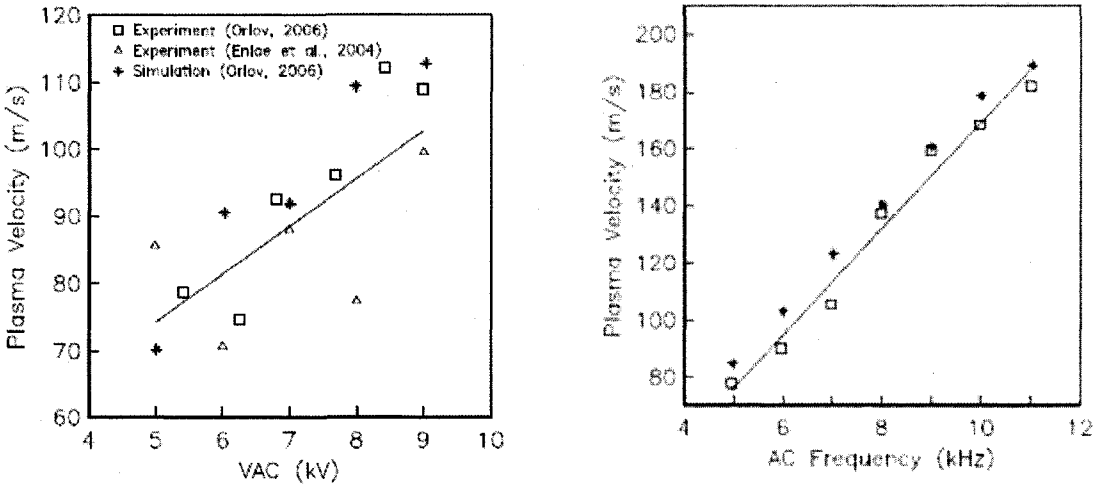

Figure 5.8 Effect of input voltage and AC frequency on velocity[134]

6. EXPERIMENTAL SETUP

6.1 Introduction

In this chapter the ODU low-speed wind tunnel, the instrumentation used for data acquisition, the model, the hot-film probe used for one-dimensional flow measurements and the Particle Image Velocimetry (PIV) system are introduced. A cylinder and an axisymmetric bluff body model were tested to provide an experimental database. The frequency of the vortex shedding for phase calculations was obtained by using a hot-film mounted on a traverse mechanism. Velocity field measurements in three planes were made by using a Particle Image Velocimetry (PIV) system in a two and/or three dimensional configuration.

6.2 Test Facility

6.2.1 The ODU Low-Speed Wind Tunnel

The Old Dominion University Low-Speed Wind Tunnel is an atmospheric pressure, closed return, fan-driven type which has two tandem closed test sections 9x8x7 ft and 3x4x8 ft respectively (Figure 6.1). The drive power of the tunnel is provided by a 125 hp AC induction motor. The motor drives a 14 bladed fan by means of a belt system. The speed of the tunnel is adjusted by a variable frequency controller[137].

As can be seen from figure 6.1, tests can be performed in either of the two tandem test sections. The present test was performed in the downstream "high-speed" test section that has a cross-section of 3x4 feet at the entrance. The floor and ceiling of the tunnel are steel

and do not diverge along the test section, although the Plexiglas sidewalls diverge at an included angle of approximately 0.6°. This divergence prevents the wall boundary layer growth from producing a longitudinal static pressure gradient. The tunnel test section dynamic pressure value is in the range of 1 to 30 psf (48 to 1436 Pa), which equates to an indicated-velocity range of 30 to 165 fps (10 to 55 m/s). The lower bound is set by the stability of the fan r.p.m. while the upper is set by the maximum drive power. The tunnel has two 20 mesh/inch, 0.017 inch wire screens with 0.564 solidity (0.436 open area ratio) which provide flow conditioning and suppression of the lateral variations of the longitudinal velocities. There is also one honeycomb with 0.512 inch (13 mm) diameter cells to break up large-scale turbulence and suppress swirl. In the empty test section, the free stream turbulence is around 0.2%, slightly decreasing at higher velocities. Although there is no thermal control for the test section, a steady-state condition is reached below about 70% of the maximum speed. The test section has a 3-axis traversing mechanism with a resolution of ±0.01 inch in the longitudinal (downstream) lateral directions, and ±0.001 inch in the vertical direction. While tunnel reference speed was obtained by Honeywell Precision Pressure Transducer (±0.05% FS, 12 bit), test section temperatures in this facility were acquired by a Hewlett Packard 3497A Data Acquisition and Control Unit (Figure 6.2).

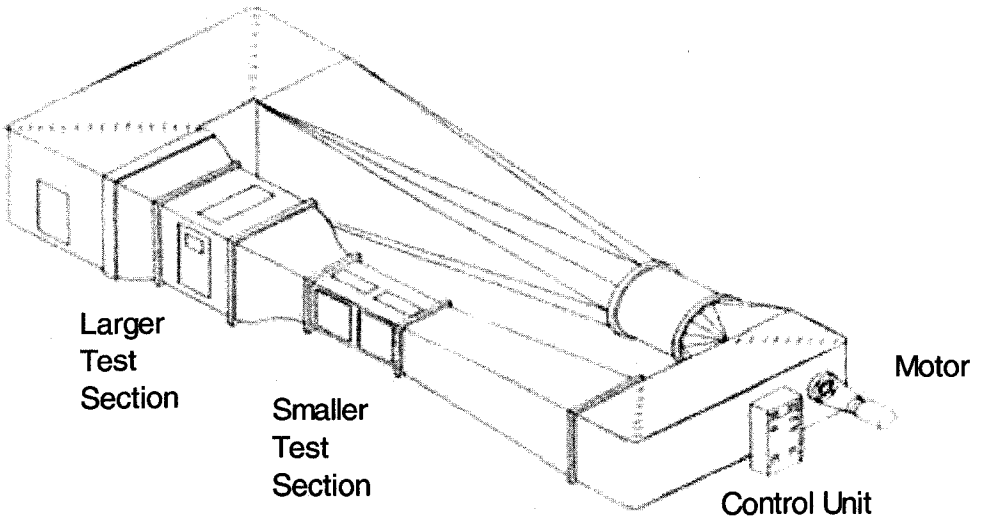

Figure 6.1 ODU Low-Speed Wind Tunnel

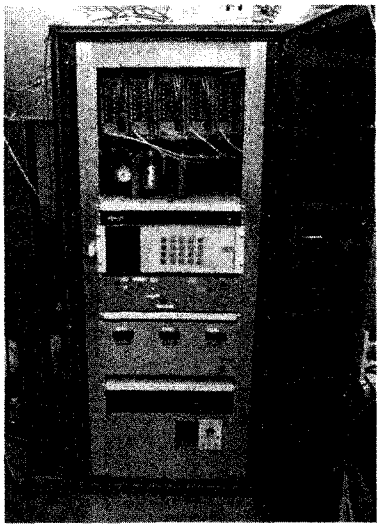

Figure 6.2: Hewlett Packard 3497A Data Acquisition and Control Unit

6.3 Models

Two circular cylinders with 3.5" and 4.5" diameters with length-to-diameter ratios 10.3:1, and 8:1, respectively were used in experiments to investigate the use of the proposed data analysis methods. However, only the larger cylinder was used in flow control applications. Both cylinders were mounted vertically in the test section allowing

study of the crossflow properties (Figure 6.3). The axisymmetric bluff body used in this work is presented in Figures 6.4 and 6.5. Aluminum and PVC bodies were built to use with the forebody inherited from the previous work[29]. The body surfaces were machined and later spray painted. The model was supported by a streamlined, wing-like strut attached to the front of the aluminum forebody which produces a favorable pressure gradient in the region of the strut. This was thought to reduce the boundary layer disturbance, whereas attaching the strut to the center body was likely to cause boundary layer tripping[29]. Existence of a turbulent boundary layer prior to the base was shown by Alcorn[29]. The overall model length-to-base ratio was 5.75:1. Blockage or other boundary corrections were considered to be unnecessary[29] since the model cross sectional area to test section area ratio was less than 1%.

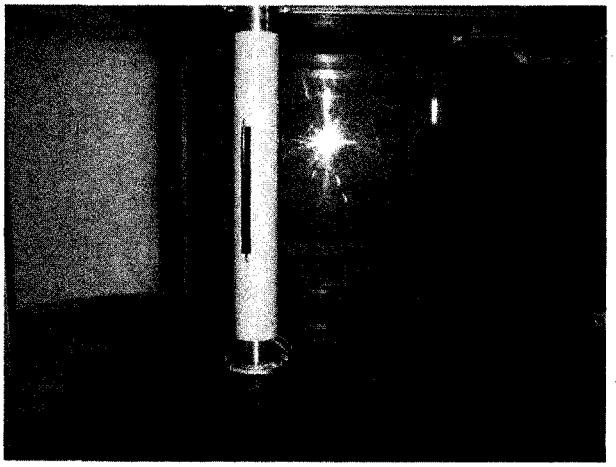

Figure 6.3 Circular Cylinder

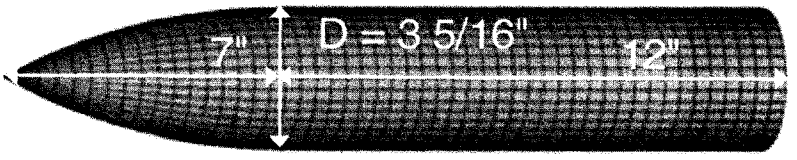

Figure 6.4 Ogive Cylinder Dimensions

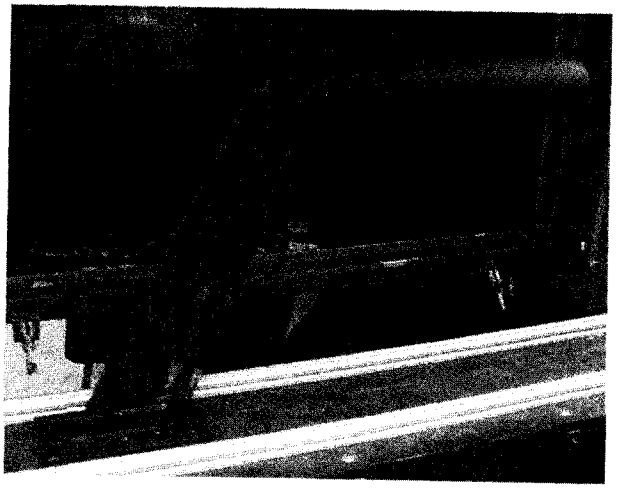

Figure 6.5 Ogive Cylinder

6.4 Hot-film Probe

A TSI, IFA-100 constant-temperature, hot-wire/hot-film anemometer was used for frequency measurements (Figure 6.6). Two custom written LabView programs (VIs) were used for probe calibration, data acquisition, and data analysis. The sensors used were commercial TSI 1201-20, operated at an overheat of 1.55. Conventional calibration processes generated a best-fit 4^{th} order polynomial relating hot-film probe voltage to velocity.

A single hot-film probe was used to extract predominant flow frequencies and to calculate phase angles to use in data grouping (Figure 6.7). Hot-films are fiber film probes that show similar characteristics to hot-wires. These probes generally have higher frequency response than the structures in the flow (frequency bandwidth up to 10 KHz). The hot-film probe was placed on a three-axis traverse system and positioned at the location, x/D=7 for the ogive cylinder and x/D=3 for the circular cylinder. The selected radial and angular position for the probe corresponded to the location where the hot-film signal was most periodic. Periodicity of the signal was determined by the help of the hot-

film VI and by the help of an oscilloscope (Figure 6.6). This set-up can be seen in Figure 6.8. Turbulence intensities at this location were below 10%, allowing proper calibration for the system. Power spectra were constructed with 200,000 velocity samples, taken at 10,000 Hz.

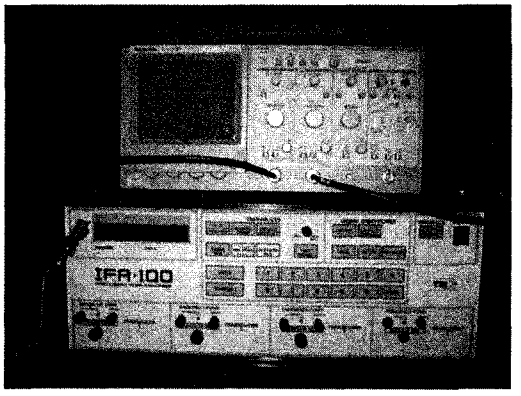

Figure 6.6 Hot-wire Anemometer and Oscilloscope

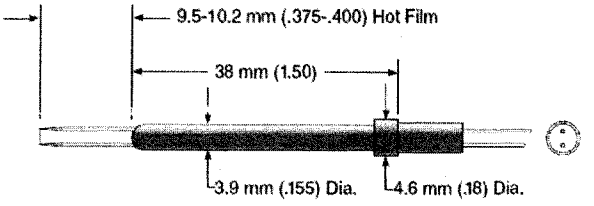

Figure 6.7 Hot-film Probe

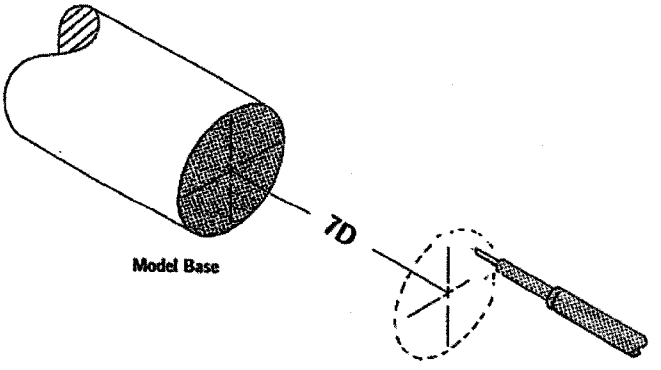

Figure 6.8 Hot-film Probe Set-up

6.5 Particle Image Velocimetry (PIV) System

6.5.1 Introduction to the PIV System

The PIV system has the ability to measure 2-D velocity vectors over a planar slice of flowfield at many points simultaneously. It can also be used in stereo configuration to obtain all three components of a velocity vector. Valuable information for understanding flowfield structures and temporal statistics can be developed from multiple sequential measurements using a PIV system.

For observation of the flowfield, illumination with two consecutive bright light flashes is required. Pulsed lasers are excellent light sources for this purpose. Velocity vectors are resolved from the displacements of the seeding particles. CCD cameras and PC based image processing are used in data processing.

6.5.2 PIV System Hardware Overview

Synchronizers for timing laser pulses, cameras and the light source are the main components of the PIV system (Figure 6.9). ODU PIV system is composed of a dual pulse Nd-YAG laser capable of 50 mJ/pulse (Figure 6.10), and a PIVCam 13-8 crosscorrelation camera which has 1280x1024 pixel resolution and 12-bit intensity dynamic range (Figure 6.11). The system is controlled by TSI Insight software with a frame rate of 3.75 fps for 2-D and 1.875 fps for stereo measurements. 2-D and stereo setup can be seen in Figure 6.12[138]. The air flow is seeded with smoke to make it visible for the CCD camera using a smoke generator (Figure 6.13).

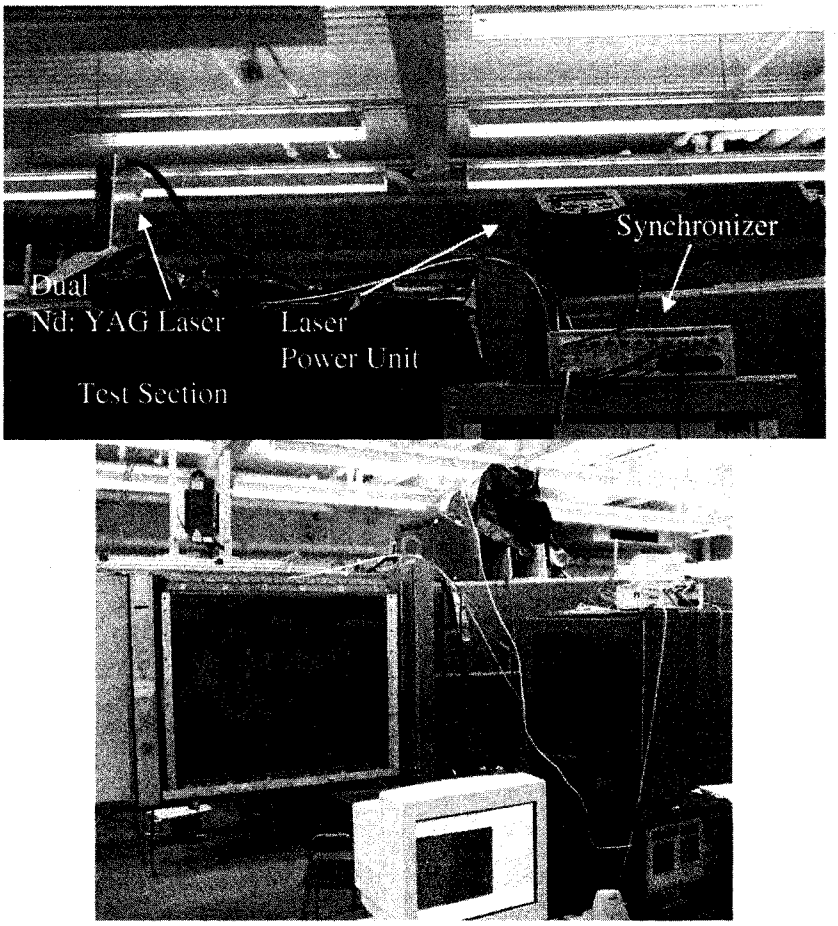

Figure 6.9 Hardware arrangements of PIV System

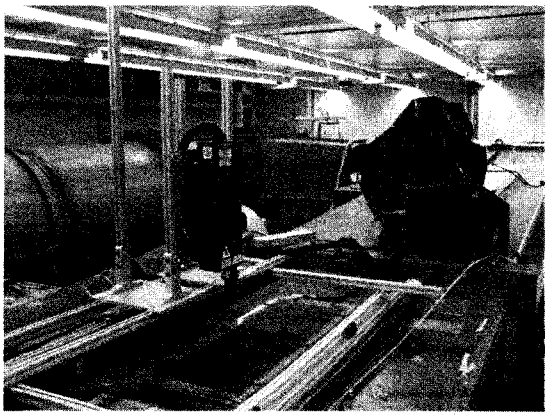

Figure 6.10 Dual Nd:YAG Laser

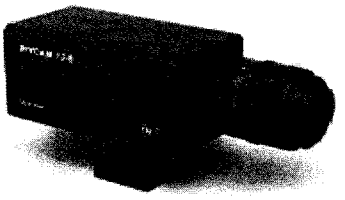

Figure 6.11: TSI PIVCAM 13-8 Model 630047

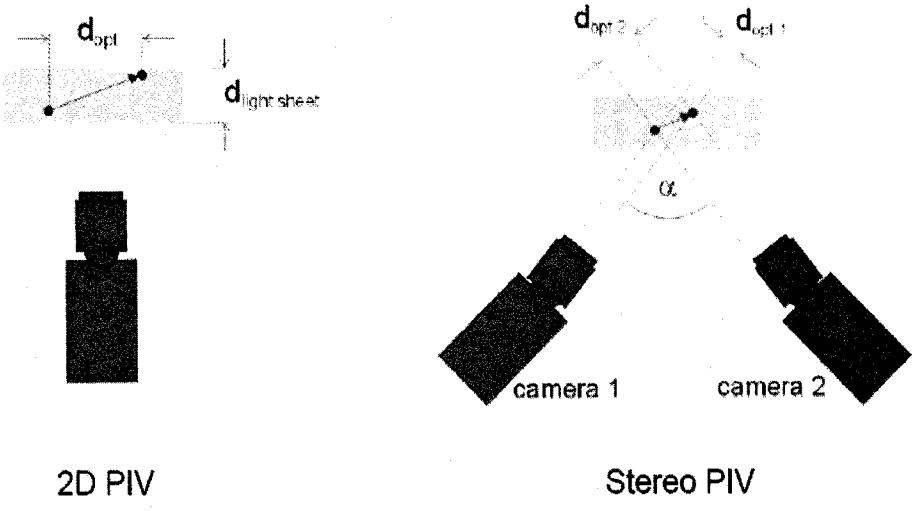

Figure 6.12 2-D and Stereo PIV Setup[138]

Figure 6.13 Smoke Generator

6.6 Other Equipment Used for Test Cases

In order to evaluate the proposed data analysis techniques some test cases were run. To compare the phase revolved images to actual locations of an object, several tests were

carried out using a system composed of a motor, an encoder and a flat plate. A flat plate spinning counterclockwise with dimensions of 3.75'' x 5.63'' on the shaft of a motor was mounted perpendicular to the tunnel floor. Pictures of the spinning plate were recorded using the CCD camera. The position of the plate was recorded using an encoder also mounted on the drive shaft. Later, images grouped using the proposed techniques were verified using the encoder data.

In the majority of these tests a Brevel motors Model #:780-953075, giving 65 rpm when 36 volts was applied, was used (Figures 6.14, 6.15). Some early runs were made with a faster (1550 rpm) motor (Figure 6.16). The order of magnitude of the speed of rotation was much faster than the structures in the actual flow case, so a replacement was made.

The encoder used was a US Digital MA2 (B8) miniature rotary absolute shaft encoder which reports the shaft position over 360° with no stops or gaps. The MA2 is available with an analog or a pulse width modulated (PWM) digital output. The analog output (MA2-A) provides an analog voltage that is proportional to the absolute shaft position with. 10-bit resolution.

After obtaining satisfactory results in the plate tests, a more complex case was analyzed. Von Karman Street vortex structures behind a cylinder with a radius of 3.5''and a cylinder with 4.5", placed from the ceiling to the floor of the tunnel, were observed. Last, tests with the ogive cylinder introduced previously were carried out.

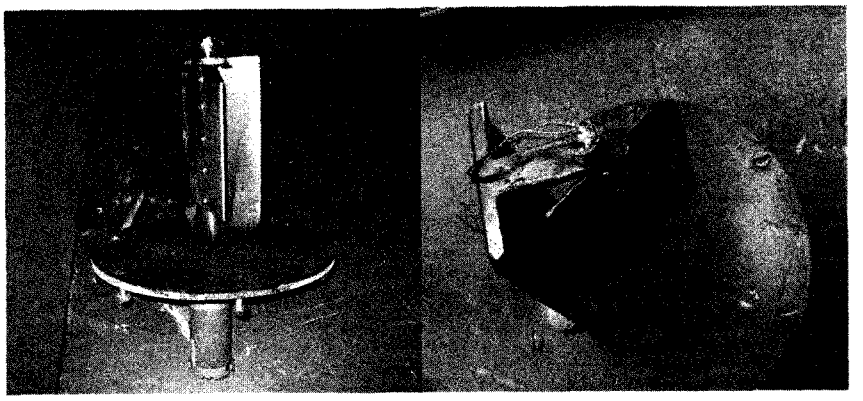

Figure 6.14 Flat plate, motor, encoder

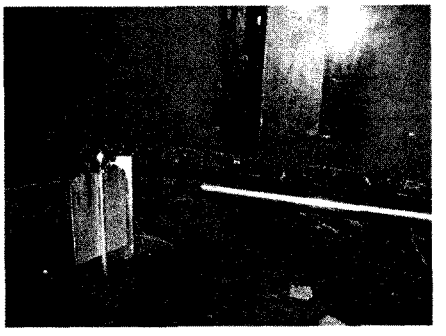

Figure 6.15 Flat plate and hot-film probe

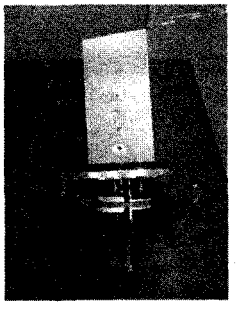

Figure 6.16 Flat plate, motor, encoder (First Case)

6.7 Plasma Actuators

Design and construction methods for the actuators are based on prior experiments by Haack[136]. Plasma actuators consist of two electrodes separated by a dielectric layer, where one of the electrodes is exposed to the air and the other one is covered by the

dielectric material. In these experiments two 1/4" strips of 2.5-mil thick copper tape were used as electrodes and one 3/4" wide strip of 5.0-mil thick Kapton tape was used as the dielectric material. The ends of the copper strips were rounded as suggested by others[136] to prevent high electric field concentrations at the corners causing dielectric failure. The actuators are constructed on the test bodies by first placing a layer of copper strip at the desired angular position, and then covering this layer with the 3/4" Kapton tape. Last the second copper strip is placed such that its downstream edge overlaps the upstream edge of the lower electrode. The size of the overlap region can be chosen in the order of mm; 1 mm for the current cases. The upper electrode is wired to ground and the lower electrode is connected to the high voltage signal resulting a downstream induced flow tangential to the surface.

6.7.1 Actuator Electronics

To produce the power needed for the actuators a signal generator, intermediate amplifier and step up transformer were used. The amplifiers and transformers were loaned by NASA Langley Research Center (Figure 6.17). Two sine waves with 90° phase were generated using a PC to input into two Compact Power Company Titan Series high voltage amplifiers. These amplifiers had a maximum output of 260 V_{rms} at 4 Amps. Signals from the amplifiers were passed through a Corona Magnetics 1:25 step up transformer designed to be used with signals with frequencies ranging from 400 Hz to 40 kHz before reaching the actuators (Figure 6.18). During operation, the transformers produced an audible tone at the operating frequency (5kHz for these tests) as reported by Haack[136].

The applied voltage and current drawn from the actuators was monitored by an oscilloscope and was read and recorded using a NI-PCI 6221 (16-Bit, 250 kS/s, 16 Analog Inputs) data acquisition card together with a NI BNC-2110 connector block. The actuator voltage was run through a Tektronix P6015A High Voltage Probe before reaching the oscilloscope. The current was read by passing an actuator lead through a current transformer. Neither actuator was tested for endurance but the lifespan of the actuators exceeded the requirements of this testing unless the applied voltage exceeded the recommended maximum, which was around as 11.8 kV_{p-p}[136].

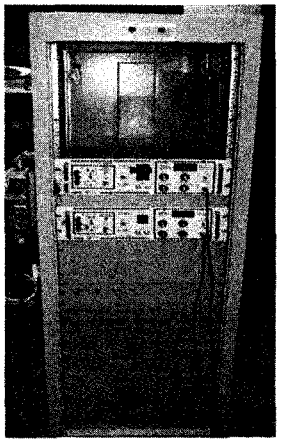

Figure 6.17 Actuator Control Unit

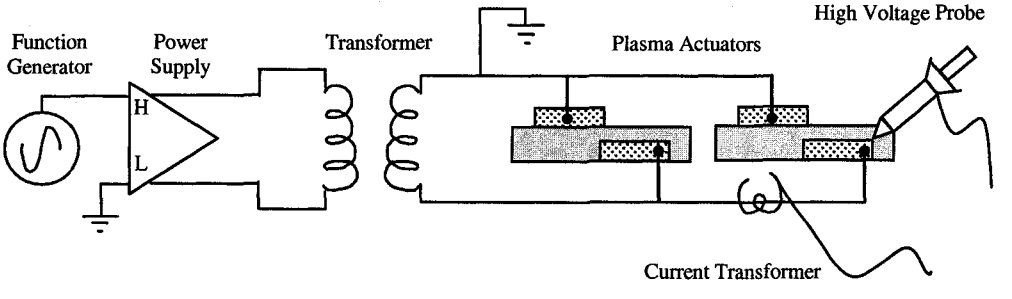

Figure 6.18 Actuator electronic setup for plasma actuators

7. RESULTS

7.1 Introduction

In this chapter the experimental results and brief explanations of the flow fields will be presented. Results include predominant frequency measurements, PIV tests with/without data processing and tests with the externally controlled PIV system on the spinning plate, cylinder in cross flow and ogive cylinder (Table 7.1). Data acquisition methods namely, predictive angular triggering technique (PATT) and tracking triggering technique (TTT), as mentioned in Chapter 3 were used to produce phase averaged images. 30 PIV images were averaged for each angular location from 0 to 180 degrees with increments of 30 degrees for the externally controlled system. 600 PIV images allowing about 15 images per angular bin collected over 10 runs were used for the phase averaging experiments.

Table 7.1 Experimental Cases

Measurements	Spinning Plate	Cylinder	Ogive Cylinder
Predominant Frequency			✓
Externally Controlled PIV	✓		
PIV with Phase Averaging	✓	✓	✓
Flow Control		✓	✓

7.2 Evaluation Tests

Before using the proposed techniques on the actual model (ogive cylinder) tests with spinning flat plates were made, due to the clear periodic wake structure. After obtaining successful results in these tests, a test with a more complex flow was made. TTT was applied to a 2-D cylinder in crossflow. Successful results proved the way for later runs with the ogive cylinder.

Flat Plate

The first experiments were conducted with a 3.75"x 5.63" flat plate mounted on a motor shaft spinning at a rate of 65 rpm. Free stream velocity was set to 25m/s giving a Reynolds number of 160,000 based on the width of the plate. This model was used for the evaluation of the both triggering techniques. PIV measurements were first made using an external trigger to test PATT and later "free" PIV measurements were made to evaluate TTT. A hot-film probe placed at x/w=3 provided the phase information to calculate triggering times and to use in the averaging techniques (Figure 7.1).

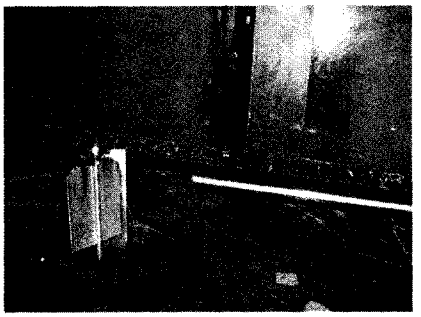

Figure 7.1 Flat plate and hot-film probe

Figure 7.2 shows the application of PATT where PIV images were recorded only at desired instances. In this figure actual images of the plate, velocity and vorticity (with streamlines) fields are presented. Here, comparison of the actual digital images and vector fields clearly shows that the external triggering system and PATT produced successful results since the increment of the rotation angle can easily be verified and repetitive results are possible. In the actual image the support of the spinning plate, encoder and the remaining part of the plate are visible. Next to the actual images velocity magnitude and vorticity plots in thirty degree increments are shown. In the velocity

magnitude and vorticity plots a digital image of the support and the encoder is superimposed in the top right corner where it actually exists. Orientation of the plate is also demonstrated by drawing a white rectangular box. A low velocity region is observed just behind the plate in the velocity plots where the flow enters from the top. Vorticity

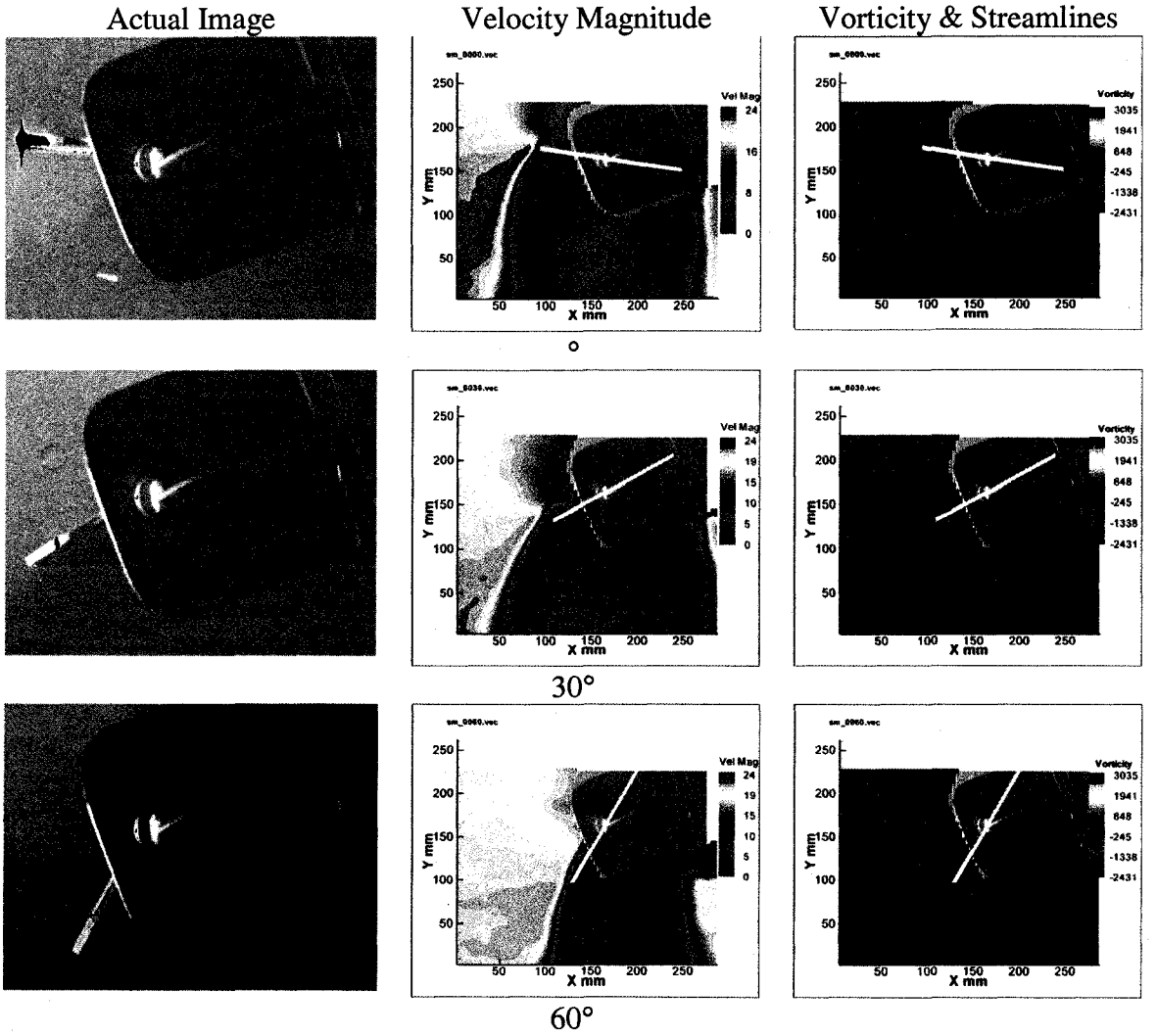

Figure 7.2 Actual position and the wake field obtained by using PATT of the spinning flat plate

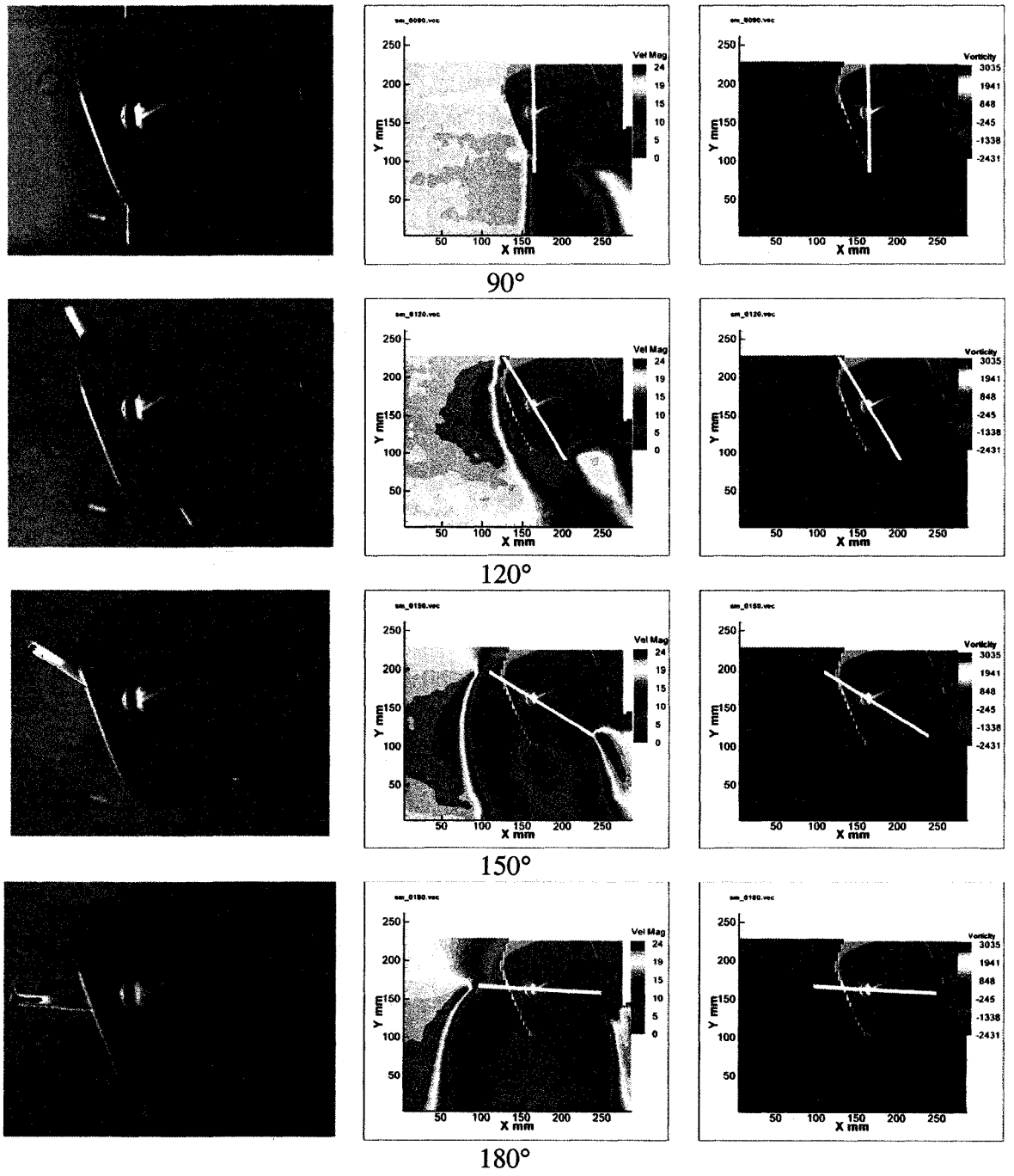

Figure 7.2 Continued

and streamline plots reveal the existence of the positive and negative shear layer as well as generation of the two vortices. While this method was suitable for periodic structures whose frequency is in the order of 1-10 Hz, it was not found to be appropriate to use for

flows with higher frequencies because of limitations of the available hardware. To overcome those limitations, the tracking triggering technique (TTT) was chosen to be used in the analysis. Before moving to this method, the support of the spinning plate was modified in order to have more viewable area. It should be noted that the location of the plate was also changed and free stream velocity was set to 30m/s. Figure 7.3 shows the velocity magnitude and vorticity-streamline plots obtained through TTT method where the flow enters from left side. Since the motion is periodic only the data from 10° to 180° is presented.

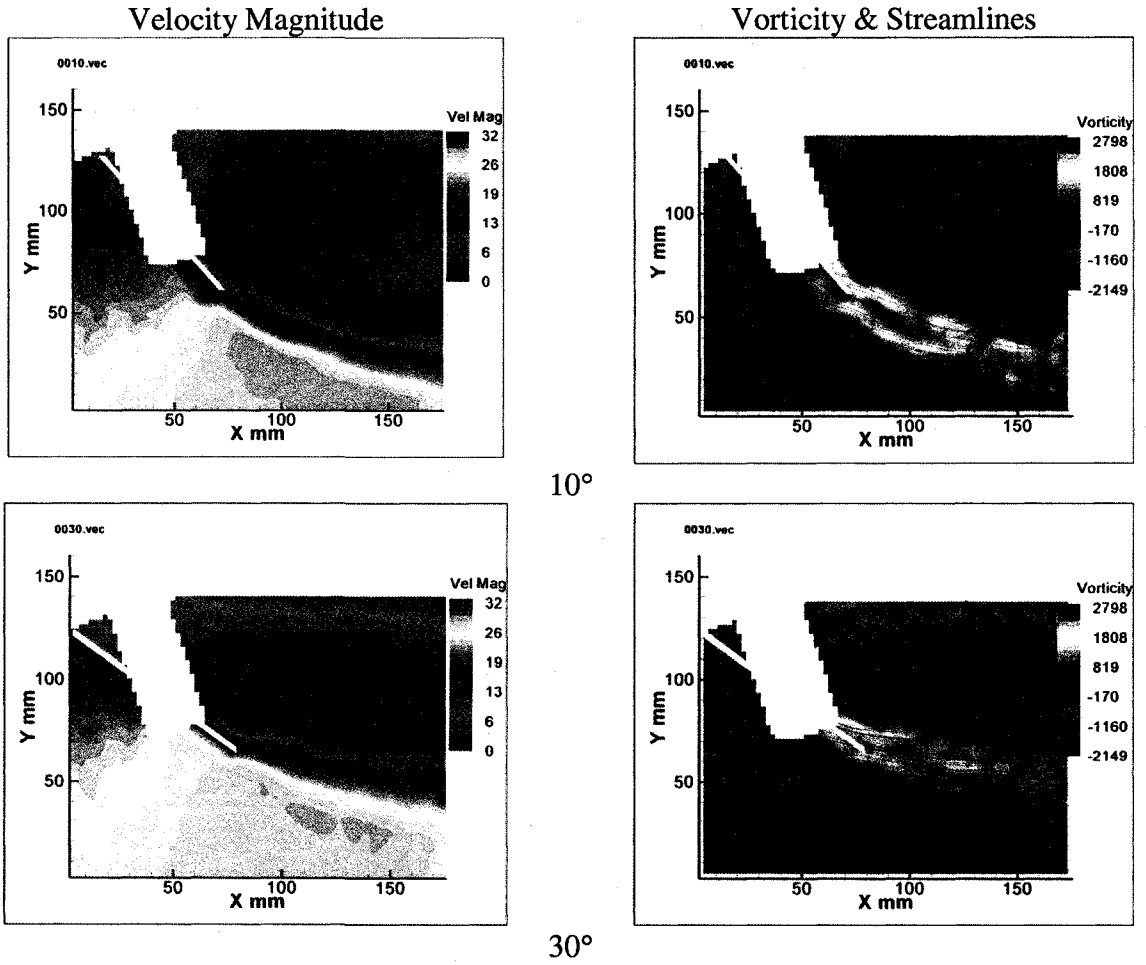

Figure 7.3 Wake field for the spinning flat plate using TTT

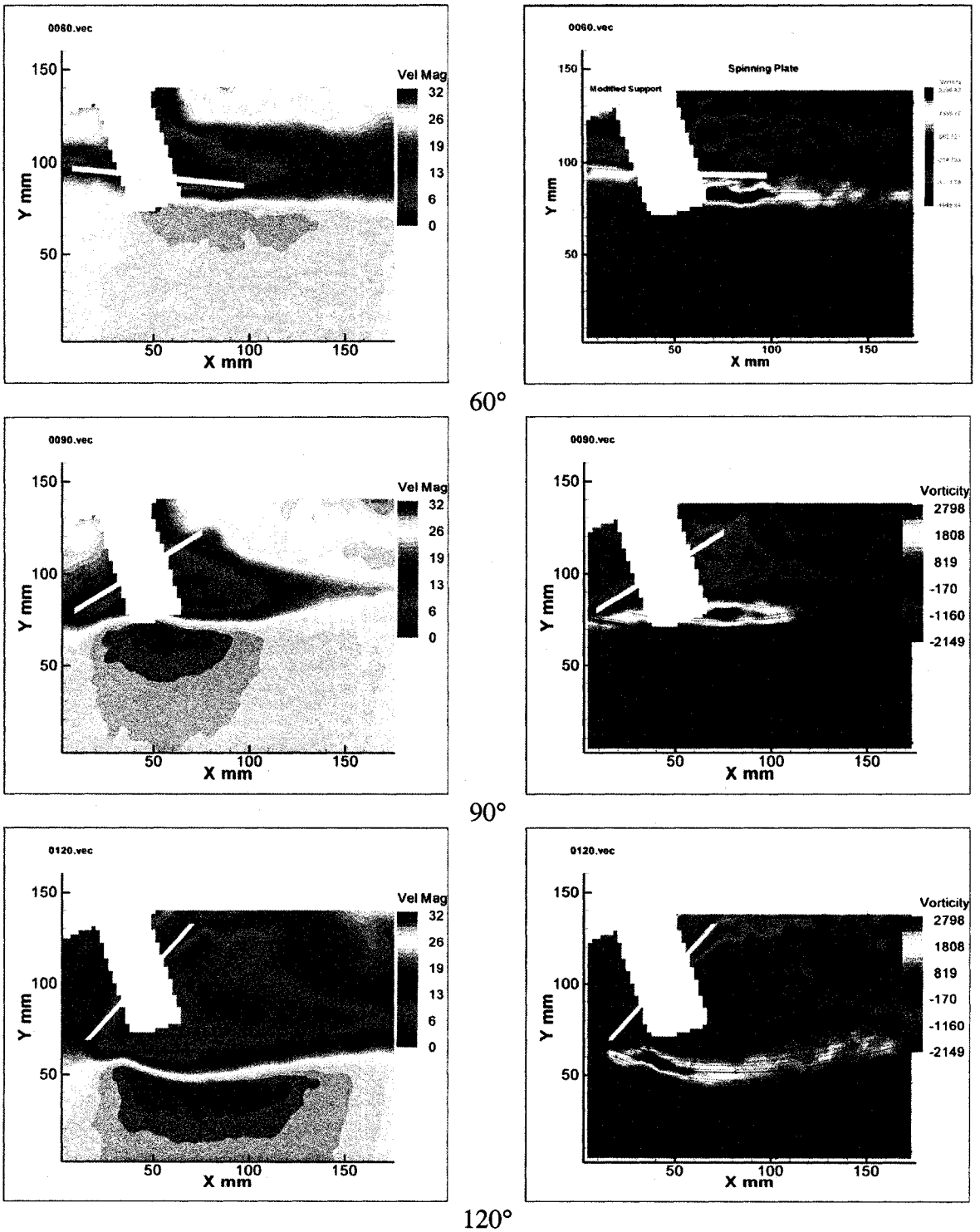

Figure 7.3 Continued

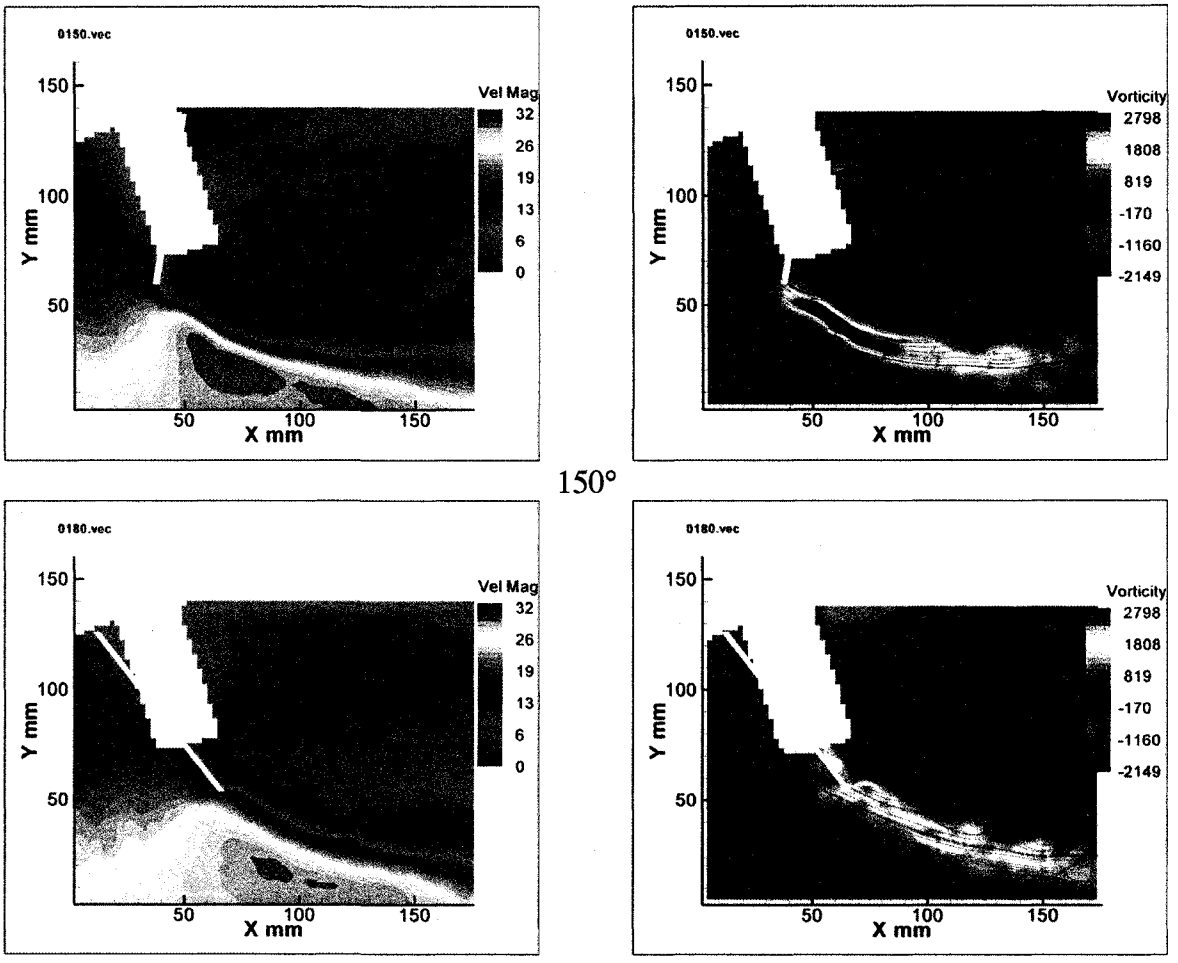

Figure 7.3 Continued

Incremental changes in the rotational angle of the plate can again be easily followed from frame to frame. It is possible to see the evolution of the low velocity region behind the flat plate. As well as a positive and negative vorticity field on each edge of the plate with successful application of TTT attention moves to a more complex flow field, that is cylinders in crossflow.

Cylinders

The near wake behind a cylinder with 3.5" diameter at 30 m/s giving a Reynolds number of 180,000 was analyzed using the TTT method. The hot-film probe was placed 3 diameters downstream from the model base. Figure 7.4 shows the very well known highly-energetic wake, characterized by the presence of a double row of alternate concentrated vortices (the Karman vortex street). This vortex shedding phenomenon is typical of all two-dimensional bluff bodies, and has a great practical importance. Sequences of phase averaged PIV images at different stages of wake development within a shedding cycle revealed the evolution of the classical vortex street for the cylinder. Immediately downstream of the cylinder, a strong recirculation region exists. The core of each developing vortex is characterized by a region of low absolute velocity (forced vortex), denoted in blue in the Figure. In the first frame a shear layer from lower side of the cylinder wraps around an incipient counterclockwise vortex. This vortex is seen to grow and convect downstream. In the last frame, one-half cycle later, a shear layer from the upper surface wraps around a clockwise vortex. Vorticity-streamline plots shows the same flow at the same times, but with vorticity highlighted and streamlines overplotted. Each vortex entrains a section of the shear layer from the appropriate side of the wake. This pair of image sequences are clearly consistent with the classical model of alternate vortex shedding from upper and lower surfaces, resulting in development of the von Karman vortex street. The average wake flow field can be seen in Figure 7.5.

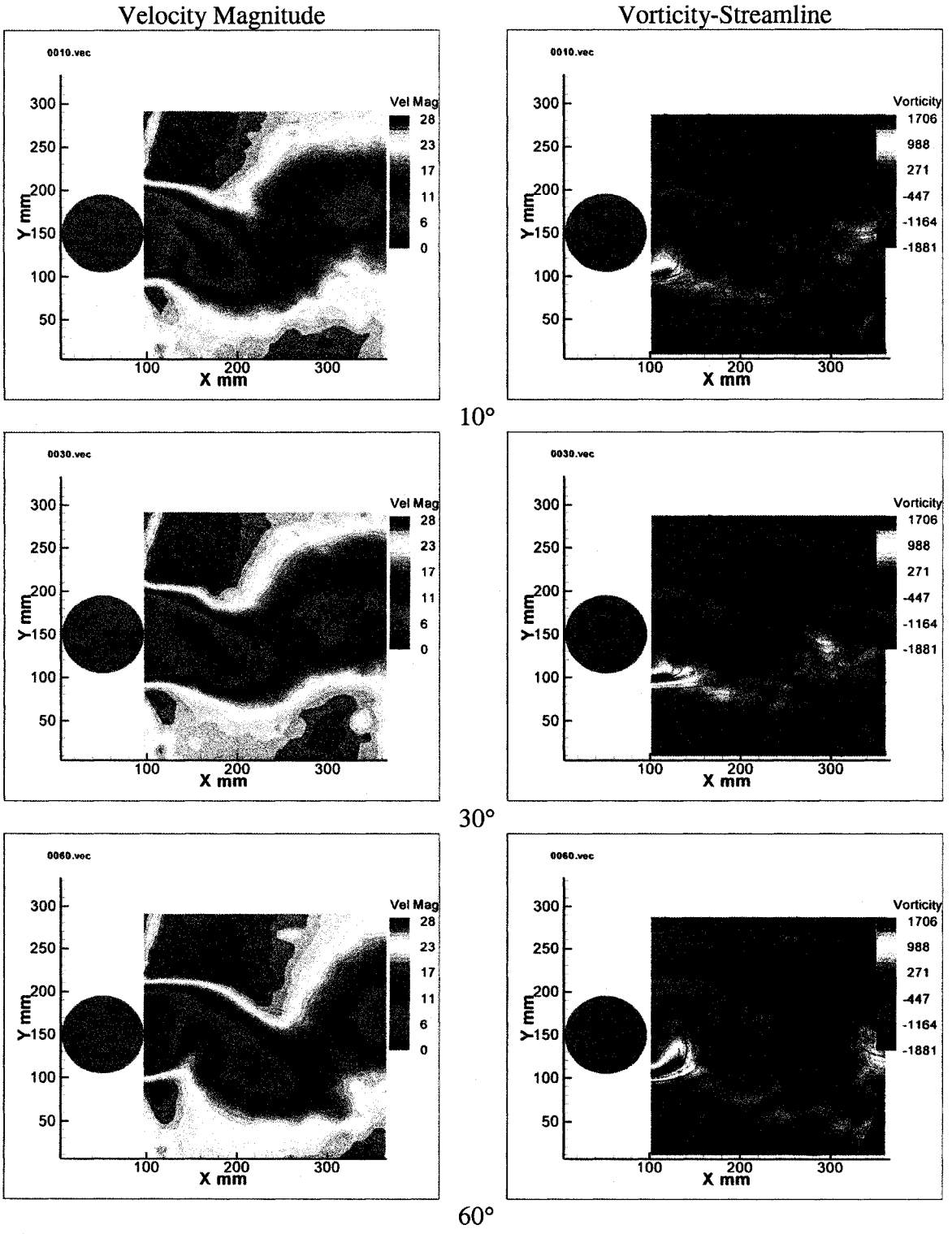

Figure 7.4 Wake field for the cylinder using TTT

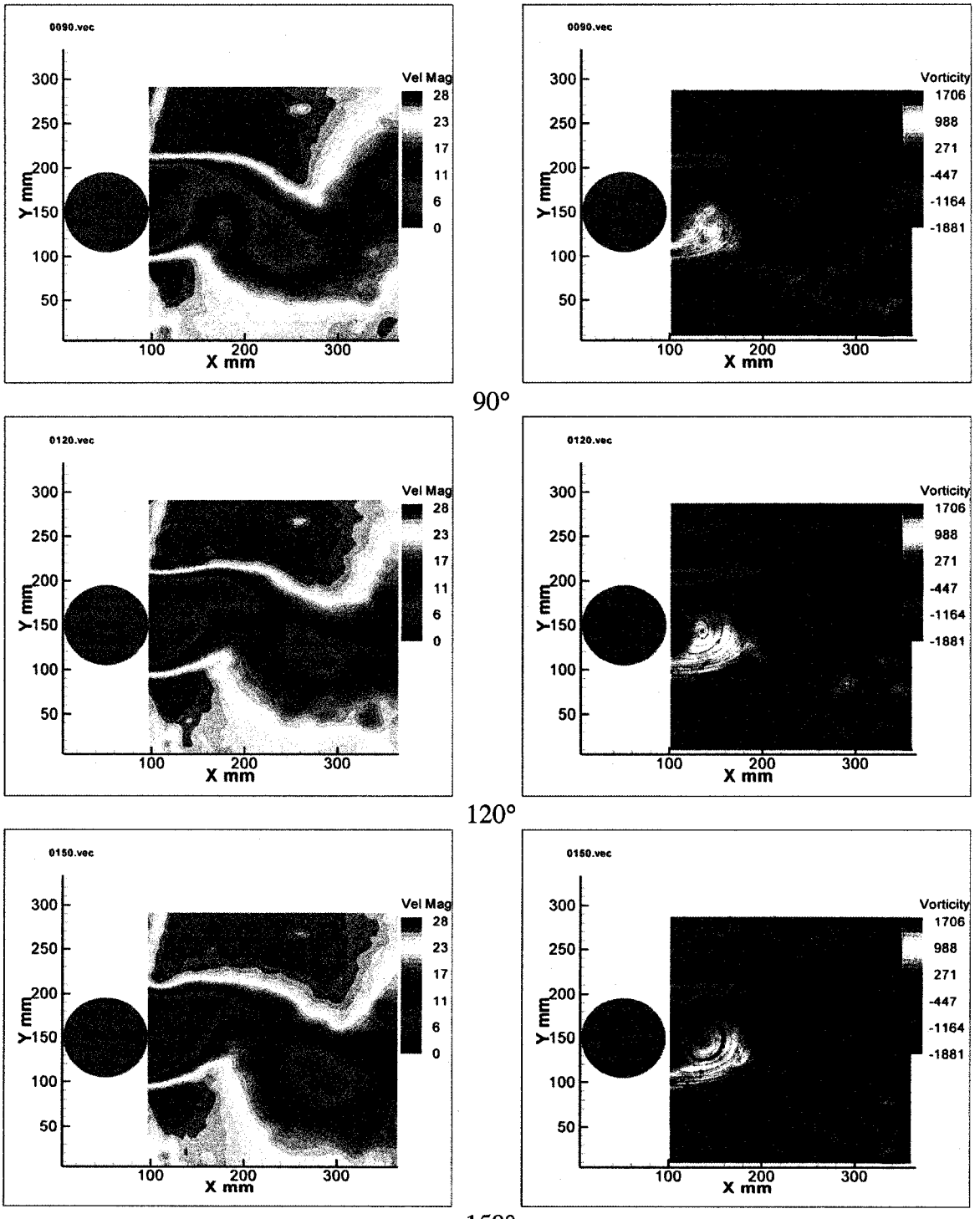

Figure 7.4 Continued

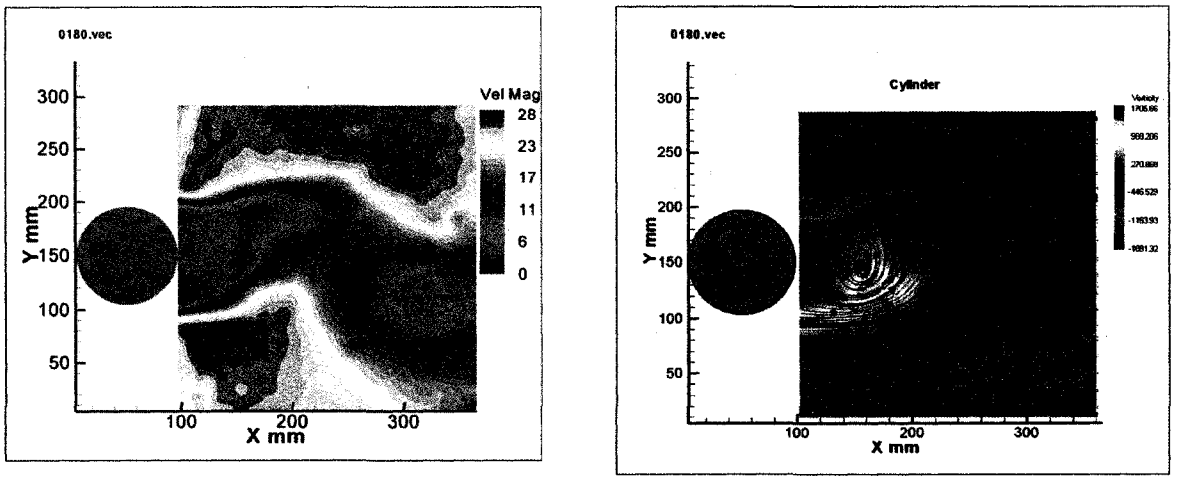

180°

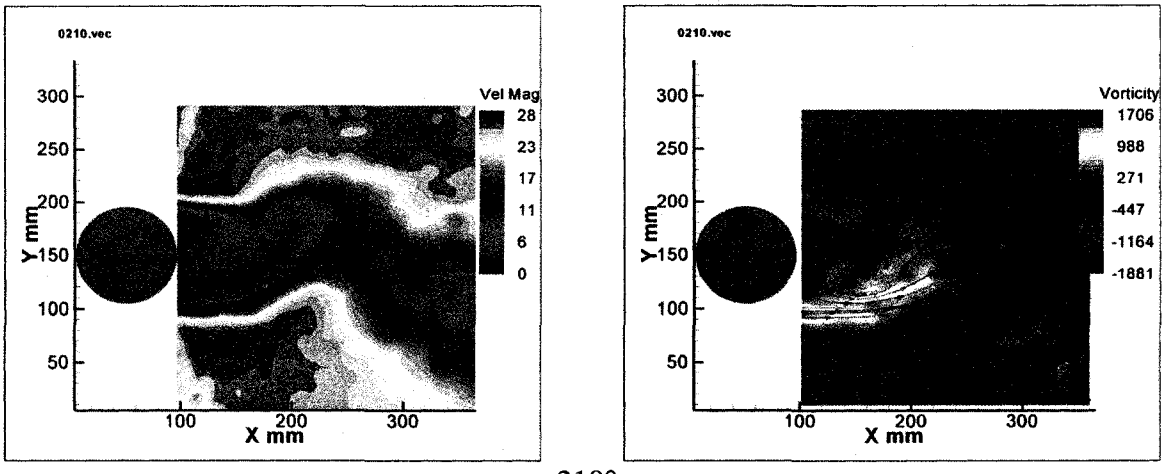

210°

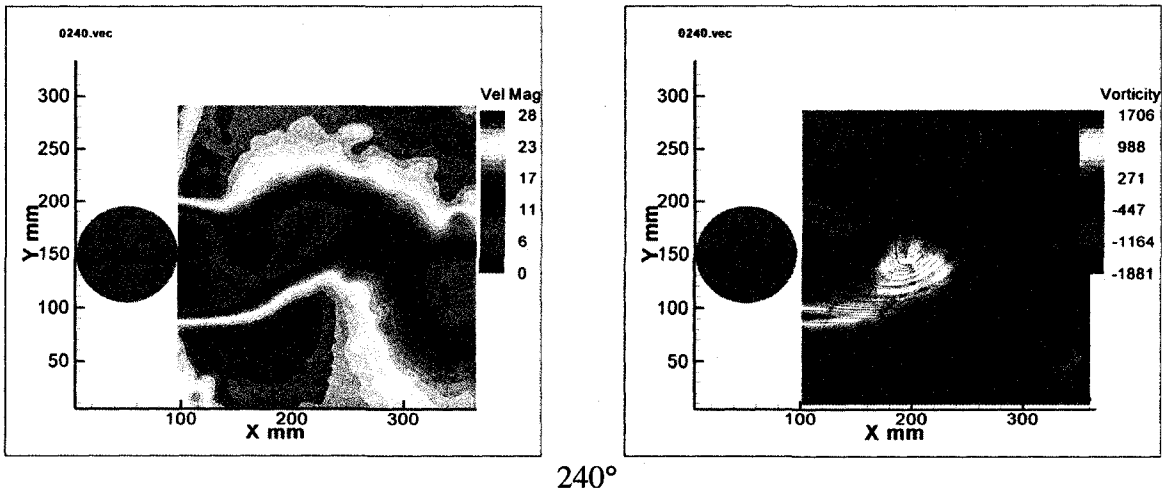

240°

Figure 7.4 Continued

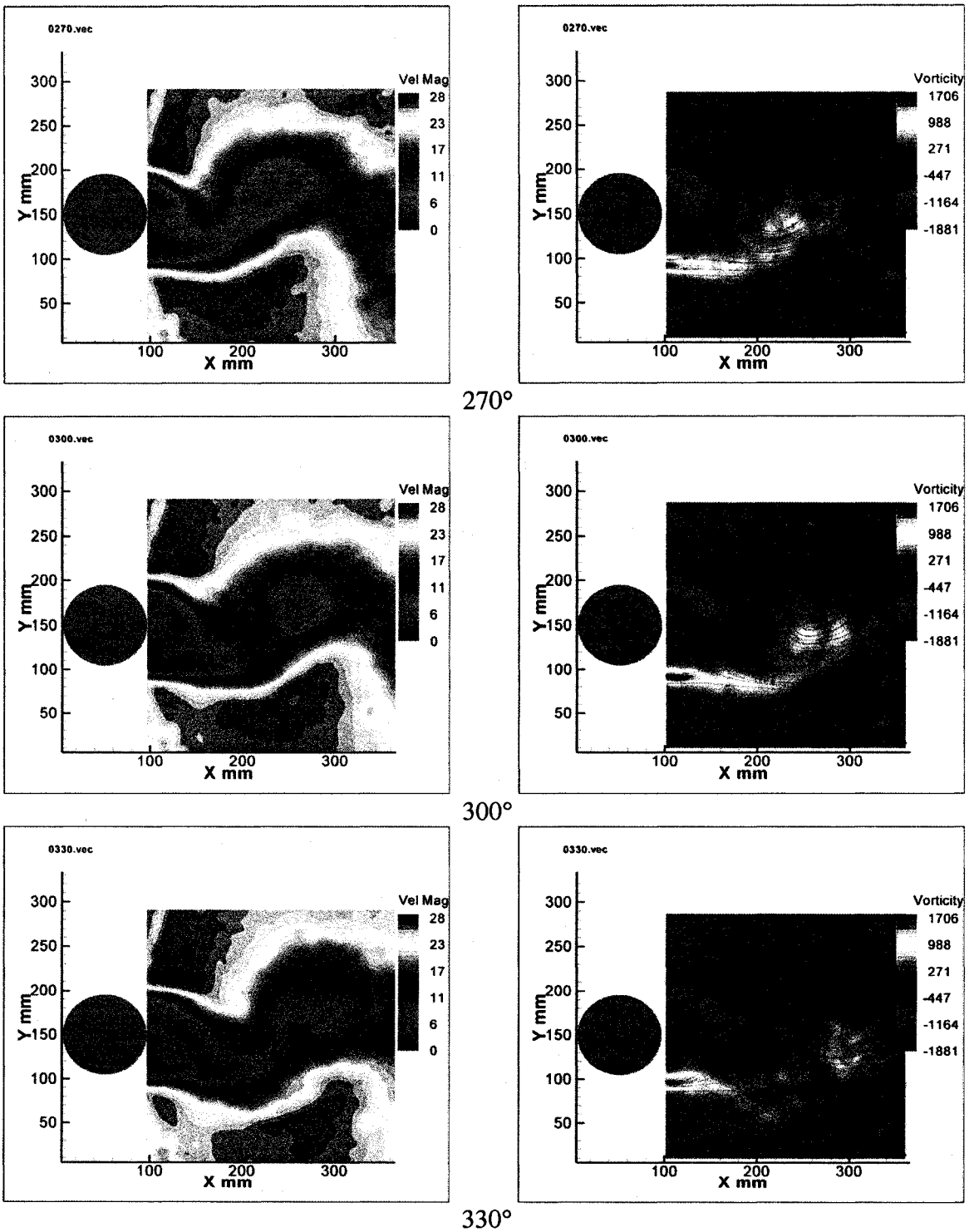

Figure 7.4 Continued

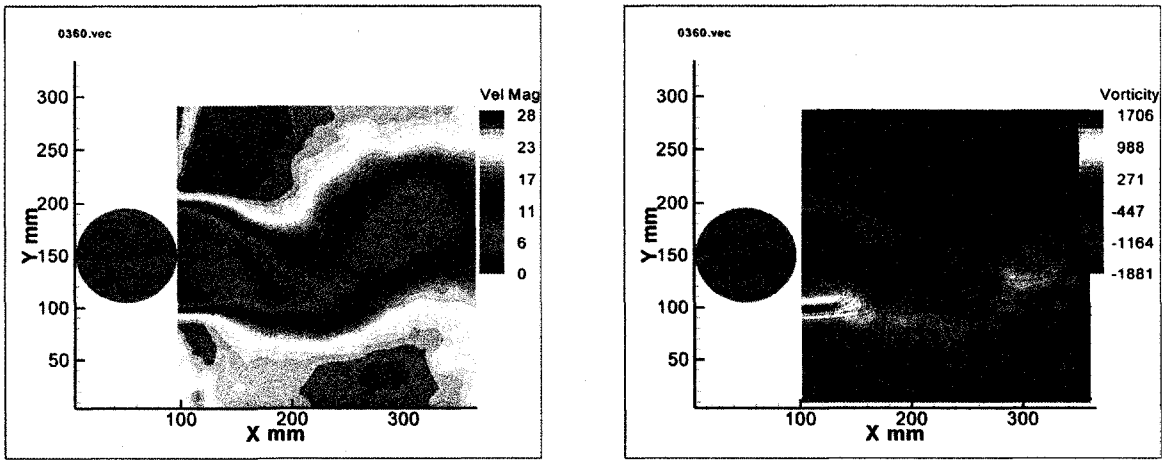

360°

Figure 7.4 Continued

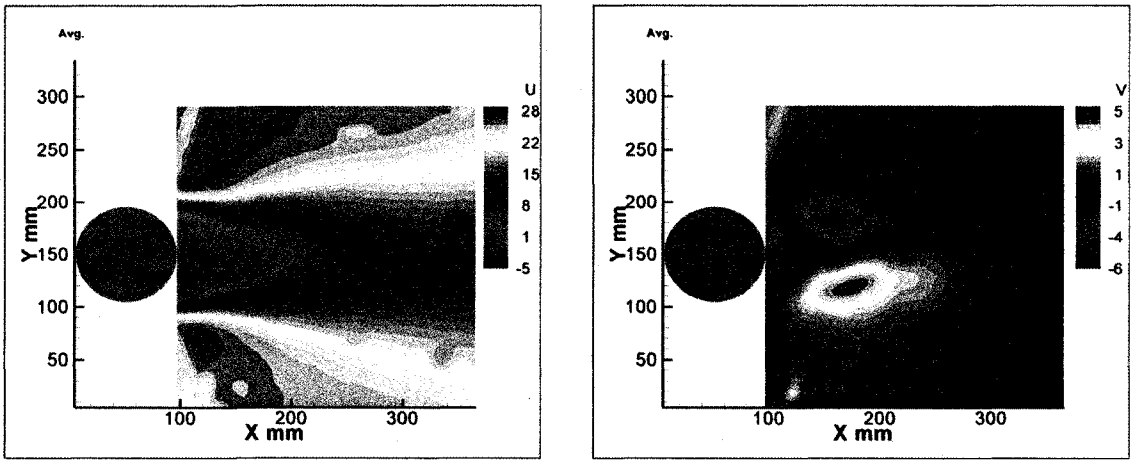

U Velocity

V Velocity

Velocity Magnitude (Contour)

Velocity Magnitude (Vector)

Figure 7.5 Average wake field

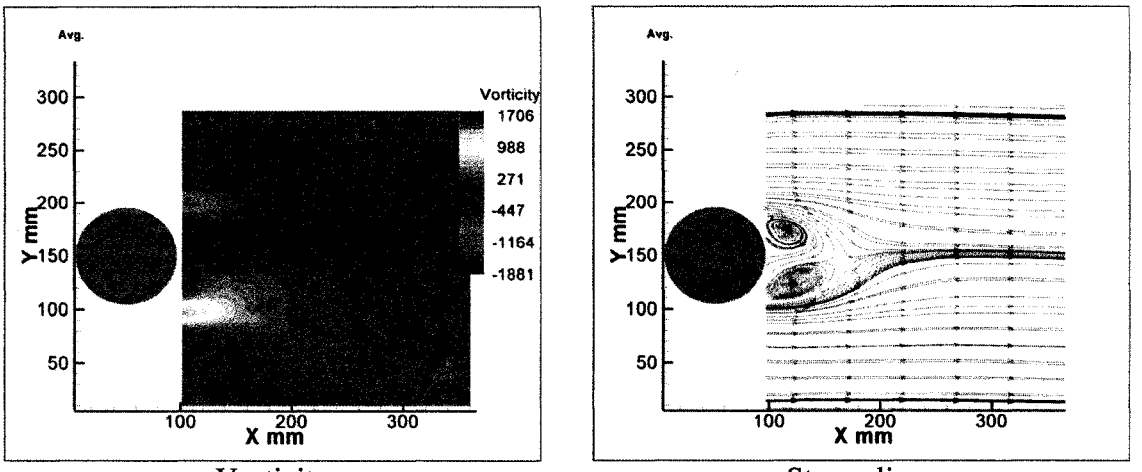

Vorticity Streamlines

Figure 7.5 Continued

Following the experiments with the first cylinder another cylinder with 4.5" diameter at 20 m/s giving a Reynolds number of 156,000 was tested. Similar but larger structures were again observed. The Von Karman vortex street was again clearly shown in velocity magnitude and vorticity-streamline plots (Figure 7.6). The average wake flow field can be seen in Figure7.7.

Velocity Vorticity-Streamline

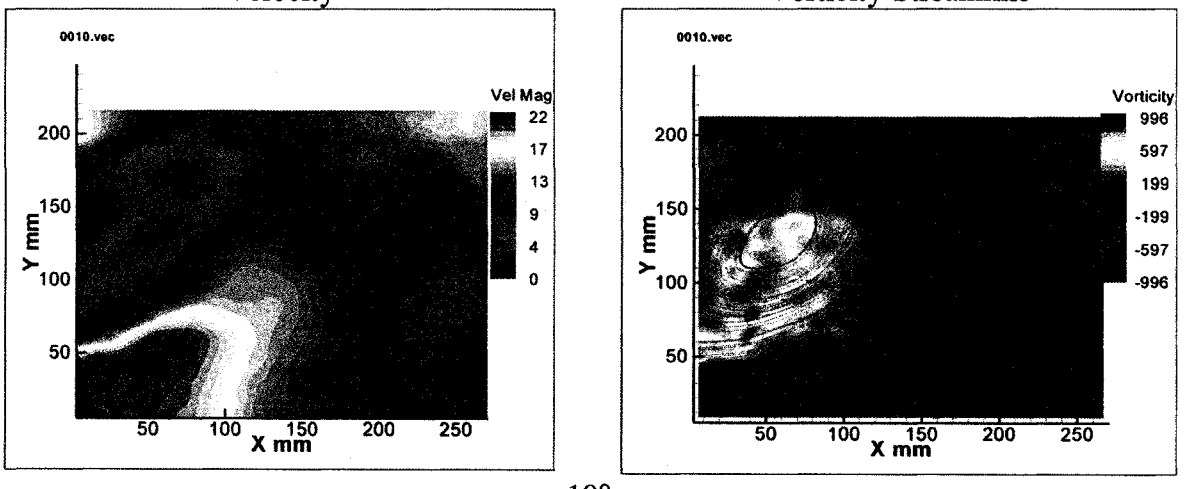

10°

Figure 7.6 Wake field for the larger cylinder using TTT

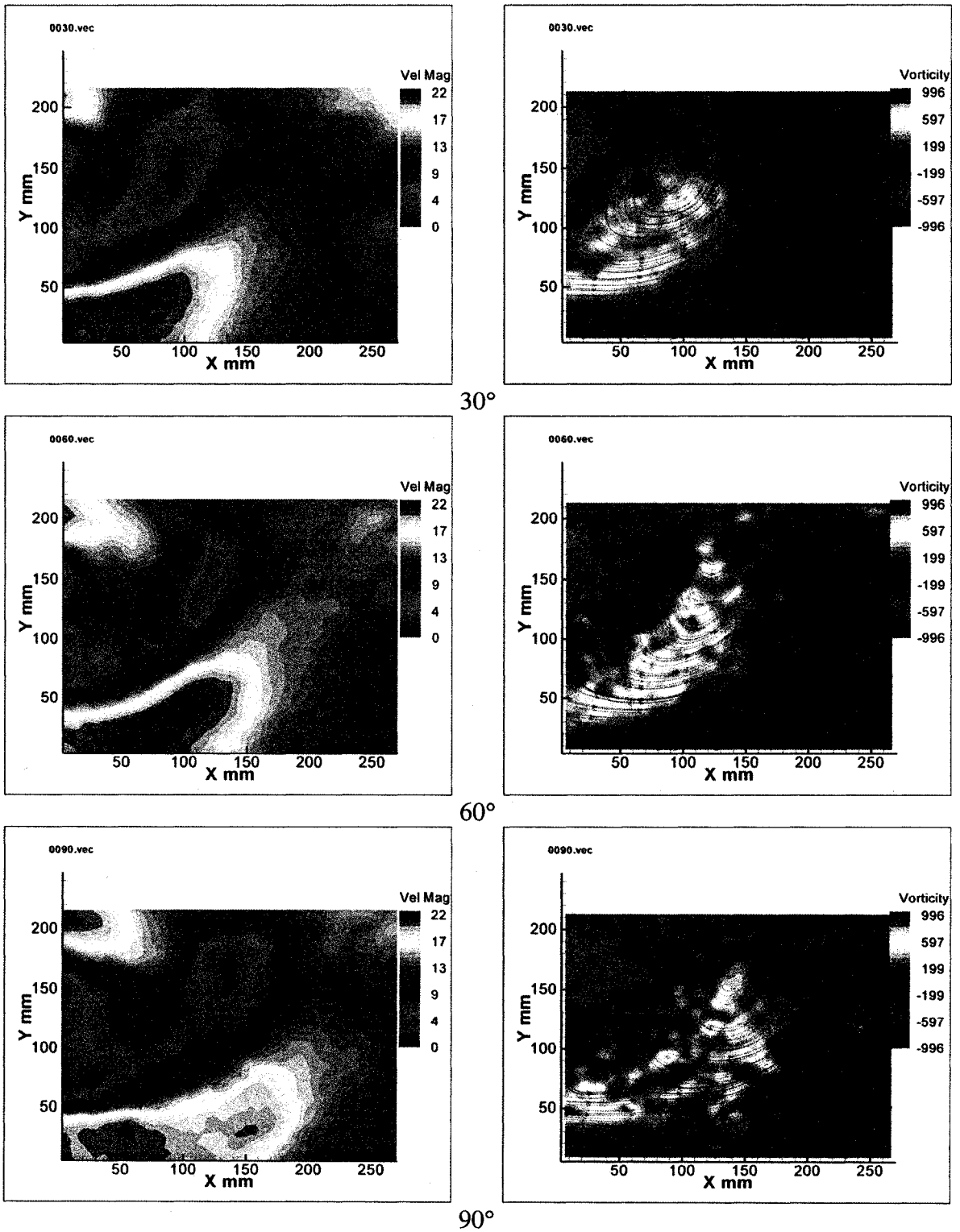

Figure 7.6 Continued

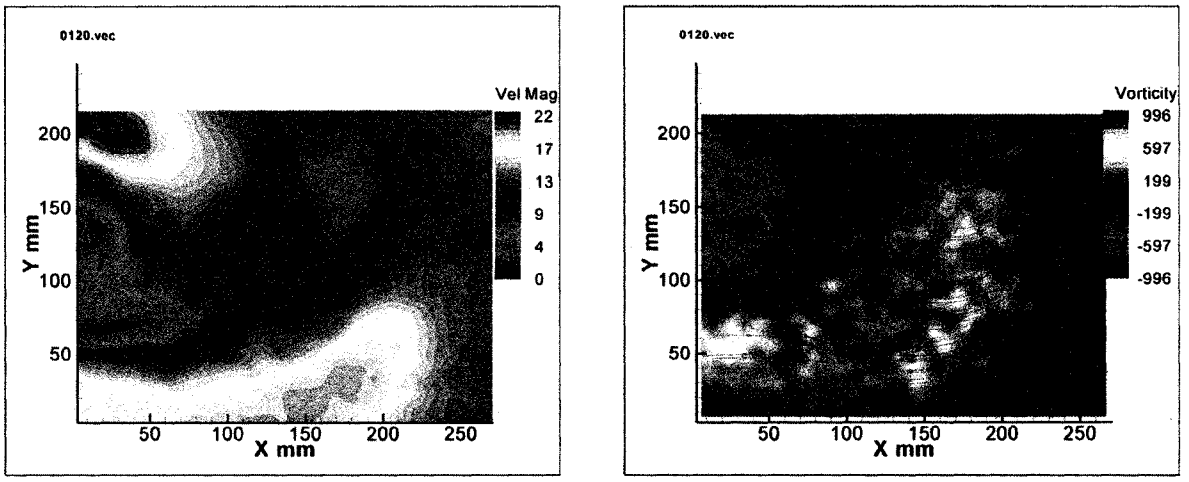

120°

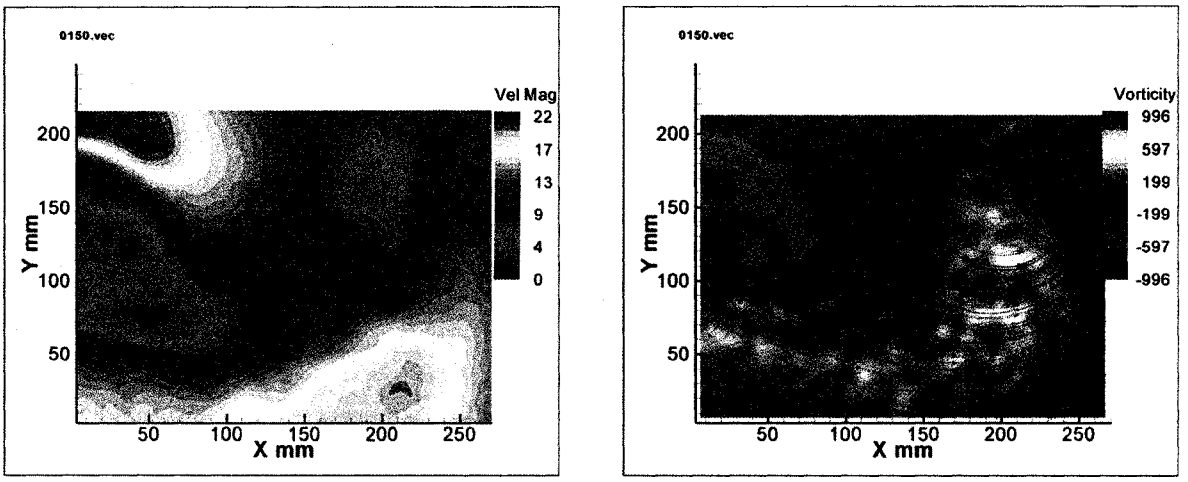

150°

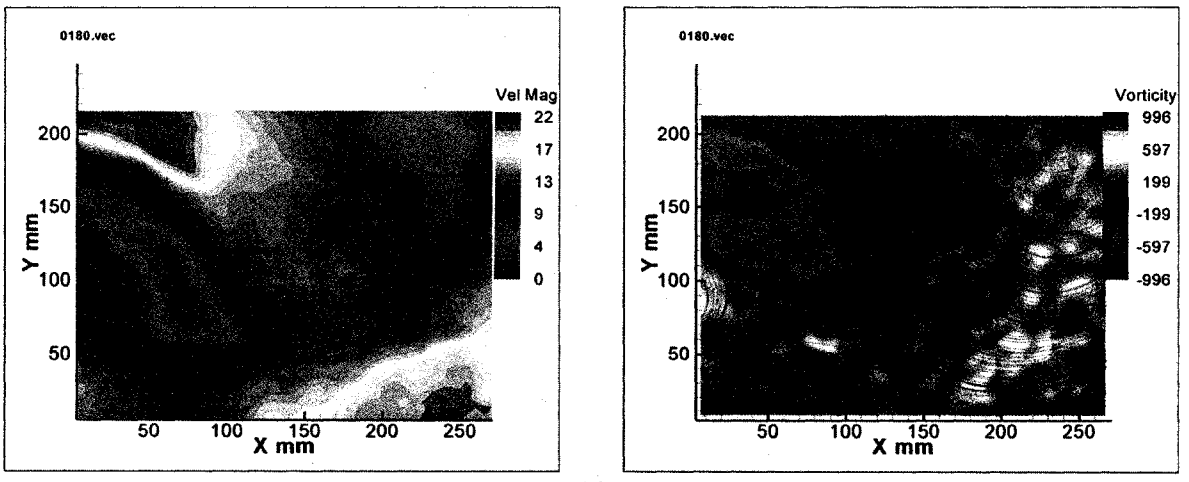

180°

Figure 7.6 Continued

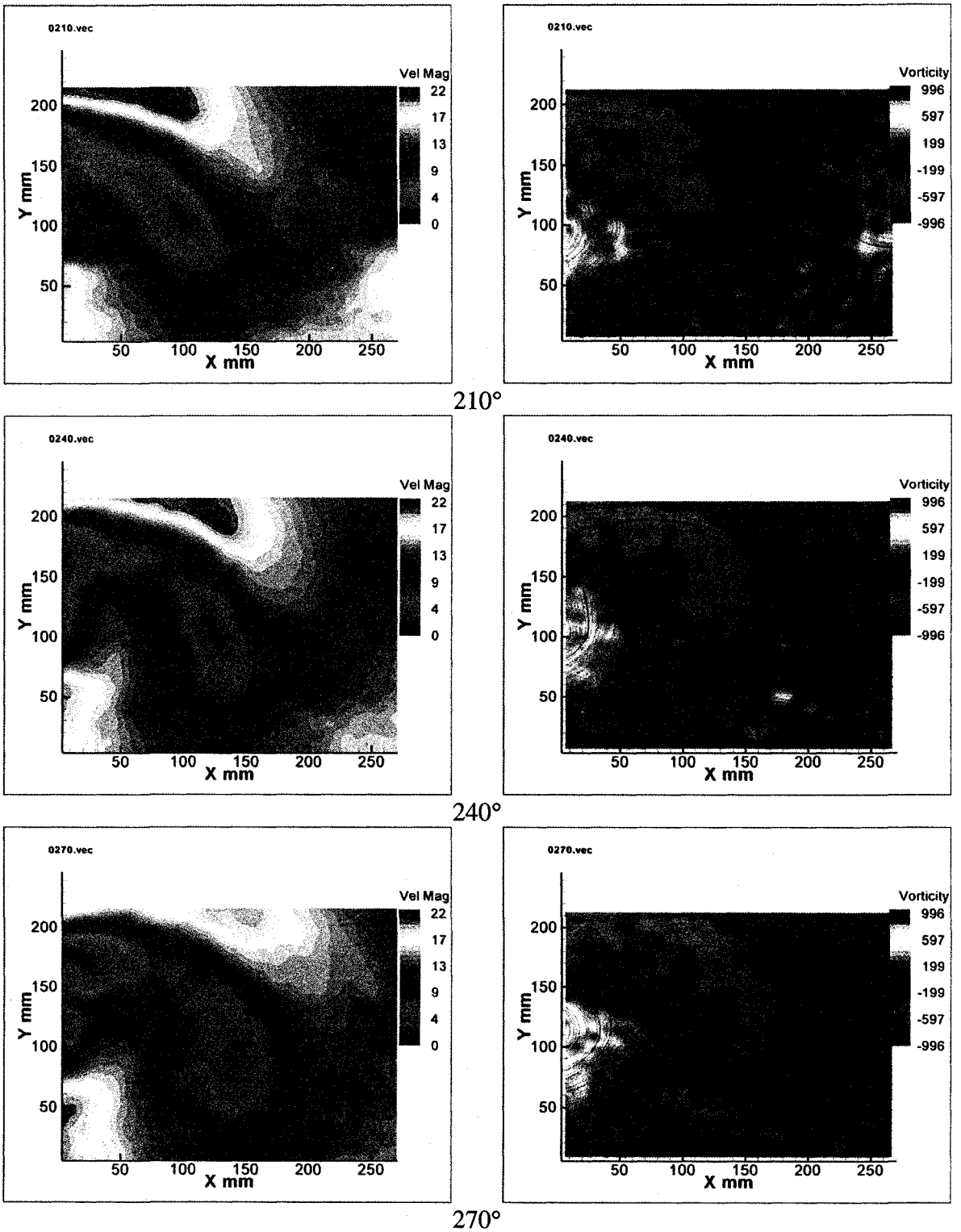

Figure 7.6 Continued

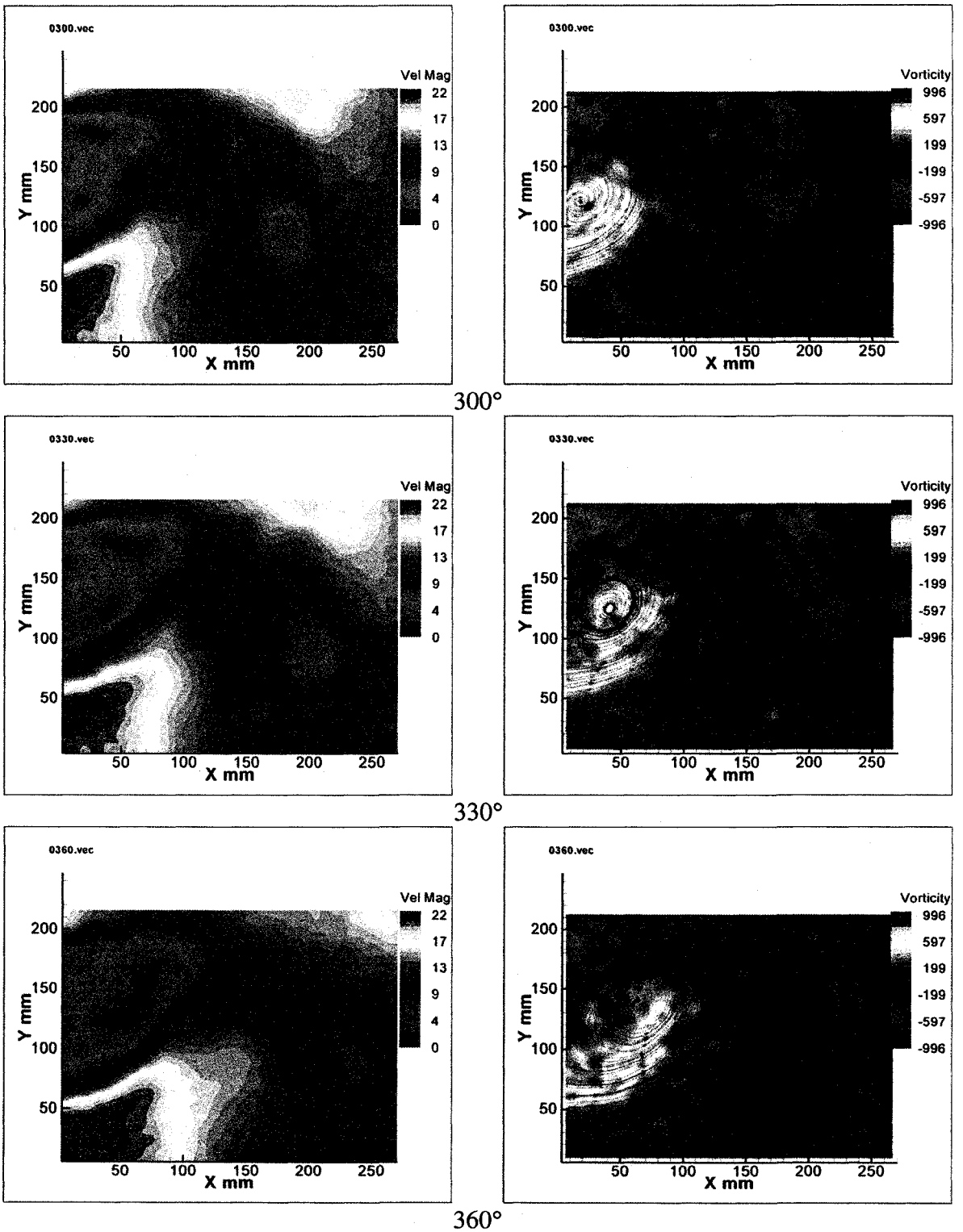

Figure 7.6 Continued

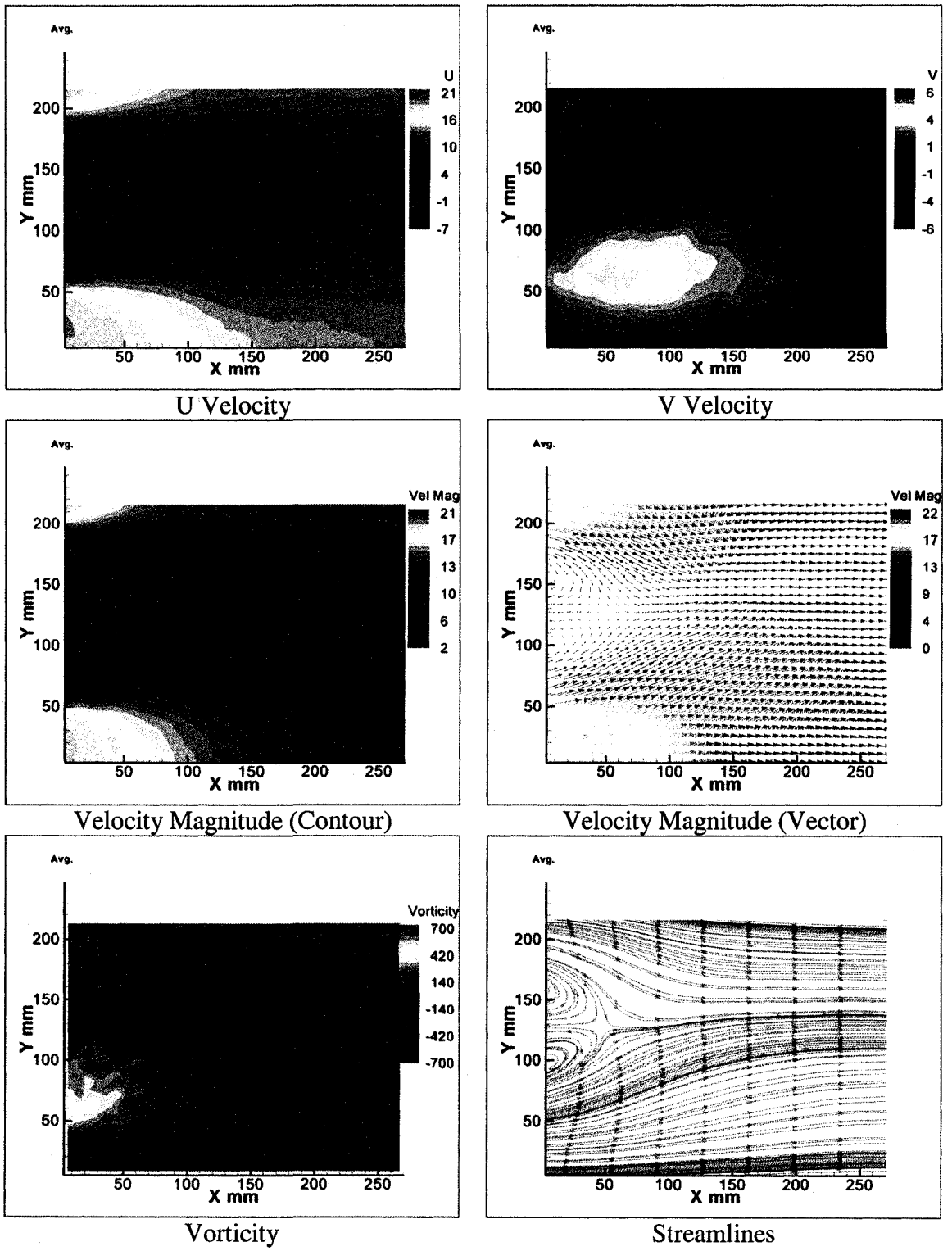

U Velocity | V Velocity

Velocity Magnitude (Contour) | Velocity Magnitude (Vector)

Vorticity | Streamlines

Figure 7.7 Average wake field

7.3 Ogive Cylinder

Detailed wake filed measurements for the ogive cylinder as described in Chapter 6was made. The model had a diameter of 3 5/16" giving a Reynolds number of 173,000 for a freestream velocity of 30 m/s. The TTT method was again used to analyze the velocity field. The hot-film probe was placed 7 diameters downstream from the model base at a radial position where the signal was most periodic as observed on the oscilloscope. The model is carefully aligned so that there was no yaw or pitch angle. First experiments to define the predominant frequency of the vortex shedding were made at several stations (Figure 7.8). These plots show ensemble averages of 20 FFTs derived from velocity files scanned at a rate of 1000 Hz for 10 seconds. It is observed that the vortex shedding was around 90 Hz. The first peak around 10 Hz is believed to be due to the oscillation of the model. PIV measurements were made in all three orthogonal planes. While a 2-component PIV setup was used for the XY plane; a stereo PIV (3-component) setup was used for the XZ and YZ planes. The X direction corresponds to being the freestream and Z to the height of the test section as shown in Figure 7.9.

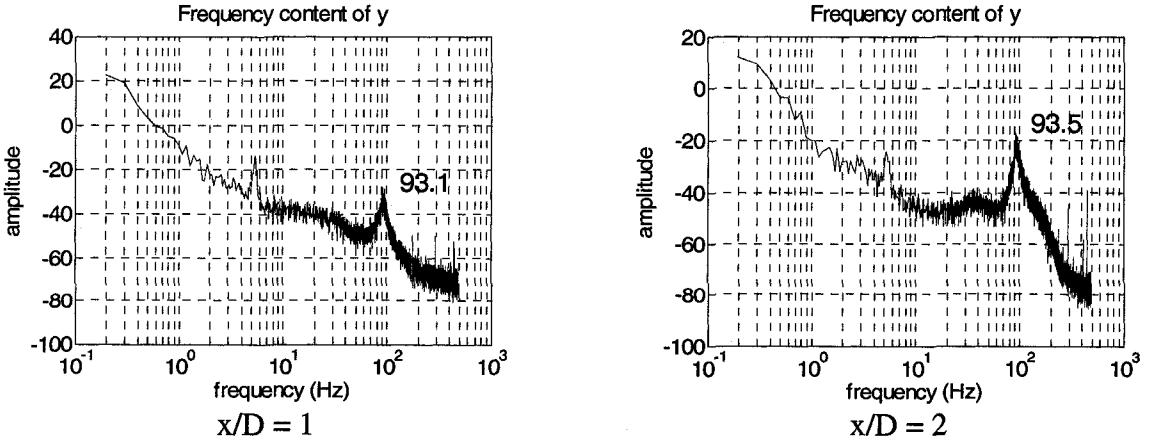

Figure 7.8 Predominant frequency measurements

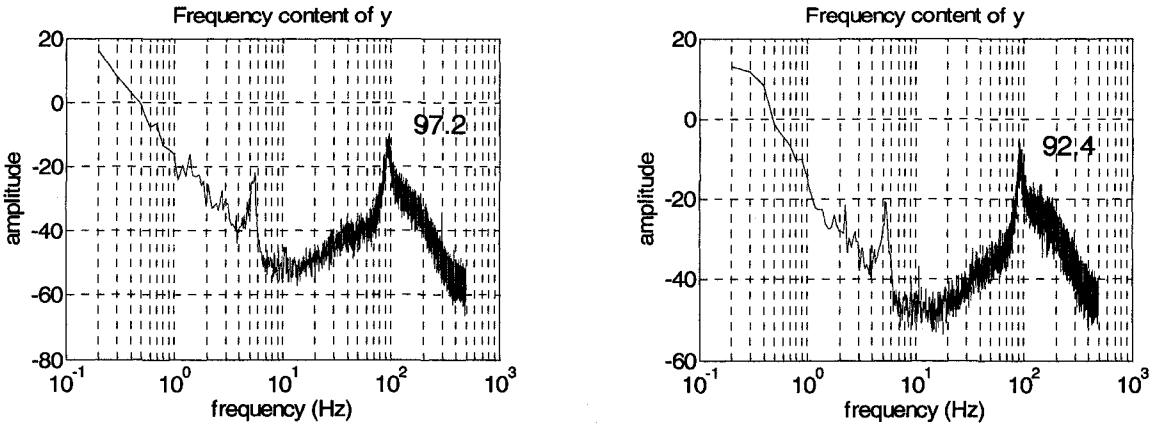

Figure 7.8 Continued

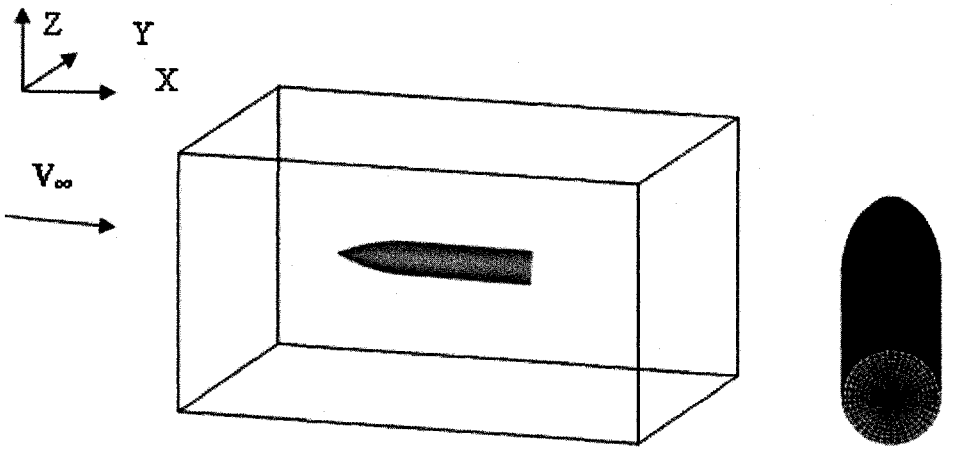

Figure 7.9 Axis system for the ogive cylinder.

XY Plane

In the first tests the camera was placed over the tunnel and the laser was placed on the right side (-y-direction) of the model. Velocity magnitude plots, as well as total turbulence, Reynolds Stress, vorticity and streamline plots are presented in Figures 7.10-7.13. The velocity plots show the wake closure point and together with the streamline plots they reveal the existence of an annular separation bubble. Again the negative and the positive vorticity regions are observed on opposite sides of the axis of symmetry.

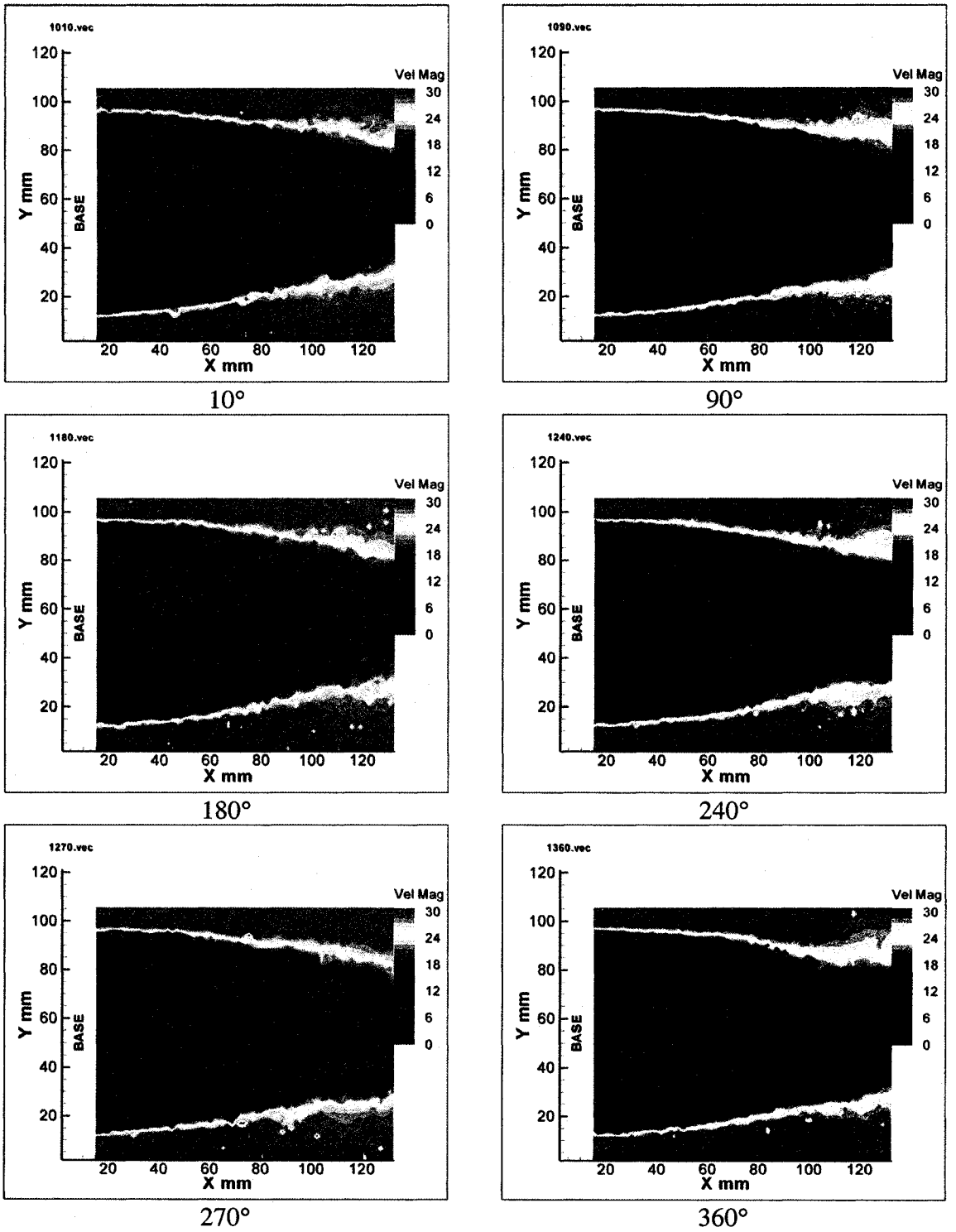

Figure 7.10 Velocity Magnitude Plots

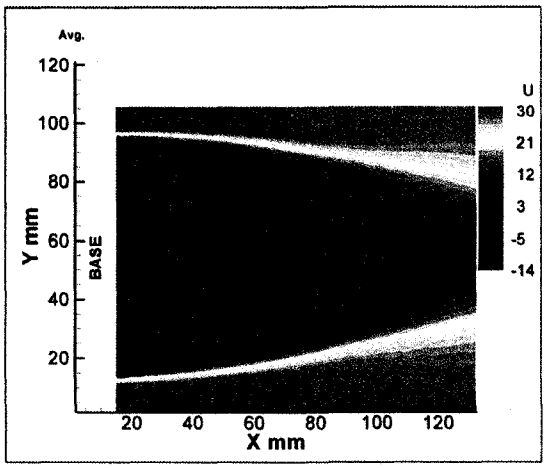

U

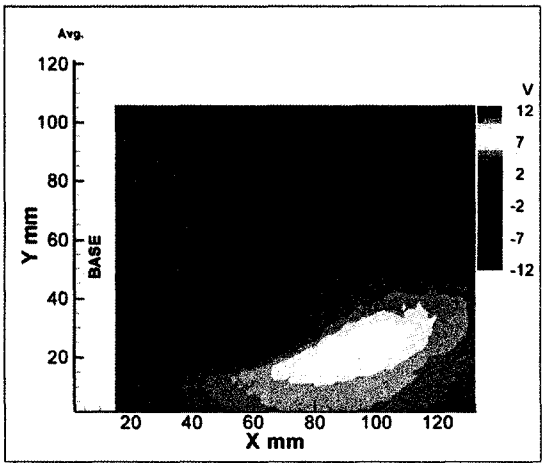

V

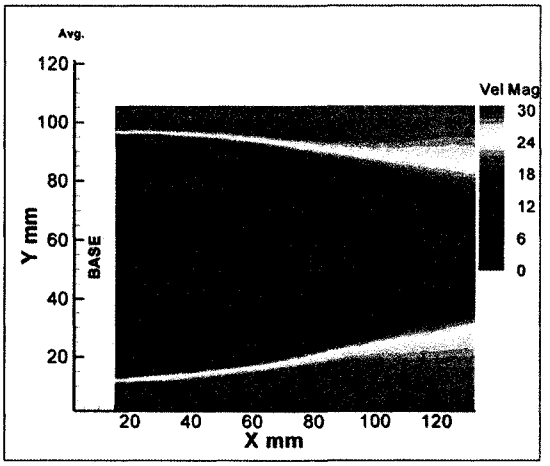

Velocity Magnitude (Contour)

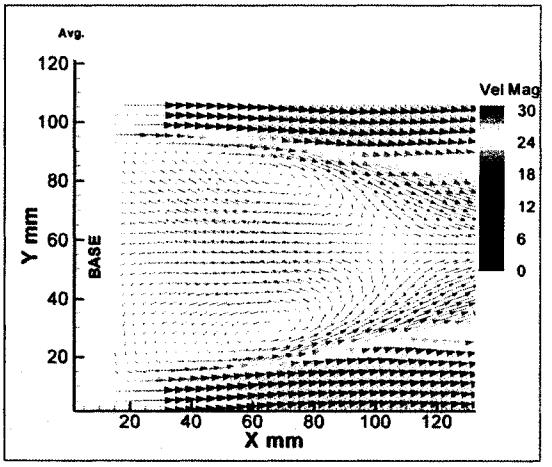

Velocity Magnitude (Vector)

Figure 7.11 Average Velocity Plots

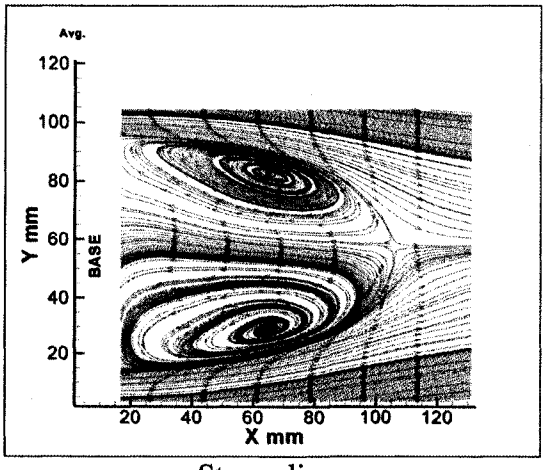

Streamlines

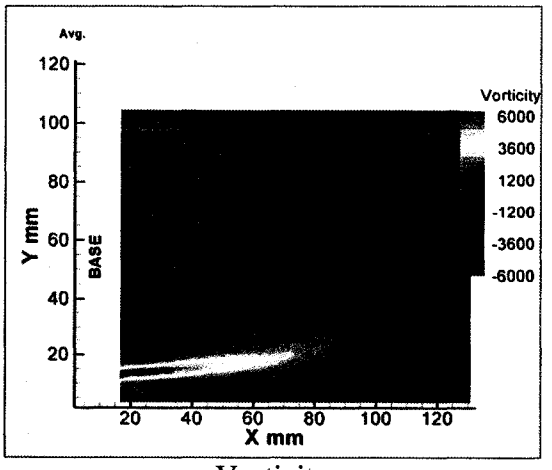

Vorticity

Figure 7.12 Streamlines and Vorticity Plots

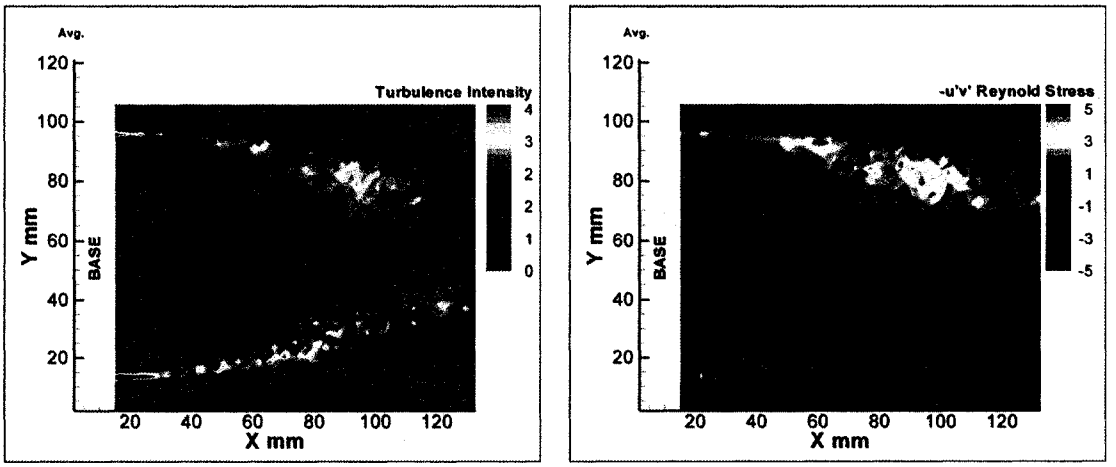

Turbulence Intensity Reynolds Stress

Figure 7.13 Total Turbulence and Reynolds Stress Plots

These measurements were only monitoring an area very close to the base so a test capturing a wider area was also made (Figures 7.14- 7.16). Similar results to the previous case were obtained. Separation bubbles, positive and negative vorticity fields are observed accordingly.

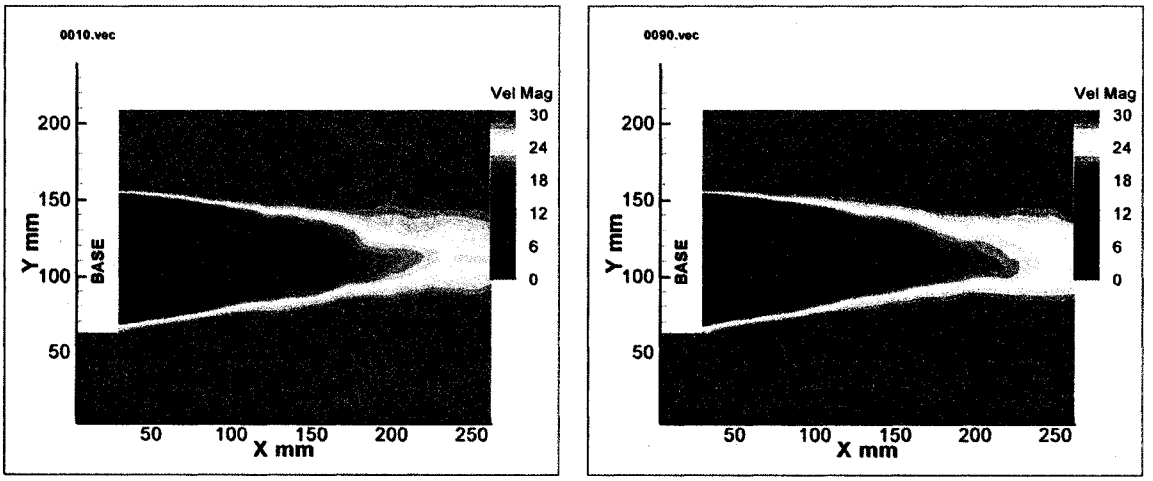

10° 90°

Figure 7.14 Velocity Magnitude Plots

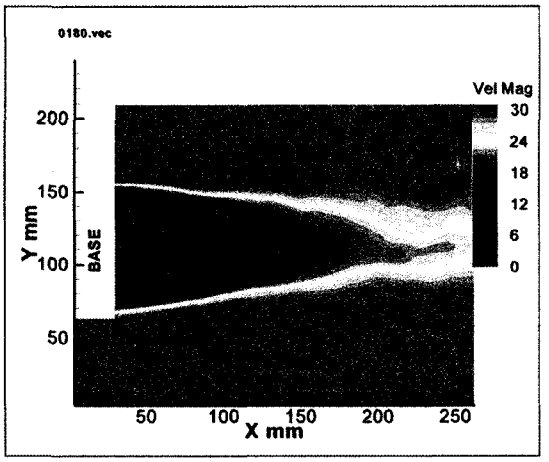

180°

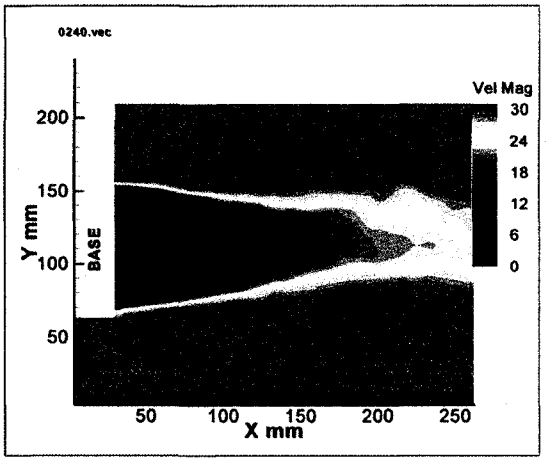

240°

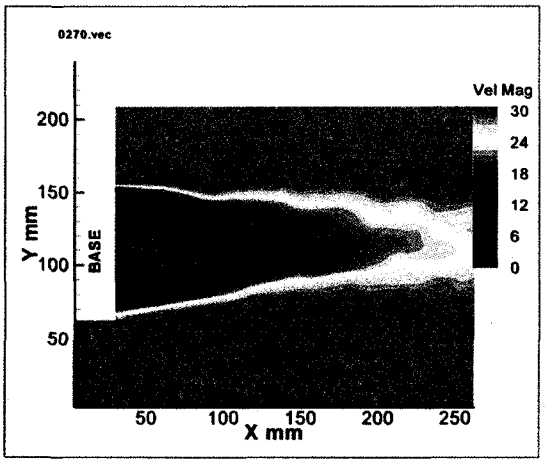

270°

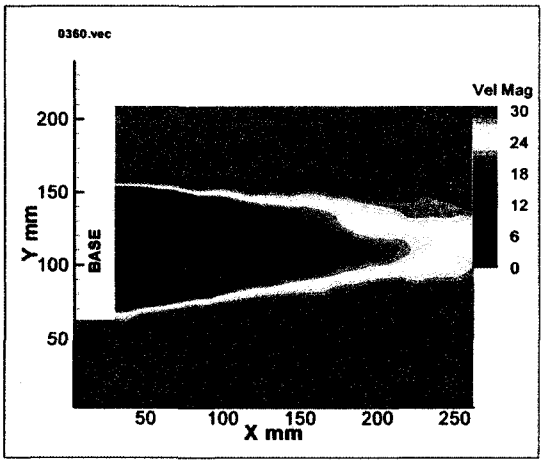

360°

Figure 7.14 Continued

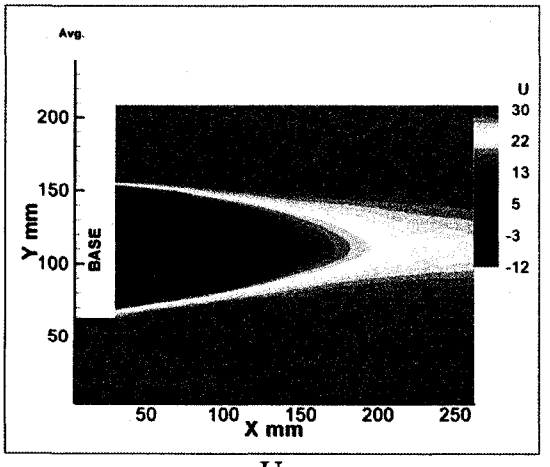

U

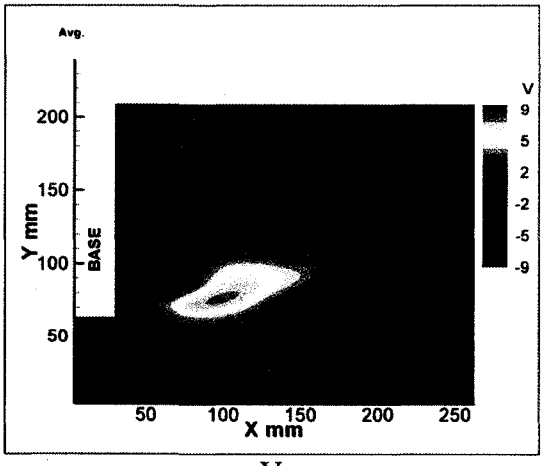

V

Figure 7.15 Average Velocity Plots

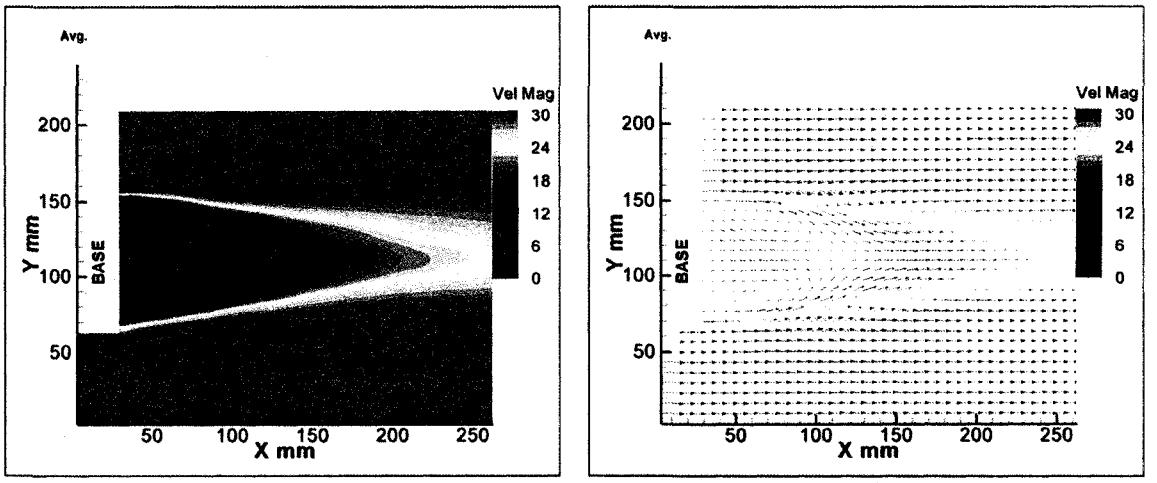

Velocity Magnitude (Contour) Velocity Magnitude (Vector)

Figure 7.15 Continued

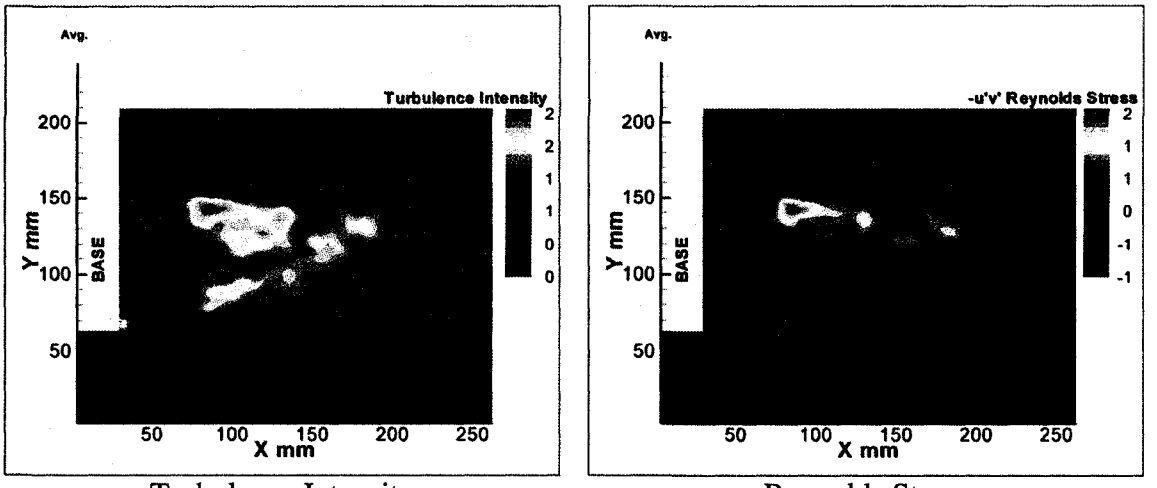

Turbulence Intensity Reynolds Stress

Figure 7.16 Total Turbulence and Reynolds Stress Plots

XZ Plane

The laser source was placed over the tunnel so as to illuminate the wake survey station, and the 2 CCD cameras were placed on the same side of the tunnel, to the right of the model. Three components of the velocity were recorded using the Stereoscopic PIV setup. In addition to the velocity, three components of the turbulence and Reynolds stress values were also obtained (Figures 7.17- 7.21).

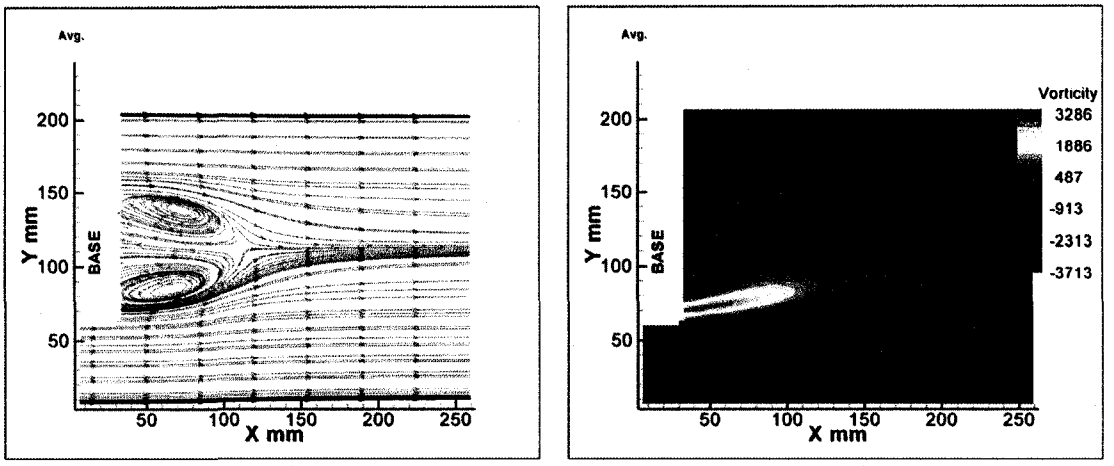

Streamlines Vorticity

Figure 7.17 Streamlines and Vorticity Plots

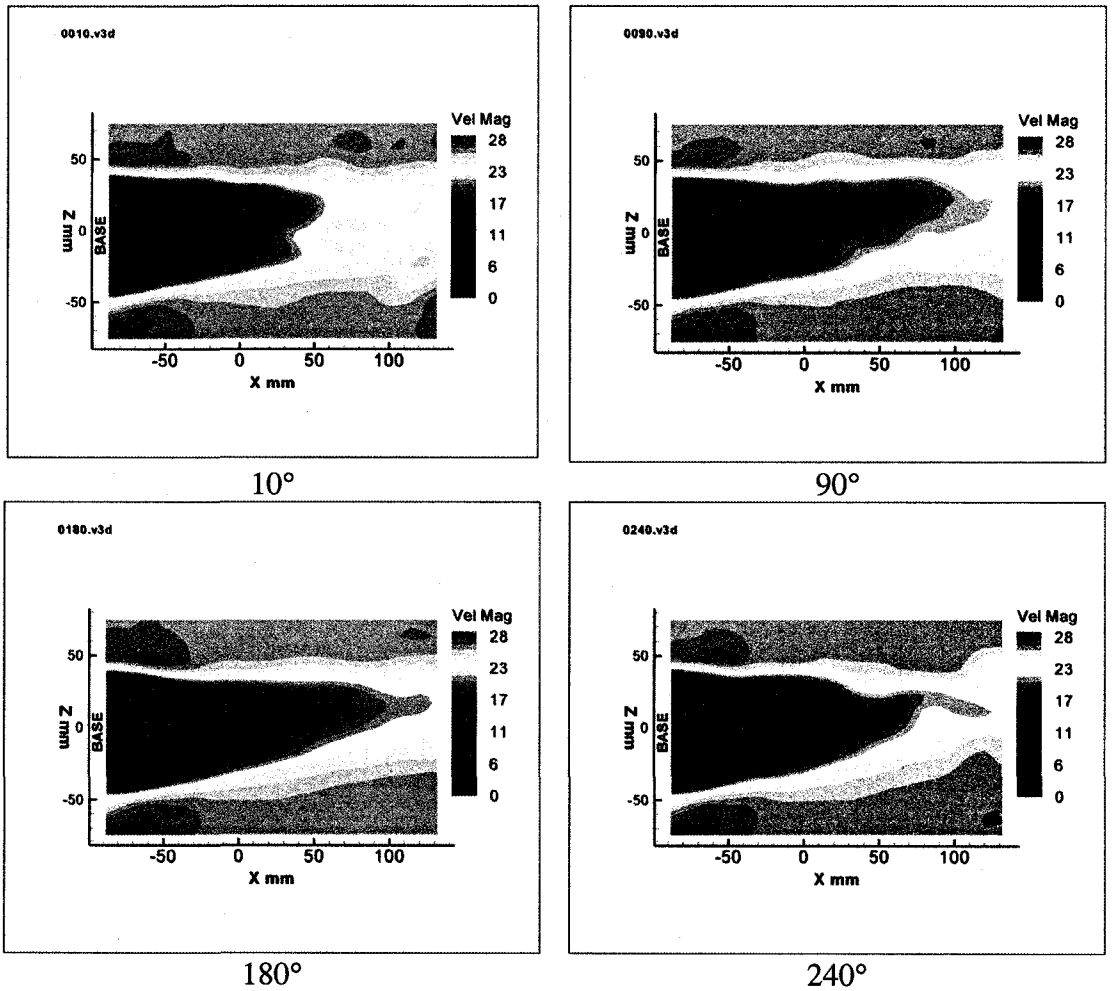

10° 90°

180° 240°

Figure 7.18 Velocity Magnitude Plots

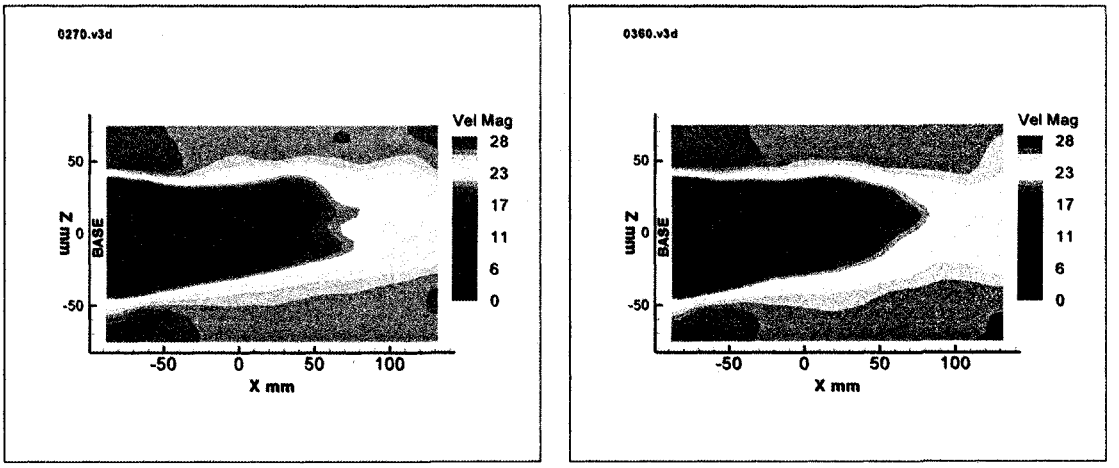

270° 360°

Figure 7.18 Continued

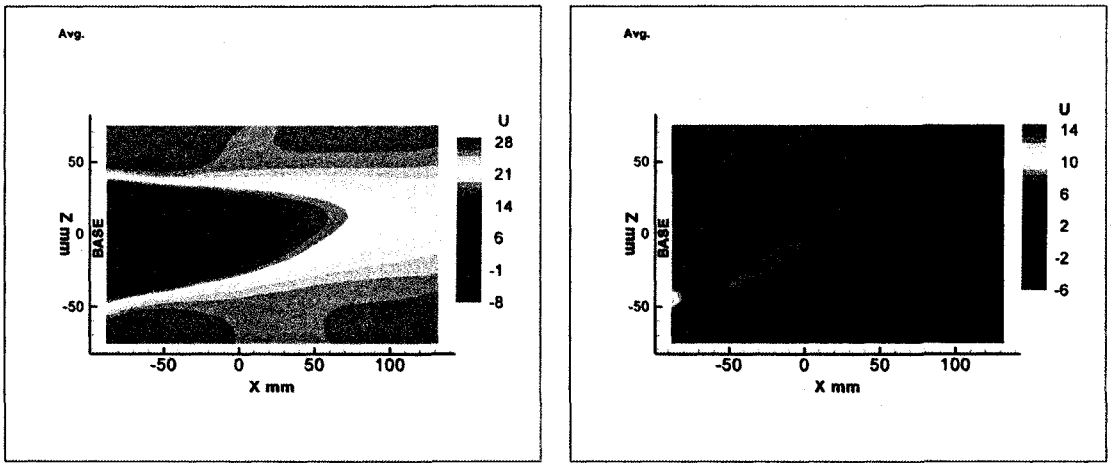

U V

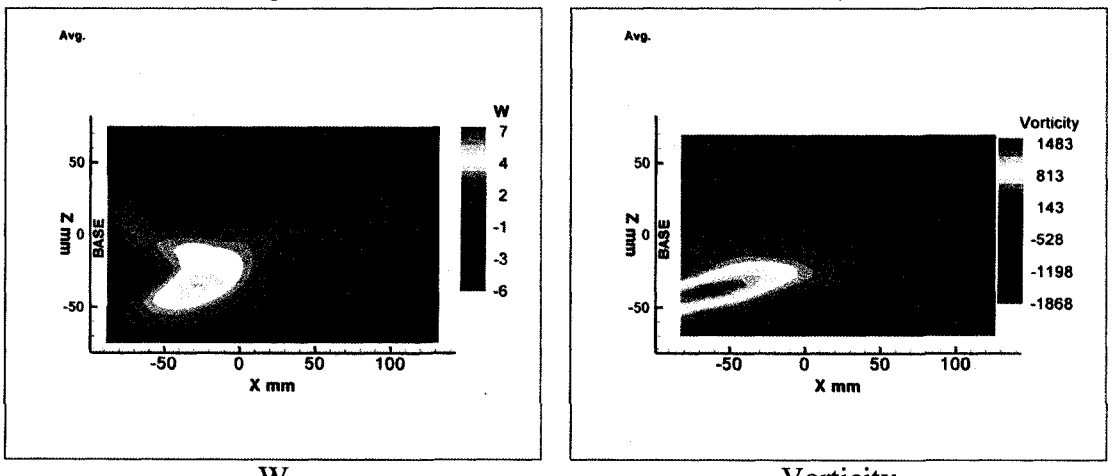

W Vorticity

Figure 7.19 Average Velocity and Vorticity Plots

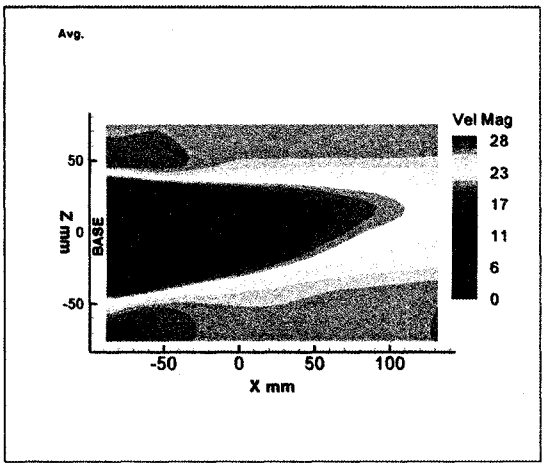

Velocity Magnitude (Contour)

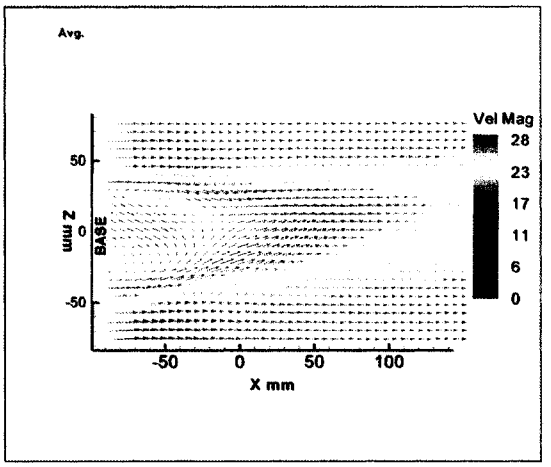

Velocity Magnitude (Vector)

Figure 7.19 Continued

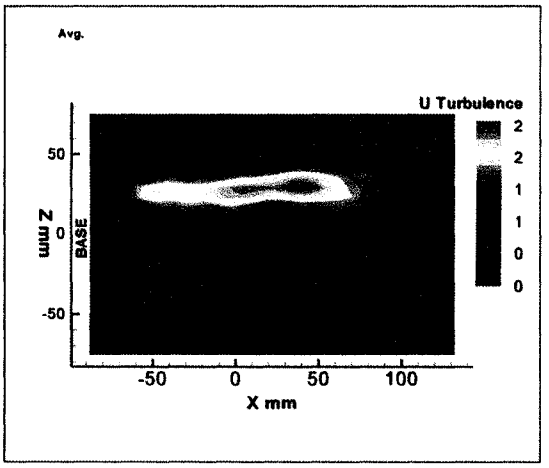

U Turbulence

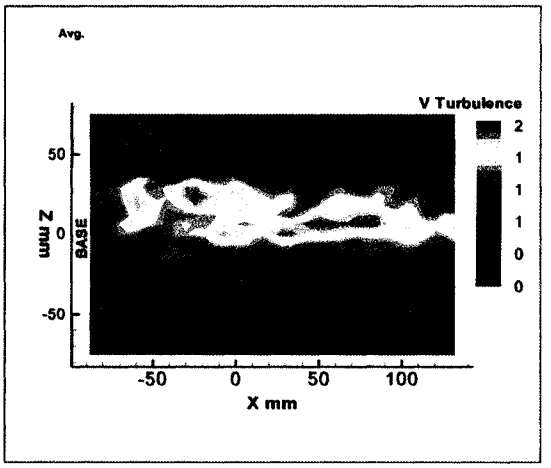

V Turbulence

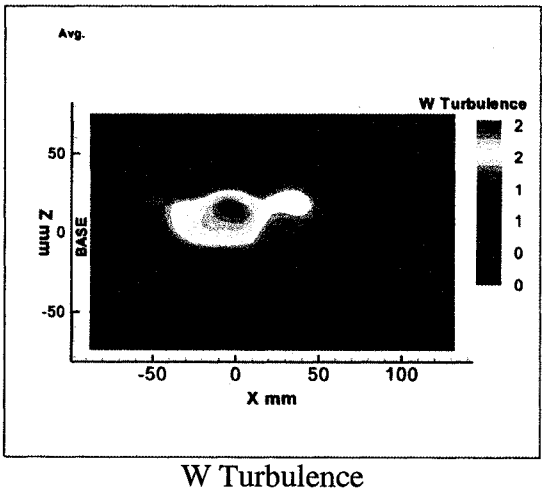

W Turbulence

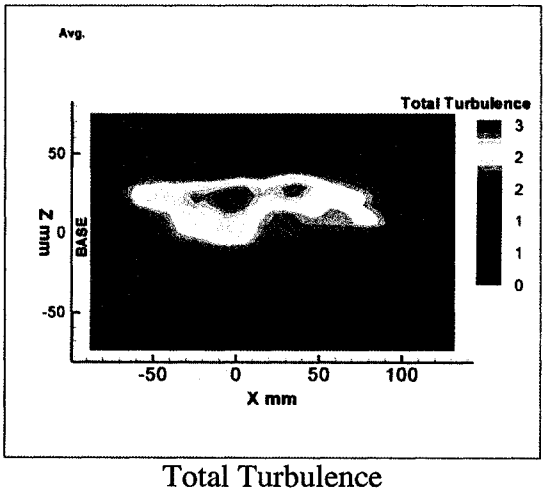

Total Turbulence

Figure 7.20 Turbulence Intensities

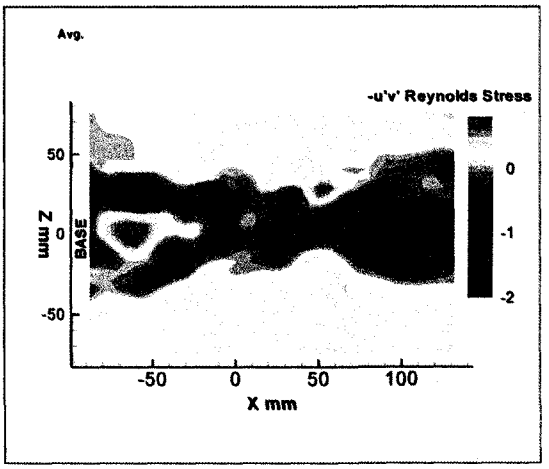

Reynold Stress- uv

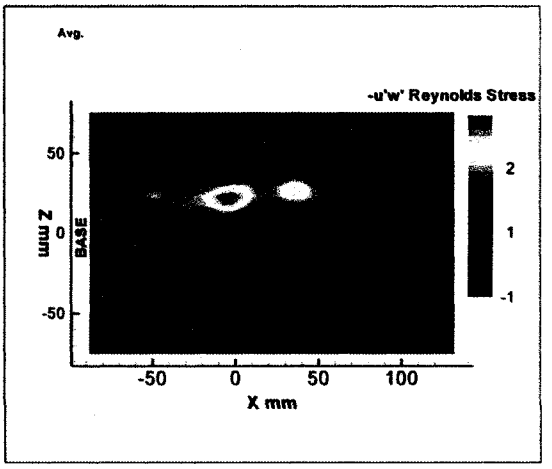

Reynold Stress- uw

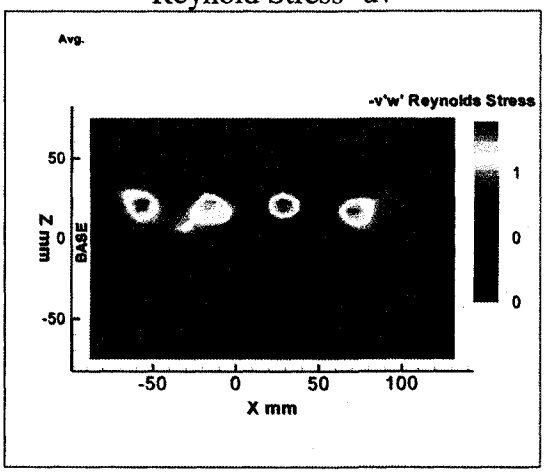

Reynold Stress- vw

Figure 7.21 Reynolds Stress Plots

YZ Plane

Crossflow velocities at the wake survey station are acquired. The laser source is placed over the tunnel and the 2 CCD cameras are placed both side of the test section. Three components of the velocity were recorded using the Stereoscopic PIV setup.

Velocity magnitude plots reveal some sense of the rotation of a vortex structure which may be a mark of the rotating spiral structure previously mentioned (Figures 7.22- 7.25).

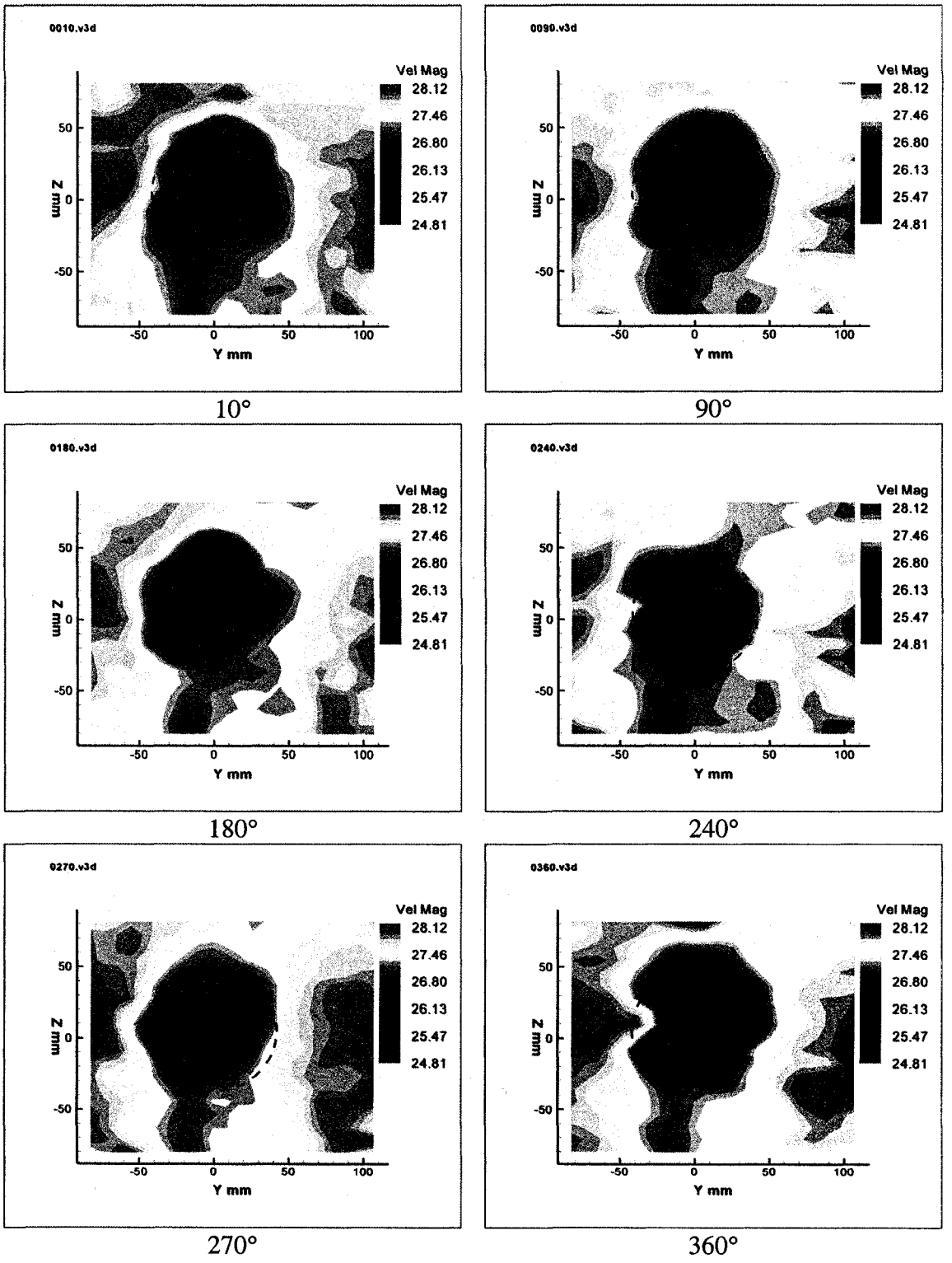

Figure 7.22 Velocity Magnitude Plots

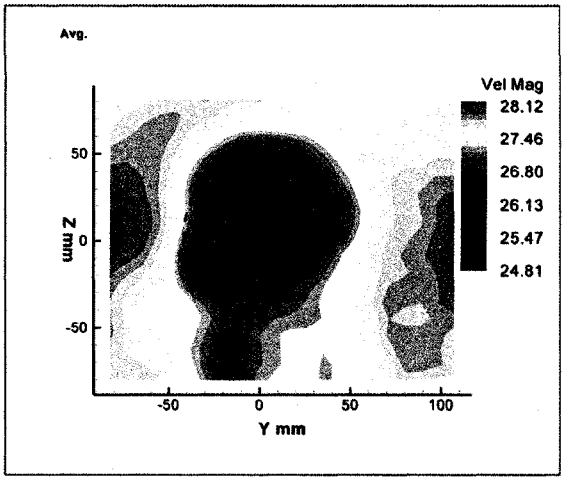

U

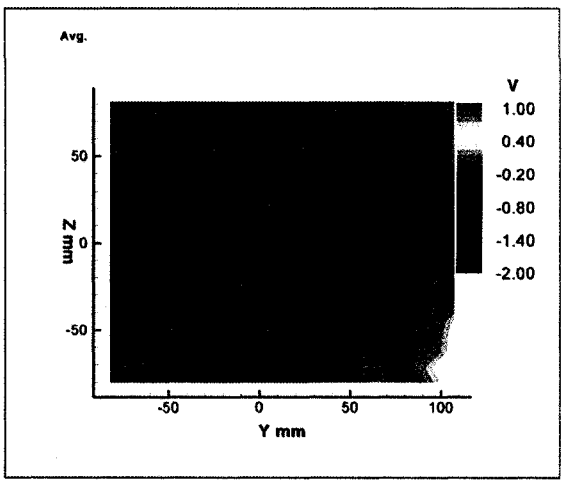

V

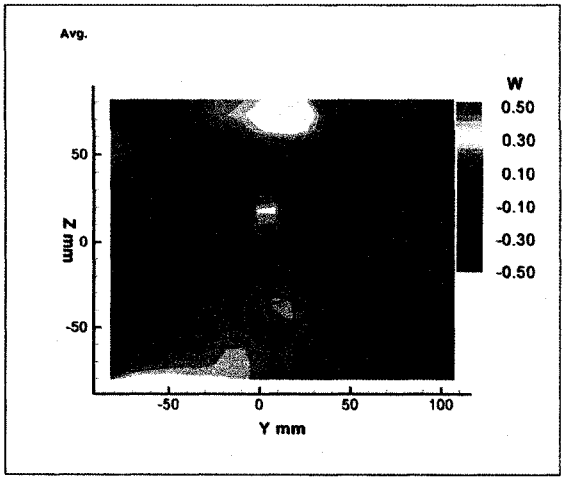

W

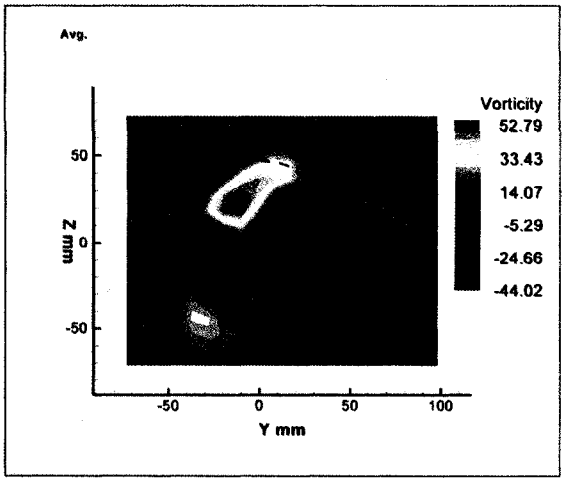

Vorticity

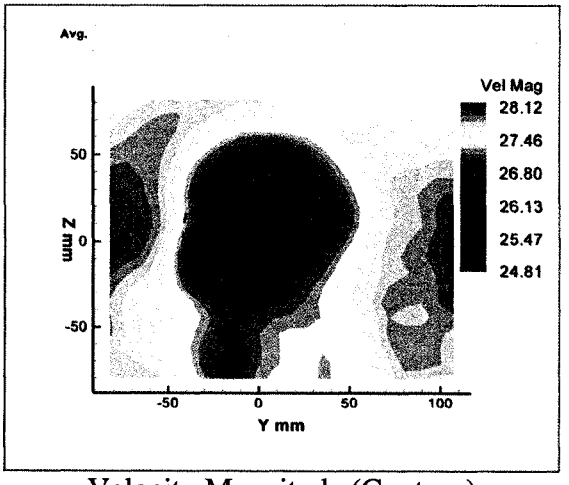

Velocity Magnitude (Contour)

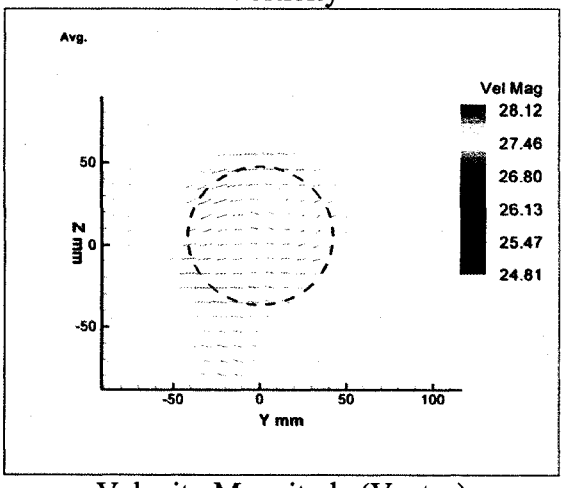

Velocity Magnitude (Vector)

Figure 7.23 Average Velocity and Vorticity Plots

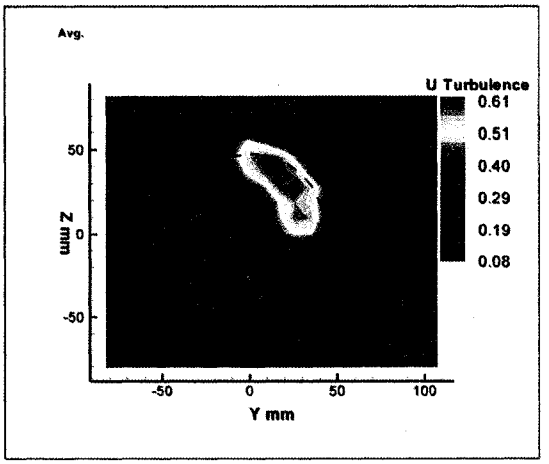

U Turbulence

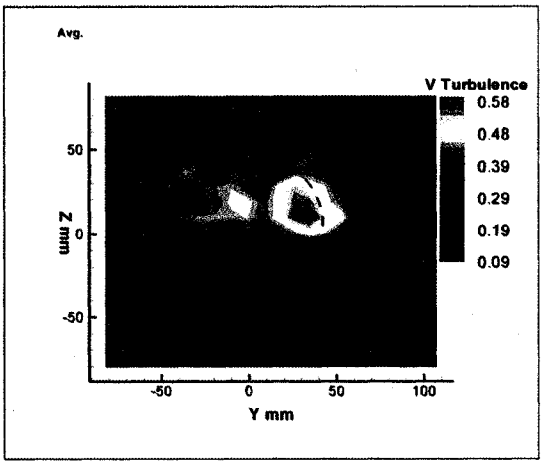

V Turbulence

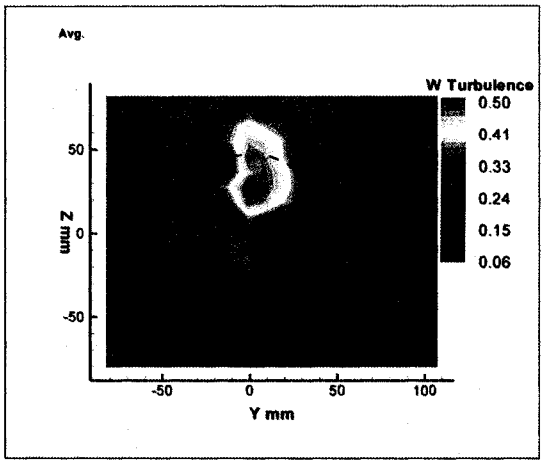

W Turbulence

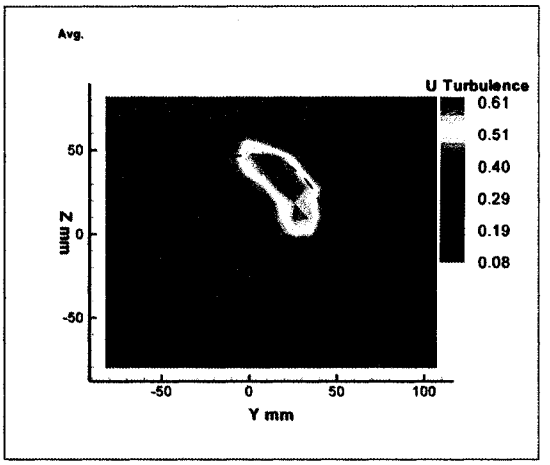

Total Turbulence

Figure 7.24 Turbulence Intensities

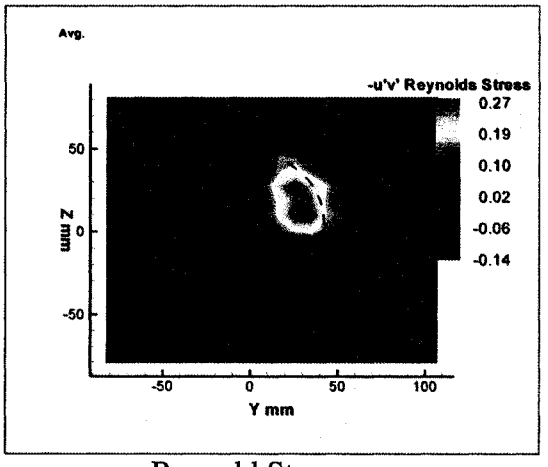

Reynold Stress- uv

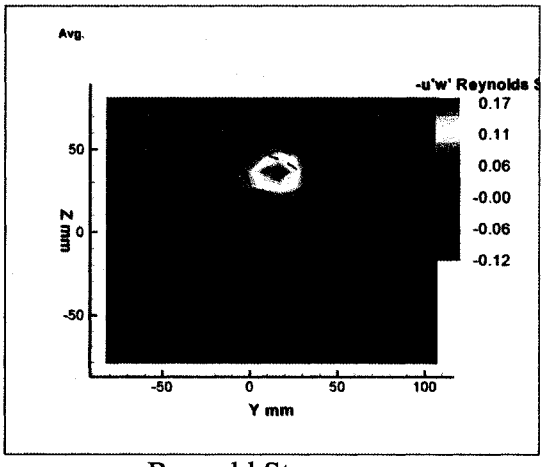

Reynold Stress- uw

Figure 7.25 Reynolds Stress Plots

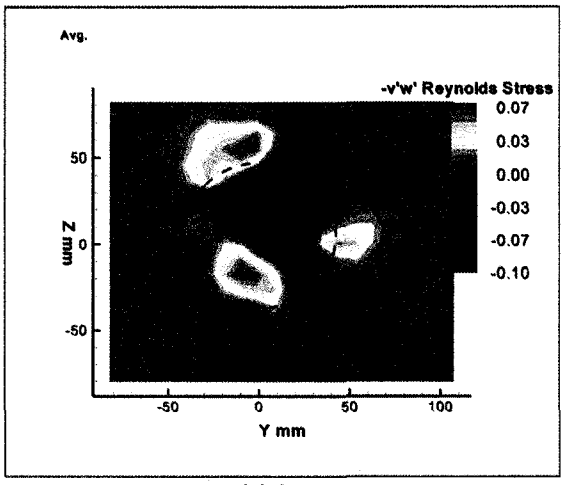

Reynold Stress- vw

Figure 7.25 Continued

7.4 Flow Control

Having analyzed and discussed wakes and phase resolving methods, experiments to investigate the effect of flow excitation by actuators on the wake structure of simple bodies are made. Plasma actuators, as described in Chapter 5, are used to modify the flow structure, hopefully in a favorable sense. Experiments with both the 2D circular cylinder in crossflow and the ogive cylinder are presented in the following sections.

7.4.1 Flow Control on a Circular Cylinder

A circular cylinder of radius 4.5" was used in the first experiments. Two ¼" wide and 12" long strip actuators were placed at 70 degrees measured from the upstream stagnation point on both sides of the cylinder as shown in Figure 7.26. Copper foil tapes were used as electrodes and Kapton tape was used as the dielectric material. This setup is somewhat similar to that described by Haack[136].

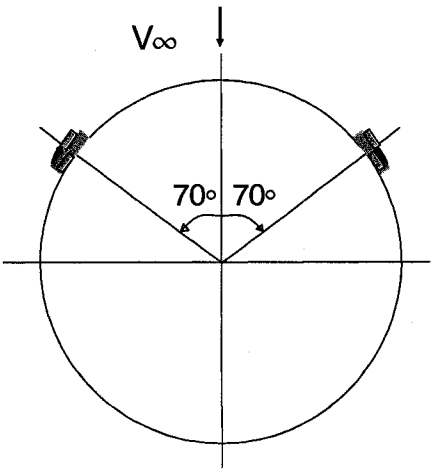

Figure 7.26 Actuator Locations for Circular Cylinder

It was found that the wake flow structure could be significantly changed compared to the reference case (no flow control). First, a single actuator was placed on the lower side of the cylinder and its effects were analyzed. Later, two actuators operating simultaneously were used. Lastly, two actuators operating independently (typically alternately) were used. All of the actuators were operated with at a carrier frequency of 5 kHz and nominally 8 kV. The TTT phase averaging method was used to produce the wake velocity maps. For all of the cases tested a favorable effect compared to no actuator case in the wake was observed, in other words the apparent width of the wake was significantly reduced in all the cases. Pressure distribution plot presented by Haack[136] was in agreement with the phenomenon of wake size reduction. Figure 7.27 shows that the separation point was around 70° and 290° for no control case. When the actuators are operated separation point was delayed to 85° and 275° which resulted in a much smaller wake behind the cylinder. Effect of plasma actuation on the wake is also presented in Figure 7.28 where the dominant frequency measurements at different plasma modulation frequencies are compared.

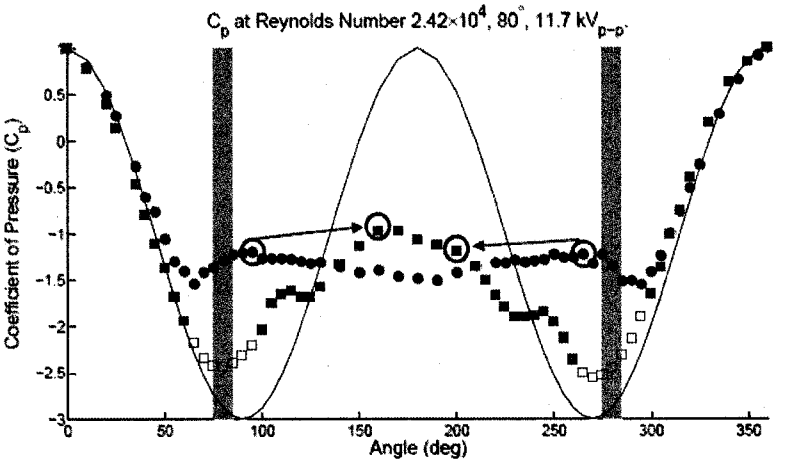

Figure 7.27 Pressure distribution showing the effect of two plasma actuators[136]

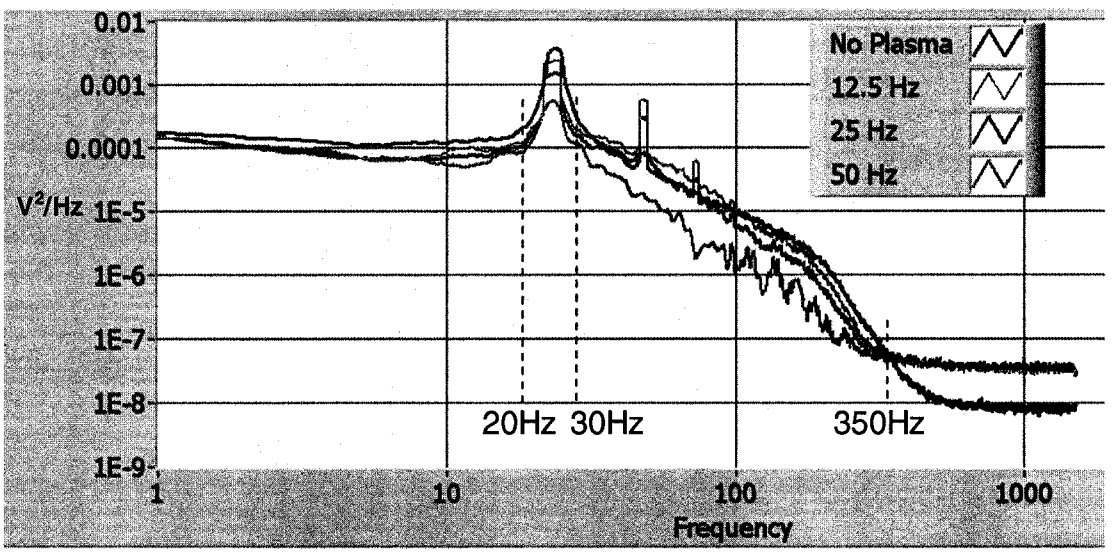

Figure 7.28 Dominant frequency at different plasma modulation frequencies

Table 7.2 presents the data obtained by integrating the areas under the power curves in Figure 7.28. Total integration as well as the integration of two focused regions are calculated. Points contaminated with electric field are eliminated for better accuracy. All of the data sets show that the amplitude of the power curves decreases with increasing modulation frequency of the actuators.

Table 7.2 Comparison of areas under the power curves, cylinder

	Total Area	30-700Hz	30-70Hz
No Plasma	0.0212	0.0183	0.0143
12.5Hz	0.0178	0.0150	0.0088
25Hz	0.0120	0.0095	0.0057
50Hz	0.0062	0.0039	0.0026

Single Actuator Case

A single actuator was placed on the lower side of the cylinder. A sine wave carrier at 5 kHz modulated by another sine wave at 25 Hz was used to operate the actuator (Figure 7.29). As seen in Figure 7.30 this actuator produced delayed separation on the lower side, causing the wake to deflect towards the upper side. This is inherently related to the generation of net circulation in the counterclockwise sense as shown. If the upper actuator were driven, the opposite effect would be observed. By this means the wake can therefore be "flipped" from side to side on demand.

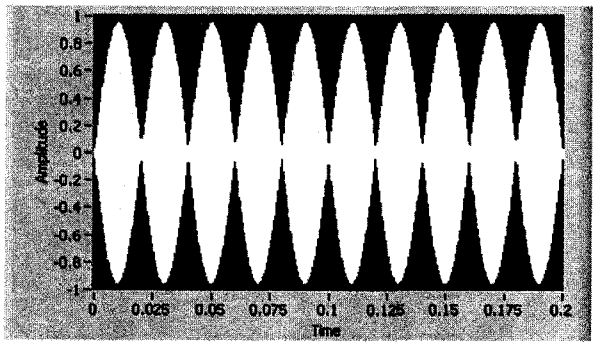

Figure 7.29 Modulated carrier frequency signal to operate a single actuator

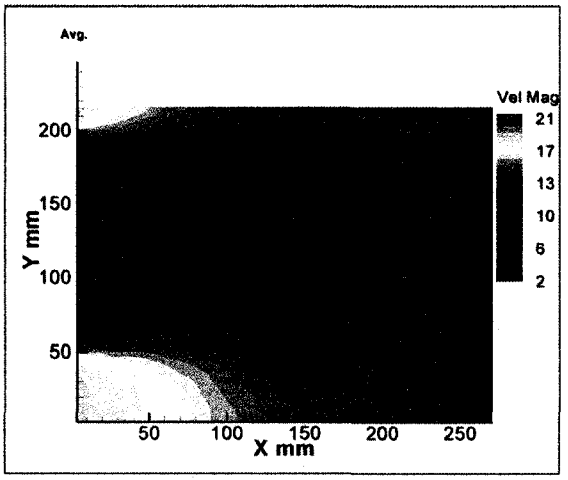

Velocity Magnitude (No control case)

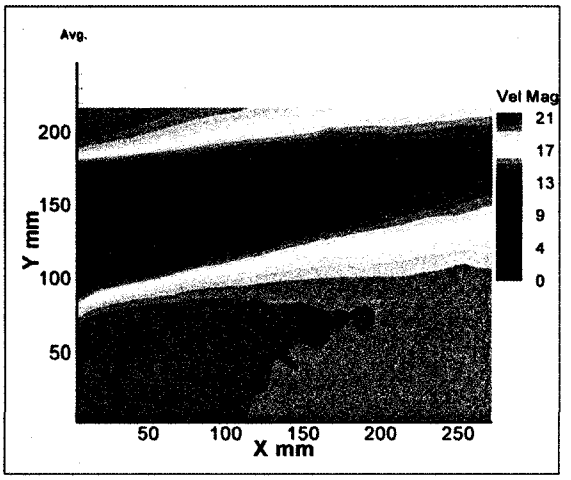

Velocity Magnitude

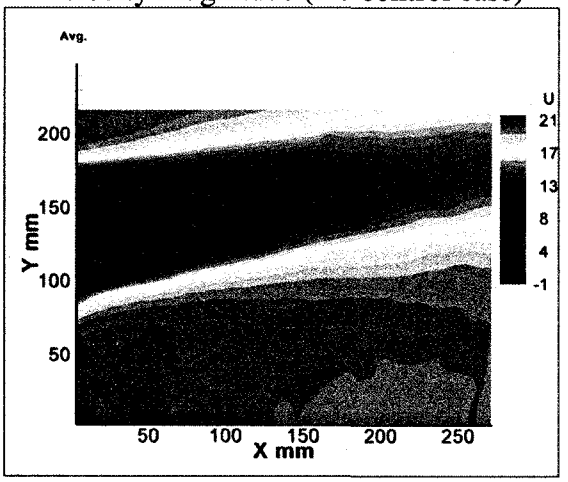

U Velocity

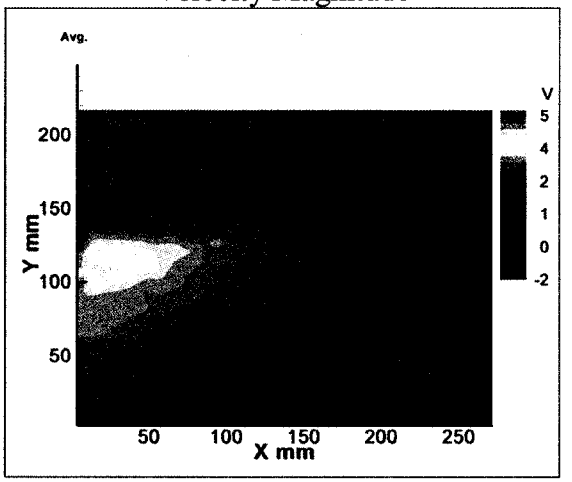

V Velocity

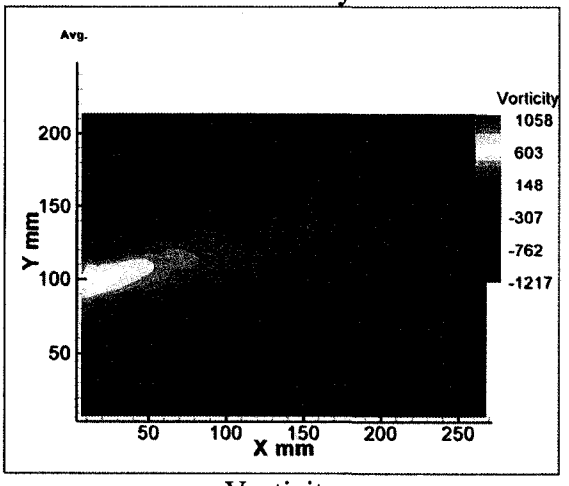

Vorticity

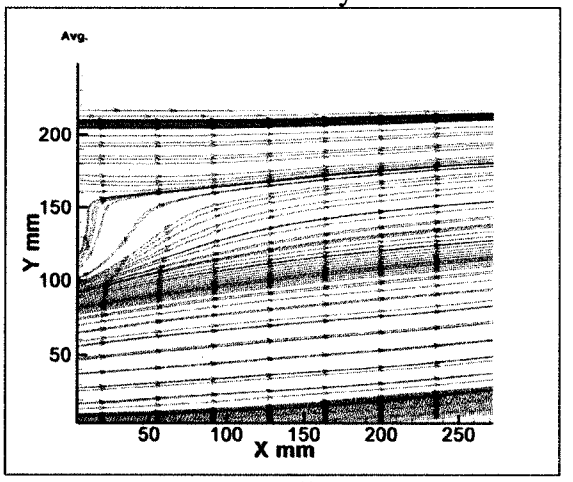

Streamlines

Figure 7.30 Average Wake Field, single actuator case

Double Actuator Operated Together

After observing the effects of a single actuator, two actuators working simultaneously with a 5 kHz carrier, modulated by a 25 Hz sine wave were tested. With two actuators operating the wake returned more-or-less to the centerline (Figure 7.31). Slight asymmetries are expected due to imperfections in placing the actuators as well as variations such as actuator thickness and the differences in the electrode overlapping region. However the wake was significantly narrower compared to the no control case.

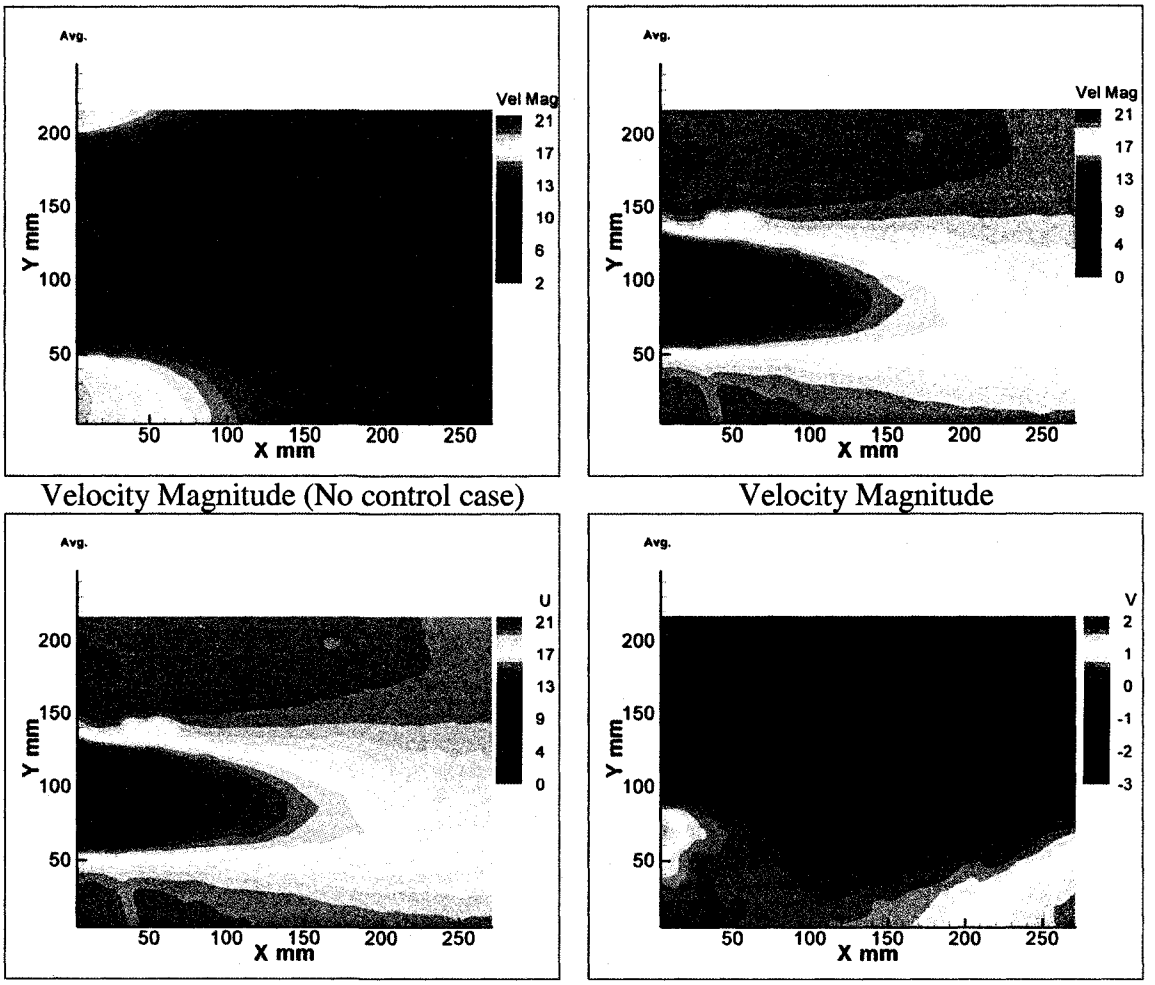

Figure 7.31 Average Wake Field, double actuator case

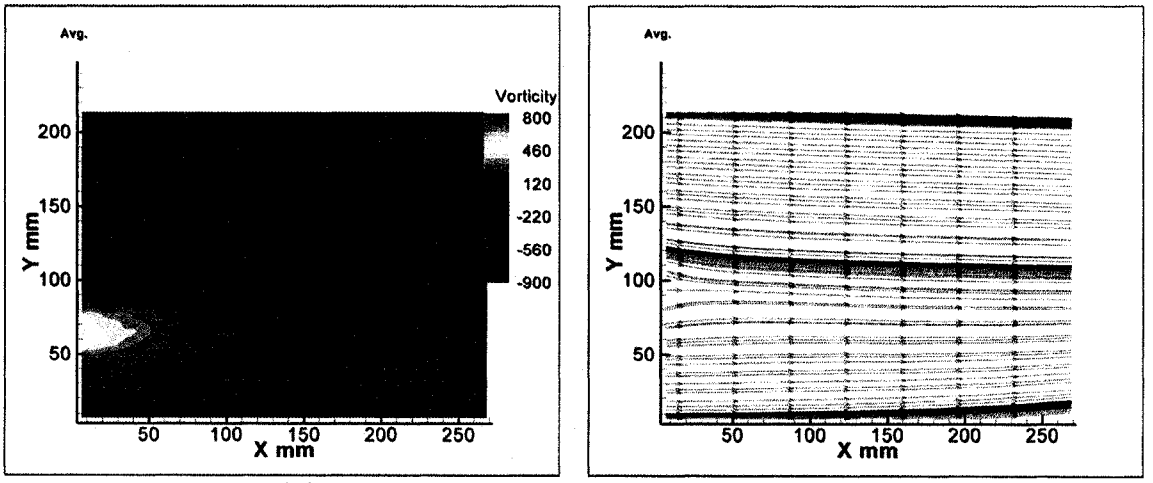

Vorticity Streamlines

Figure 7.31 Continued

Double Actuators Operated Independently

Finally, two actuators were operated with a 5 kHz carrier frequency but with a 90° phase shift in the low frequency modulating signal (Figure 7.32). This causes only one actuator to be active at any given time in order to control the state of the wake. In principle, the wake should "flip" from side to side at the modulating frequency, with associated changes in circulation. The modulation frequency was varied as a control parameter and it was observed that for a narrow frequency band (24.5-25.5 Hz) around the natural shedding frequency of the cylinder it was possible to "lock on" to the vortex structure and drive it at the desired values over this small range. This is flow control in the proper sense - a causal relationship between input and output. It was also seen that running the actuators at the half or double the natural shedding frequency caused complete disorganization of the periodicity of the vortex shedding.

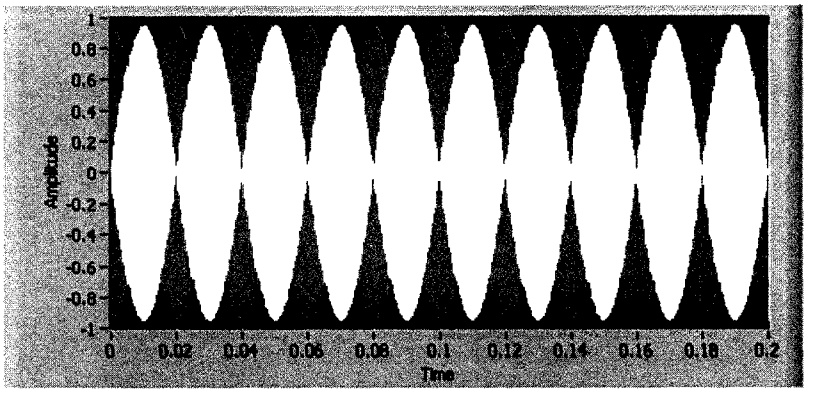

Figure 7.32 Modulated carrier frequency signal to operate double actuators with 90° phase

Figure 7.33 shows the case where the actuators were operated with 12.5 Hz modulation frequency. It is seen that the wake size is reduced and its periodicity has disappeared (at least at the modulation frequency).

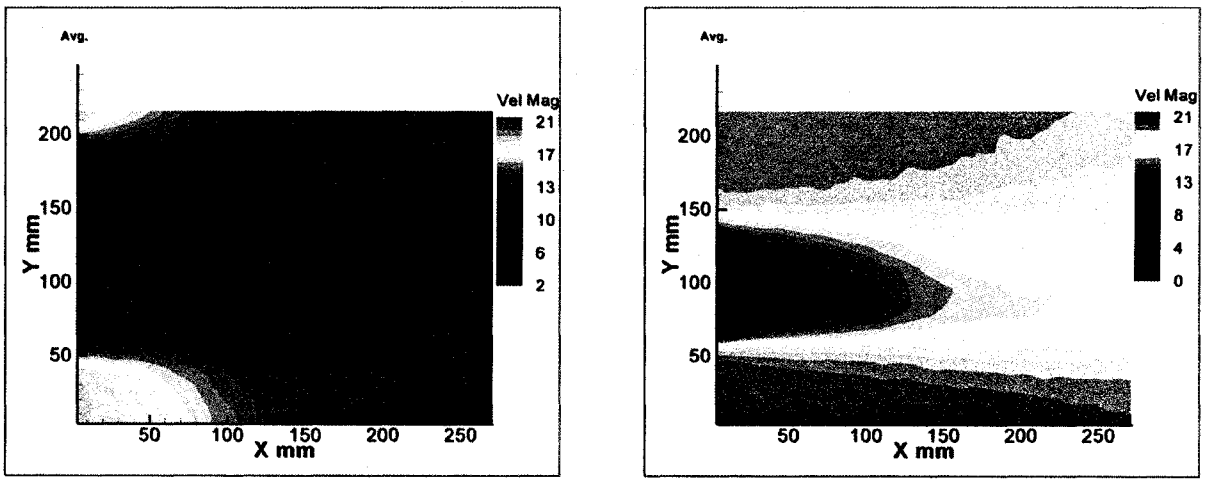

Velocity Magnitude (No control case) Velocity Magnitude

Figure 7.33 Average Wake Field, double actuator-12.5 Hz

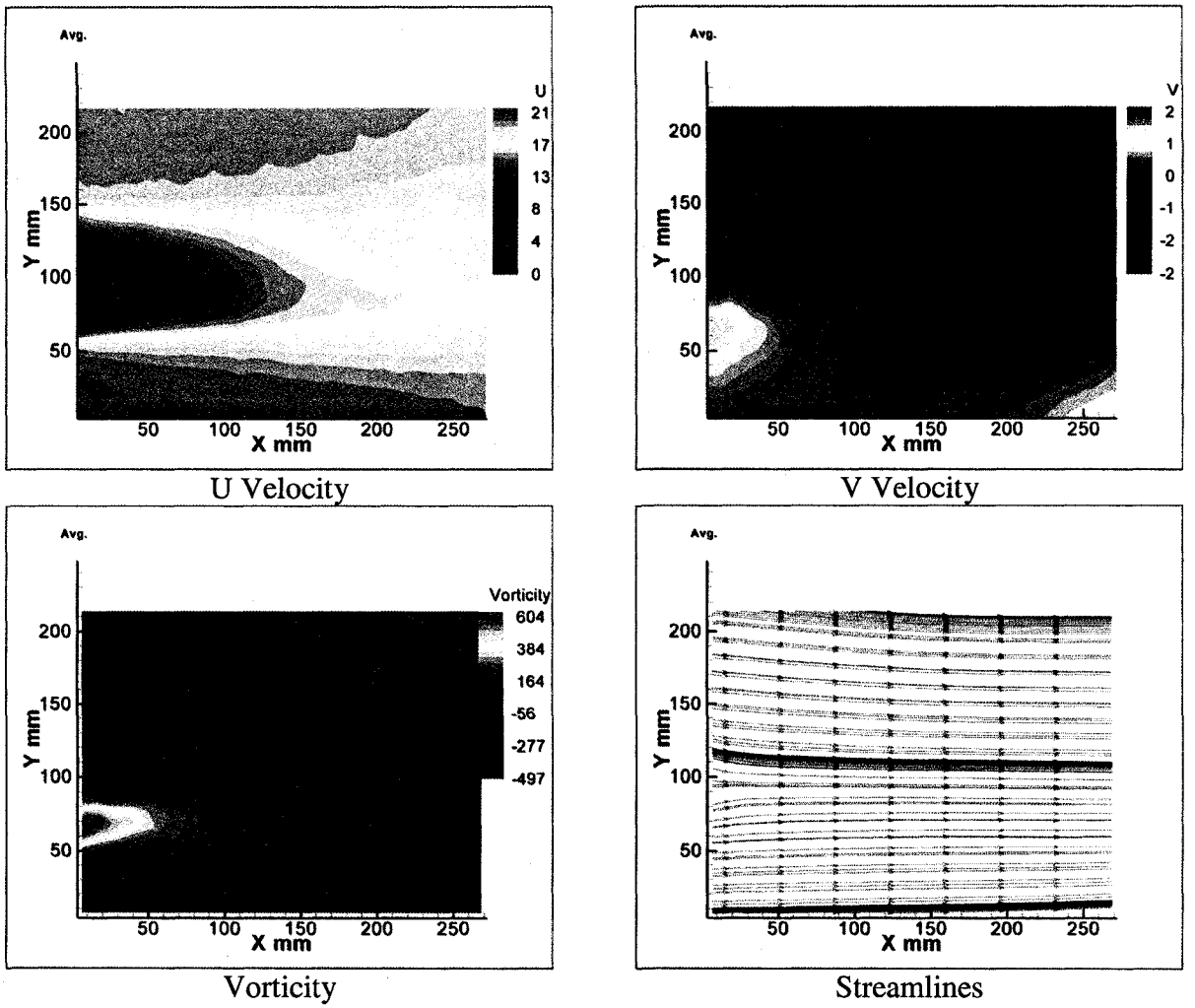

Figure 7.33 Continued

Similar effects to those for the 12.5 Hz case were observed for the 50 Hz case where the width of the wake was reduced and the periodicity at the modulation frequency disappeared (Figure 7.34).

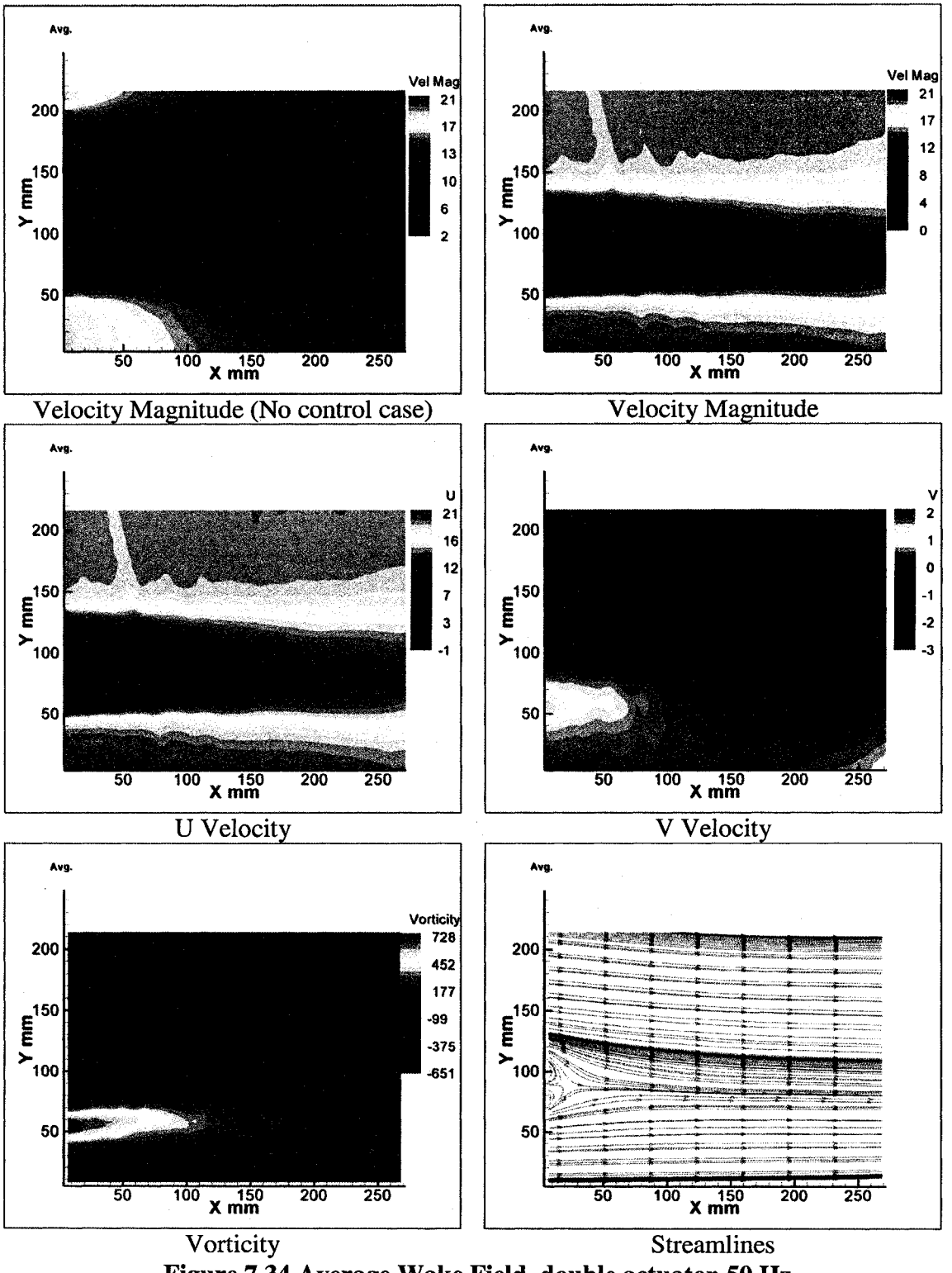

Figure 7.34 Average Wake Field, double actuator-50 Hz

As was mentioned earlier, "lock on" to vortex shedding was possible for frequencies between 24.5- 25.5 Hz. In Figure 7.35 a classical vortex street, derived from 600 binned images with an angular resolution of 10°, can be easily seen. Evaluation of the V velocity component and vorticity can be seen frame by frame in Figures 7.35 and 7.36, respectively. "Lock on" must be occurring otherwise the binned images would not resolve to distinct vortex patterns, rather would tend to the time average, which is shown in Figure 7.37.

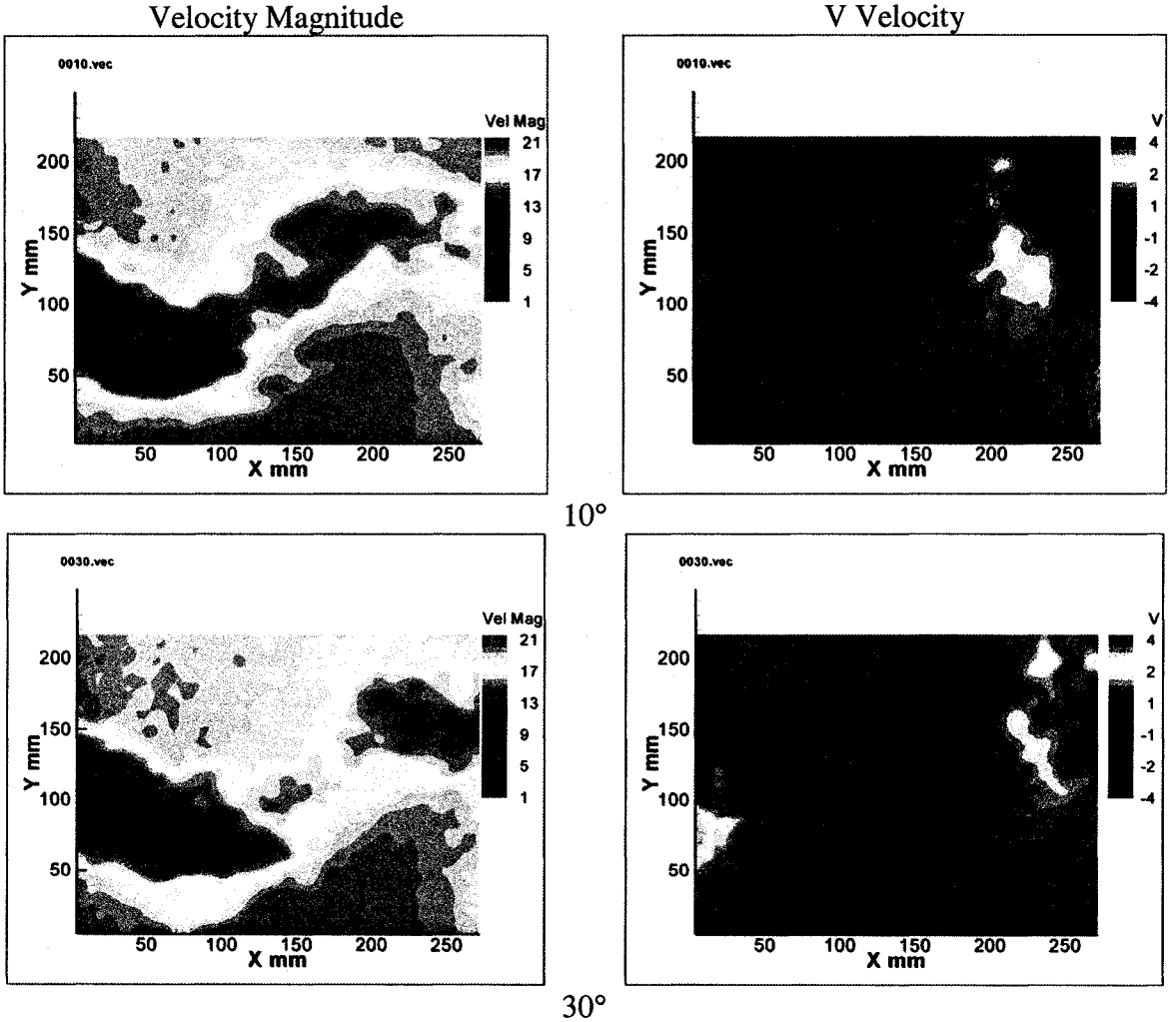

Figure 7.35 Wake field for the larger cylinder using TTT, double actuator-24.5 Hz

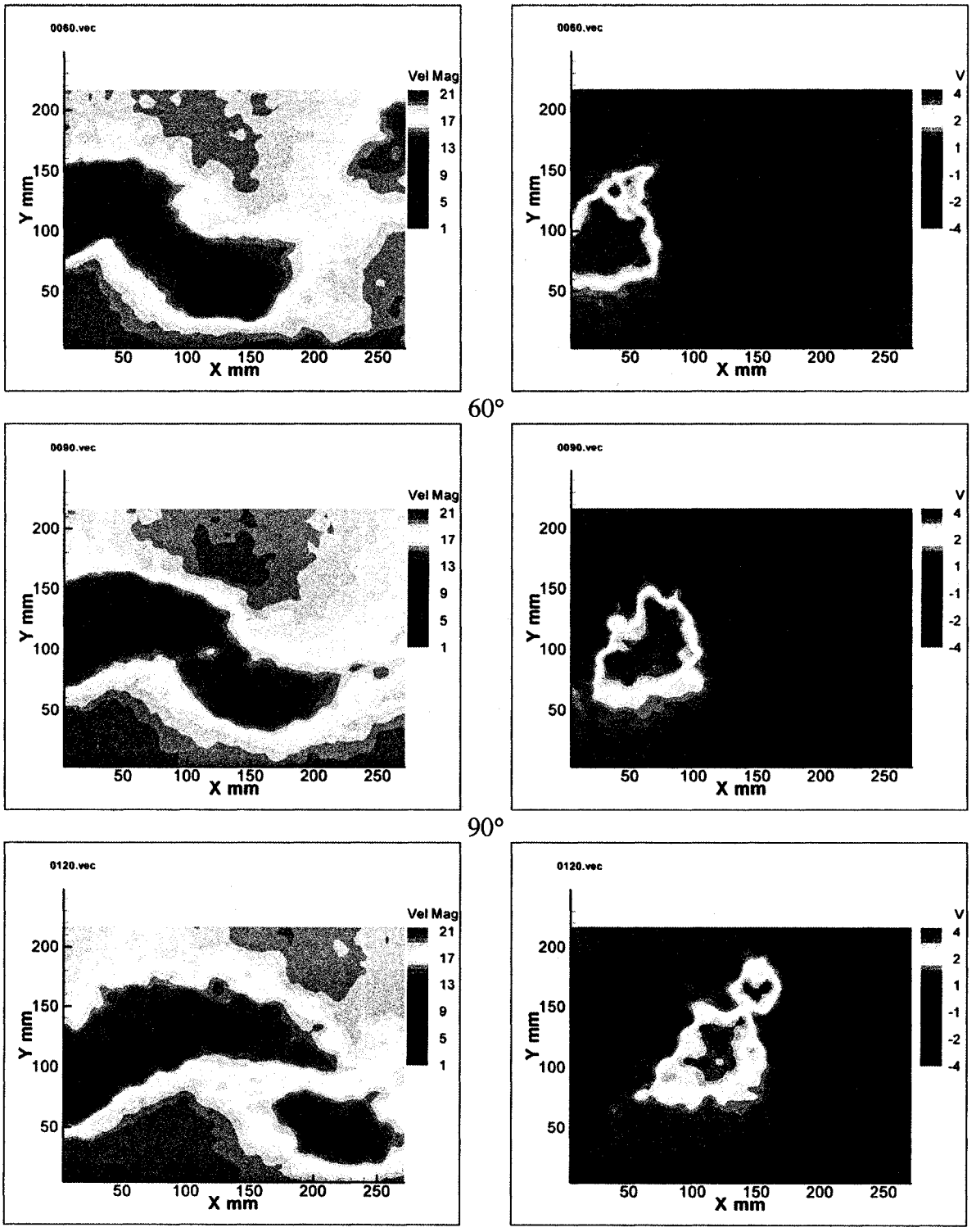

Figure 7.35 Continued

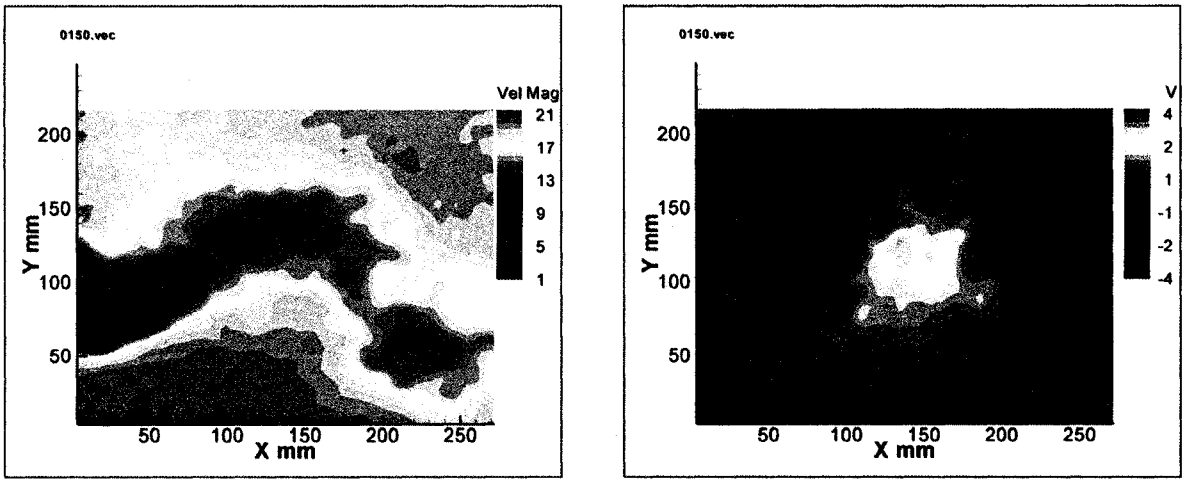

150°

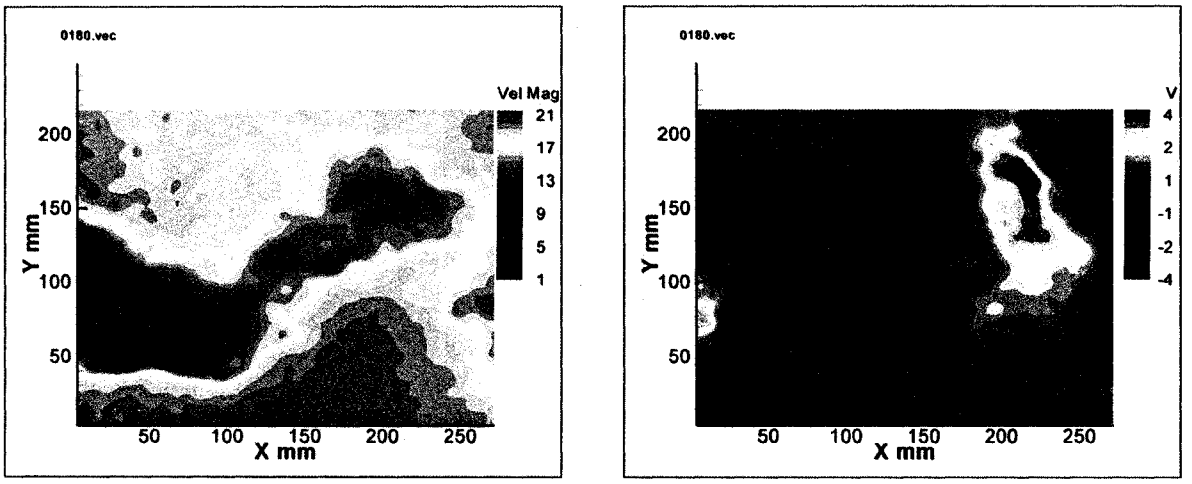

180°

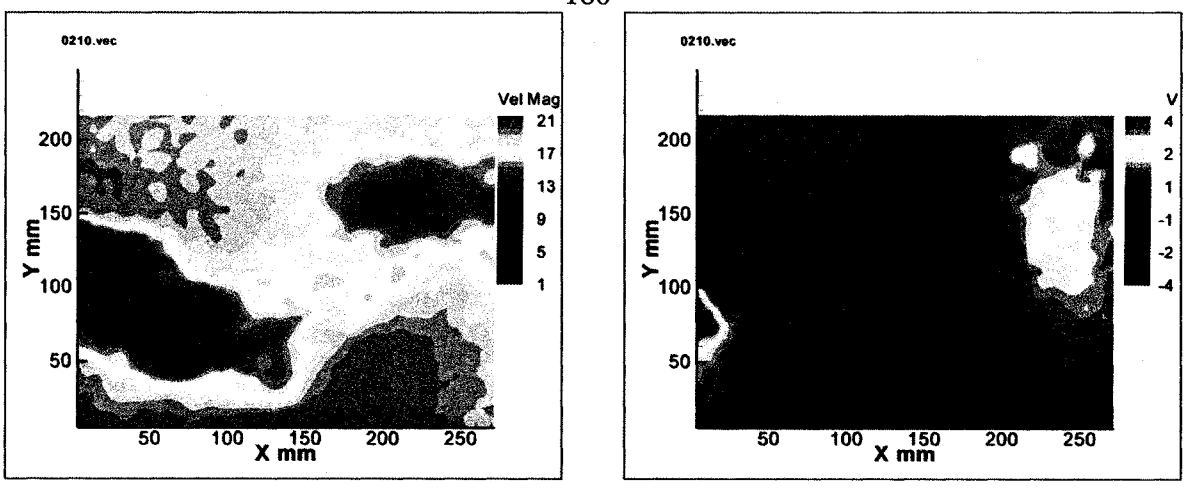

210°

Figure 7.35 Continued

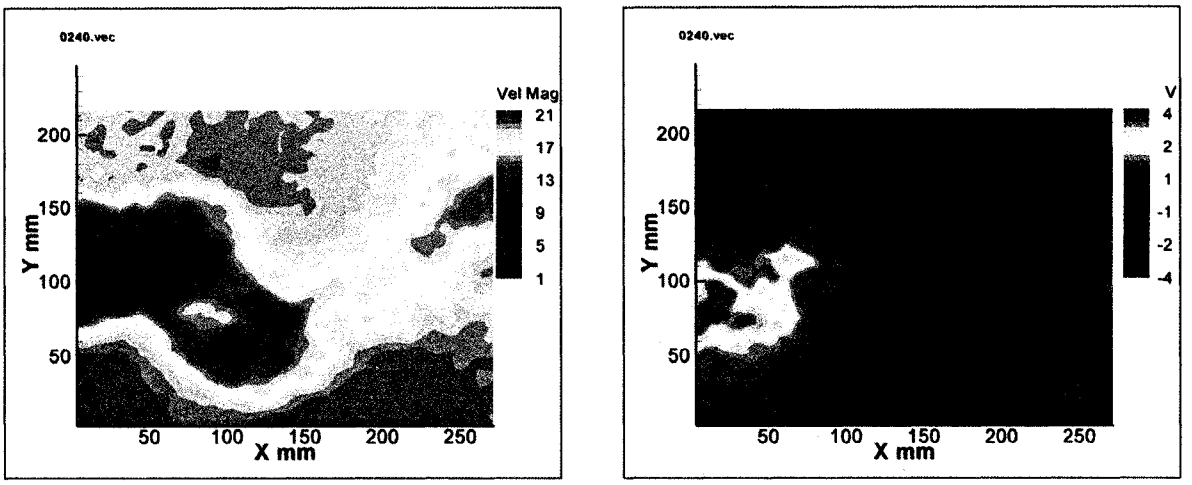

240°

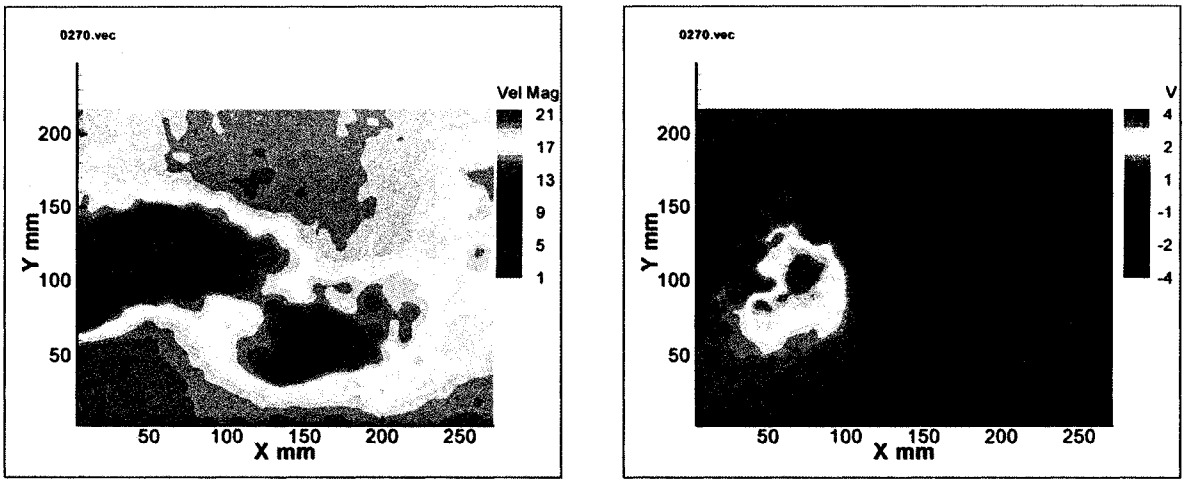

270°

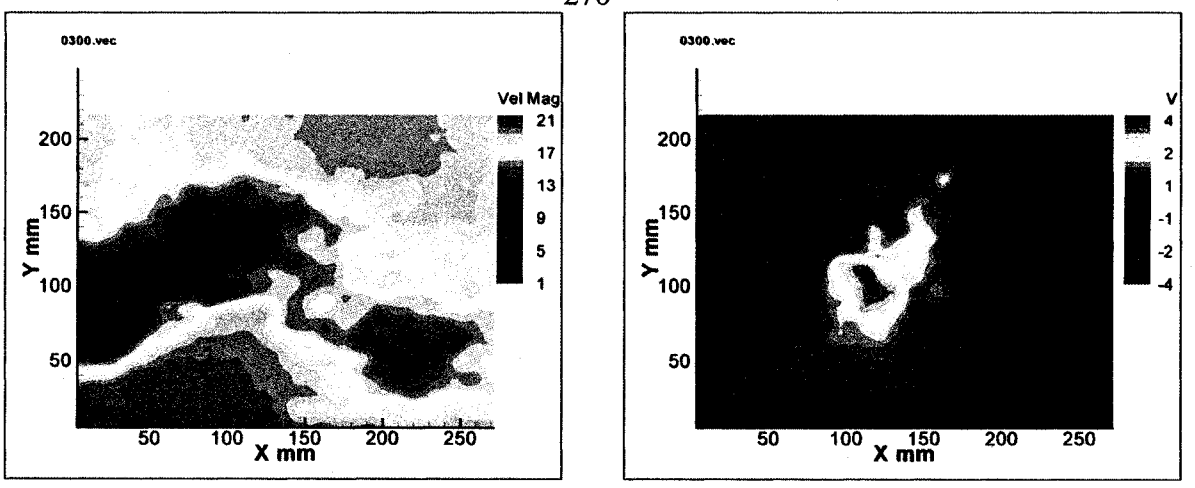

300°

Figure 7.35 Continued

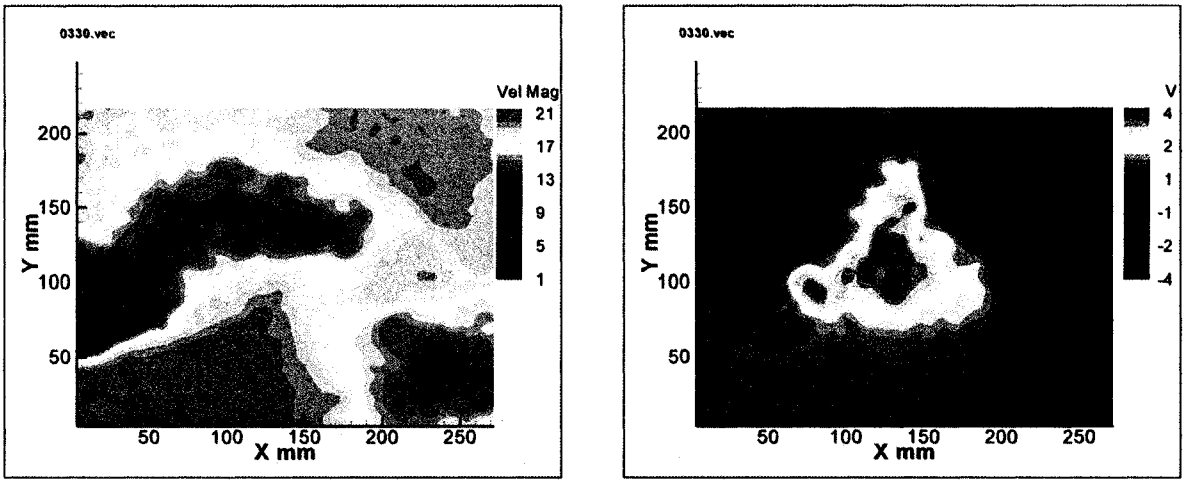

330°

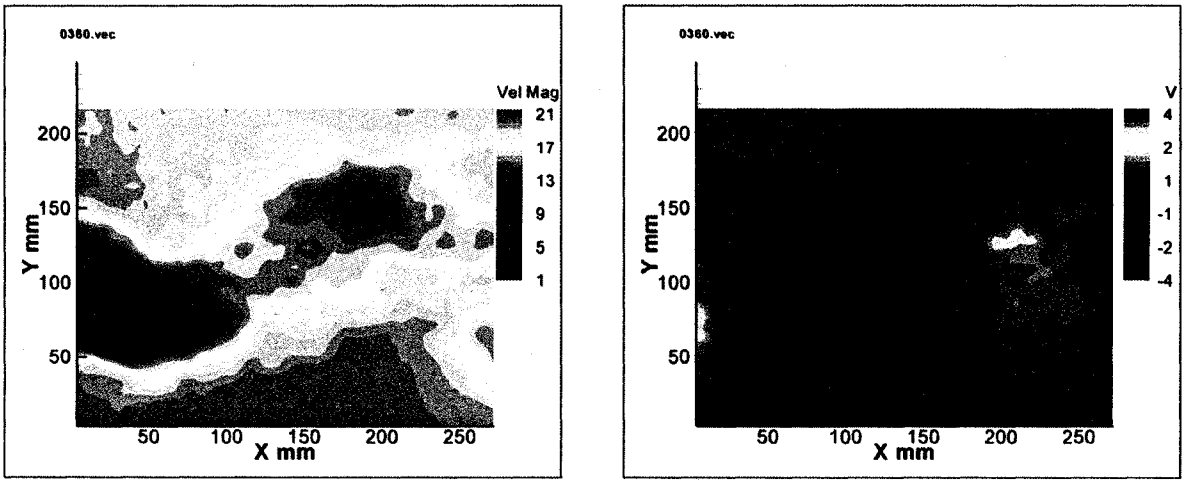

360°

Figure 7.35 Continued

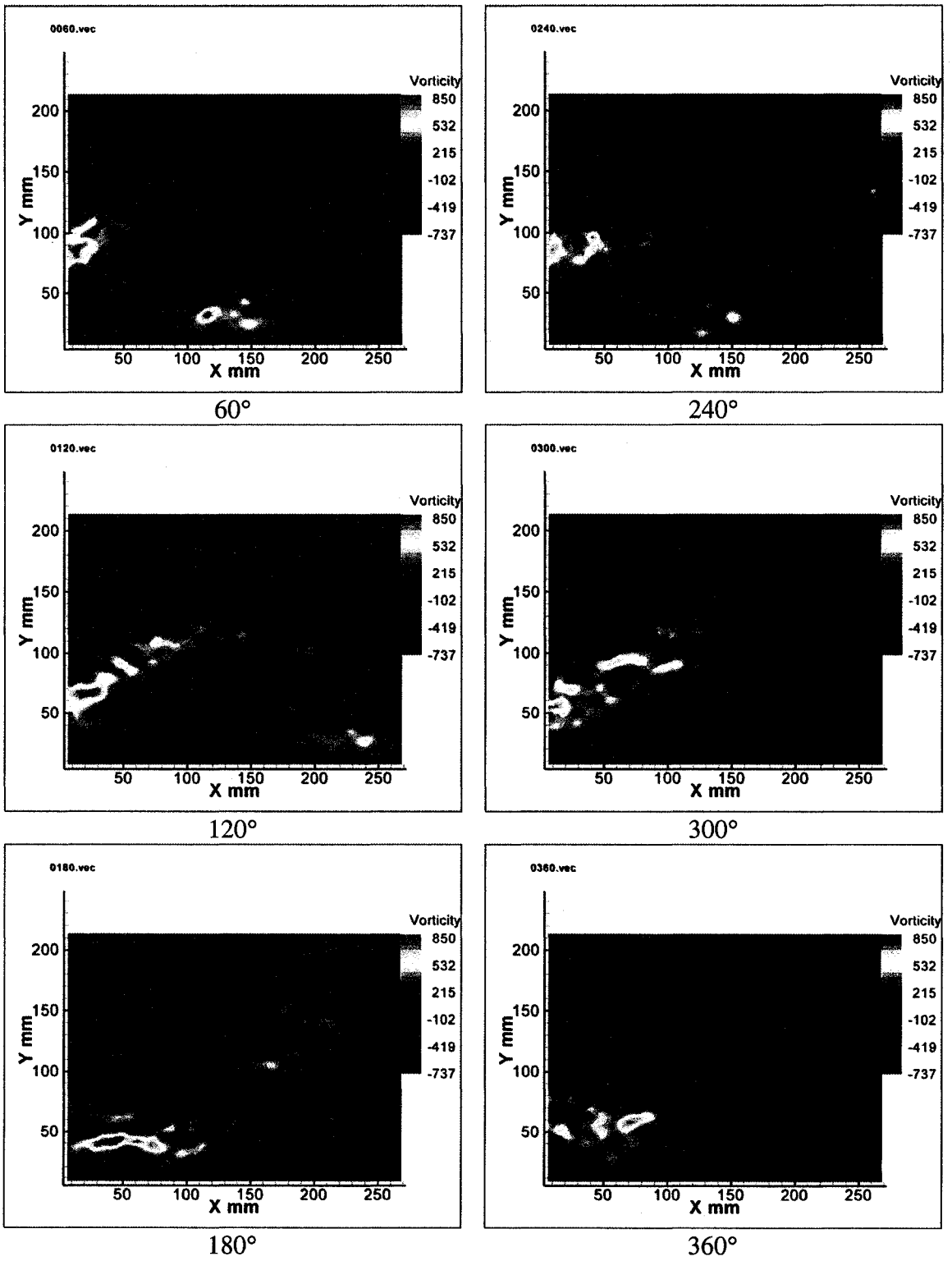

Figure 7.36 Vorticity field for the larger cylinder using TTT, double actuator-24.5 Hz

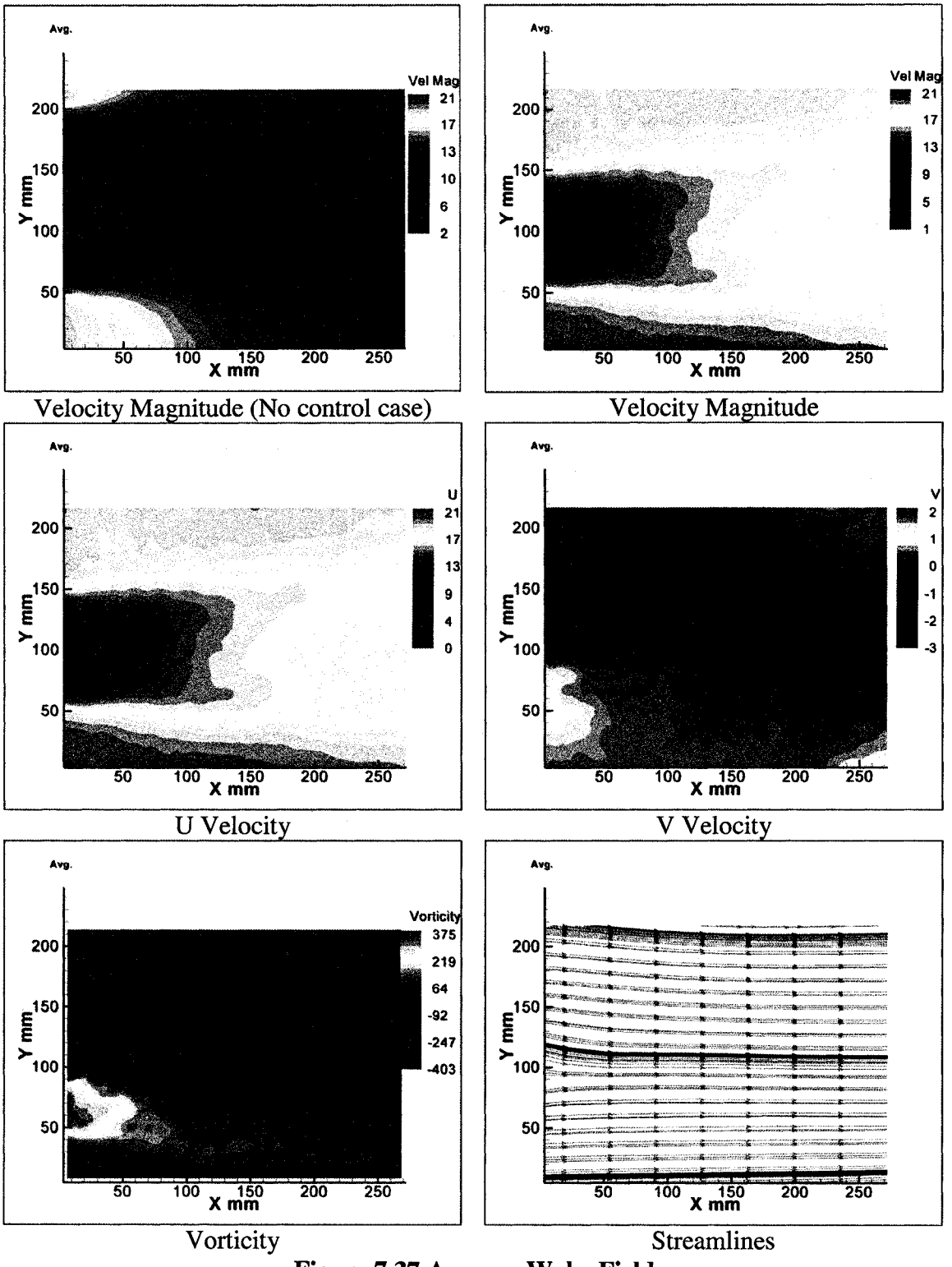

Figure 7.37 Average Wake Field

After 24.5 Hz, 25 Hz was used as modulating frequency for the actuators. Similar structures to the previous case were experienced. Lock on was successful, and a vortex street was clearly observed (Figures 7.38-40).

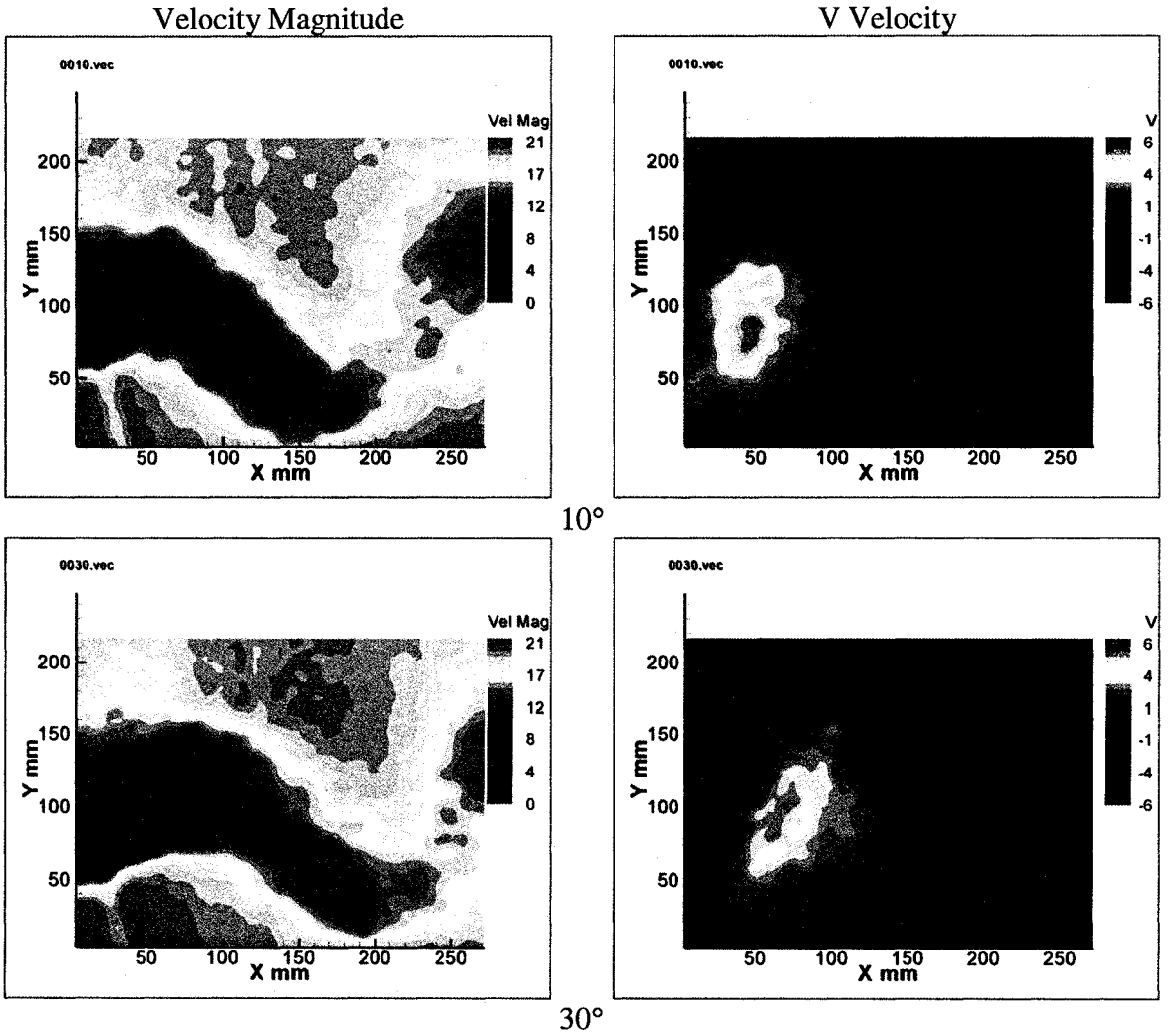

Figure 7.38 Wake field for the larger cylinder using TTT, double actuator-25 Hz

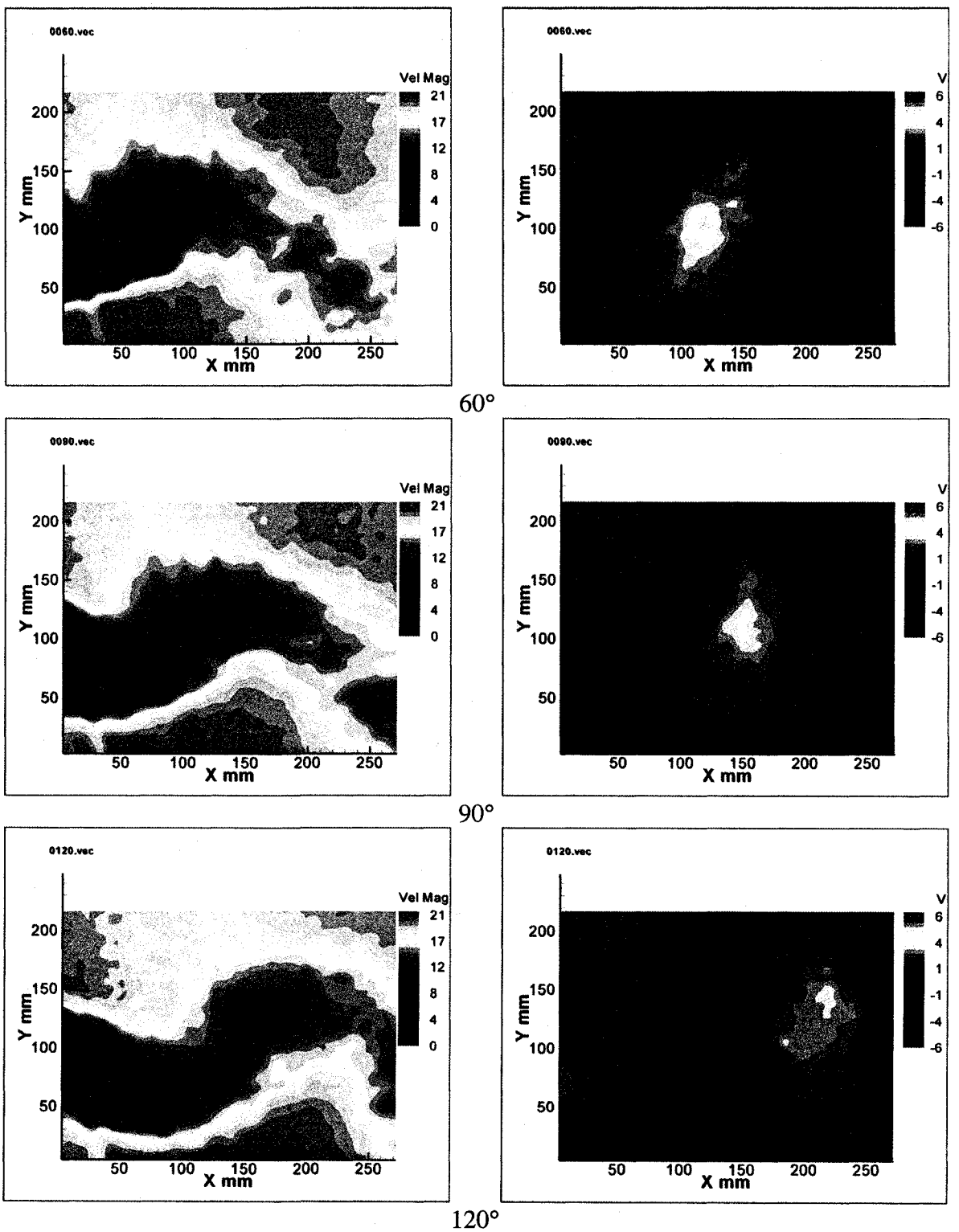

Figure 7.38 Continued.

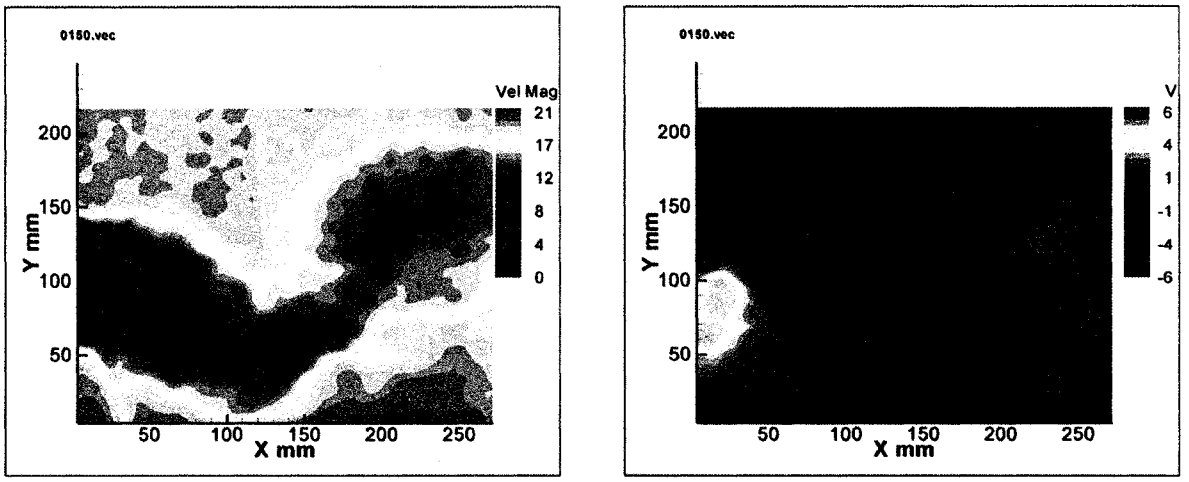

150°

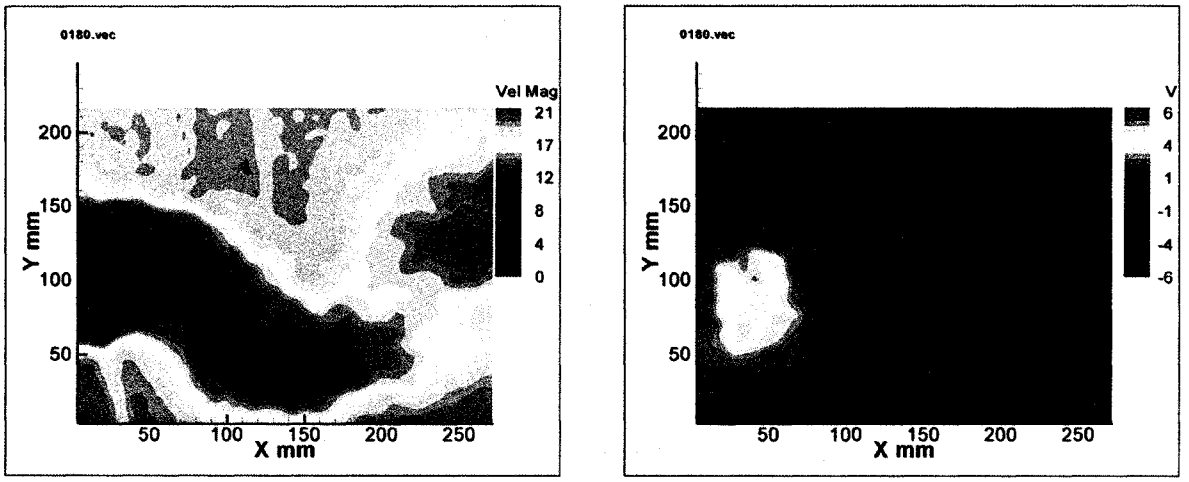

180°

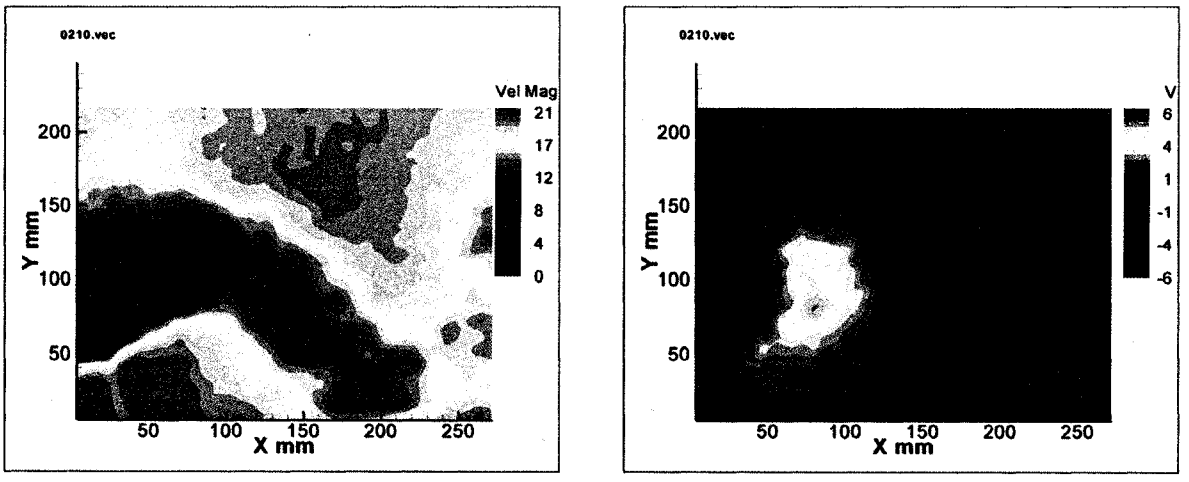

210°

Figure 7.38 Continued

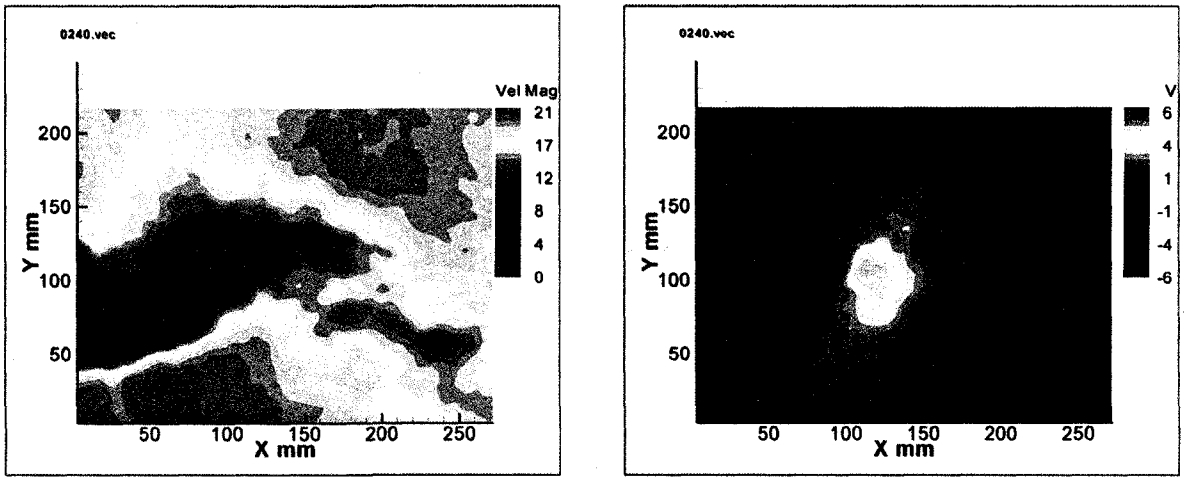

240°

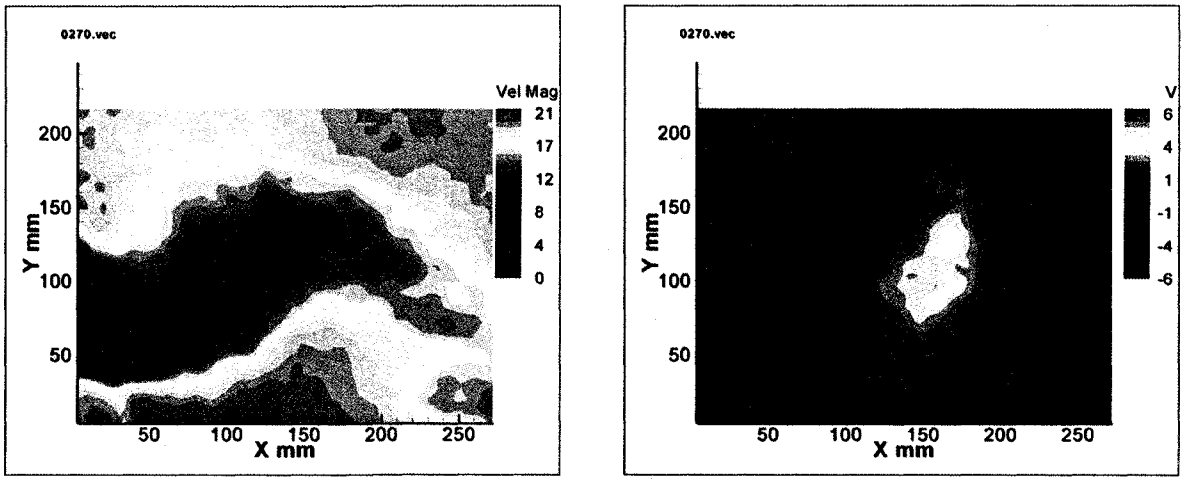

270°

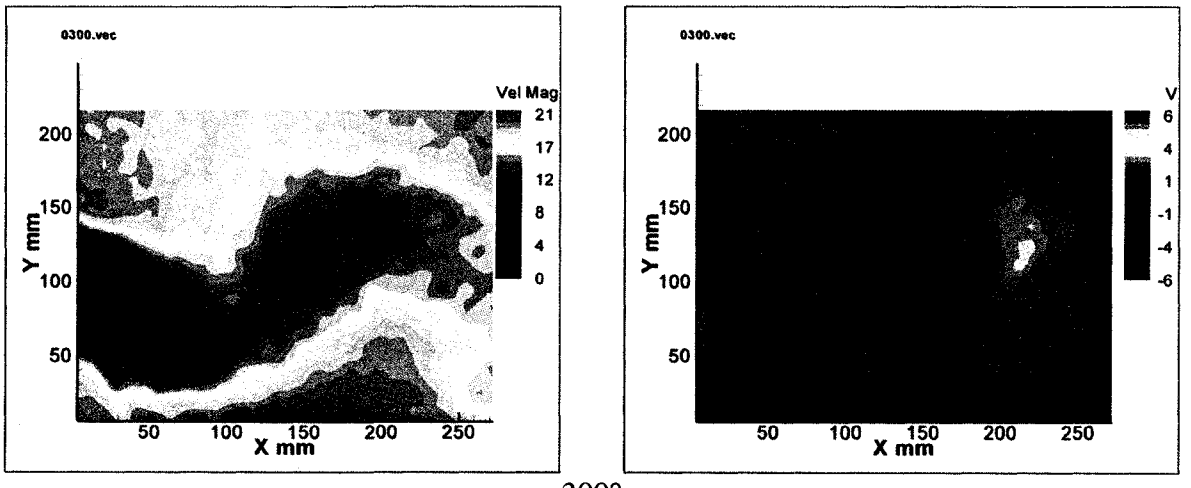

300°

Figure 7.38 Continued

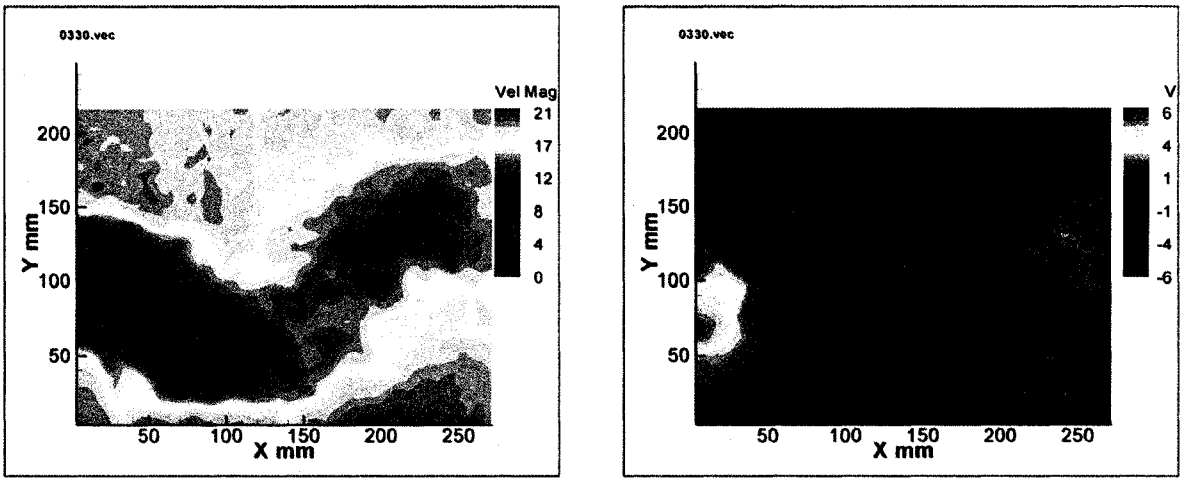

330°

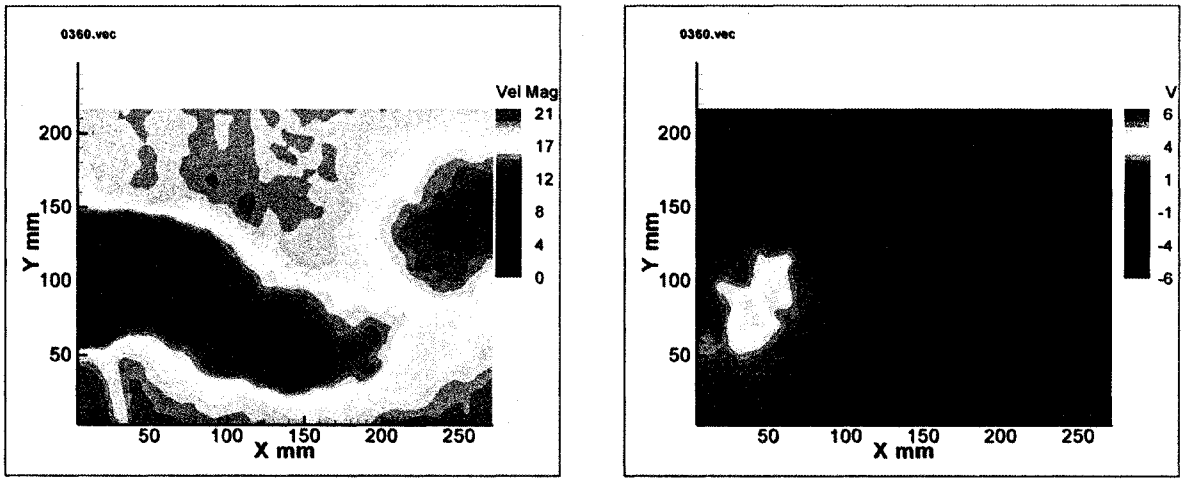

360°

Figure 7.38 Continued

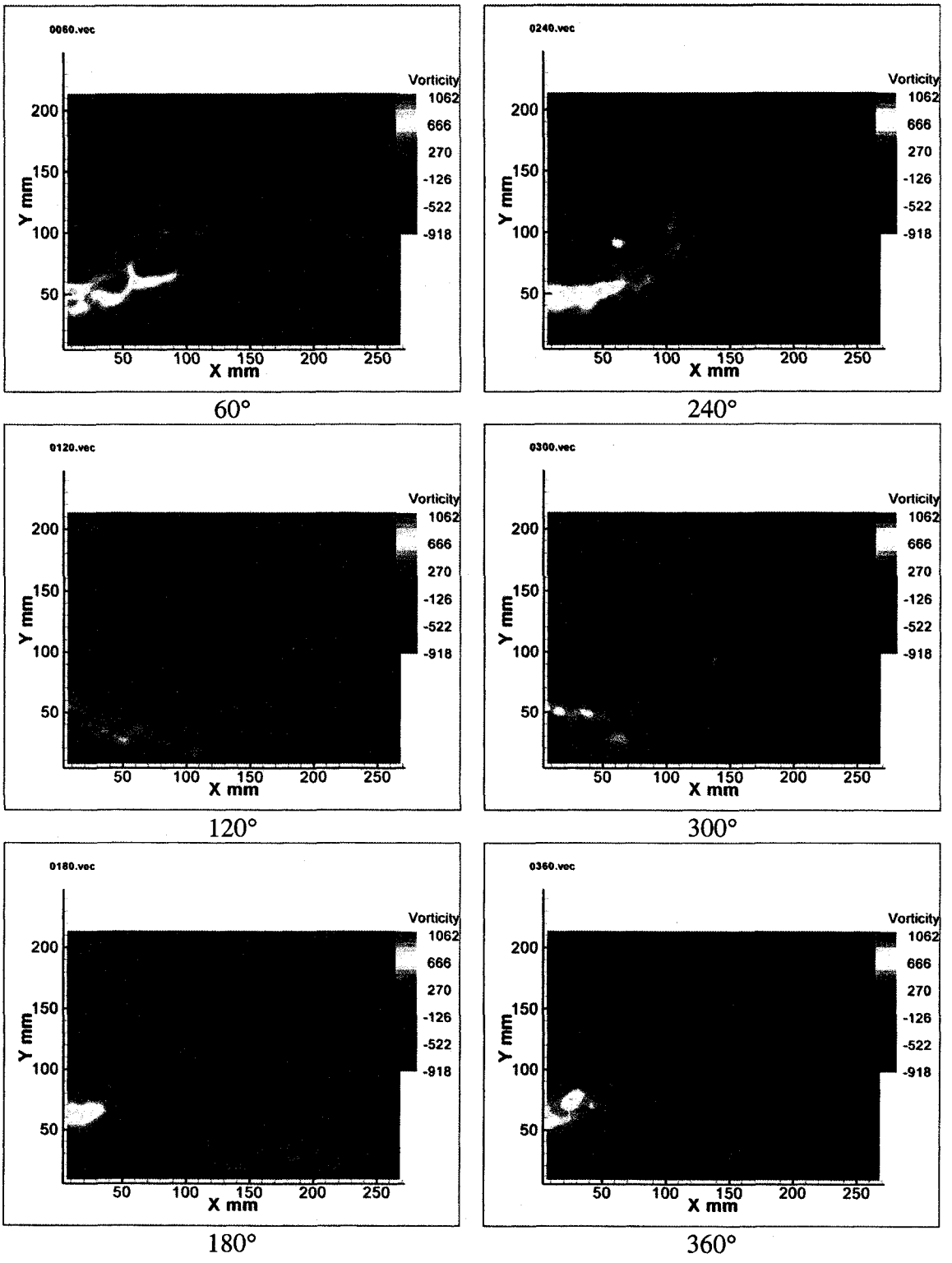

Figure 7.39 Vorticity field for the larger cylinder using TTT, double actuator-25 Hz

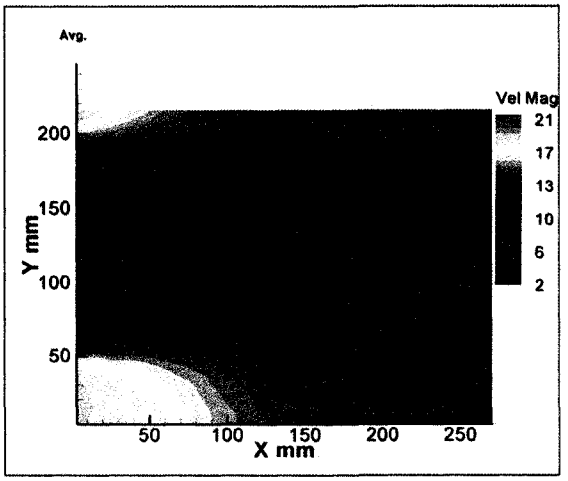

Velocity Magnitude (No control case)

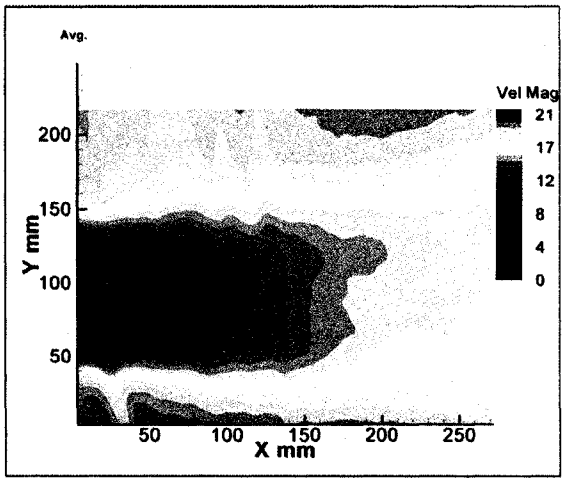

Velocity Magnitude

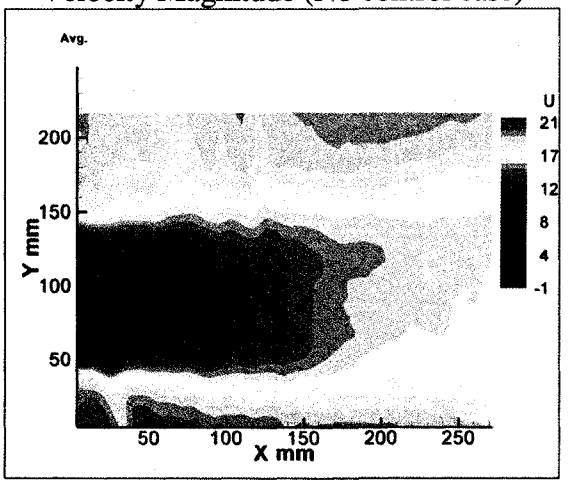

U Velocity

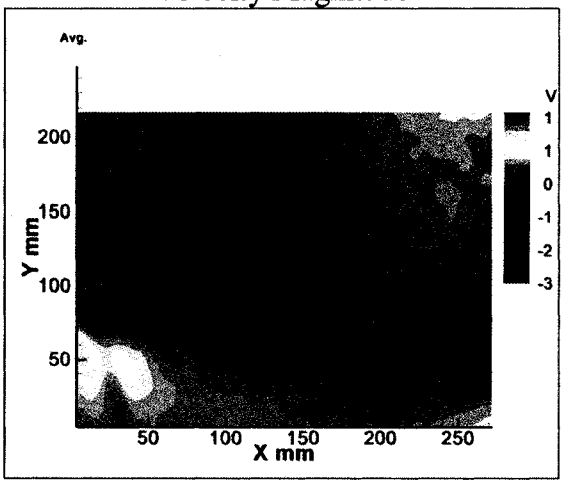

V Velocity

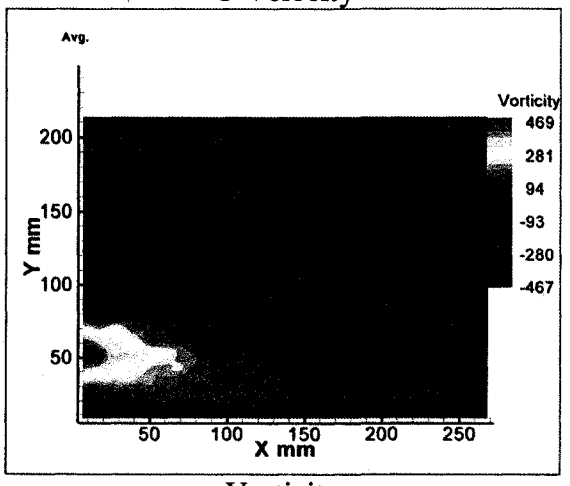

Vorticity

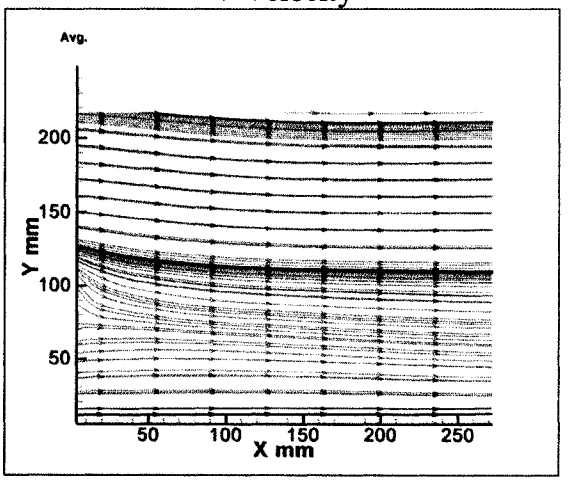

Streamlines

Figure 7.40 Average Wake Field

Lastly 25.5 Hz sine waves were used to drive the actuators. Vortex structures were easily identified and lock on was successful (Figures 7.41-43).

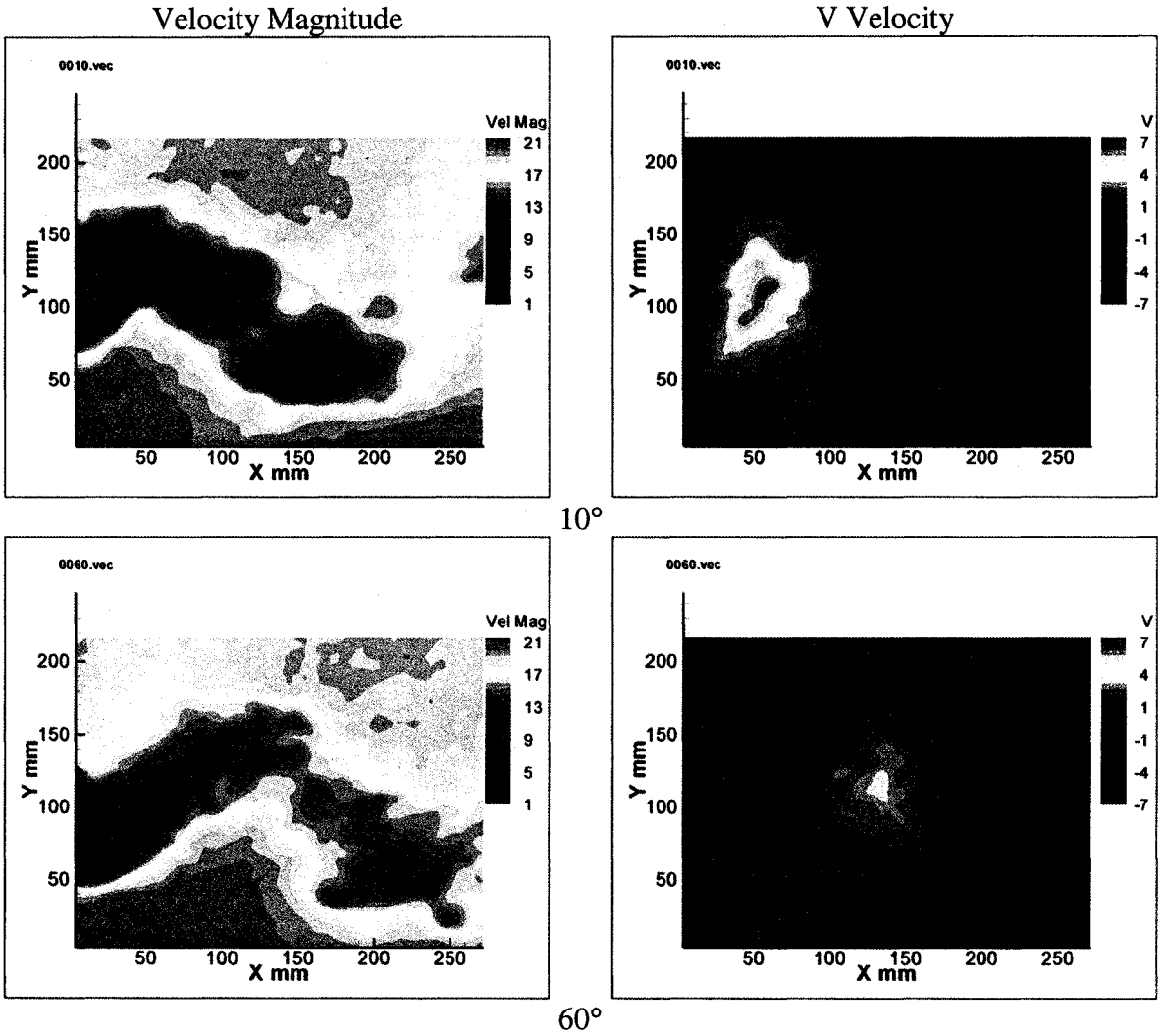

Figure 7.41 Wake field for the larger cylinder using TTT, 25 kHz

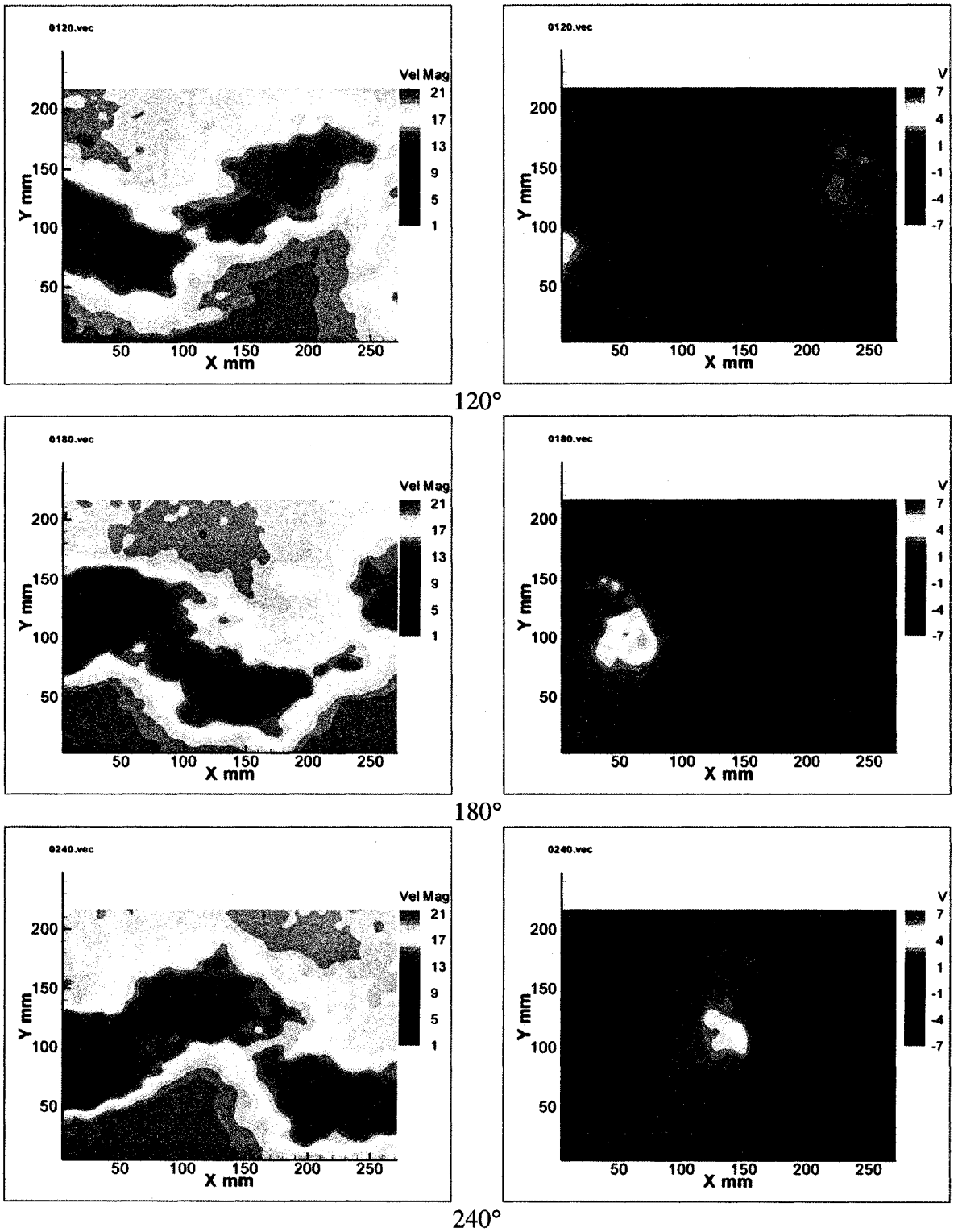

Figure 7.41 Continued

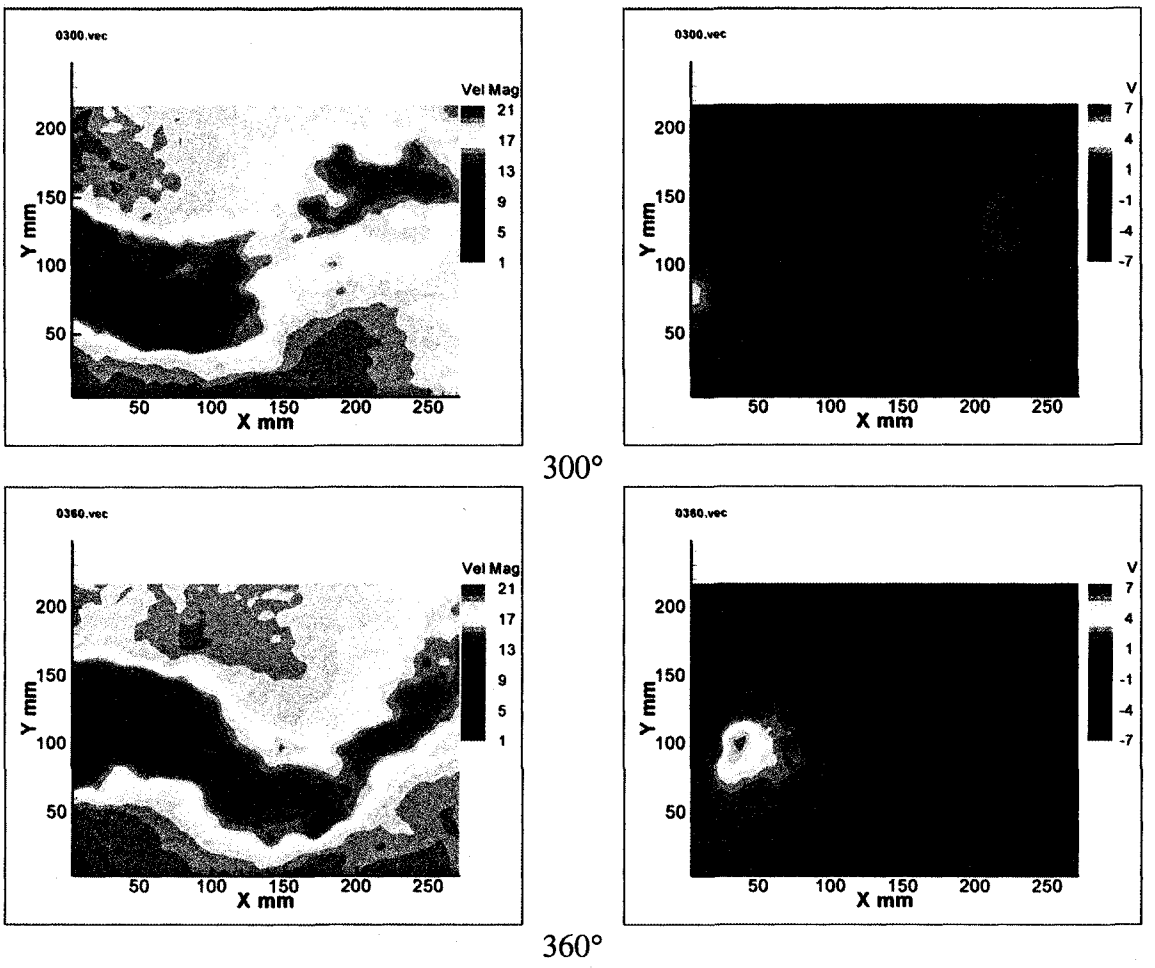

Figure 7.41 Continued

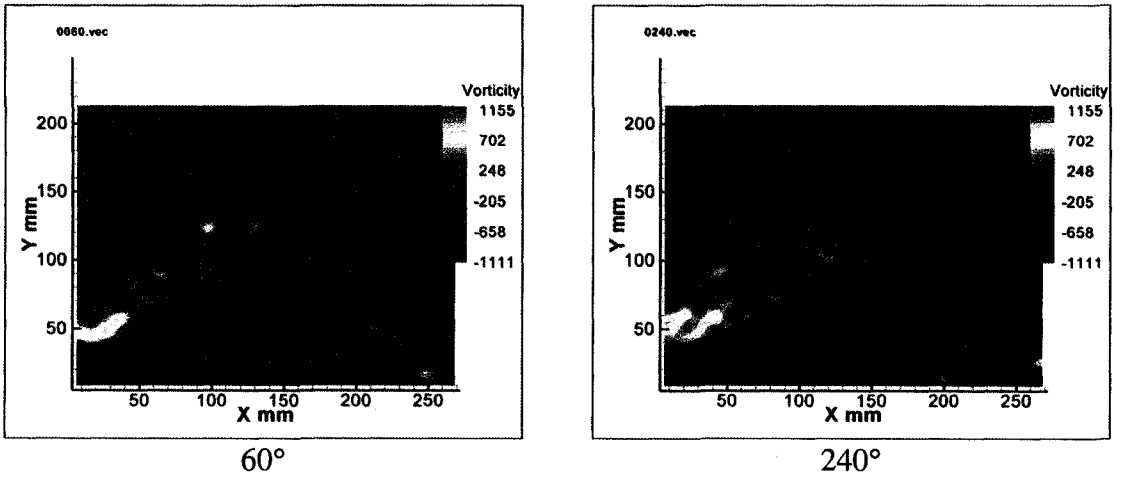

Figure 7.42 Vorticity field for the larger cylinder using TTT, double actuator-25.5 Hz

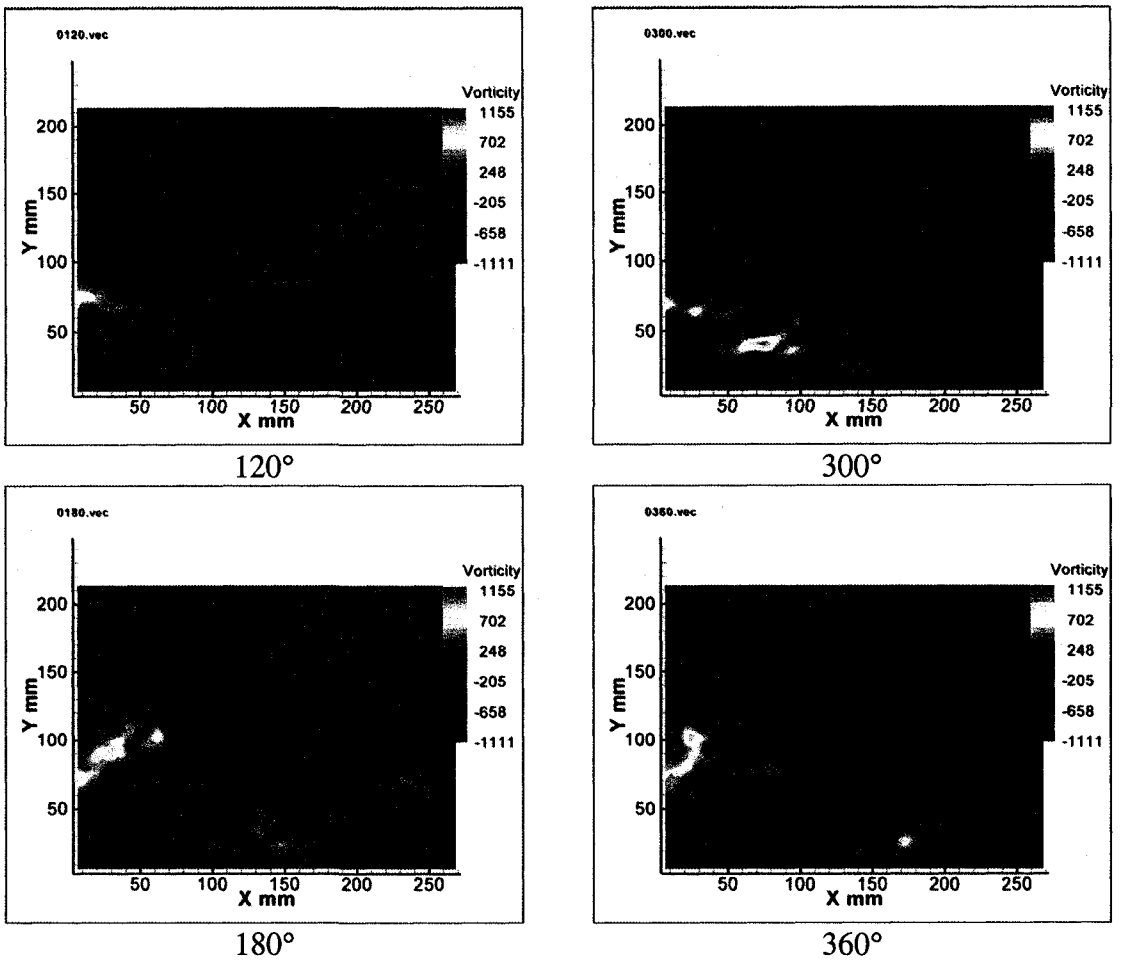

120° 300°

180° 360°

Figure 7.42 Continued

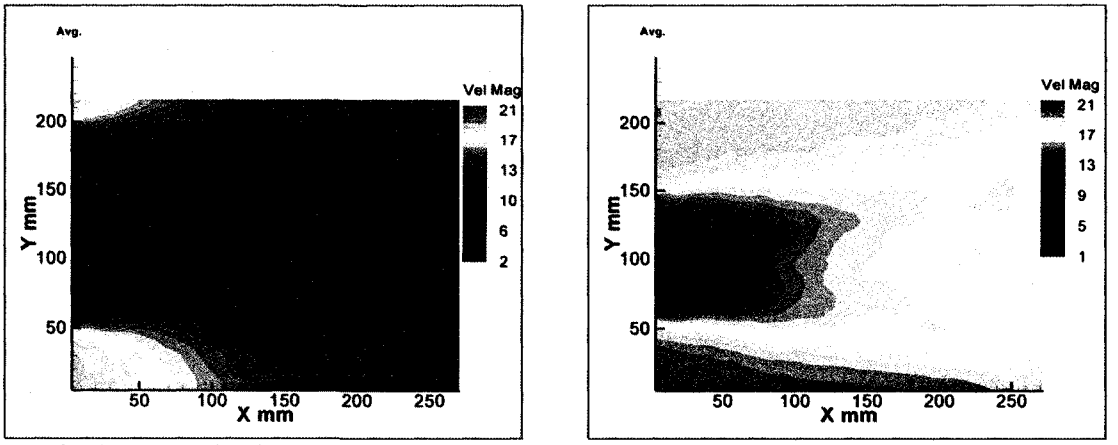

Velocity Magnitude (No control case) Velocity Magnitude

Figure 7.43 Average Wake Field

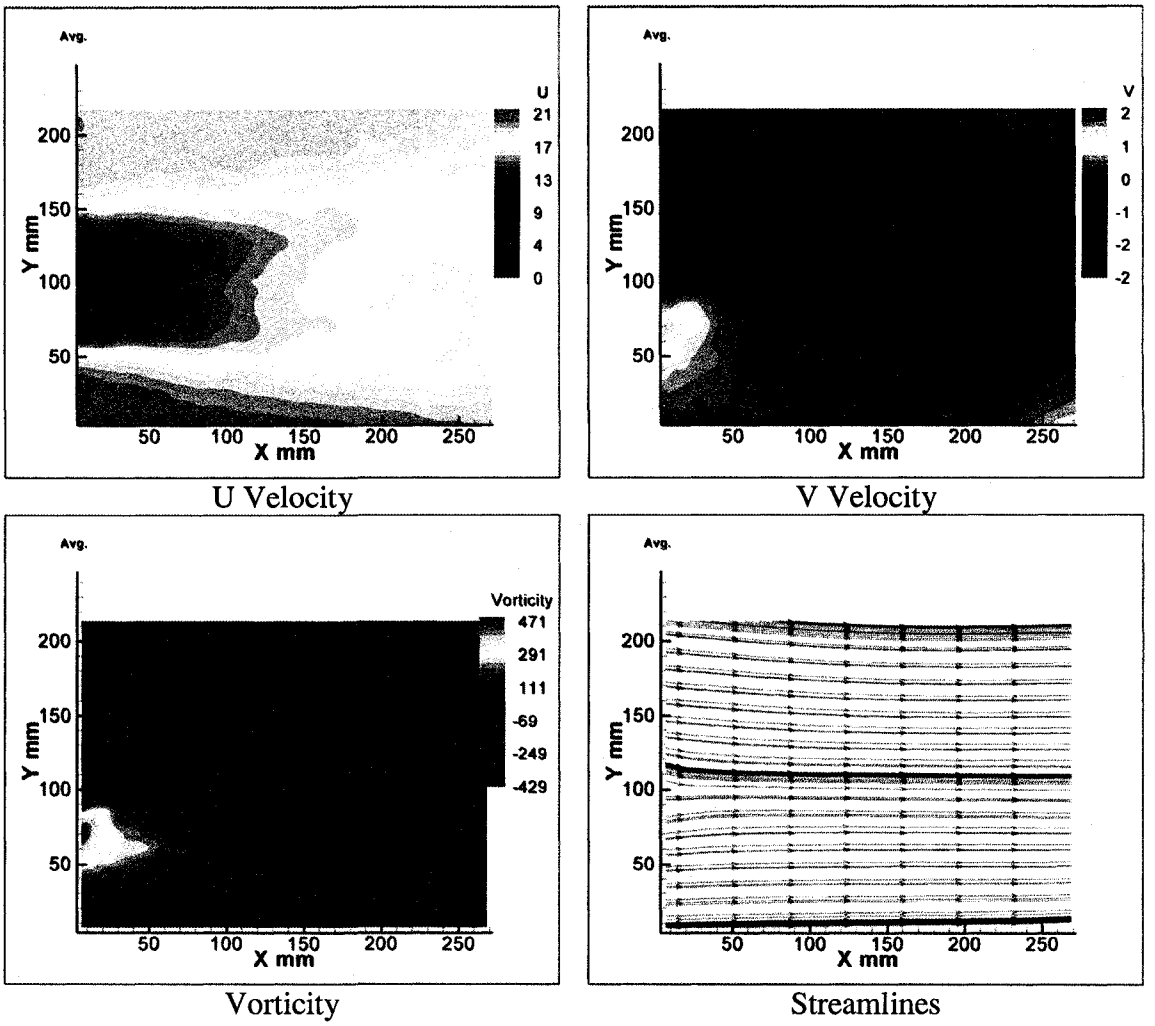

Figure 7.43 Continued

7.4.2 Flow Control on the Ogive Cylinder

Flow control was attempted on the ogive cylinder described in section 7.3. To better see the relative effectiveness of the actuators the freestream velocity was reduced to 20 m/s. Copper electrodes of ¼" wide and ¾" wide Kapton tape were used to build the actuators. An overlap of 1mm was chosen for the electrodes. Four different configurations of actuators were tested. First, four actuators (60° arcs separated by 15°) on the circumference operating as two pairs at same frequency were used. Later two actuators (150° arcs separated by 30°) on the circumference operating independently were tested.

After that two actuators placed on the base (2" long), "blowing" outwards were tested. Lastly, two actuators (12" long) oriented in the streamwise direction on top and bottom of the body were investigated. Placement of the electrodes is illustrated in Figure 7.44. It was observed that direct alteration of the mean flow about a body was not as effective as the boundary layer flow control where the flow instabilities are exploited in the cylinder case. Also, as mentioned before, ogive cylinder had a complex three dimensional flow field. For this reason it was harder to propose a flow control method to have a favorable effect.

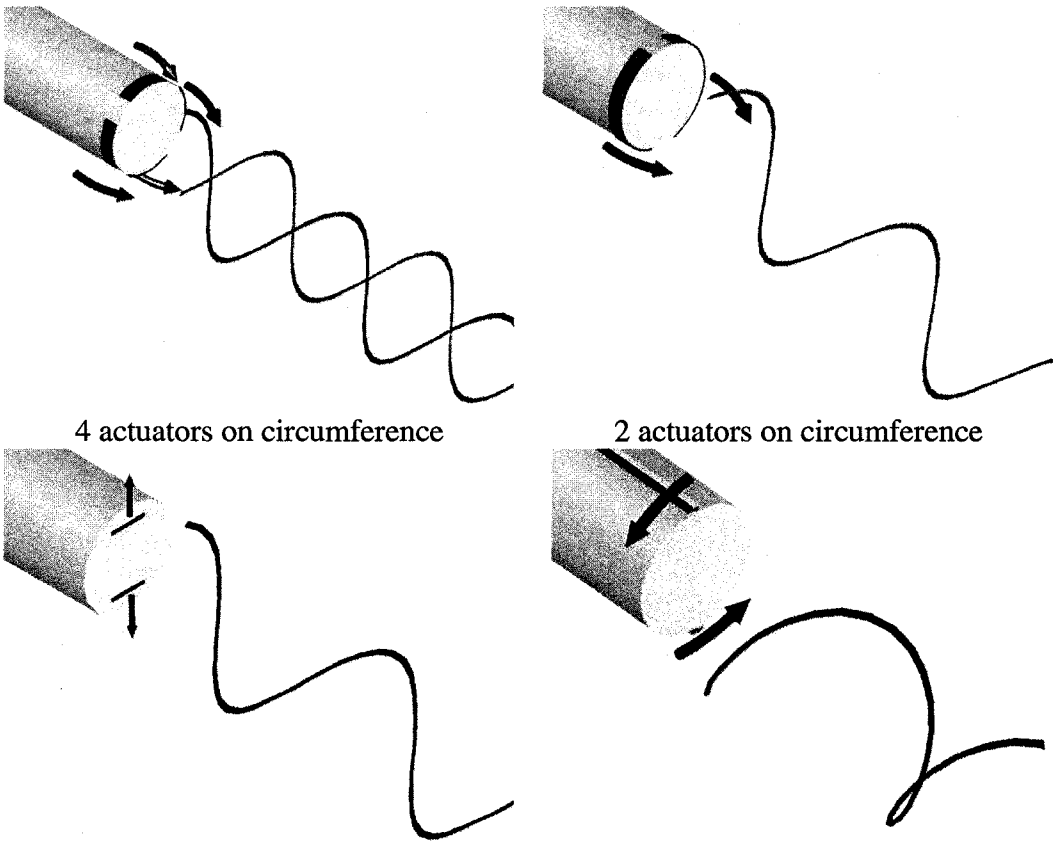

Figure 7.44 Actuator Locations for Ogive Cylinder

Figure 7.45 shows the dominant frequency measurements at different plasma modulation frequencies. It is observed that the frequency characteristics for all cases almost overlapped.

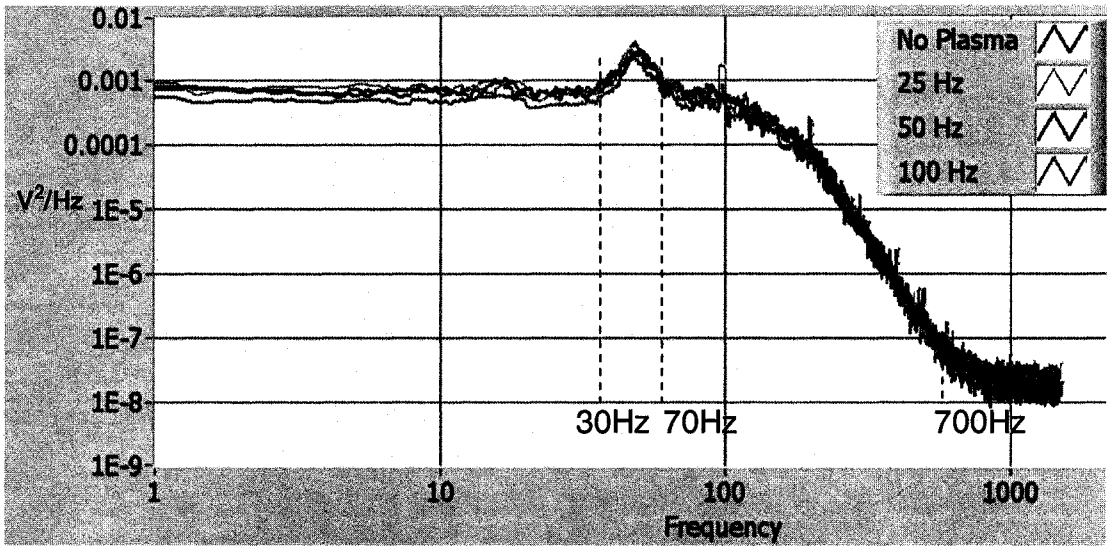

Figure 7.45 Dominant frequency at different plasma modulation frequencies

Table 7.3 presents the data obtained by integrating the areas under the power curves in Figure 7.45. Total integration as well as the integration of two focused regions are calculated. All of the data sets show that there is no distinct relation between amplitude of the power curves and the modulation frequency of the actuators. The difference between the data sets may be attributed to the random component of the data. These results also show that the effect of the actuator on the ogive cylinder was very small.

Figure 7.46 shows the wake field for one of the control cases where the four actuators were operated with 50 Hz carrier signal. Velocity magnitude plot for control

case is presented with the velocity magnitude plot for no control case. It is observed that there is only a small effect generated by the actuators which caused wake to shrink a

Table 7.3 Comparison of areas under the power curves, ogivecylinder

	Total Area	30-700Hz	30-70Hz
No Plasma	0.085	0.0637	0.0440
25Hz	0.088	0.0665	0.0455
50Hz	0.0876	0.0670	0.0470
100Hz	0.0882	0.0669	0.0463

small amount. U velocity plot shows the classical wake pattern where the wake closure point is observed. V velocity plot shows the existence of two vortices with opposite signs. Vorticity plot shows the two shear layer with opposite signs as well.

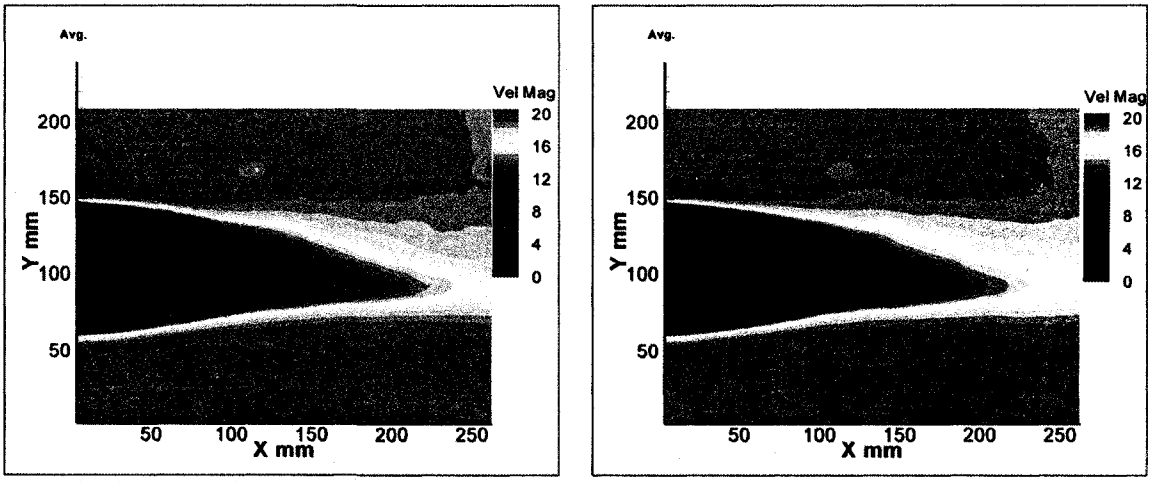

Velocity Magnitude (No control case) Velocity Magnitude

Figure 7.46 Average Wake Field

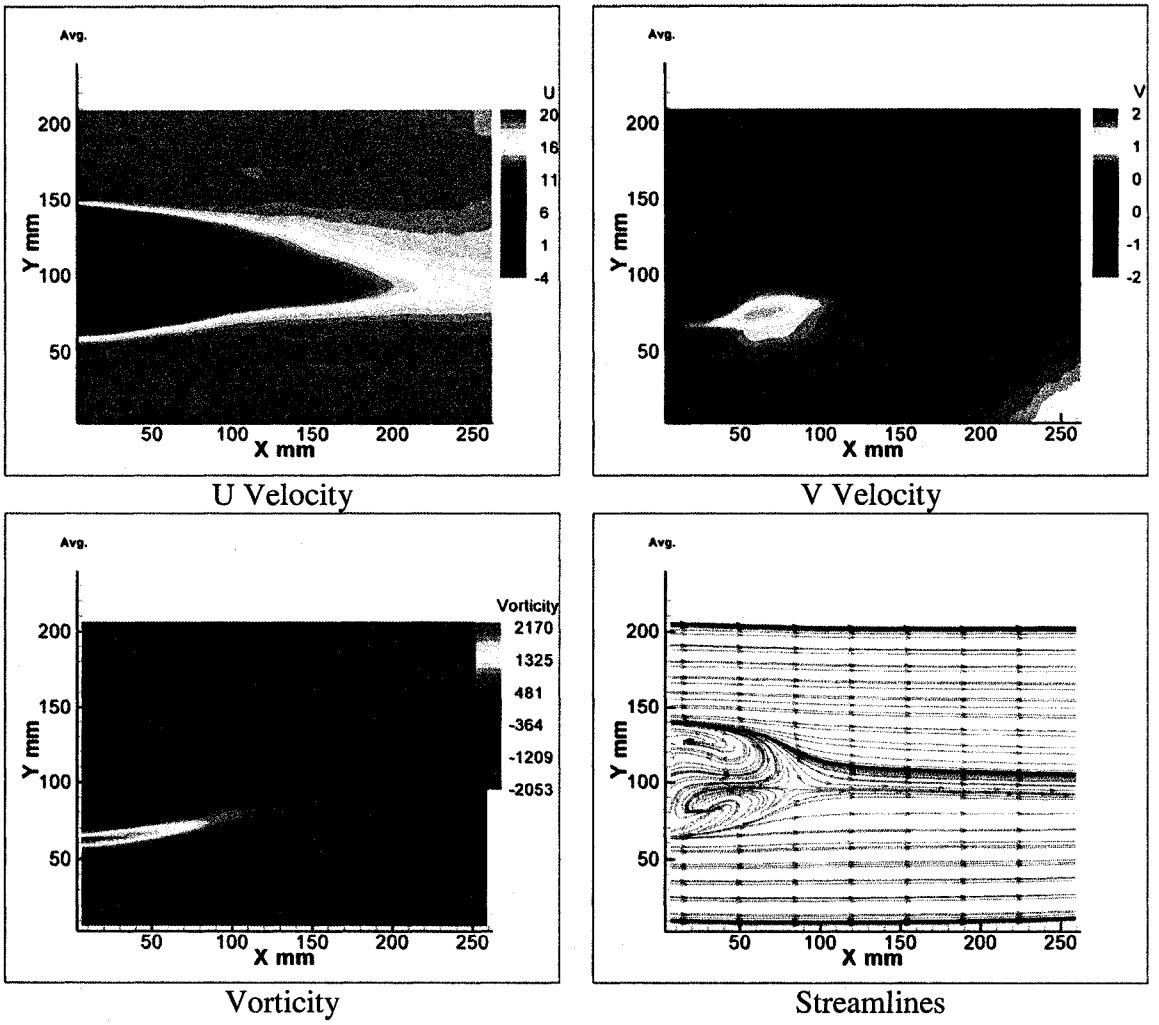

Figure 7.46 Continued

Due to the difficulties stated earlier not much difference was observed for the flow control of ogive cylinder compared to no control case. Tests at different Reynolds numbers, different actuator or carrier frequencies (not presented here) and different geometries mentioned above did not reveal any effect of the plasma actuators either.

8. CONCLUSIONS AND FUTURE WORK

8.1 Conclusions

The present work was involved with the aerodynamic characteristics of a circular cylinder at Re=156,000 and an axisymmetric body (ogive cylinder) at Re=170,000 as well as manipulation of their wakes using plasma actuators. Detailed wake data was obtained through the PIV technique.

Investigation of the wake fields were made by using two phase averaging techniques. First, an implementation of an angular triggering technique, the Predictive Angular Triggering Technique (PATT), which uses the flow frequency and phase information to predict a future trigger point at which to record PIV images was used. Second, the Tracking Triggering Technique (TTT) which uses the detection of the PIV laser signal's pulse occurrence then tags each PIV image with the angular position at its measurement time, allowing grouping into angular slots or bins was used. These two methods were applied first on a spinning plate where the physical location of the plate could be measured. Results proved that the phase averaging system worked effectively. Later a circular cylinder in crossflow was used to observe the wake vortex structure. Here, the phase information was derived from flow measurements, specifically a hot-wire in the wake. Sequences of phase averaged PIV images at different stages of wake development within a shedding cycle revealed the evolution of the classical vortex street for the cylinder. Observations of an ogive cylinder wake showed that resolution of the wake field was not as simple as the cylinder case due to complex three dimensionalities in the flow,

however detailed wake analysis using 2-D and stereoscopic PIV measurements were completed. These analyses showed that there is a highly turbulent unsteady periodic wake behind the ogive cylinder base. However it was very hard to establish the periodicity using the techniques mentioned. The spiral mode of vortex shedding was confirmed with difficulty.

After analyzing the wakes, investigation of the effects of plasma actuators on the wakes were conducted. A similar setup to previous studies of 2D cylinders was explored. First, a single actuator was placed on the lower side of the cylinder. Later, two actuators operating simultaneously were used. Lastly, two actuators operating independently (typically alternately) were used. All of the actuators were operated with at a carrier frequency of 5 kHz and nominally 8 kV. The TTT phase averaging method was used to produce the wake velocity maps. For all of the cases tested, a favorable effect compared to the no actuator case in the wake was observed; in other words, the apparent width of the wake was significantly reduced in all the cases. Actuators were placed 70° measured from the upstream stagnation point on both sides of the cylinder. Using a single actuator produced delayed separation on the lower side, causing the wake to deflect towards the upper side. This is inherently related to the generation of net circulation in the counterclockwise sense. Since it was expected that if the upper actuator were driven, the opposite effect would be observed (and by this means the wake could therefore be "flipped" from side to side on demand) tests with two actuators operating independently were carried out. Test results showed that for a narrow frequency band (24.5 - 25.5 Hz) of modulating frequency around the natural frequency (25 Hz) it was possible to "lock on" to the shedding and drive it at the desired values over this small range. This is flow

control in the proper sense- a causal relationship between input and output. To the knowledge of the author there has not been any proper flow control case for this high Reynolds number (Re= 156,000) on cylinders previously presented in the literature. It was also seen that running the actuators at half or double the natural shedding frequency caused complete disorganization of the periodicity of the vortex shedding. Analysis of the power spectra of the dominant frequency for different actuator modulation was also investigated. It was seen that there was a linear relation and the amplitude of the power curves decreased with increasing modulation frequency.

Flow control was also attempted on the ogive cylinder. Several arrangements of the actuators were tried. Attempts to influence off-surface flow field showed that the effect was small. Only little effect was observed on the wake with open loop excitation. It was concluded that feedback control was not practical with the present weak actuators.

First, four actuators on the circumference operating as two pairs at same frequency were used. Later two actuators on the circumference operating independently were tested. After that two actuators placed on the base, blowing outwards were tested. Last two actuators on streamwise direction on top and bottom of the body were investigated. It was observed that direct alteration of the mean flow about a body was not as effective as the boundary layer flow control where the flow instabilities are exploited in the cylinder case. Also as was mentioned before ogive cylinder had a complex three dimensional flow field. For this reason it was harder to develop a flow control method which had a favorable effect. Analysis of the power spectra of the dominant frequency for different actuator

modulation for the four actuator case also showed that there was not a distinct relationship.

8.2 Future Work

The results presented in this dissertation demonstrated the capability of the plasma actuators to control vortex shedding for a limited range of frequencies on bluff body shapes. Future work is required for a more complete analysis of the potential and limitations of the actuators on bluff bodies.

First of all, the frequency range of the control needs to be improved. Factors affecting this can be the parameters which are related to actuator performance such as operating frequency, location, size, and size of overlapping region of the actuator.

A better understanding of the three dimensional flow field on axisymmetric bodies is needed. Different phase resolving techniques can be developed to analyze this complex structure. After completely analyzing the three dimensional wake a proper control technique could be proposed. For flow control cases an external synchronization signal other than a hot-wire can be used since the hot-wire data showed traces of contamination from the high electrical field in the wake region.

A numerical approach to analyze the complete evolution of the vortex shedding should be pursued. However, for these types of high Reynolds number flows where time accuracy is important it is not simple to analyze the flow field numerically mainly due to lack of computer power. Also, a multi-physics solver should be explored to take the plasma actuators into account, but this is also challenging since the plasma physics is not

completely understood and the combined affects of the local heating and momentum input may not be simulated properly.

REFERENCES

[1]Fox, R.W., *Introduction to Fluid Mechanics*, 4th ed., Wiley, New York, 1994.

[2]Shih, C., "Turbulent Wake Flow Behind A Circular Cylinder," http://www.eng.fsu.edu/~shih/, Florida State University, [cited in 2007].

[3]Schlichting, H., *Boundary Layer Theory*, 4th ed., McGraw-Hill, 1962.

[4]Buresti, G., "Wind effects on buildings and structures," Jubileum Conference on Wind Effects on Buildings and Structures, Porto Alegre, Brazil, 25-29 May 1998.

[5]Dyke, M.V., *An Album of Fluid Motion*, The Parabolic Press, Stanford, California, 1982.

[6]http://www.itsc.com/movies/index.htm, [cited in 2006].

[7]http://www.ceemast.csupomona.edu/nova/vonK.html, [cited in 2005].

[8]Lienhard, J.H., "Synopsis of Lift, Drag and Vortex Frequency for Rigid Circular Cylinders," College of Engineering Research Division Bulletin 300, Tech. Extension Service, Washington State University, 1966.

[9]Blevins, R.D., *Flow-Induced Vibration*, 2nd ed., VNR, New York, 1990.

[10]Roshko, A., "On the drag and shedding frequency of two-dimensional bluff bodies," NACA TN 3169, 1954.

[11]Bearman, P.W., "On vortex shedding from a Circular Cylinder in the Critical Reynolds Number Regime," *Journal of Fluid Mechanics*, Vol. 37, 1969, pp. 577-586.

[12]Roshko, A., "Experiments on the Flow past a Circular Cylinder at Very High Reynolds Number," *Journal of Fluid Mechanics*, Vol. 10, 1961, pp. 345-356.

[13]Schafer, J.W., Eskinazi, S., "An Analysis of the Vortex Street Generated in a Viscous Fluid," *Journal of Fluid Mechanics*, Vol. 6, 1959, pp. 241-260.

[14]Sarpkaya, T., "Vortex-Induced Oscillations," *Journal of Applied Mechanics*, Vol. 46, 1979, pp. 241-258.

[15]Griffin, O.M., Ramberg S. E., Davies, M. E, Calculation of the Fluid Dynamic Properties of Coherent Vortex Patterns in Vortex Flows, ASME, New York, 1980.

[16]Yeh, T.T., Robertson, B., Mattar. "LDV Measurements Near a Vortex Shedding Strut Mounted in a Pipe," *Journal of Fluids Engineering*, Vol. 105, 1983, pp. 185-194.

[17]Jones, G.W., Cincotta, J.J. and Walker, R.W., "Aerodynamic Forces on a Stationary and Oscillating Circular Cylinder at High Reynolds Numbers," NASA TR-300, 1969.

[18]Techet, A.H., "Vortex Induced Vibrations," http://web.mit.edu/13.42/www/lectsupp.html, Massachusetts Institute of Technology, [cited in 2005].

[19]Williamson, C.H.K., "Vortex dynamics in the cylinder wake," *Annu. Rev. Fluid. Mech*, Vol. 28, 1996, pp. 477-526.

[20]McCormick, W., Barnes, W., *Aerodynamics Aeronautics and Flight Mechanics*, 2nd ed., John Wiley & Sons Inc., 1995.

[21]Delery, J.M., "ROBERT LEGENDRE AND HENRIWERLÉ: Toward the Elucidation of Three-Dimensional Separation," *Annu. Rev. Fluid. Mech*, Vol. 33, 2001, pp. 129-154.

[22]Buresti, G., "Bluff Body Aerodynamics," International Advanced School on Wind-Excited and Aeroelastic Vibrations of Structures, June 12-16 2000.

[23]Karman, T.V., "Uber den Mechanismus des Widerstandes, den ein bewegter Korper in einer Flussigkeit erfahrt, 1 Teil.," *Gott. Nachr*, Vol. (C.W. 15), 1911, pp. 509-517.

[24]Karman, T.V., "Uber den Mechanismus des Widerstandes, den ein bewegter Korper in einer Flussigkeit erfahrt, 2 Teil.," *Gott. Nachr*, Vol. (C.W. 16), 1912, pp. 547-556.

[25]Roshko, A., "On the development of turbulent wakes from vortex streets," NACA TN 1191, 1954.

[26]Weickgenannt, A., Monkewitz, P. "Control of vortex shedding in an axisymmetric bluff body wake," *Eur. J. Mech. B-Fluids*, Vol. 19, 2000, pp. 789-812.

[27]Taneda, S., "Visual observations of the flow past a sphere at Reynolds number between 10^4 and 10^6," *Journal of Fluid Mechanics*, Vol. 85, 1978, pp. 185-192.

[28]Rodi, W., "On the simulation of turbulent flow past bodies," *Journal of Wind Engineering and Industrial Aerodynamics*, Vol. 46-47, 1993, pp. 3-19.

[29]Alcorn, C., "Boundary Layer Influences on the Subsonic Near-Wake of a Family of Three-Dimensional Bluff Bodies," PhD Thesis, Aerospace Engineering Dept., Old Dominion University, Norfolk, VA, August 1993.

[30]Fuchs, H.V., Mercker, E., Michel, U, "Mode expansion of Coherent Structures in the Wake of a Circular Disk," Second International Symposium on Turbulent Shear Flows, Imperial College, London, July 1979.

[31]Fuchs, H.V., Mercker, E., Michel, U. "Large-Scale Coherent Structures in the Wake of Axisymmetric Bodies, part 1," *Journal of Fluid Mechanics*, Vol. 93, 1979, pp. 185-207.

[32]Sarpkaya, T., "Computational methods with vortices, The 1988 Freeman Scholor Lecture," *ASME Journal of Fluids Engineering*, Vol. 111, 1989, pp. 5-52.

[33]Chorin, A.J., "Numerical Study of slightly viscous flow," *Journal of Fluid Mechanics*, Vol. 57, 1973, pp. 785-796.

[34]Sevilla, A., Martinez-Bazan, C. "Vortex Shedding in high Reynolds number axisymmetric bluff-body wakes: Local linear instability and global bleed control," *Physics of Fluids*, Vol. 16 (6), 2004, pp. 3460-3469.

[35]Honohan, A.M., "The Interaction of Synthetic Jets with Cross Flow and the Modification of Aerodynamic Surfaces," PhD Thesis, Georgia Institute of Technology, 2003.

[36]Schubauer, G.B., "Forced Mixing in Boundary Layers," *Journal of Fluid Mechanics*, Vol. 8 (part 1), 1960, pp. 10-32.

[37]Stykowski, P.J., Sreenivasan, K.R. "On the formation and Suppression of Vortex Shedding at Low Reynolds Numbers," *Journal of Fluid Mechanics*, Vol. 218, 1990, pp. 71-107.

[38]Mair, W.A., "The effect of a rear-mounted disk on the drag of a blunt-based body of revolution," *Aeronautical Quarterly*, Vol. 16, 1965, pp. 350-360.

[39]Roshko, A., "On the wake and drag of bluff bodies," *Journal of Aeronautical Sciences*, Vol. 22, 1955, pp. 124-137.

[40]Kwon, K., Choi, H. "Control of laminar vortex shedding behind a circular cylinder using splitter plates," *Physics of Fluids*, Vol. 8, 1996, pp. 479-486.

[41]Maull, D.J., "Vortex shedding from bluff bodies in a shear flow," *Journal of Fluid Mechanics*, Vol. 60, 1973, pp. 401-409.

[42]Ashgar, A., "Controlling Shedding from Circular Cylinders Using Plasma Actuators," PhD Thesis, University of Notre Dame, Indiana, 2004.

[43]Lin, J.C., Howard, F.G. and Selby, G.V., "Turbulent Flow Separation Control through Passive Techniques," AIAA Paper 89-0976, 1989.

[44]Howard, F.G., Goodman, W.L. and Walsh, M.J., "Axisymmetric Bluff-Body Drag Reduction Using Circumferential Grooves," AIAA Paper 83-1788, 1983.

[45]Bushnell, D. and Wilkinson, S.P., "Flow Separation Control ", Applied Aerodynamic Drag Reduction, The University of Kansas, 1993.

[46]Tanner, M., "Reduction of base drag," *Progress in Aerospace Sciences*, Vol. 16 (4), 1975, pp. 369-384.

[47]Zdravkovich, M.M., "Review and classification of various aerodynamic and hydrodynamic means of suppressing vortex shedding," *Journal of Wind Engineering and Industrial Aerodynamics*, Vol. 7, 1981, pp. 145-189.

[48]Vadillo, J.L., "Numerical Studies of the Application of Active Flow Control to Subsonic and Transonic Airfoil Flows Using a Synthetic Jet Actuator," PhD Thesis, Washington University, 2005.

[49]Gad-el-Hak, M., Flow Control - Passive, Active, and Reactive Flow Management, Cambridge University Press, 2000.

[50]Bearman, P.W., "The effect of the base bleed on the flow behind a two-dimensional model with a blunt trailing edge," *Aeronautical Quarterly*, Vol. 18, 1967, pp. 207-224.

[51]Maull, D.J., "Mechanisms of two and three-dimensional base drag," Symposium proceedings, Aerodynamic Drag Mechanisms of Bluff Bodies and Road Vehicles, New York, 191–226, 1978.

[52]Ahuja, K.K., Burrin R. H, "Control of Separation by Sound," 9th AIAA/NASA Aeroacoustics Conference, AIAA Paper 84-2298, Williamsburg, VA, 1984.

[53]Huang, L.S., Maestrello L., Bryant T. D, "Separation Control Over an Airfoil at High Angles of Attack by Sound Emanating from the Surface," AIAA Paper 87-1261, 1987.

[54]Hsiao, F.B., Liu C. F., Shyu J. Y. "Control of Wall-Separated Flow by Internal Acoustic Excitation," *AIAA Journal*, Vol. 28 (8), 1990, pp. 1440-1446.

[55]Liu, W.P., Brodie, G. H. "A Demonstration of MEMS-Based Active Turbulence Transitioning," *International Journal of Heat and Fluid Flow*, Vol. 21, 2000, pp. 297-303.

[56]Bar-Sever, A., "Separation control on an airfoil periodic forcing," *AIAA Journal*, Vol. 27 (6), 1989, pp. 820-823.

[57]Schumm, M., Berger, E., Monkewitz, P. A. "Self-Excited Oscillations in the wake of Two-Dimensional Bluff Bodies and Their Control," *Journal of Fluid Mechanics*, Vol. 271, 1994, pp. 17-53.

[58]Fujisawa, N., Kawaji, Y., Ikemoto, K. "Feedback Control of Vortex Shedding from a Circular Cylinder by Rotational Oscillations," *Journal of Fluids and Structures*, Vol. 15, 2001, pp. 23-37.

[59]Sun, X., "Closed-Loop Control of Vortex Shedding By Means of Lorentz force," PhD Thesis, New Jersey Institute of Technology, 2003.

[60]Henoch, C. and Stace, J., "Experimental investigation of a salt water turbulent boundary layer modified by an applied streamwise magneto hydrodynamic body force," *Physics of Fluids*, Vol. 7 (6), 1995, pp. 1371-1383.

[61]Roussopoulos, K., "Feedback control of vortex shedding at low Reynolds numbers," *Journal of Fluid Mechanics*, Vol. 133, 1993, pp. 265-285.

[62]Park, D.S., Ladd, D. M., Hendricks, E. W. "Feedback control of Von Karman vortex shedding behind a circular cylinder at low Reynolds numbers," *Physics of Fluids*, Vol. 6, 1984, pp. 2390.

[63]Smith, B.L., Trautman, M. A., Glezer, A., "Controlled Interactions of Adjacent Synthetic Jets," AIAA Paper 99-0669, 1999.

[64]Rizzetta, D.P., Visbal, M. R., Stanek, M. J. "Numerical Investigations of Synthetic Jets," *AIAA Journal*, Vol. 37 (8), 1999, pp. 919-927.

[65]Smith, B.L., Glezer, A, "Vectoring and Small-Scale Motions Effected in Free Shear Flows Using Synthetic Jet Actuators," 35th AIAA Aerospace Meeting, AIAA Paper 97-0213, Reno, NV, 1997.

[66]Roth J. R., S.D.M., Wilkinson S. P., "Electrohydrodynamic flow control with a glow-discharge surface plasma," *AIAA Journal*, Vol. 38, 2000, pp. 1166-1172.

[67]Artana, G., D'Adamo, J., Leger, L., Moreau, E. and Touchard, G., "Flow control with electrohydrodynamic actuators," *AIAA Journal*, Vol. 9, 2002, pp. 1773-1779.

[68]Artana, G., Sosa, R., Moreau, E. and Touchard, G., "Control of the near-wake flow around a circular cylinder with electrohydrodynamic actuators," *Experiments in Fluids*, Vol. 35, 2003, pp. 580-588.

[69]Roth J.R., "Aerodynamic flow acceleration using paraelectric and peristaltic electrohydrodynamic effect of a one atmosphere uniform glow discharge plasma," *Physics of Plasmas*, Vol. 10, 2003, pp. 2117-2126.

[70]Enloe CL, M.T., Van Dyken RD, Kachner KD, Jumper EJ, Corke TC, Post M, Haddad O. "Mechanisms and responses of a single dielectric barrier plasma actuator: geometric effects," *AIAA Journal*, Vol. 42, 2004, pp. 2177-2184.

[71]Enloe CL, M.T., Van Dyken RD, Kachner KD. "Mechanisms and response of a single dielectric barrier plasma actuator: plasma morphology," *AIAA Journal*, Vol. 42, 2004, pp. 589-594.

[72]Post ML, C.T., "Separation control on a high angle of attack airfoil using plasma actuators," *AIAA Journal*, Vol. 42, 2004, pp. 2177-2184.

[73]Sung Y, K.W., Mungal M. G., Cappelli M. A. "Aerodynamic modification of flow over bluff objects by plasma actuation," *Experiments in Fluids*, Vol. 41 (Research Article), 2006, pp. 479-486.

[74]Malik MR, W.L., Hussani MY, "Ion wind drag reduction," AIAA Paper 83–0231, 1983.

[75]Santhanakrishnan, A., Jacob, J.D. and Suzen, Y.B., "Flow Control Using Plasma Actuators and Linear/Annular Plasma Synthetic Jet Actuators," 3rd AIAA Flow Control Conference, AIAA Paper 2006-3033, San Francisco,CA, 2006.

[76]Hyun, K.T. and Chun, C.H., "The wake flow control behind a circular cylinder using ion wind," *Experiments in Fluids*, Vol. 35, 2003, pp. 541-552.

[77]El-Khabiry S, C.G., "Drag reduction by dc corona discharge along an electrically conductive flat plate for small Reynolds number flow," *Physics of Fluids*, Vol. 9, 1997, pp. 587-599.

[78]Moreau, E., Leger, L. and Touchard, G., "Effect of a DC surface non-thermal plasma on a flat plate boundary layer for airflow velocity up to 25 m/s modification of flow over bluff objects by plasma actuation," *Journal of Electrostatics*, Vol. 64, 2006, pp. 215-225.

[79]Roth, J.R. and Dai, X., "Optimization of the Aerodynamic Plasma Actuator as an Electrohydrodynamic (EHD) Electrical Device," 44th AIAA Aerospace Sciences Meeting and Exhibit, AIAA Paper 2006–1203, Reno, NV, 2006.

[80]Wilkinson, S.P., "Investigation of An Oscillating Surface Plasma For Turbulent Drag Reduction," 41st AIAA Aerospace Sciences Meeting and Exhibit, AIAA Paper 2003–1023, Reno, NV, 2006.

[81]Santhanakrishnan, A. and Jacob, J.D., "Flow control with plasma synthetic jet actuators," *Journal of Physics D: Applied Physics*, Vol. 40, 2007, pp. 637-651.

[82]Goksel, B., Greenblatt, D., Rechenberg, I., Nayeri, C.N. and Paschereit, C.O., "Steady and unsteady plasma wall jets for separation and circulation control," 3rd AIAA Flow Control Conference, AIAA Paper 2006–3686 San Francisco,CA, 2006.

[83]Sosa, R. and Artana, G., "Steady control of laminar separation over airfoils with plasma sheet actuators," *Journal of Electrostatics*, Vol. 67, 2006, pp. 604-610.

[84]Corke, T.C., Jumper, E.J., Post, M., Orlov, D. and McLaughlin, T.E., "Application of weakly-ionized plasmas as wing flow-control devices," 40th AIAA Aerospace Sciences Meeting and Exhibit AIAA Paper 2002–0350, Reno, NV, 2002.

[85]Corke, T.C., Mertz, B. and Patel, M.P., "Plasma flow control optimized airfoil " 44th AIAA Aerospace Sciences Meeting and Exhibit AIAA Paper 2006–1208, Reno, NV, 2006.

[86]Corke, T.C., He, C. and Patel, M.P., "Plasma Flaps and Slats: An Application of Weakly Ionized Plasma Actuators," 2nd AIAA Flow Control Conference, AIAA Paper 2004-2127, Portland, OR, 2004.

[87]List, J., Byerley, A., McLaughlin, T. and Dyken, V.R., "Using a plasma actuator to control laminar separation on a linear cascade turbine blade," 41st AIAA Aerospace Sciences Meeting and Exhibit AIAA Paper 2003–1026, Reno, NV, 2003.

[88]Hultgren, L. and Ashpis, D., "Demonstration of separation delay with glow-discharge plasma actuators," 41st AIAA Aerospace Sciences Meeting and Exhibit AIAA Paper 2003–1025, Reno, NV, 2003.

[89]Huang, J., Corke, T.C. and Thomas, F.O., "Unsteady Plasma Actuators for Separation Control of Low-Pressure Turbine Blades," *AIAA Journal*, Vol. 44 (7), 2006, pp. 1477-1487.

[90]Ramakumar, K., "Active flow control of low pressure turbine blade separation using plasma actuators," Master's Thesis, University of Kentucky, Lexington, Kentucky, 2006.

[91]Asghar, A. and Jumper, E.J., "Phase syncrhonization of vortex shedding from multiple cylinders using plasma actuators," 41st AIAA Aerospace Sciences Meeting and Exhibit AIAA Paper 2003–1028, Reno, NV, 2003.

[92]McLaughlin, T.E., Munska, M.D., Vaeth, J.P., Dauwalter, T.E., Goode, J.R. and Siegel, S.G., "Plasma-based actuators for cylinder wake vortex control " 2nd AIAA Flow Control Conference, AIAA Paper 2004–2129, Portland, OR, 2004.

[93]Thomas, F.O., Kozlov, A. and Corke, T.C., "Plasma actuators for landing gear noise reduction," 11th AIAA/CEAS Aeroacoustics Conference, AIAA Paper 2005–3010, Monterey, CA, 2005.

[94]Siegenthaler, J., Jumper, E.J. and Asghar, A., "A preliminary study in regularizing the coherent structures in a planar, weakly compressible, free shear layer " 41st AIAA Aerospace Sciences Meeting and Exhibit, AIAA Paper 2003–0680, Reno, NV, 2003.

[95]Samimy, M., Adamovich, I., Kim, J., Webb, B., Keshav, S. and Utkin, Y., "Active control of high speed jets using localized arc filament plasma actuators " 2nd AIAA Flow Control Conference, AIAA Paper 2004–2130, Portland, OR, 2004.

[96]Shyy, W., Jayaraman, B. and Andersson, A., "Modeling of Glow Discharge-Induced Fluid Dynamics," *Journal of Physics D: Applied Physics*, Vol. 92 (11), 2002, pp. 6434-6443.

[97]Suzen, Y.B., Huang, P.G., Jacob, J.D. and Ashpis, D.E., "Numerical Simulation of Plasma Based Flow Control Applications," 35th AIAA Fluid Dynamics Conference and Exhibit, AIAA Paper 2005–4633, Toronto, Ontario, 2005.

[98]Suzen, Y.B. and Huang, P.G., "Simulations of Flow Separation Control Using Plasma Actuators," 44th AIAA Aerospace Sciences Meeting and Exhibit, AIAA Paper 2006–877, Reno, NV, 2006.

[99]Hall, K.D., Jumper, E.J., Corke, T.C. and McLaughlin, T.E., "Potential Flow Model of a Plasma Actuator as a Lift Enhancement Device," 43rd AIAA Aerospace Sciences Meeting and Exhibit, AIAA Paper 2005–783, Reno, NV, 2005.

[100]Orlov, D.M. and Corke, T.C., "Numerical Simulation of Aerodynamic Plasma Actuator Effects," 43rd AIAA Aerospace Sciences Meeting and Exhibit, AIAA Paper 2005–1083, Reno, NV, 2005.

[101]Orlov, D.M., Corke, T.C. and Patel, M.P., "Electric Circuit Model for Aerodynamic Plasma Actuator," 43th AIAA Aerospace Sciences Meeting and Exhibit, AIAA Paper 2006–1206, Reno, NV, 2006.

[102]Font, G.I., "Boundary Layer Control with Atmospheric Plasma Discharges," 40th AIAA/ASME/SAE/ASEE Joint Propulsion Conference and Exhibit, AIAA Paper 2004–3574, Fort Lauderdale, FL, 2004.

[103]Font, G.I. and Morgan, W.L., "Plasma Discharges in Atmospheric Pressure Oxygen for Boundary Layer Separation Control," 35th Fluid Dynamics Conference and Exhibit, AIAA Paper 2005–4632, Toronto, Ontario, 2005.

[104]Font, G.I., Jung, S., Enloe, C.L., McLaughlin, T.E., Morgan, W.L. and Baughn, J.W., "Simulation of the Effects of Force and Heat Produced by a Plasma Actuator on Neutral Flow Evolution," 44th AIAA Aerospace Sciences Meeting and Exhibit, AIAA Paper 2006–167, Reno, NV, 2006.

[105]Shang, J.S., "Electromagnetic Field of Dielectric Barrier Discharge," 36th AIAA Plasmadynamics and Lasers Conference, AIAA Paper 2005–5182, Toronto, Ontario, 2005.

[106]Pons, J., Moreau, E. and GTouchard. "Asymmetric surface dielectric barrier discharge in air at atmospheric pressure: electrical properties and induced airflow characteristics," *Journal of Physics D: Applied Physics*, Vol. 38, 2005, pp. 3635-3642.

[107]Baughn, J.W., Porter, C.O., Peterson, B.L., McLaughlin, T.E., Enloe, C.L., Font, G.I. and Baird, C., "Momentum transfer for an aerodynamic plasma actuator with an imposed boundary layer," 44th AIAA Aerospace Sciences Meeting and Exhibit, AIAA Paper 2006–168, Reno, NV, 2006.

[108]Porter, C.O., Baughn, J.W., McLaughlin, T.E., Enloe, C.L. and Font, G.I., "Temporal force measurements on an aerodynamic plasma actuator," 44th AIAA Aerospace Sciences Meeting and Exhibit, AIAA Paper 2006–104, Reno, NV, 2006.

[109]Mittal, R. and Balachandar, S., "Effect of three dimensionality on the lift and drag of nominally two-dimensional cylinders," *Physics of Fluids*, Vol. 7, 1995, pp. 1841-1865.

[110]Bendat, J.S. and Piersol, A.G., *Random Data Analysis and Measurement Procedures*, 3rd ed., John Wiley & Sons Inc., 1971.

[111]Sonnenberger, R., Graichen, K. and Erk, P., "Fourier-averaging: a phase-averaging method for periodic flow," *Experiments in Fluids*, Vol. 28, 2000, pp. 217-224.

[112]Stella, A., Guj, G. and Felice, F.D., "Propeller Wake Flowfield Analysis by Means of LDV Phase Sampling Techniques," *Experiments in Fluids*, Vol. 28, 2001, pp. 1-10.

[113]Cui, J., "The Interaction of Synthetic Jets with Turbulent Boundary Layers," PhD Thesis, Washington University, 2004.

[114]Gregory, J.W., "Development of Fluidic Oscillators as Flow Control Actuators," PhD Thesis, Purdue University, 2005.

[115]D. Rapoport, I.F., K. Cohen, A. Seifert. "Closed-Loop Vectoring Control of a Turbulent Jet Using Periodic Excitation," *Journal of Propulsion and Power*, Vol. 19 (4), 2003, pp. 646-654.

[116]Stansby, P.K., "The effects of end plates on the base pressure coefficient of a circular cylinder " *Aeronautical Journal*, Vol. 78, 1974, pp. 36-37.

[117]Apelt, C.J. and West, G.S., "The effects of wake splitter plates on bluff-body flows in the range 10^4<Re<5x10^4," *Journal of Fluid Mechanics*, Vol. 71 (part 2), 1975, pp. 145-160.

[118]Strykowski, P.J. and Sreenivasan, K.R., "On the formation and supression of vortex shedding at low Reynolds numbers," *Journal of Fluid Mechanics*, Vol. 218, 1990, pp. 71-107.

[119]Roth, J.R., Madhan, R.C., Yadav, M., Rahel, J. and Wilkinson, S.P., "Flow Field Measurements of Paraelectric, Peristaltic and Combined Plasma Actuators Based on the One Atmospheric Uniform Glow Discharge Plasma (OAUGDPTM)," 42nd Aerospace Sciences Meeting and Exhibit, AIAA 2004 - 0845, Reno, NV, 2004.

[120]Glezer, A. and Amitay, M., "Synthetic Jets," *Annu. Rev. Fluid. Mech*, Vol. 34, 2002, pp. 503-529.

[121]Griffin, O.M. and Hall, K.C., "Review-Vortex Shedding Lock-on and Flow Control in Bluff Body Wakes," *Journal of Fluids Engineering*, Vol. 113 (4), 1991, pp. 526-537.

[122]Armstrong, B.J., Barnes, F.H. and Grant, I., "The Effect of a Perturbation on the Flow over a Bluff Cylinder," *Physics of Fluids*, Vol. 29 (7), 1986, pp. 2095-2102.

[123]Okajima, A., Takata, H. and Asanuma, T., "Viscous Flow Around a Rotationally Oscillating Circular Cylinder," Institute of Space and Aeronautical Sciences Report, University of Tokyo, No:532, 1975.

[124]Blevins, R.D., "The Effect of Sound on Vortex Shedding from Cylinders," *Journal of Fluid Mechanics*, Vol. 161, 1985, pp. 217-237.

[125]Seifert, A., *Closed-Loop Active Flow Control Systems: Actuators*, Springer Berlin / Heidelberg, 2007.

[126]Madhan, R.C.M., "Boundary Layer Flow Acceleration by Paraelectric and Peristaltic EHD Effects of Aerodynamic Plasma Actuators," Master's Thesis, University of Tennessee, 2004.

[127]Corke, T., "Single Dielectric Barrier Discharge Plasma Enhanced Aerodynamics: Physics, Modelling and Applications," *Experiments in Fluids*, Vol., 2008, pp. (to be published).

[128]Kogelschatz, U., Eliasson, B. and Egil, W., "Fundamentals and applications of dielectric barrier discharges," Proceedings of the 23rd ICPIG, 1-20, 1997.

[129]Roth, J.R., Dai, X., Rahel, J. and Sherman, D.M., "The Physics and Phenomenology of Paraelectric One Atmosphere Uniform Glow Discharge Plasma (OAUGDP™) Actuators for Aerodynamic Flow Control," 43rd AIAA Aerospace Sciences Meeting & Exhibit, AIAA Paper 2005–781, Reno, NV, 2005.

[130]Opaits, D.F., Roupassov, D.V., Starikovskaia, S.M., Starikovskii, A.Y., Zavialov, I.N. and Saddoughi, S.G., "Plasma Control of Boundary Layer Using Low-Temperature Non-Equilibrium Plasma of Gas Discharge," 43rd AIAA Aerospace Sciences Meeting & Exhibit Reno, AIAA Paper 2005-1180, Reno, NV, 2005.

[131]Roth, J.R., Rahel, J. and Dai, X., "Three Dimensional Flow Acceleration Using Plasma Aerodynamic Actuators," APS Gaseous Electronics Conference, Reno, NV, 2003.

[132]Yadav, M., Dai, X. and Roth, J.R., "Measurement of the Boundary Layer Velocity Induced by Paraelectric Plasma Actuators using an Inexpensive High Voltage Power

Supply," 31st IEEE International Conference on Plasma Science, Baltimore, Maryland, 2004.

[133]Dai, X., Rahel, J. and Roth, J.R., "Maximum Flow Velocity and Dielectric Heating in Electrohydrodynamic (EHD) Plasma Actuators using Paraelectric Effects of a One Atmosphere Uniform Glow Discharge Plasma (OAUGDPTM)," 31st IEEE International Conference on Plasma Science, Baltimore, Maryland, 2004.

[134]Orlov, D.M., "Modelling And Simulation Of Single Dielectric Barrier Discharge Plasma Actuators," PhD Thesis, University of Notre Dame, Indiana, 2006.

[135]Post, L.M., "Plasma Actuators for Separation Control on Stationary and Oscillating Airfoils," PhD Thesis, University of Notre Dame, Indiana, 2004.

[136]Haack, S., "Flow Control Using Plasma And Synthetic Jet Actuators On Bluff Bodies," Master's Thesis, University of Maryland, 2007.

[137]Koc, I., "An Experimental Study of Automotive Wakes For Drag Breakdown," Master's Thesis, Aerospace Engineering Dept., Old Dominion University, Norfolk, VA, August 2003.

[138]www.dantecdynamics.com, [cited in 2002].

VITA

DEGREES

Master of Science Aerospace Engineering

Old Dominion University, Norfolk, VA, Aug. 2003

Bachelor of Science Mechanical Engineering

Gazi University, Ankara, Turkey June 2001

PROFESSIONAL CHRONOLOGY

Aerospace Engineering Department, Old Dominion University, Norfolk, VA

Research Assistant, August 2001- August 2008

PROFESSIONAL MEMBERSHIPS

American Institute of Aeronautics and Astronautics (AIAA) - *Student Member,* (Chapter President at Old Dominion University; www.orgs.odu.edu/aiaa)

American Society of Mechanical Engineers (ASME) - *Student Member*

Tau Beta Pi Engineering Honor Society, Member

SCHOLARY ACTIVITIES

Koc, I. and Britcher, C. P., Phase Averaged Velocity Fields For Bluff Bodies Using PIV System, Proceedings of IMECE2008, 2008 ASME International Mechanical Engineering Congress and Exposition, Nov. 2-6, 2008, Boston, MA, USA

Koc, I. and Britcher, C. P., An Experimental Study of Bluff-Body Wakes for Drag Breakdown, AIAA Region I YPSE Conference, Johns Hopkins University Applied Physics Lab, November 10-11 2006

W. Mokhtar, X. Zheng, **I. Koc** and K. Kara, Aerodynamics and Flow Control of Flapping Wings, AIAA-2006-1059, 44th AIAA Aerospace Sciences Meeting and Exhibit, Reno, Nevada, Jan. 9-12, 2006

Koc, I. and Britcher, C. P., Wake Surveys Of Automobile Geometries For Drag Breakdown Using 2D And 3D PIV Systems, 11.Int. Symp. on Flow Visualization, August 9-12, 2004, University of Notre Dame, Notre Dame, Indiana, USA

Koc, I. and Britcher, C. P., An Experimental Study of Automotive Wakes for Drag Breakdown Using PIV System, AIAA Region I-MA Conference, Virginia Tech., April 2004

An Experimental Study of Automotive Wakes for Drag Breakdown, MS Thesis, Old Dominion University, August 2003.

An Experimental Study of Automotive Wakes for Drag Breakdown and Aerodynamics of Ground Vehicles, Seminar, Old Dominion University, October 2003.

Koc, I., Britcher C. P.; "Phase-Resolved Characterization of Wake Flows," Poster Session, 5th Annual Research Exposition, Norfolk, VA, April 2008